WATER ANALYSIS BY REMOTE SENSING: A MODEL FOR THE INTERPRETATION OF OPTICAL SPECTRAL MEASUREMENTS

by
Peter Gege

Translated from Forschungsbericht 94-15

Translated text has been reviewed by the author.

Gewässeranalyse mit passiver Fernerkundung: Ein Modell zur Interpretation optischer Spektralmessungen

Peter Gege

Deutsche Forschungsanstalt für Luft- und Raumfahrt e.V.
Institut für Optoelektronik Oberpfaffenhofen, Germany

Deutsche Forschungsanstalt für Luft- und Raumfahrt
Forschungsbereich Nachrichtentechnik und Erkundung
Institut für Optoelektronik
Abteilung Optische Fernerkundung
D-82230 Weßling

Head of Institute: Prof. Dr. F. Lanzl

Head of Department: Dr. M. Schroeder

Author: Dipl.-Phys. P. Gege

Copies of the original report in German, published by the DLR, can be obtained from: Deutsche Forschungsanstalt für Luft- und Raumfahrt e. V, Abteilung ZL-ID, D-51140 Köln, Germany.

Remote sensing, Lake Constance, spectroscopy, Fresnel reflection, phytoplankton

ABSTRACT

Spectral analysis of sunlight reflected in water allows determination of concentrations of water constituents from remote sensing data. By comparison of shipborne spectrometer data with *in situ* measurements for Lake Constance, algorithms for data analysis have been developed based on physical models:

- A model for "cloud correction". Measurement of radiation leaving the water is particularly critical when the sky is cloudy, since specular surface reflections of clouds falsify the signal from the water body. An algorithm has been developed which corrects such errors.

- A model for determining the concentrations of inorganic suspended matter, dissolved organic matter (yellow substance) and 4 phytoplankton classes from reflectance spectra. The separation of different phytoplankton classes, achieved here for the first time, permits more accurate determination of the concentration of the important pigment chlorophyll *a*.

Table of Contents

1. Introduction 7

2. Passive spectroscopy with variable cloud cover . 13
   2.1 Incident radiation analysis 14
      2.1.1 Four-source model 14
      2.1.2 Measurement of incident radiation 17
      2.1.3 Determination of the spectrum of direct solar radiation 19
      2.1.4 Determination of the cloud spectrum 28
      2.1.5 Normalization of the base spectra 30
      2.1.6 Resolution of incident radiation into 4 components 32
   2.2 Measurement of radiation reflected from water 35
   2.3 Calculation of reflectance 38
      2.3.1 Dependence of radiation measurements on the field of view of the sensor 38
      2.3.2 Definition of the terms reflectance and albedo 41
      2.3.3 Relationship between reflectance and albedo 42
      2.3.4 Specular surface reflections . . . 43
      2.3.5 Cloud correction 45
3. Optical properties of water and its constituents 51
   3.1 Absorption and scattering theory 53
      3.1.1 Quantum-mechanical derivation of the complex refractive index 53
      3.1.2 Classical derivation of the complex refractive index 57
      3.1.3 The complex refractive index . . . 59
      3.1.4 Mie theory for spherical particles. 64
      3.1.5 Absorption of arbitrarily shaped articles 70
   3.2 Determination of optical properties . . . 73
      3.2.1 Inherent optical properties . . . 73
      3.2.2 Modelling of scattering 81

3.3 Pure water 92
3.4 Important pigments 97
3.4.1 Yellow substance 100
3.4.2 Chlorophylls 103
3.4.3 Phaeophytins 109
3.4.4 Phycobiliproteins 110
3.4.5 Carotenes 115
3.4.6 Xanthophylls 117
3.5 Phytoplankton 119
3.5.1 Absorption 119
3.5.2 Scattering 124
4. Reflectance model 125
4.1 Relationship of reflectance with absorption and scattering 125
4.2 Model input spectra 127
4.2.1 Water 127
4.2.2 Yellow substance 129
4.2.3 Phytoplankton 130
4.3 Inversion of reflectance spectra 135
4.3.1 The problem of inversion 135
4.3.2 General program structure 137
4.3.3 The INVERS program 139
4.3.4 The WASSER program 141
5. Measurements 142
5.1 Instruments 142
5.1.1 Spectrometer 142
5.1.2 HLPC system 144
5.1.3 Photometer 147
5.2 Correlation between chlorophyll a and other measurements 149
5.2.1 Phaeophytin a 150
5.2.2 Carotenoids 151
5.2.3 Chlorophylls b and c 153
5.2.4 Abundance 155
5.2.5 Biovolume 156
5.2.6 Secchi depth 157
5.3 Yellow substance 158
5.3.1 Literature data on yellow substance in Lake Constance 158

5.3.2 Measurement of yellow substance on 25.6.91 160
5.4 Description of the measurement site . . . 162
5.5 Seasonal development of phytoplankton . . 164
6. Determination of water constituents from reflectance spectra 169
6.1 Spectral characterization of the phytoplankton in Lake Constance 169
6.2 Pigment determination 171
6.2.1 Chlorophyll a 172
6.2.2 Phaeophytin a 180
6.2.3 Carotenoids 181
6.3 Phytoplankton classification 184
6.3.1 Reflectance spectra fitting by the INVERS program and comparison with *in situ* data 184
6.3.2 Optical class: Cryptophyceae . . . 190
6.3.3 Optical class: diatoms 191
6.3.4 Optical class: green algae 192
6.3.5 Optical class: dinoflagellates . . 193
6.4 The spectral region in the vicinity of 685 nm 194
7. Summary 198
8. References 204
Acknowledgements 218

Appendix A: Kramers-Kronig relations 221
Appendix B: Simplex algorithm 227
Appendix C: Software outline 230

1. Introduction

Remote sensing of water

Research and surveillance of waters is no longer conceivable without the use of image-forming instruments on aircraft or satellites, since two-dimensional structures, such as the distribution of dissolved and suspended matter in water, can only be recognized by pictorial representation. Although sampling from a ship does permit considerably more substances to be determined, even as a depth profile, the time required for sampling and analysis of water samples is very great and only a few sites are ever studied for routine measurements. A higher level of sampling is only carried out during labour-intensive campaigns. During such campaigns, the samples can be confirmed as being representative of the body of water if it is shown that the water constituents are fairly homogeneously distributed. However, inhomogeneous distributions are frequently found, so-called "patches", and then only a picture ensures reliable extrapolation of the measured values to the area under study.

It is sufficient for some applications to document marked differences in water colour by aerial photography. However, quantitative information on concentrations may only be derived from conventional photographs with great effort. In the case of routine studies, this is only possible if the "water colour" is characterized in a defined manner spectrally and radiometrically, that is using a calibrated sensor.

For determining concentrations, generally only the visible region of the electromagnetic spectrum is suitable, since in other spectral regions the depth of

penetration is less than 1 cm.* If the sun is used as light source, this is termed *passive* measurement; if the water is illuminated with a suitable light source such as a laser, the process is termed *active*. The accuracy of determination is greater with active measurements, since the light source may be optimized with respect to optical properties of individual substances in the water. Moreover, depth profiles can be measured in pulsed mode and active measurements may also be taken at night. However, image generation is associated with a high technical effort. Most active systems make point measurements which are combined to form a ground track. This work concentrates on passive measurements.

The classic example of the value of passive spectral measurements is the *Coastal Zone Color Scanner* (CZCS) on the American *Nimbus-7* satellite which operated from 1978 to 1986. Oceanic chlorophyll concentration could be mapped for the first time from its measurements. The book by Barale and Schlittenhardt (1993) gives a survey of the variety of the applications of this data set. It also contains an article which introduces the future satellite-borne sensors for oceanic observation (van der Piepen and Doerffer 1993). They offer more spectral channels than the CZCS, as a result of which it may be expected that water analysis in coastal areas will be considerably improved.

Satellites are essential for global observations, but for measurements on smaller areas, aircraft are considerably more flexible. Since earth observation satellites overfly the same area at intervals of 1 to 2 weeks or more, specific observations of brief occurrences such as algal blooms which are often of particular interest may only be carried out with aircraft. Favourable weather conditions

---

* These spectral regions may be used to study the water surface, for example in measurement of the surface temperature (thermal infrared in the vicinity of 10 μm) or to determine the length and height of water waves (microwaves in the centimetre range).

may also be exploited here. Furthermore, for many inland waters, the high spatial resolution of aircraft measurements is indispensable; raster sizes below 10 metres are achieved without problem. An example of a modern aircraft instrument which is optimized for remote sensing of water is the German ROSIS (Doerffer et al. 1989).

The aim of any analysis of waters is to determine the concentrations of the water constituents. For this purpose, in the case of remote sensing measurements, the light reflected in the water must be related to the constituents via a model. This model is termed a *bio-algorithm*, since many constituents have a biological nature. However, in the case of aircraft and satellite measurements, two problems must first be solved which do not occur in the case of comparable underwater measurements:

1. The scattered light from the atmosphere which arrives at the sensor and attenuation of the signal at the surface on passing through the atmosphere must be taken into account (atmospheric correction),

2. The light reflected at the water surface must be calculated and subtracted from the signal at the surface.

A good description of these problems and approaches to their solution is given by Gordon (1993). Satisfactory results have only been obtained previously when the following conditions are satisfied:

- cloudless sky,

- the aerosol type is known,

- the light penetrating into the water is absorbed for at least one spectral channel.

When the sky is clear, the distribution of radiation of the sky can be calculated and, from this, the light reflected at the water surface, if the position of the sun, angle of observation and wind speed are known. If this component is subtracted from the measured value, the light scattered by the atmosphere is obtained for spectral channels at which the reflection in water is zero. If the type of aerosol is known, that is the particle size distribution and refractive index of the aerosols, the scattered light component can be extrapolated to other wavelengths.

This standard method leads to good results in the open ocean, since in this case the reflection of water in the infrared is negligible and the scattering behaviour of maritime aerosols has been reliably characterized. However, in the case of waters having a high suspended matter content or having surface films - marine coastal areas, rivers, inland waters - the water frequently reflects over the entire spectral range. Furthermore, the scattering behaviour of aerosols occurring in the vicinity of land can only be estimated roughly. In this case it is not possible to differentiate in the measurement signal between light reflected in the water, at the water surface and in the atmosphere. Separation of these three components is only possible with a model which includes both the atmosphere and also the waters.

In the case of measurements made on board ship, the problem simplifies, since light scattered by the atmosphere into the sensor may be ignored. It is possible to study how well the light which is backscattered in the water can be separated from the light which is reflected at the water surface. In the present work, a method is developed which makes this separation successfully, even if the distribution of radiation in the sky is unknown. This fulfils the precondition for the actual aim of the work, development of a bioalgorithm for waters in which the reflection is not negligible in the infrared and in

which different types of substances are dissolved or suspended.

Outline of the work

The measurements for the present work were collected in the course of 36 trips of the research ship "Robert Lauterborn" on Lake Constance. The spectral measurements were made from deck with a spectrometer. Furthermore, extensive *in situ* data were available which had been obtained by Constance University by analysis of water samples. The data set covers the biologically interesting period from April to November.

The measurements were taken in a weekly cycle, independently of the weather. The sky was very frequently cloudy or overcast, and in such cases the specular reflections of the clouds at the water surface present great problems in the evaluation of spectral measurements. This produced the necessity of developing a method by which the reflections at the water surface could be corrected, even when the radiation distribution of the sky is not known. This "cloud correction" is the subject of Chapter 2.

Other parts of the work deal with the development of a bioalgorithm. It was not the aim of the work to obtain the best possible agreement between parameters of the spectral measurements and *in situ* data by means of statistical evaluation, since such an empirical algorithm is not suited to other types of waters. The aim was rather to represent systematically the optical properties of waters in order to obtain a description in terms of a model which can be applied to other types of water bodies. This systematic part is covered by Chapter 3.

On the basis of the findings of this systematic part, two PC programs were written which enable determination of the concentrations of pigments or individual phytoplankton classes by so-called "inverse modelling". The

programs are described in Chapter 4.

Before the results of modelling could be compared with *in situ* measurements, they had to be evaluated with respect to remote sensing requirements. The *in situ* data set and the conclusions drawn therefrom are given in Chapter 5.

In Chapter 6, *in situ* data are compared with modelling results. The model is a significant improvement on other models: it permits the differentiation between 4 "optical classes" of the phytoplankton, independent of the weather conditions.

Outlook

Since the modelling of water body albedo, introduced in the present work, functions reliably, it offers a good basis for a coupled atmosphere-water model by which aircraft and satellite measurements can be evaluated even for critical types of waters and light conditions. Implementation of such a model for evaluation of data from existing and future sensors in image-processing software will be the subject of future work.

2. Passive spectroscopy with variable cloud cover

Whereas active spectroscopic methods are independent of the lighting conditions, passive methods have the disadvantage of only yielding useable data under certain weather conditions. In the case of spectroscopic study of water bodies, especially, where a large part of the radiation detected is reflections at the water surface, the accuracy with which information on the water body can be extracted depends considerably on the roughness of the water surface and on the cloud cover. Because of such effects of the weather, large amounts of data obtained in routine measurements are not evaluated or else measurements are only carried out at all under favourable conditions.

It is unsatisfactory for the continuity of a data set if the potential observations are restricted in this way. Therefore, a method has been developed in order to derive useable reflectance spectra even from measurements which contain an unknown specular surface reflection component or in which accompanying measurement of incident radiation does not correctly represent the influence of cloud cover.

It is shown that the spectrum of the incident radiation can be modelled in the range 400 to 800 nm at a resolution of 2 nm with an accuracy better than 99.8 per cent by addition of only 4 base spectra. These base spectra do not change in the course of a day or in the course of the year. The reflectance spectrum can therefore be calculated without measuring the incident radiation if the relative proportions of the 4 base spectra are known for a radiance measurement of the water. These proportions can be derived from the reflectance spectrum itself, since they generate characteristic errors in this if they are not correct.

This chapter first introduces the model by which the incident radiation may be represented as a sum of 4 base spectra. Two of these base spectra can be calculated, and the other two are derived from a large number of measurements. This model forms the basis for cloud correction in measurement of water body albedo spectra. Use of an inversion method is shown for simultaneous determination of the correct incident radiation and reflectance spectra. Comparison of the corrected and not corrected reflectance spectra shows that in the case of cloud cover, only corrected spectra can generally be meaningfully interpreted.

2.1 Incident radiation analysis

2.1.1 Four-source model

Quantitative interpretation of spectral measurements requires that the incident radiation be known.

The light incident on the water surface arrives from the upper hemisphere, that is from all points (θ,Φ) of the sky having zenith angles θ of 0 to $\pi/2$ and azimuth angles Φ from 0 to 2π. A detector having a small angular aperture measures the light intensity in the unit mW m^{-2} nm^{-1} sr^{-1}. This parameter is termed *radiance* (L). If the detector is pointed towards the sky (more precisely towards the upper hemisphere) it detects the downwelling radiation which is indicated by the subscript "d"; otherwise it records the upwelling radiation, designated by subscript "u". The integral of the downwelling radiance over the upper hemisphere - weighted by $\cos\theta$ because of the projection - is the *irradiance* E_d:*

$$E_d(\lambda) = \int_{\Phi=0}^{2\pi} \int_{\theta=0}^{\pi/2} L_d(\lambda,\theta,\Phi) \cos\theta \sin\theta \, d\theta \, d\Phi. \qquad (2.1)$$

---

* The nomenclature is based on the recommendations of the *International Association of Physical Oceanography, IAPO* (Morel and Smith 1982).

The downwelling radiance at the coordinates (θ,Φ) of the sky is composed of two components: transmitted and scattered light. If $E_0(\lambda)$ is the irradiance outside the atmosphere (solar constant), the following therefore applies:

$$L_d(\lambda) = E_0(\lambda)\ (c_1'\ t(\lambda) + c_2'\ b(\lambda)).$$

$t(\lambda)$ and $b(\lambda)$ denote the spectral course of transmission and scattering, c'_1 and c'_2 give the particular proportion. To simplify the equations, the arguments (θ,Φ) have been omitted.

For the analysis of measured irradiance spectra, the assumption is now made that the radiance $L_d(\lambda)$ can be written as the sum of four radiation sources:

$$L_d(\lambda) = E_0(\lambda)\ (c_1\ t_A(\lambda) + c_2\ \lambda^{-4} + c_3\ \lambda^{-n} + c_4\ t_c(\lambda)\ ). \qquad (2.2)$$

In this equation, $t_A(\lambda)$ is the transmission spectrum of the atmosphere, λ^{-4} and λ^{-n} are the Rayleigh and Mie components of the scattering, respectively. The "cloud spectrum" $t_C(\lambda)$ is a combination of the transmission spectrum and scattering spectrum of the atmospheric water (in the form of vapour or clouds) which cannot be further separated within the framework of this model.

The Mie component λ^{-n} of the scattering represents the aerosol scattering. Aerosols are usually treated as spherical particles having a specific size distribution (Mie theory, see Section 3.1.4). Apart from the refractive index, the size distribution is the most important parameter governing the wavelength dependency of scattering. Therefore, the differentiation between different aerosol types (for example maritime, continental) essentially denotes different size distribution. The aerosol scattering is approximately proportional to λ^{-n},

the *Ångström coefficient* n depending on the size distribution (see, for instance, Gordon 1993). The more the refractive index approaches that of water and the larger the particles are, the smaller n becomes. n is generally between 0.5 and 2.

Since the spectra $t_A(\lambda)$ and $t_C(\lambda)$ used in practice contain an unknown Mie component (see 2.1.3 and 2.1.4), the parameter n is not the correct Ångström exponent from the Mie calculations, but a value which parametrizes in $t_A(\lambda)$ and $t_C(\lambda)$ the aerosol scattering relative to the Mie component. n is therefore termed below the *relative* Ångström exponent. The correct Ångström exponent cannot be determined with the present model.

Assuming that at different points (θ,Φ) of the sky only the relative proportions c_i of the four sources change but not their spectral dependency, (2.2) can be inserted into (2.1) and all λ-dependent functions can be moved in front of the integral. From this follows the following equation:

$$E_d(\lambda) = \alpha\, E_{sun}(\lambda) + \beta\, E_{sky}(\lambda) + \gamma\, E_{Mie}(\lambda,n) + \delta\, E_{cloud}(\lambda). \qquad (2.3)$$

The four sources $E_x(\lambda)$ are referred to in the following text by the designations below:

$E_{sun}(\lambda)$	$= E_0(\lambda) \cdot t_A(\lambda)$	=	direct solar radiation
$E_{sky}(\lambda)$	$= E_0(\lambda) \cdot (\lambda/\lambda_0)^{-4}$	=	blue sky
$E_{Mie}(\lambda,n)$	$= E_0(\lambda) \cdot (\lambda/\lambda_1)^{-n}$	=	Mie scattering, aerosol scattering
$E_{cloud}(\lambda)$	$= E_0(\lambda) \cdot t_C(\lambda)$	=	clouds

λ_0 and λ_1 are reference wavelengths which are specified in the normalization of the sources (Section 2.1.5). The relative proportions α, β, γ and δ of the 4 sources $E_x(\lambda)$ vary from measurement to measurement and are obtained

from the parameters $c_i(\theta,\Phi)$ of Equation (2.2) by integration over the upper hemisphere.

The spectrum $E_0(\lambda)$ is known from the literature (Neckel and Labs 1981); the spectra $t_A(\lambda)$ and $t_C(\lambda)$ are derived from measurements in Sections 2.1.3 and 2.1.4 below. As is shown in Section 2.1.6, the resolution of a measured spectrum by Equation (2.3) functions very well in practice, even if n is set at 0: the error is at most 0.24%, and on average is even as low as 0.11%.

2.1.2 Measurement of incident radiation

The downwelling irradiance $E_d(\lambda)$ can in principle be measured by two methods: with a cosine detector or with a Lambert reflector.

A cosine detector integrates the radiance $L_d(\lambda,\theta,\Phi)$ in accordance with Equation (2.1), that is it measures the irradiance directly, in which case it weights the component from the direction (θ,Φ) with the cosine of the zenith angle θ. With a reflector, $E_d(\lambda)$ is measured indirectly: the radiation scattered by the reflector is detected. If the reflector reflects the incident radiation diffusely without any direction being preferred, it is termed a Lambert reflector. A sensor which is directed at a Lambert reflector records a radiance $L_d(\lambda) = E_d(\lambda)/\pi$.

Since no cosine detector was available, the radiance reflected by a white Teflon plate was measured. Teflon plate is not an ideal Lambert reflector. However, a weather-resistant reflector was required since measurements were made in all weathers, so that the usual white standards (compressed barium sulphate, magnesium oxide or titanium dioxide) could not be considered.

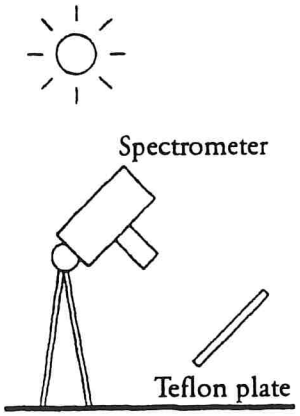

In order to maintain a diffuse reflection over the largest possible angular range, the surface of the Teflon plate was roughened with sandpaper. As a result, specular reflections only occur at angles above about 45°. To avoid these specular reflections, care was taken during measurement to ensure that the angle between the sun and the line normal to the plate was small. As is shown in the adjacent diagram, the head of the tripod on which the spectrometer was mounted was tilted in such a way that the spectrometer faced as diametrically as possible to the sun. The Teflon plate was held perpendicularly to the optical axis of the spectrometer.

Even if an ideal Lambert reflector had been available, it would not have been possible to correctly determine the spectrum $E_d(\lambda)$ relevant for calculation of reflectance for the following reasons:

1. To calculate the reflectance, knowledge of the irradiance *below water* is necessary. It cannot be derived from the measurement of $E_d(\lambda)$ above water since the downwelling radiance from the zenith angle θ is weighted with $\cos\theta$ by a sensor above water in accordance with Equation (2.1), but below water is weighted with $\cos\theta'$, the angle θ' being related to the angle θ by Snell's law, $\sin\theta = n \sin\theta'$ (n = refractive index of water). Since $\theta' < \theta$, the

weighting factors below water are greater than above water. As θ increases, the difference in the weighting increases. For example, for radiation in the vicinity of the horizon ($\theta = 90°$, $\theta' = 48.6°$ = critical angle for total reflection), the weighting above water is $\cos\theta = 0$, but below water is $\cos\theta' = 0.66$. In addition to the increased proportion of radiation from large zenith angles, a detector below water measures radiation in the angle range $48.6° < \theta' < 90°$ which cannot leave the water body (scattered light from the water).*

2. Depending on the cloud cover, a water radiance measurement takes between 5 and 40 seconds. The water surface in the angle of view of the spectrometer moves during this time and thus the irradiance for the water column beneath this surface also changes. Correct averaging in the subsequent measurement of irradiance is not possible.

3. While the water radiance is being measured, or in the time up to measurement of E_d, the irradiation can change if clouds are moving across the sky.

Since correct measurement of the downwelling irradiance is not possible with the spectrometer used, both in principle and for instrumental reasons, a correction method has been developed by which the reflectance can still be approximately correctly determined. It is described in Section 2.3.5.

2.1.3 Determination of the spectrum of direct solar radiation

The direct solar radiation spectrum is made up of the solar constant $E_0(\lambda)$ and the transmission spectrum $t_A(\lambda)$.

---

* The problems mentioned here will be discussed in detail in Section 2.3.1.

The solar constant is depicted in Figure 2.1. It was taken from the article by Neckel and Labs (1981), where it is tabulated for a spectral resolution of 2 nm. This is also about the resolution of the spectrometer used to record the spectra for this work.*

It can be seen from Equation (2.3) that when $\delta = 0$, the only unknown spectral function is $t_A(\lambda)$, so that $t_A(\lambda)$ may be determined in principle by comparison of two measurements if they differ significantly in the components α, β and γ. These parameters and n are unknown and must be determined by comparison, whereas λ_0 and λ_1 are arbitrary. Up to the point where values of λ_0 and λ_1 are specified in the normalization of the 4 sources in Section 2.1.5, they are set equal to 1 nm and are omitted in the equations.

$\delta = 0$ represents an atmosphere without water vapour and without clouds. This is never the case, but when measurements made on cloudless days are examined, the day having minimum water content may be identified, as will be explained later. If the spectrum $t_A(\lambda)$ is determined for this day, it completely satisfies the aim of separating the *variable* spectra. Therefore δ is set to zero for the day having minimum atmospheric water content.

---

* Spectrometer details are given in Section 5.1.1

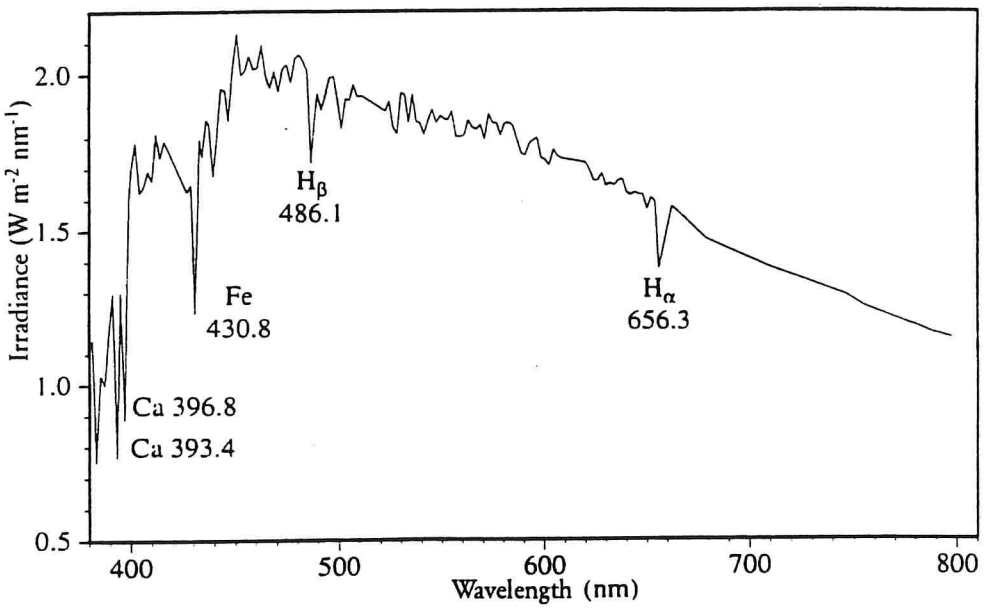

Figure 2.1: Solar constant $E_0(\lambda)$. From Neckel and Labs (1981). Spectral resolution: 2 nm. Absorption lines assigned as in Bergmann and Schäfer (1981).

For a measurement E_1 made on a day where $\delta = 0$, from (2.3), the desired function

$$t_A(\lambda) = \frac{E_1(\lambda) - \beta_1 E_0(\lambda) \lambda^{-4} - \gamma_1 E_0(\lambda) \lambda^{-n}}{\alpha_1 E_0(\lambda)} \qquad (2.4)$$

may be calculated if the factors α_1, β_1 and γ_1 and the relative Ångström coefficient n are known. In order to determine these factors, the measurement must be compared with a second measurement E_2. If $t_A(\lambda)$ is identical for both measurements, it follows that

$$\frac{E_1(\lambda) - \beta_1 E_0(\lambda) \lambda^{-4} - \gamma_1 E_0(\lambda) \lambda^{-n}}{\alpha_1 E_0(\lambda)} = \frac{E_2(\lambda) - \beta_2 E_0(\lambda) \lambda^{-4} - \gamma_2 E_0(\lambda) \lambda^{-n}}{\alpha_2 E_0(\lambda)}$$

and thus after rearranging,

$$E_0(\lambda) \lambda^{-4} = \frac{\alpha_2 E_1(\lambda) - \alpha_1 E_2(\lambda) + (\alpha_1\gamma_2 - \alpha_2\gamma_1) E_0(\lambda) \lambda^{-n}}{\alpha_2\beta_1 - \alpha_1\beta_2} .$$

On the left side there is a known function, on the right side, the functions $E_1(\lambda)$, $E_2(\lambda)$, $E_0(\lambda)$ are known and the parameters α_1, β_1, γ_1, α_2, β_2, γ_2 and n are wanted. Although the right side can be matched to the left side by variation of these parameters in an inversion method, the result does not have a single value because the 6 factors only correspond to 3 established functions. Only 3 factors x, y and z can be unambiguously determined as follows:

$$E_0(\lambda)\,\lambda^{-4} = x\,E_1(\lambda) - y\,E_2(\lambda) + z\,E_0(\lambda)\,\lambda^{-n} \equiv f_1(\lambda). \qquad (2.5)$$

If x, y and z are known, the ratio α_1/α_2 can then be stated, which, as can be seen, is

$$\frac{y}{x} = \frac{\alpha_1}{\alpha_2}.$$

This ratio is useful, since when it is known, there exists a fitting function $f_2(\lambda)$ which links 4 free parameters to 4 known functions so that the 4 parameters can be unambiguously determined. This fitting function follows directly from (2.4):

$$\frac{\alpha_1}{\alpha_2} = \frac{\alpha_1\,t_A\,E_0}{\alpha_2\,t_A\,E_0} = \frac{E_1(\lambda) - \beta_1\,E_0(\lambda)\,\lambda^{-4} - \gamma_1\,E_0(\lambda)\,\lambda^{-n}}{E_2(\lambda) - \beta_2\,E_0(\lambda)\,\lambda^{-4} - \gamma_2\,E_0(\lambda)\,\lambda^{-n}} \equiv f_2(\lambda). \qquad (2.6)$$

If the free parameters β_1, γ_1, β_2, γ_2 and n are determined with the aid of this equation, the spectrum $t_A(\lambda)$ may be calculated from Equation (2.4) except for a multiplying factor α_1.

The method described for calculating the spectrum $t_A(\lambda)$ has been realized as a Pascal program with the name SKY. This first carries out a fitting operation on the function $f_1(\lambda)$ according to Equation (2.5), the sum

$$\sum_i \left(E_0(\lambda_i)\, \lambda_i^{-4} - f_1(\lambda_i) \right)^2$$

being minimized by a least square fit (λ_i = spectral channel number i). Because the sum of the three spectra $E_1(\lambda)$, $E_2(\lambda)$ and $E_0(\lambda)\lambda^{-n}$ must result in a strong wavelength dependency of λ^{-4} which cannot be observed in the individual spectra, even a small error in $f_1(\lambda)$ leads to a significant deviation from the theoretical curve. Since the fitting reacts so sensitively to deviations, the accuracy of E_1, E_2 and E_0 determines the accuracy of the fit; the fitting parameters x, y and z are therefore highly precise. Just the ratio $y/x = \alpha_1/\alpha_2$ is used further.

In a second step, the program fits the function $f_2(\lambda)$ to the ratio α_1/α_2 and determines the parameters β_1, γ_1, β_2, γ_2 and n. This fitting is performed in both steps by the Simplex algorithm which is explained in Appendix B.

In the last step, the desired function $t_A(\lambda)$ is calculated in accordance with Equation (2.4). Since the parameter α_1 is not determined $t_A(\lambda)$ is specified except for a multiplying factor. This is determined by calibration of the function $E_0(\lambda) \cdot t_A(\lambda)$ as explained in Section 2.1.5.

The process described which ultimately leads to the spectrum $t_A(\lambda)$ is illustrated in Figures 2.2 to 2.5.

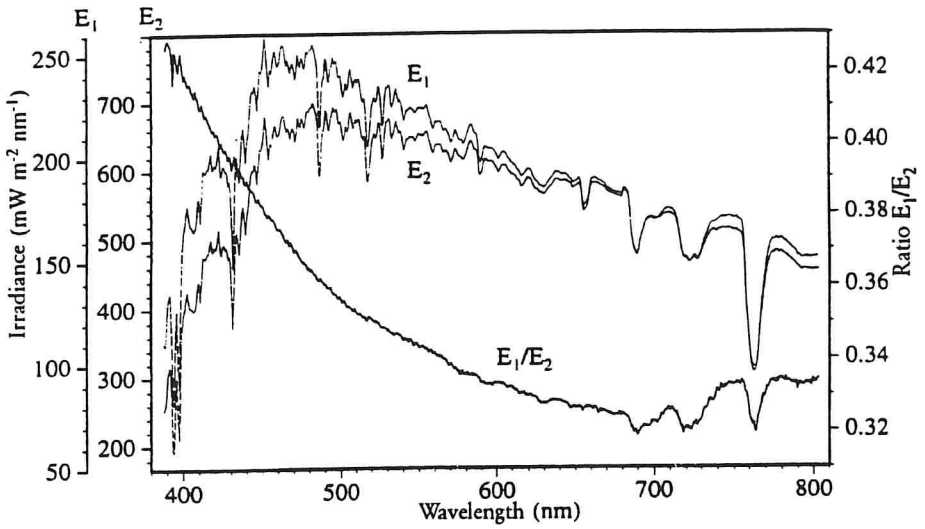

Figure 2.2: Comparison of two measurements E_1 and E_2 of the downwelling irradiance.

Figure 2.2 shows two irradiance measurements E_1 and E_2 made on 23.4.91 and the ratio E_1/E_2. It can be seen from the ratio that the two measurements differ spectrally, that is the relative proportions of α, β and γ are different. This is a precondition for deriving the spectrum $t_A(\lambda)$.

Figure 2.3 shows the result of the fit according to Equation (2.5). The thick curve is the blue sky spectrum $E_0(\lambda)\lambda^{-4}$, the thin curve is the function $f_1(\lambda)$ where $x = 28.05$, $y = 66.17$, $z = 0.8491$, $n = 0$. Since the ratio $y/x = \alpha_1/\alpha_2$ is the only information which will be used further from the fit shown in Figure 2.3, the deviation of the fitted curve from the theoretical curve, restricted to some narrow spectral regions, does not lead to any significant error in the function $t_A(\lambda)$.

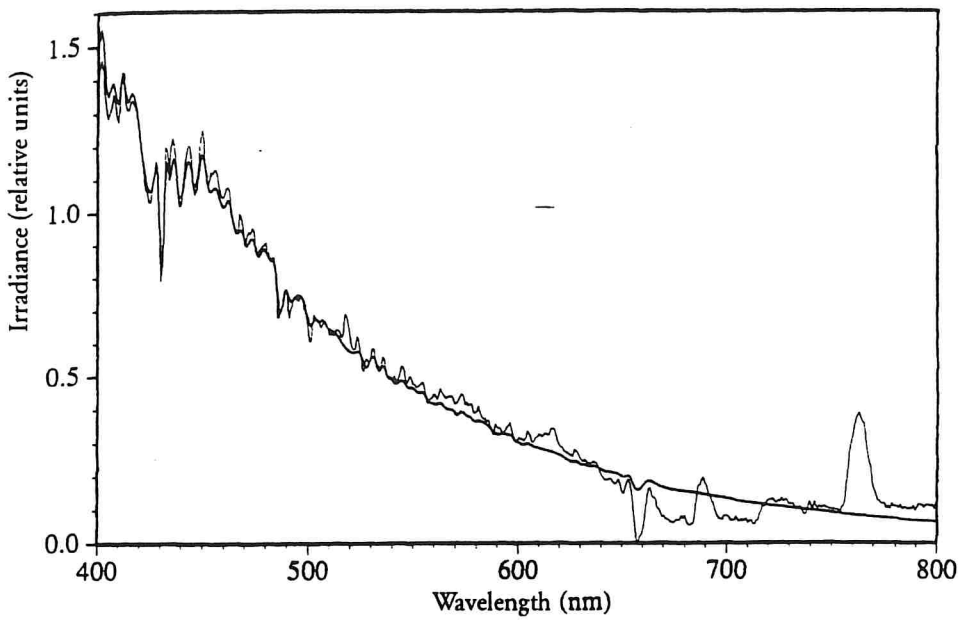

Figure 2.3: Fitting the two measurements of Figure 2.2 to the blue sky spectrum by Equation (2.5).

The fit shown in Figure 2.3 corresponds to a ratio $\alpha_1/\alpha_2 = 2.359$. The function $f_2(\lambda)$ is fitted to this ratio by Equation (2.6) and the result is shown in Figure 2.4. The fitting seems to be very successful.

The result of the comparison of the two measurements E_1 and E_2 of Figure 2.2 leads to the spectrum $t_A(\lambda)$ of Figure 2.5. Since α_1 is unknown, the scaling factor of the y axis is first arbitrary. A suitable normalization method is described in Section 2.1.5; this has already been carried out in Figure 2.5.

Figure 2.5, moreover, depicts a calculated atmospheric transmission spectrum. Calculation was carried out by the program LOWTRAN 7 (Kneizys et al. 1988) for a standard atmosphere (US Standard).

As the comparison shows, $t_A(\lambda)$ correctly represents the atmospheric transmission qualitatively: the position and shape of the oxygen and water absorption bands are in agreement and the order of magnitude of the transmission

is correct. However, structures can be recognized in $t_A(\lambda)$ which can be unambiguously assigned to the solar spectrum, the most conspicuous of these being the Fe line at 430.8 nm and the H_α line at 656.3 nm.

The reason for the solar spectral characteristics appearing in the spectrum $t_A(\lambda)$ is the different spectral resolution of solar constant and spectrometer. Because $E_0(\lambda)$ has many absorption lines especially in the blue and green, the amplitude $E_0(\lambda_i)$ in channel λ_i is highly sensitive to the position and width of the channel. This is the reason for the "noise" of $t_A(\lambda)$ in the range 400 - 600 nm.

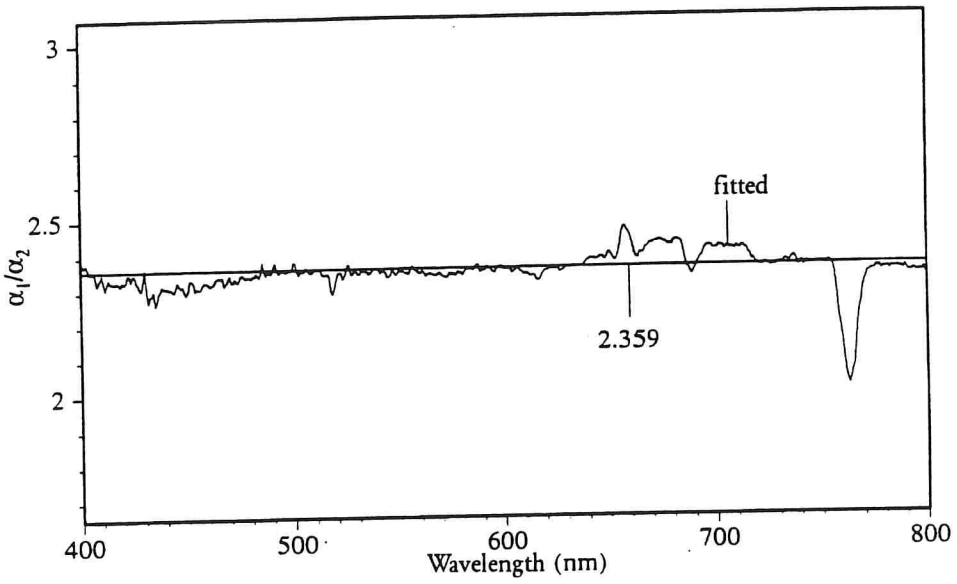

Figure 2.4: The fitted function $f_2(\lambda)$ for the measurements of Figure 2.2.

The transmission curve calculated by LOWTRAN 7 is less dependent on λ than $t_A(\lambda)$ over the entire spectral range. The reason is that the Mie scattering cannot be completely separated from the transmission by the algorithm described.

This is because the statement $\delta = 0$ which is necessary to eliminate $t_C(\lambda)$ from the equations does not correctly

represent reality. The fact that the atmosphere was not actually water-free on 23.4.91 can be recognized from the presence of the water absorption band at 715 - 730 nm. Since $t_C(\lambda)$ is the sum of a transmission and a scattering term of the water droplets, ignoring $t_C(\lambda)$ leads to errors in the remaining spectra in (2.3). The Rayleigh scattering is not affected, but the direct solar radiation spectra and the Mie scattering spectra are affected. They cannot be properly separated: the Mie scattering component of the water vapour which has not been taken into consideration is superimposed on the direct solar radiation spectrum. The wavelength dependency of the aerosol scattering can therefore only be established relative to this Mie component: the value n in the equations is not the correct Ångström exponent. As will be shown in Section 2.1.6, in practice, n can be set at 0.

In order to separate the variable components in the solar spectrum by Equation (2.3), it is unimportant that $t_A(\lambda)$ is not the correct transmission spectrum and n is not the correct Ångström exponent. The resolution (2.3) fulfils the purpose for which it is used in practice, that is enhancing reflectance spectra, without limiting accuracy.

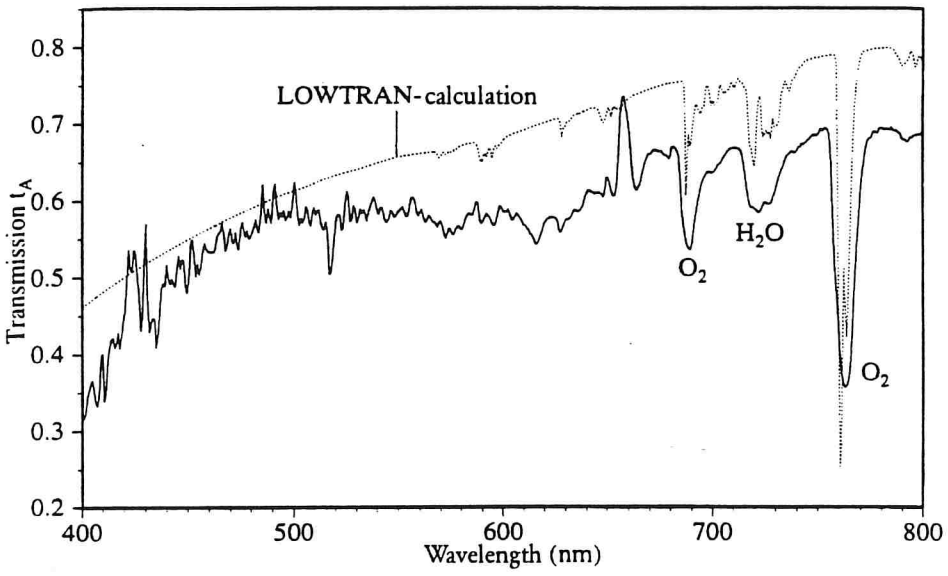

Figure 2.5: Atmospheric transmission spectrum $t_A(\lambda)$,

derived from the two measurements of Figure 2.2. The LOWTRAN spectrum is based on the atmosphere type "1976 US Standard", aerosol type "rural".

Several transmission spectra were calculated in each case in the manner described for days without cloud cover or with low cloud cover and clear air (57 spectra in total). Since the transmission in the region 715 - 730 nm depends considerably on the concentration of water in the atmosphere, the strength of this absorption band (relative to the absorption just outside this band) was used as a criterion of water vapour concentration. The band was least marked on 23.4.91, therefore the spectrum $t_A(\lambda)$ utilized in the further evaluation was derived from a measurement made on this day.

2.1.4 Determination of the cloud spectrum

The program CLOUD was written to determine the cloud spectrum $t_C(\lambda)$. It proceeds very similarly to the determination of $t_A(\lambda)$: for $\delta_1 > 0$, it can be calculated from a measurement $E_1(\lambda)$ via the relationship

$$t_C(\lambda) = \frac{E_1(\lambda) - \alpha_1 E_0(\lambda) t_A(\lambda) - \beta_1 E_0(\lambda) \lambda^{-4} - \gamma_1 E_0(\lambda) \lambda^{-n}}{\delta_1 E_0(\lambda)} \qquad (2.7)$$

if the factors α_1, β_1 and γ_1 and the relative Ångström coefficient n are known. These parameters may be determined as previously by comparing $E_1(\lambda)$ with a second measurement $E_2(\lambda)$ which has a different cloud component δ_2. The 7 parameters α_1, β_1, γ_1, α_2, β_2, γ_2 and **n** are determined in a very similar manner to (2.6) by fitting the function $f_3(\lambda)$ to the ratio δ_1/δ_2:

$$\frac{\delta_1}{\delta_2} = \frac{E_1(\lambda) - \alpha_1 E_0(\lambda) t_A(\lambda) - \beta_1 E_0(\lambda) \lambda^{-4} - \gamma_1 E_0(\lambda) \lambda^{-n}}{E_2(\lambda) - \alpha_2 E_0(\lambda) t_A(\lambda) - \beta_2 E_0(\lambda) \lambda^{-4} - \gamma_2 E_0(\lambda) \lambda^{-n}} \equiv f_3(\lambda). \qquad (2.8)$$

The two-stage process of Section 2.1.3, in which the ratio δ_1/δ_2 is first determined, has not proved to be expedient here. The reason is that the ratio δ_1/δ_2 cannot be established with sufficient accuracy because the equation corresponding to (2.5) in this case, with 4 free parameters for 4 given curves, has too great an error tolerance. Instead of this, δ_1/δ_2 is fitted as an eighth fitting parameter in (2.8).

Whereas the spectra used in the determination of $t_A(\lambda)$ are those where the water content of the atmosphere is at a minimum, the spectra used in the determination of $t_C(\lambda)$ are just those where this content is at a maximum. As before, the water content is estimated by means of the absorption band at 715-730 nm.

In total, 52 spectra $t_C(\lambda)$ were calculated. Figure 2.6 shows the spectrum for which the atmospheric water content is at a maximum. Normalization of the y-axis is described in Section 2.1.5.

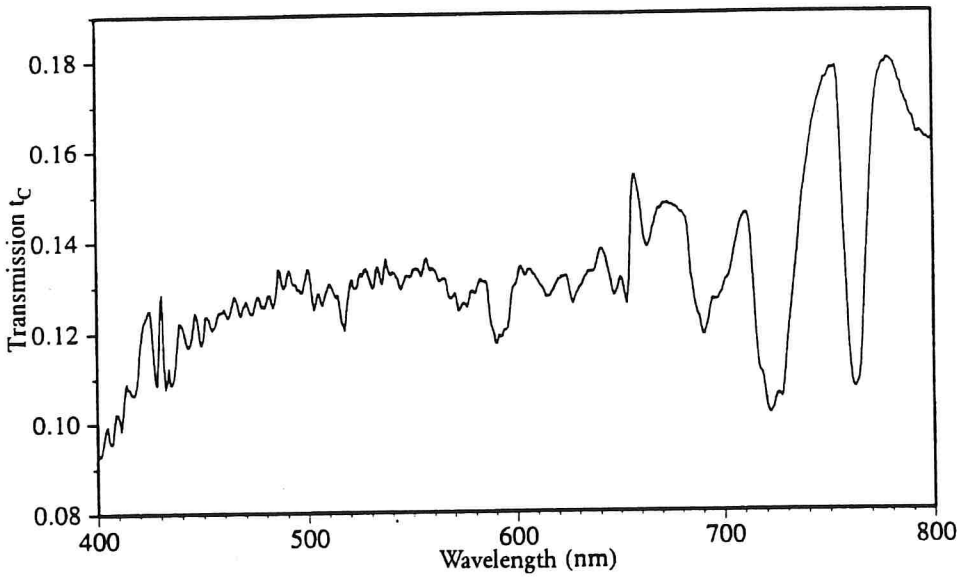

Figure 2.6: Cloud spectrums $t_C(\lambda)$.

2.1.5 Normalization of the base spectra

In order that the parameters α, β, γ and δ represent the proportions of the sources E_{sun}, E_{sky}, E_{Mie} and E_{cloud} of the irradiance E_d in the resolution (2.3), normalization of the sources is necessary, that is the integral over the wavelength must be the same for all sources:

$$I_0 = \int_{\lambda_{min}}^{\lambda_{max}} E_x(\lambda)\, d\lambda. \qquad (2.9)$$

The reference value I_0 is arbitrary. Here, the value for the solar constant ($E_x(\lambda) = E_0(\lambda)$) is used:

$$I_0 = 674.7\ W\ m^{-2},$$

with the limits λ_{min} = 387.86 nm and λ_{max} = 803.46 nm, the range of values over which measurements were made. If λ_{min} was set to 0 and λ_{max} was set to ∞, this would yield the known value of 1372 W m^{-2}.

Since $E_x(\lambda)$ is the product of $E_0(\lambda)$ with a function $g(\lambda)$, normalization (2.9) represents a rescaling of $g(\lambda)$. The spectra $t_A(\lambda)$ and $t_C(\lambda)$ were calculated in Sections 2.1.3 and 2.1.4 except for a multiplying factor α_1 and δ_1 respectively. These factors are established in the normalization on the basis of Equation (2.9).

The normalization factor of the Rayleigh scattering (blue sky) is λ_0. From (2.9), λ_0 = 528.16 nm. The scaling factor of the Mie scattering, λ_1, is a function of n: for n = 1, λ_1 = 559.46 nm; for n = 0.1, λ_1 = 576.58 nm; for n = 0, no scaling is required.

The 4 normalized base spectra $E_{sun}(\lambda)$, $E_{sky}(\lambda)$, $E_{Mie}(\lambda)$ and $E_{cloud}(\lambda)$ are depicted in Figure 2.7.

An index which is suitable for characterizing the "brightness" of a measurement $E_d(\lambda)$ is the ratio of the integrated irradiance

$$I_d = \int_{\lambda_{min}}^{\lambda_{max}} E_d(\lambda)\, d\lambda$$

to the integrated solar constant:

$$\Lambda = \frac{I_d}{I_0} .$$

Because of the normalization (2.9), it follows from (2.3) that:

$$\Lambda = \alpha + \beta + \gamma + \delta .$$

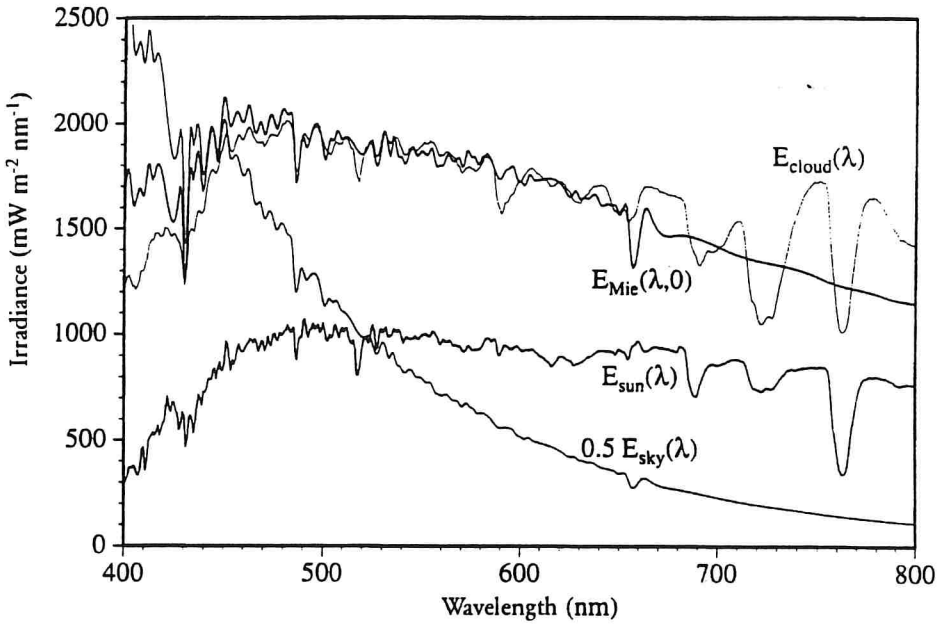

Figure 2.7: The 4 base spectra of the model.

Since Λ is known, in the fitting, only three of the factors α, β, γ and δ are independent of each other. The factors α, β, γ and δ can be compared with each other more readily if they are related to the total Λ. The primed values

$$\alpha' = \frac{\alpha}{\Lambda},\ \beta' = \frac{\beta}{\Lambda},\ \gamma' = \frac{\gamma}{\Lambda},\ \delta' = \frac{\delta}{\Lambda}$$

then give the relative proportions of the individual radiation sources of a measurement, since $\alpha' + \beta' + \gamma' + \delta' = 1$.

2.1.6 Resolution of incident radiation into 4 components

Since the spectra $t_A(\lambda)$ and $t_C(\lambda)$ are now known, a measured spectrum $E_d(\lambda)$ may be resolved according to Equation (2.3) into its 4 constituents $E_{sun}(\lambda)$, $E_{sky}(\lambda)$, $E_{Mie}(\lambda)$ and $E_{cloud}(\lambda)$. This is carried out by the program WEISS. It fits the fitting function $f_4(\lambda)$ to $E_d(\lambda)$ by variation of the five parameters α, β, γ, δ and n:

$$E_d(\lambda) = \alpha\, E_{sun}(\lambda) + \beta\, E_{sky}(\lambda) + \gamma\, E_{Mie}(\lambda,n) + \delta\, E_{cloud}(\lambda) \equiv f_4(\lambda). \qquad (2.10)$$

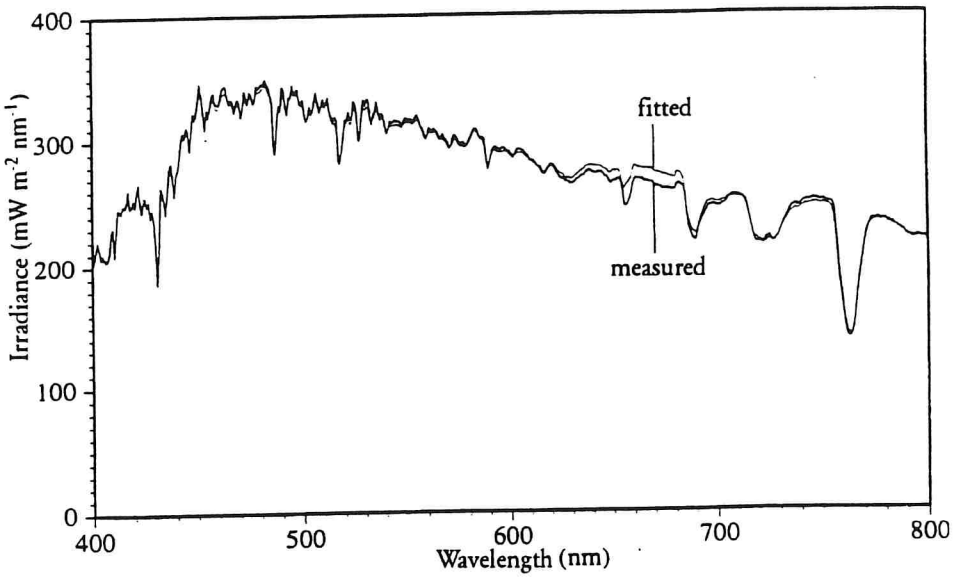

Figure 2.8: Example of modelling of incident radiation $E_d(\lambda)$.

The result of the resolution of $E_d(\lambda)$ is the 4 factors α, β, γ and δ and the relative Ångström exponent n. The error in the resolution is the difference

$$E_R(\lambda) = E_d(\lambda) - f_4(\lambda), \tag{2.11}$$

the relative mean square deviation

$$\Delta_R = \frac{1}{K}\sqrt{\sum_{i=1}^{K}\left(\frac{E_R(\lambda_i)}{E_d(\lambda_i)}\right)^2} \tag{2.12}$$

is designated the mean error (λ_i = channel number i, K = number of channels).

Figure 2.8 shows that the resolution functions well in practice. The thick curve is the measured spectrum $E_d(\lambda)$ and the thin curve is the fitted $f_4(\lambda)$. The fitting parameters are α' = 0.7177, β' = 0.0415, γ' = 0.09987, δ' = 0.1420, = 0.1654, n = 0 and the mean error is Δ_R = 0.108%. This was not an extraordinarily good result

which was selected, but an average one.

In order to investigate what influence the relative Ångström exponent n has on the quality of the fit, fitting was carried out twice for 33 measurements of irradiance: the first time the program fitted the parameter n, the second time n was fixed at 0. The result is shown in Figure 2.9.

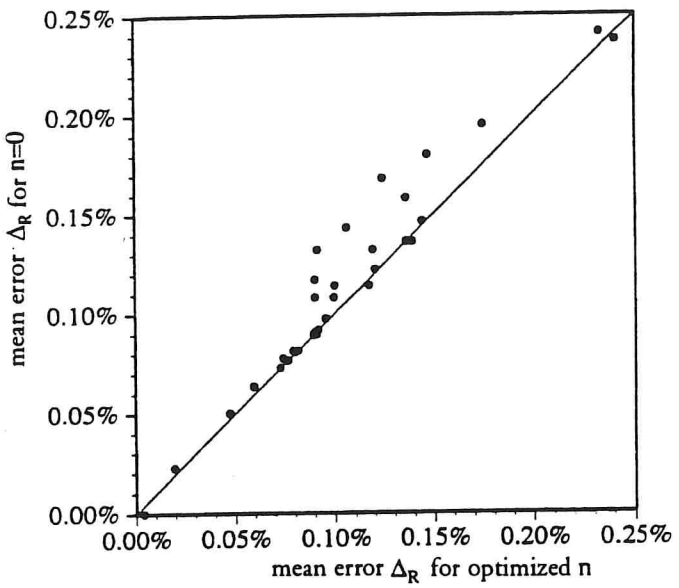

Figure 2.9: Influence of the relative Ångström exponent n on the quality of fit of the incident radiation.

The mean error Δ_R of the fit where n is optimized is plotted on the abscissa of Figure 2.9 and that for n = 0 on the ordinate. Although in some cases the fit is better if n is a fitted variable, there is generally no great difference: if Δ_R is averaged over all 33 fits, an error of 0.105% is obtained for variable n and 0.114% for n = 0. The relative Ångström coefficient n does not therefore need to be taken into account in the modelling of irradiance.

Figure 2.9 also makes clear that the error in the modelling of the irradiance is very small: the greatest observed error was 0.241%, and the mean error was 0.114% (at n = 0).

To a good approximation, therefore, the irradiance may be represented by a sum of only 4 base spectra. This conclusion is also drawn in the article by Condit and Grum (1964) in which 191 so-called daylight spectra and 60 so-called skylight spectra were analysed to develop filters for colour photography. For this purpose, light reflected by a white barium sulphate plate was measured with a resolution of 5 nm in dependence on the position of the sun, the cloud cover and the orientation of the plate relative to the sun. The spectra were divided into two groups: *skylight* spectra, where no direct sunlight could reach the plate for geometric reasons (shadows), and *daylight* spectra (all others). An eigenvector analysis was carried out for each group (Simonds (1963). In each case 4 eigenvectors were sufficient to account for the spectral differences: in the case of the daylight spectra they accounted for 98.2% of the variability and in case of the skylight spectra they accounted for 99.4% (sum of the first 4 eigenvalues of the covariance matrix, normalized by the trace).

To what extent the model introduced here is generally valid is difficult to estimate, however. Although the measurements of Condit and Grum confirm the statement that the irradiance may be represented by 4 base spectra, their measurements as well as those used here were always carried out at the same site. However, Middleton (1954) showed that the intensity and spectral distribution of the irradiance, in the case of an overcast sky, depend considerably on the albedo of the earth's surface. It is therefore probable that at least over land surfaces the base spectra of the model introduced must be modified in order to model the irradiance when the sky is overcast.

2.2 Measurement of radiation reflected from water

All the spectral measurements on Lake Constance were made from the research ship "Robert Lauterborn" of Constance

University. The spectrometer was mounted on a tripod and attached to the railing, as shown in the diagram.

When the upwelling radiance of the water is being measured, in order to minimize the proportion of surface reflections, it is necessary to aim at an angle of 90° between the optical axis of the spectrometer and the water surface. However, since the distance from the water surface is only about 2 meters, at an angle of 90°, the field of view of the spectrometer would completely include its own mirror image. The actual angle was therefore less than 90° and was determined by the best possible compromise between avoiding shadows and minimizing solar reflections:

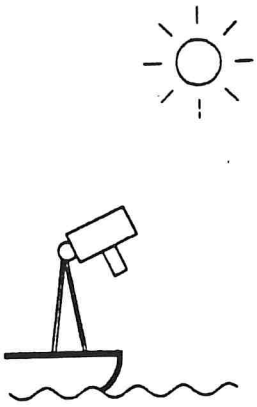

• When the water surface is rough, the spectrometer unavoidably includes direct solar reflections. The amount of this "sun glint" depends on the position of the sun, on the roughness of the water surface and on the angle of view relative to the sun. It is small when the sun is at the rear, that is when the spectrometer is mounted on the side of the ship facing away from the sun. However, measurements in the ship's shadow are unusable as the angular distribution and intensity of the solar irradiation cannot be determined in the shadow so that correct calculation of the reflectance is not possible. If the spectrometer is mounted on the side of the ship facing the sun the shadow is avoided but sun glint is obtained in exchange.

• If solar reflections were observable on the side of the ship facing the sun, measurements were made on the side facing away from the sun, the spectrometer being inclined to the vertical sufficiently to avoid under any circumstances measurement in the shadow. The angle to the water surface was therefore in the range 70-85°.

The angle of inclination of the spectrometer to the water surface additionally depends on the inclination of the ship: depending on the waves, the ship sometimes pitches and tosses very violently; the change in angle can be up to 25°.

For the reasons described, measurement from the ship does not give the correct radiance of the water, but light reflected at the surface is additionally detected. This component can vary from measurement to measurement. It is critically dependent on cloud cover and wave conditions.

To calculate the reflectance, for each radiance measurement of the water a corresponding measurement of the downwelling irradiance would have to be carried out. However, this cannot be determined correctly as has been explained in Section 2.1.2.

Since both measurement of the radiance of the water and measurement of the downwelling irradiance are subject to error, the reflectance spectra contain errors. Particularly on days with a cloudy sky, it is frequently the case that not a single reflectance spectrum can be derived from the measurements in which at least the apparent errors are small. A method is introduced in the following section by which the errors may be satisfactorily corrected.

2.3 Calculation of reflectance

2.3.1 Dependence of radiation measurements on the field of view of the sensor

Downwelling radiation. In the case of a sensor which has a small field of view, the measurement of radiation is the radiance L, see Section 2.1.1. From this, the irradiance E can be calculated by Equation (2.1) if the spatial radiation distribution $L(\theta,\Phi)$ is known. If a reflector is used which uniformly reflects radiation from all zenith angles θ and azimuth angles Φ without giving any preference to any one direction (Lambert reflector), the product of π and the radiance measured at the reflector gives the irradiance. If the reflector is arranged parallel to the water surface, the following therefore applies*

$$E_d^+(\lambda) = \pi\, L_d^+(\lambda). \qquad (2.13)$$

A planar detector having a field of view of 2π measures $E_d^+(\lambda)$ directly by integrating the radiance from the upper hemisphere according to Equation (2.1) (*cosine detector*). The direction of the light beam is indicated by the subscripts "u" and "d" (u: upwelling, d: downwelling) and the measurement site is indicated by the superscripts "+" and "-" (+: above water, -: below water).

Below water, the downwelling radiance in the nadir direction is

$$L_d^-(\lambda) = (1-\sigma^+)n^2\, L_d^+(\lambda) + \sigma^-\, L_u^-(\lambda). \qquad (2.14)$$

The first term is the downwelling radiance after passage

---

* As described in 2.1.2, a white Teflon plate was used as reflector for the Lake Constance measurements. It does not reflect the light uniformly, that is the determination of $E_d^+(\lambda)$ by Equation (2.13) is subject to error.

through the water surface, the second term is upwelling radiance which is reflected at the water surface. Since, by refraction at the water surface, a light beam having a solid angle $d\Omega$ is focused below water into a narrower cone having a solid angle $d\Omega/n^2$, more light falls into a sensor having a small but unchangeable aperture angle. In addition to this gain (factor n^2), the loss by reflection at the surface (factor $1-\sigma^+$) is virtually negligible. The refractive index n and *Fresnel reflection* σ are almost wavelength-independent in the visible range (the changes are 4% and 6% respectively: Jerlov 1976, pages 22 and 80).

The downwelling irradiance E_d^- is obtained from L_d^- by integration over the upper hemisphere:

$$E_d^-(\lambda) = \int_{\phi=0}^{2\pi} \int_{\theta=0}^{\pi/2} \left[(1-\sigma^+(\theta'))\ n^2\ L_d^+(\lambda,\theta',\phi) + \sigma^-(\theta)\ L_u^-(\lambda,\theta,\phi)\right] \cos\theta \sin\theta\ d\theta\ d\phi.$$

In this equation, θ' is the zenith angle in air, θ is the zenith angle in water. Because $n \sin\theta = \sin\theta'$, $n^2 \cos\theta \sin\theta\ d\theta = \cos\theta' \sin\theta'\ d\theta'$, and it follows that:

$$E_d^-(\lambda) = \int_{\phi=0}^{2\pi} \int_{\theta=0}^{\pi/2} \left[(1-\sigma^+(\theta))\ L_d^+(\lambda,\theta,\phi) + \sigma^-(\theta)\ L_u^-(\lambda,\theta,\phi)\right] \cos\theta \sin\theta\ d\theta\ d\phi. \quad (2.15)$$

This value is measured with a cosine detector below water. In order to determine E_d^- correctly from radiance measurements, L_d^+ and L_u^- would have to be measured for all solid angles and the dependence of σ^+ and σ^- on the zenith angle θ would have to be taken into account. The former is too complex for routine measurements and even the latter is imprecise: although $\sigma(\theta)$ may be calculated in principle from Fresnel's equations (for instance see Jerlov 1976, page 73), because σ is dependent on polarization, the polarization of the radiation would have to be taken into account for all spatial directions. This can be calculated at most for idealized conditions

(sun and clear sky or uniform cloud cover) which rarely occur in practice.

The dependency of σ on the zenith angle denotes that the proportion of the light reflected at the surface depends on the angle of incidence. According to the model (2.3), the spectral course of the incident light may be approximated by a sum of 4 radiation sources E_x. In accordance with the mean angle of incidence θ_x of each of these sources, for each source, its own reflection factor $\sigma_x = \sigma(\theta_x)$ can be given. The equation for the reflected radiation E_r is then:

$$E_r^+(\lambda) = \sigma_{sun}\,\alpha E_{sun}(\lambda) + \sigma_{sky}\,\beta E_{sky}(\lambda) + \sigma_{Mie}\,\gamma E_{Mie}(\lambda) + \sigma_{cloud}\,\delta E_{cloud}(\lambda). \qquad (2.16)$$

In Equation (2.15), the term $\sigma^+(\theta)\ L_d^+(\lambda,\theta,\phi)$ represents the radiance $L_r^+(\lambda,\theta,\phi)$ reflected at the surface. The integration of this value over the upper hemisphere yields the irradiance of Equation (2.16). If the relationship

$$E_r^+(\lambda) \equiv \sigma^+(\lambda)\ E_d(\lambda), \qquad (2.17)$$

is formulated, that is if the spectrum $E_d(\lambda)$ is used for the reflected radiation, the angle dependency of σ^+ becomes a wavelength dependency; this applies similarly to σ^-. It then follows from Equation (2.15):

$$E_d^-(\lambda) = [1-\sigma^+(\lambda)]\ E_d^+(\lambda) + \sigma^-(\lambda)\ E_u^-(\lambda). \qquad (2.18)$$

The function $\sigma^+(\lambda)$ is discussed in more detail in Section 2.3.4. The reflection factor $\sigma^-(\lambda)$ for the upwelling radiation is in the order of magnitude 0.52 to 0.56 (Jerome et al. 1990), that is its wavelength dependency is low.

Upwelling radiation. $E_u^-(\lambda)$ may be calculated from $L_u^-(\lambda,\theta,\phi)$ in a similar manner to Equation (2.1). L_u^- is generally measured perpendicularly to the water surface and the angle dependency is generally not determined. In order to calculate E_u^-, the statement $E_u^-(\lambda) = Q\ L_u^-(\lambda)$ is generally made, with the approximation that the proportionality factor Q is independent of wavelength. Q depends on the scattering behaviour of the water body. Measurements show that Q is generally between 4.4 and 5.4 (Tyler 1960, Smith 1974, Austin 1979, Clark 1981, Prieur 1976). According to Kirk (1983, page 117) Q = 5 is a good approximation for a solar elevation around 45°:

$$E_u^-(\lambda) \approx 5\ L_u^-(\lambda). \qquad (2.19)$$

When a light beam leaves the water, the beam angle increases by the factor n^2 and some of the beam is reflected back into the water. A sensor with a small field of view which is directed towards the water surface therefore receives

$$L_u^+(\lambda) = \frac{1-\sigma^-}{n^2}\ L_u^-(\lambda) + L_r^+(\lambda). \qquad (2.20)$$

By integrating this equation over all solid angles, $E_u^+(\lambda)$ is obtained. For the same reasons discussed under equation (2.15), $E_u^+(\lambda)$ can be estimated only inadequately from a single measurement of $L_u^+(\lambda)$ in the nadir direction. If the spectral change of the light reflected at the surface is compensated for again by wavelength-dependent reflection factors $\sigma^+(\lambda)$, $\sigma^-(\lambda)$, then the following applies:

$$E_u^+(\lambda) = [1-\sigma^-(\lambda)]\ E_u^-(\lambda) + \sigma^+(\lambda)\ E_d^+(\lambda). \qquad (2.21)$$

2.3.2 Definition of the terms reflectance and albedo

Reflectance is generally defined as the ratio of upwelling to downwelling irradiance beneath the water surface (see for instance Gordon et al. 1975, Jerlov

1976, Bukata et al. 1980, Siegel 1987):

$$R(\lambda) = \frac{E_u^-(\lambda)}{E_d^-(\lambda)}. \qquad (2.22)$$

Above water, only the parameter

$$\rho(\lambda) = \frac{E_u^+(\lambda)}{E_d^+(\lambda)} \qquad (2.23)$$

can be measured. It is termed *albedo* (Jerlov 1976, page 78).

2.3.3 Relationship between reflectance and albedo

The substances which are dissolved or suspended in water influence the *reflectance* of the water body; light reflected at the surface, moreover, determines the *albedo*. Since the reflectance is the decisive parameter for determining the concentrations of water constituents, but the albedo is measured by remote sensors, a relationship must be made between the two parameters. This is as follows:

$$\rho(\lambda) = \frac{[1-\sigma^-(\lambda)]\,[1-\sigma^+(\lambda)]}{1 - \sigma^-(\lambda)\,R(\lambda)}\,R(\lambda) + \sigma^+(\lambda). \qquad (2.24)$$

Proof: From Equation (2.21) it follows for the albedo:

$$\rho(\lambda) = \frac{E_u^-(\lambda)}{E_d^-(\lambda)} = (1-\sigma^-(\lambda))\,\frac{E_u^-(\lambda)}{E_d^-(\lambda)} + \sigma^-(\lambda).$$

Equation (2.22) provides the relationship with the reflectance: $\frac{E_u^-(\lambda)}{E_d^-(\lambda)} = R(\lambda)\,\frac{E_d^-(\lambda)}{E_d^-(\lambda)}$, and from equation (2.18) $\frac{E_d^-(\lambda)}{E_d^-(\lambda)} = 1-\sigma^-(\lambda) + \sigma^-(\lambda)\,\frac{E_u^-(\lambda)}{E_d^-(\lambda)}$. The albedo is thus

$$\rho(\lambda) = (1-\sigma^-(\lambda))\,R(\lambda)\left[(1-\sigma^-(\lambda)) + \sigma^-(\lambda)R(\lambda)\left[(1-\sigma^-(\lambda)) + \sigma^-(\lambda)R(\lambda)\left[(1-\sigma^-(\lambda)) + \ldots\right]\right]\right] + \sigma^-(\lambda) =$$

$$[1-\sigma^-(\lambda)]\,[1-\sigma^-(\lambda)]\,R(\lambda)\cdot\sum_{i=0}^{\infty}[\sigma^-(\lambda)\,R(\lambda)]^i + \sigma^-(\lambda) \quad \text{with} \quad \sum_{i=0}^{\infty} x^i = \frac{1}{1-x} \quad (2.24) \text{ follows.}$$

In practice, the exponential series development is restricted to the linear element (Equation 2.24a, page 46).

2.3.4 Specular surface reflections

A sensor which is located outside the water and is directed at the water surface, in accordance with Equations (2.20) and (2.21), apart from the radiation from the water body, also detects light which is reflected at the surface. This component $\sigma^+(\lambda)$ is termed here *specular surface reflection*. Depending on wavelength, $\sigma^+(\lambda)$ can achieve the order of magnitude of the reflectance or can be above this - in particular above 600 nm. The quality of the correction for these specular reflections is therefore critical for the quality of the reflectance spectrum.

For the light from specular reflections at the water surface, the law angle of incidence = angle of exit applies. If the water is not made rough by waves, the light reflected at the surface originates from a solid angle which corresponds to the angle of aperture of the sensor. $\sigma^+(\lambda)$ is thus sensitive to the angle of aperture of the sensor and its orientation.

To calculate the reflectance from the albedo, the function $\sigma^+(\lambda)$ defined in Equation (2.17) is required in which the sensor has an aperture of 2π and is orientated perpendicularly to the water surface. A sensor of this type measures $E_d^+(\lambda)$ and when the relative proportions α, β, γ and δ of the 4 sources are determined from this measurement, $\sigma^+(\lambda)$ can be estimated from Equation (2.16), since the order of magnitude of the individual reflection factors is known: the reflection factor for the direct solar radiation (σ_{sun}) is tabulated in the book by Jerlov (1976) (Table XVIII page 74; when the sun is high, σ_{sun} = 2.0%); for diffuse radiation (σ_{sky}, σ_{Mie}, for a uniformly overcast sky also σ_{cloud}), Jerlov gives 5.2% to 6.6% as typical values (page 75). The changes in these values when the water surface becomes rough may be

approximated as a function of wind speed by the equations which were established by Cox and Munk (1956). A cloudy sky, however, remains a problem, since σ_{cloud} is greatly dependent on the position of the clouds.

Since the estimation of $\sigma^{+}(\lambda)$ is highly subject to error, especially in the case of a sensor having a small angle of aperture, another method has been developed for correcting reflectance spectra. This is based on the fact that an erroneous $E_d^{-}(\lambda)$, just as an erroneous $\sigma^{+}(\lambda)$, is made noticeable by characteristic errors in the reflectance spectrum. In contrast, when the correct spectrum $E_d^{-}(\lambda)$ is used (which can only be measured with a cosine detector under water), the reflectance spectrum would not be influenced by the spectral properties of the illumination. If the signatures of the light source are now minimized in the reflectance spectrum by an iterative process by dividing $E_d^{-}(\lambda)$ into the 4 radiation sources by Equation (2.3) and varying the relative proportions α, β, γ and δ, the correct spectrum $E_d^{-}(\lambda)$ may be determined as an approximation. Because this correction of reflectance spectra is particularly important with cloud cover, the method is termed *cloud correction*. It is described in more detail in the next section.

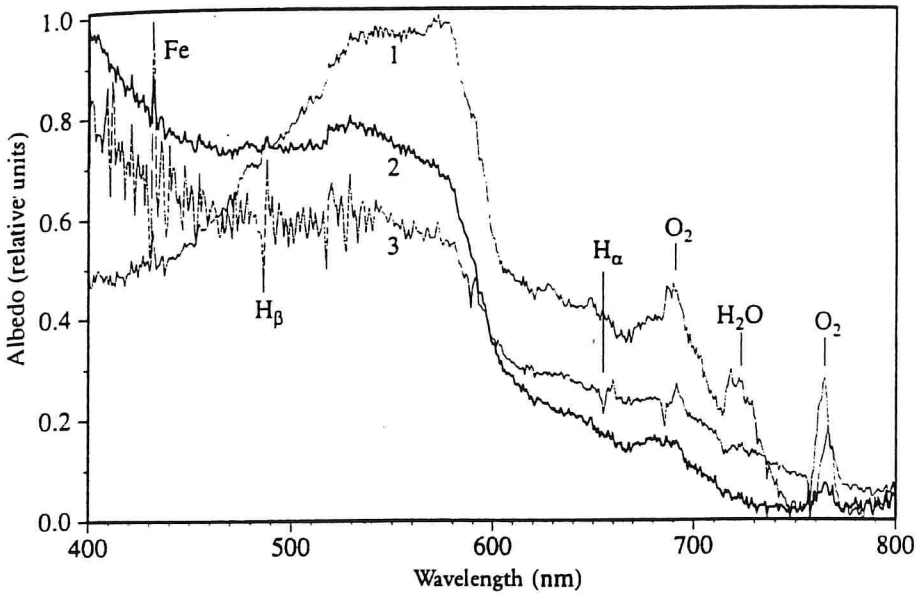

Figure 2.10: Examples of influences on the albedo spectrum due to changes in incident radiation.

2.3.5 Cloud correction

A typical example of how problematic are measurements made on days with rapidly changing cloud cover is shown in Figure 2.10. Here, the radiation reflected from the water (E_u^+) has been divided by three measurements of incident radiation (E_d^+) made in quick succession. Three completely different albedo spectra are obtained.

The proportion of direct solar radiation changed constantly on this day (23.4.91) since the clouds varied in thickness and intermittently completely exposed the sun. The incident radiation thus varied very rapidly in intensity and spectrum. The specular surface reflections therefore also constantly varied, an effect which was further amplified by the variable wind. This type of weather situation occurred on many days when measurements were taken. It is a chance occurrence if a reasonably good reflectance spectrum can be extracted without correction from the measurements made on such a day.

A reflectance spectrum is termed "good" if spectral characteristics of the illumination are observable to only a slight extent. If the spectral dependency of the surface reflections σ^+ and σ^- were ignored in the conversion of albedo to reflectance by Equation (2.24), albedo and reflectance would essentially differ by a constant scaling factor and a constant offset. Of the three examples given in Figure 2.10, spectrum 2 would then be the only one to be rated as "good". In the other two, structures are present in the spectrum which can clearly be assigned to the incident radiation; the most obvious are indicated in the figure.

If the one measurement E_d^+ which leads to albedo 2 and, after determination of offset and scaling factor, permits calculation of a "good" reflectance spectrum had not been made, not a single useable reflectance spectrum would have been obtained for this day. In fact, on many days it is impossible to derive even a single "good" reflectance spectrum from the measured spectra. Measurements on these days would be unusable without cloud correction.

The cloud correction starts from the relationship (2.24) between reflectance and albedo, at any rate in the approximated form

$$\rho(\lambda) \approx [1-\sigma^-]\,[1-\sigma^+(\lambda)]\,R(\lambda) + \sigma^+(\lambda). \qquad (2.24a)$$

The albedo $\rho(\lambda)$ is, by definition, the measured ratio $E_u^+(\lambda)/E_d^+(\lambda)$. As mentioned above, no reliable information on water constituents can be derived from this in many weather situations. However, if it is possible to determine the function $\sigma^+(\lambda)$ which describes the spectral shifts between reflectance and albedo (the wavelength dependency of σ^- does not play a great role and is ignored), the water constituents may be determined from the reflectance spectrum $R(\lambda)$, see Chapter 4. It is less complex and mathematically equivalent to modify $E_d^+(\lambda)$ by

the model (2.3) in such a way that the remnants of the illumination are minimized in the albedo $\rho(\lambda)$ and σ^+ thus becomes a constant. This method is implemented as PC program REF ("Reflectance").

The measured incident radiation spectrum, $E_d^+(\lambda)$, is resolved as in program WEISS (see Section 2.1.6) into the 4 sources E_{sun}, E_{sky}, E_{Mie}, E_{cloud} in order to determine the relative proportions α, β, γ and δ. The difference between the fitted and measured spectrum is stored as "residual spectrum" $E_R(\lambda)$; its factor ε has the value 1. $E_R(\lambda)$ represents a fifth radiation source. Although its amplitude is small in comparison to the other 4 sources, its use markedly decreases the noise in the reflectance spectrum.

If the relative proportions of the 5 sources are changed, another spectrum $E_d^+(\lambda)$ is obtained. If the albedo is calculated therefrom, the spectral characteristics of the 5 sources occur with a different amplitude: if the factor x of the radiation source $E_x(\lambda)$ is weighted wrongly, structures are visible in the albedo spectrum which characterize this radiation source; if the factor x is correct, these structures are absent. The strategy for optimizing the spectrum $\rho(\lambda)$ is therefore to minimize signatures in the spectrum which may clearly be assigned to the incident radiation.

The most prominent signature is the absorption band of atmospheric water at 722 nm which occurs in the sources E_{sun} and E_{cloud} (see Figure 2.7). In practice, this signature is highly important because the cloud proportion is frequently not correct. If the factor α of E_{sun} or the factor δ of E_{cloud} is erroneous, in addition, the other prominent atmospheric structures appear in the albedo, especially the oxygen absorption bands at 685 nm and 762 nm. All 3 bands lead to peaks in the albedo at the wavelengths mentioned; these peaks disappear after

successful correction. The length L of the curve in the region of these bands is therefore a measure of how correct are the factors α and δ:

$$L_{H_2O} = \sum_{(722nm)} \sqrt{[\rho(\lambda_{i+1})-\rho(\lambda_i)]^2 + 1}$$

$$L_{O_2} = \left(\sum_{(685nm)} + \sum_{(762nm)} \right) \sqrt{[\rho(\lambda_{i+1})-\rho(\lambda_i)]^2 + 1}$$

$\sum_{(722\ nm)}$ denotes that the summation index i proceeds over the channels which are relevant to the absorption of water at 722 nm. This applies similarly to $\sum_{(685\ nm)}$ and $\sum_{(762\ nm)}$.

For the sources E_{sky} and E_{Mie}, there are no peaks which could be minimized in order to determine the factors β and γ. However, since the sources E_{sun} and E_{cloud} are very noisy in the blue and green because they compensate for the differing spectral resolution of solar constant and spectrometer, a change in α or δ leads to a changed noise pattern in $E_d^+(\lambda)$. If the factors β or γ are erroneous, the noise compensation by $\alpha E_{sun}(\lambda) + \delta E_{cloud}(\lambda)$ is not complete which leads to a noisy albedo, see Figure 2.10, curve 3. Therefore, the noise in the range 400-600 nm is a criterion which can be used to optimize β and γ. The albedo smoothness G is used as a measure of the noise:

$$G = \sum_{\lambda_i=400\ nm}^{600\ nm} \left| 1 - \frac{\rho(\lambda_{i+1})}{\rho(\lambda_i)} \right| .$$

The program REF therefore calculates the albedo from Equation (2.23), rates its quality via the value of

$$L_{H_2O} + L_{O_2} + G$$

(minimized) and calculates a new spectrum $E_d^+(\lambda)$ with other values for α, β, γ, δ and ε. This cycle is repeated until the process converges.

Figure 2.11 shows that the cloud correction functions well in practice. In this case, the albedo was first calculated with a measured spectrum $E_d^+(\lambda)$ (thin curve; this is curve 1 of Figure 2.10). It apparently contains remnants of the water and oxygen bands, so that cloud correction is necessary. $E_d^+(\lambda)$ was resolved by Equation (2.10) into the 4 base spectra and the function $E_R(\lambda)$ was calculated. Values smaller by 20 per cent were then inserted for the parameters α and δ and values larger by 20 per cent were inserted for β and γ and the fitting operation was started. After 300 iterations the albedo no longer changed. The result is the thick curve.

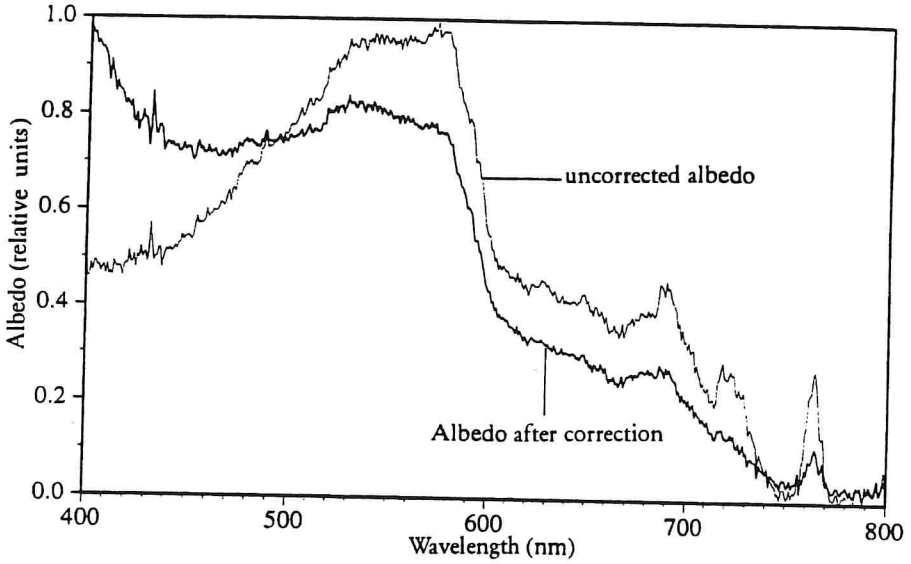

Figure 2.11: Example of the effect of cloud correction.

As comparison with Figure 2.10 shows, the result is very similar to curve 2 which is considered as a reasonably correct albedo. Cloud correction therefore performs satisfactorily.

Figure 2.11 shows the importance of cloud correction very clearly: under some lighting conditions, the albedo spectrum can change very markedly, especially in the blue. If in the reflectance spectrum derived therefrom the course of the curve in the blue and the green is

correlated, as is conventional, with the chlorophyll concentration, completely erroneous results are obtained without cloud correction. However, the maximum at 685 nm which is frequently employed for determining the chlorophyll *a* concentration is also effected by an error of this type because of a marked O_2 absorption band.

A good indicator of whether cloud correction is necessary is provided by the water absorption band at 722 nm. If this can be discerned in the albedo (or reflectance) spectrum, cloud correction is highly advisable.

3. Optical properties of water and its constituents

Using the "cloud correction" described in the preceding chapter, it is possible to derive useful reflectance spectra even from radiance measurements which are usually discarded because of variable cloud cover or rough water surface. The objective is now to find a correlation between the reflectance spectrum and the concentrations of individual water constituents.

For the open ocean, the ratio of the radiances in the blue and the green is a current method for determining the chlorophyll concentration from remote sensing data, for instance data from the *Coastal Zone Color Scanner* (CZCS) on the Nimbus-7 satellite. However, this method is only successful as long as no pigment other than chlorophyll a and phaeophytin a noticeably influences the optical properties of the open ocean at the wavelengths selected; the derived "chlorophyll concentration" is the sum of these two pigments. However, in the coastal areas of the oceans and in inland waters, the pigmentation of water is more complex. The reflection is generally made up here from contributions of different substances. In order to separate these, the values of reflectance or radiance have to be considered at several wavelengths and separation performed with the aid of a model.

The basis of any model of "water colour" is the optical properties of water and its constituents. These form the subject of this chapter; the model for reflectance based thereon will be formulated and applied in the following chapters.

The optical properties can be summarized in a single parameter, the complex refractive index. In addition to the particle size, it determines the absorption and scattering behaviour. The fundamental physical

relationships are described in detail in Section 3.1. The reasoning followed clearly shows the close linkage between absorption and scattering. Because of this linkage, the Kramers-Kronig relations which are valid in a wide range of cases can be used to calculate, when the absorption is known, the spectral course of the refractive index. Otherwise this may only be ascertained by determining the characteristic molecular parameters (eigenfrequencies, line widths, oscillator strengths) from the absorption spectrum. This complex method is used in the only comparable model given in the literature (Bricaud and Morel 1981), as far as I am aware, on the optical properties of water bodies.

The scattering can be calculated from the absorption and refractive index spectrum with the aid of Mie theory, if the shape and size of the particles are known. Since phytoplankton has a wide range of shapes, in practice scattering can only be calculated to an approximation. In Section 3.1.4, the useful approximation of van de Hulst (1957) for spherical particles having a relative refractive index close to one is described. It is used in 3.2 in order to estimate attenuation and scattering of algae. These spectra are employed in the modelling of the reflectance in later chapters, since useful measurements are found in the literature at most for the absorption of the various algal species, but scarcely at all on scattering.

The discussion of fundamental relationships and the description of computation methods is followed by a set of important information on water and its constituents. The nomenclature corresponds to recommendations of the *International Association of Physical Oceanography*, IAPO (Morel and Smith 1982). This nomenclature is conventional in literature on optical oceanography; limnological publications frequently use other terms and symbols.

3.1 Absorption and scattering theory

3.1.1 Quantum-mechanical derivation of the complex refractive index

The elementary processes in the interaction of light with matter are shown in Figure 3.1.

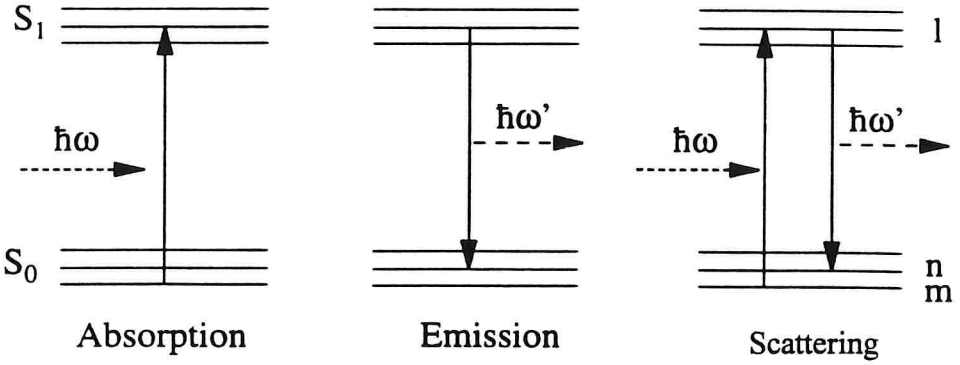

Figure 3.1: Energy level diagrams for absorption, emission and scattering of a photon at a molecule.

When a molecule absorbs a quantum of light (photon), one electron absorbs its energy $\hbar\omega$*. If the molecule is, for example, a pigment** in the electronic ground state and if the wavelength of the photon is in the visible region of the electromagnetic spectrum, the electron changes from the electronic ground state S_0 to the first excited singlet state S_1. The molecule is said to be converted into the excited state. At temperatures above absolute zero, the molecules are not in the lowest energy state, but they rotate and vibrate about their equilibrium position. In the representation of Figure 3.1, this means that the electronic ground state S_0 is split

---

* Energy is a parameter of fundamental importance in the description of elementary physical relationships, therefore for spectroscopy any parameter proportional to energy is a "natural" variable, for which the equations have a particularly simple form. In addition to energy E itself, conventional variables are frequency ω (s^{-1}) and wavenumber ν (m^{-1}), $E = \hbar\omega = hc\nu$, h = Planck's constant, $\hbar = h/2\pi$. The wavelength λ (m) is indirectly proportional to these variables: $\lambda = 1/\nu$.

** Pigment = a molecule which absorbs in the visible.

into many sublevels; each sublevel corresponds to one degree of freedom of rotation or vibration.

Emission is the reverse process: the excited molecule gives off its excitation energy by transferring one electron from S_1 to S_0, one photon of energy $\hbar\omega'$ being emitted. The molecule is then in the ground state.

Scattering in this quantum-mechanical scenario is absorption with simultaneous emission (Landau-Lifschitz 1986, p. 206). When the probability of absorption and emission is known, the probability of scattering may therefore be obtained.

All of the information on the interaction of a photon with a molecule is contained in the scattering tensor* (Hassing and Mortenson 1980)

$$\alpha_{\rho\sigma}^{mn}(\omega) = \sum_{l} \frac{\langle n|M_\rho|l\rangle\langle l|M_\sigma|m\rangle}{E_l - E_m - \hbar\omega - i\Gamma_l} + \frac{\langle n|M_\sigma|l\rangle\langle l|M_\rho|m\rangle}{E_l - E_n + \hbar\omega - i\Gamma_l}.$$

It is related to the amplitude of the scattered wave. The quantity in the numerator

$$\langle l|M_\sigma|m\rangle \equiv \int \psi_l^*(r)\, M_\sigma\, \psi_m(r)\, d^3r$$

describes, in quantum-mechanical formalism, the probability that the electron undergoes a dipole transition from level E_m to level E_l. E_m is the energy of the bound electron. Its path in the molecule - its orbital - is described by the wave function

$$|m\rangle \equiv \psi_m(r).$$

The square of its absolute value, $\langle m|m\rangle = |\psi_m(r)|^2$, is the probability of the electron being at position r. An

---

* The expressions in the numerator are read from right to left.

electromagnetic wave whose E vector points in direction σ can cause the electron to transfer to another orbital $|l\rangle$. Whether the transition takes place depends on two factors: the polarization σ of the wave - described by the operator M_σ - and the scalar product

$$\langle l|m\rangle \equiv \int \psi_l^*(r)\ \psi_m(r)\ d^3r,$$

which is a measure of the overlap of the two wave functions. The operator M_σ describes the probability w_σ that the incident wave has the "matching" polarization σ, the overlap $\langle l|m\rangle$ gives the probability of transition of the electron from the orbital $|m\rangle$ into orbital $|l\rangle$. Since the two probabilities are independent from each other, the total probability for absorption of the photon is the product of these individual probabilities:

$$\langle l|M_\sigma|m\rangle = w_\sigma\langle l|m\rangle.$$

Similarly,

$$\langle n|M_\rho|l\rangle = w_\rho\langle n|l\rangle$$

is the probability of emission of a photon of polarization ρ by transition of the electron from the orbital $|l\rangle$ into orbital $|n\rangle$. Overall, the numerator

$$\langle n|M_\rho|l\rangle\ \langle l|M_\sigma|m\rangle = w_\rho w_\sigma\ \langle n|l\rangle\ \langle l|m\rangle$$

is thus a product of four probabilities, that it is real and is greater than or equal to zero.

If the levels E_1, over which the summation in the scattering tensor proceeds, are rotational and vibrational states of the first electronically excited state S_1, the scattering tensor gives the probability of a photon being scattered at this molecule. The tensor is composed of a resonant and a nonresonant term. The resonance is given

by the expression in the denominator

$$E_l - E_m - \hbar\omega - i\Gamma_l \quad .$$

This means that the photon can only be absorbed if an electron can absorb its energy $\hbar\omega$ by undergoing a transition from level E_m to level E_1. The law of conservation of energy requires that $E_1 - E_m = \hbar\omega$. Since the probability that an electron has energies $E_1 \pm \varepsilon$ is not zero, the photon can also be absorbed if its energy does not exactly match the transition. However, the probability decreases with increasing ε: the probability distribution is a Lorentzian function with $2\Gamma_1$ as line width as will be shown later (Equation 3.4b, page 59).

The nonresonant term of the scattering tensor describes the "time-reversed" process, in which the initial state and final state are exchanged (Landau-Lifschitz 1986, p. 206). This term is generally ignored since it is several orders of magnitude smaller than the resonant term if the molecule can absorb the photon. The scattering tensor thus simplifies to the expression

$$A_{mn}(\omega) = \sum_l \frac{w_\sigma w_\rho \langle n|l\rangle\langle l|m\rangle}{E_l - E_m - \hbar\omega - i\Gamma_l}.$$

m is the initial state, and n the final state of the molecule. If conditions are restricted to elastic scattering at the ground state (m=n=0) and the energy of the ground state is set as usual to zero, then

$$N(\omega) \equiv A_{00}(\omega) = \sum_l \frac{A_l}{\omega_l - \omega - i\Gamma_l} \qquad (3.1)$$

is obtained ($A_1 \geq 0$, real). To describe the interaction of light with matter on a macroscopic level, the contributions of the individual molecules must be appropriately averaged. According to Hassing and Mortenson (1980), the

contributions of the molecules add in the area of validity of *linear optics* (that is for the absorption and scattering processes, but not, for example, for Raman scattering or birefringence).* $N(\omega)+1$ is the complex refractive index $m(\omega)$ (Tehver 1981).

3.1.2 Classical derivation of the complex refractive index

The quantum-mechanical derivation of the complex refractive index presented here is still of rare occurrence in the literature. A "classical" derivative is conventional via the differential equation

$$m_e\ddot{r} + g\dot{r} + qr = eE(t) \qquad (3.2)$$

for the damped motion of an electron (amplitude r(t), mass m_e, charge e, damping g) under the influence of an electric field E(t), see for instance Born and Wolf (1989) p. 92. If $E(t) = E_0e^{-i\omega t}$ and $r(t) = r_0e^{-i\omega t}$, then

$$(-m_e\omega^2 - i\omega g + q)\, r(t) = e\, E(t).$$

The electron performs a forced vibration of frequency ω. The amplitude r(t) increases if ω approaches the resonance frequency $\omega_0 = \sqrt{q/m_e}$; the damping g restricts the amplitude.

If N electrons perform this vibration, the macroscopic dipole moment P likewise changes at this frequency:

$$P(t) = Ner(t) = \frac{Ne^2}{m_e(\omega_0^2-\omega^2)-i\omega g}\cdot E(t).$$

---

* This even applies to inelastic scattering ($m \neq n$), in which coherent and incoherent components must be differentiated. In coherent scattering the amplitudes of the scattered waves add, interference occurs in the case of incoherent scattering.

The dielectric susceptibility χ is defined in electrodynamics as the proportionality constant between incident wave E(t) and the induced dipole moment P(t): $P = \chi E$. In isotropic substances and in media having cubic symmetry χ is related to the complex refractive index m via the relationship $4\pi\chi = m^2-1$ (Kittel 1983, page 439). From this it follows that:

$$m^2(\omega)-1 = 4\pi \frac{P(t)}{E(t)} = \frac{4\pi Ne^2}{m_e(\omega_0^2-\omega^2)-i\omega g}.$$

If the N electrons do not all have the same resonance frequency ω_0, but if $N \cdot f_1$ electrons are in resonance (damping g_1) at frequency ω_1, Equation (3.3) follows

$$m^2(\omega)-1 = \frac{4\pi Ne^2}{m_e} \sum_l \frac{f_l}{\omega_l^2-\omega^2-i\omega g_l}. \qquad (3.3)$$

This equation links the macroscopic quantity m with microscopic parameters of the model (3.2). It was discovered by a remarkable coincidence virtually simultaneously by two physicists having almost the same name: by H.A. Lorentz 1880 and L. Lorenz 1881.

Mueller (1973) used the Lorentz-Lorenz equation to model absorption spectra of phytoplankton pigments (page 108). In his work, the constant in front of the sum is $Ne^2/\pi m_e c^2$, since he was using SI units, whereas the notation in (3.3) applies to the CGS system.

Several variants of the Lorentz-Lorenz equation are found in the literature, since, depending on the symmetry of the dispersing substance, different relationships between χ and m apply. For example, in van de Hulst (1957, page 191) there appears on the left side $3(m^2-1)/(m^2+2)$. He uses the equation to describe absorption spectra of spheres having a refractive index close to one. In this case ($m \approx 1$), $m^2+2 \approx 3$, that is his equation virtually

corresponds to (3.3).

The classical equation (3.3) and the quantum-mechanical equation (3.1) for the refractive index obviously differ. The reason is the differing expression for the electron path: in the quantum-mechanical derivation, the electron path is its orbital in the molecule; in the classical derivation it simply performs a damped harmonic vibration. The quantum-mechanical equation is therefore the more correct one.

3.1.3 The complex refractive index

Real and imaginary parts of the complex refractive index can be given explicitly for both the quantum-mechanical equation (3.1) and the classical equation (3.3). Since the quantum-mechanical equation is both simpler and more exact, the following discussion is restricted thereto. From (3.1) are obtained the following expressions for the real and imaginary parts of the complex refractive index $m(\omega) = n(\omega) + in'(\omega)$:

$$n(\omega) = Re\ N(\omega) + 1 = 1 + \sum_l \frac{A_l\,(\omega_l-\omega)}{(\omega_l-\omega)^2+\Gamma_l^2} \qquad (3.4a)$$

$$n'(\omega) = Im\ N(\omega) = \sum_l \frac{A_l\,\Gamma_l}{(\omega_l-\omega)^2+\Gamma_l^2} \qquad (3.4b)$$

In Figure 3.2 these two functions are illustrated for a single line; in the case of several lines, the amplitudes of the individual lines add. In order to illustrate the difference from the classical equation (3.3), their real and imaginary parts are also drawn (dotted lines). Interestingly, these lack the symmetry properties of the quantum-mechanical equations.

In an individual line, the amplitude A, the line width Γ and the resonance frequency ω_0 determine the course of

the curve of both the real part and the imaginary part. If the spectrum of the imaginary part is known in a spectral region for which the curve parameters A, Γ and ω_0 can be readily determined, the real part can be calculated therewith and vice versa. This conversion is also possible for several lines but as the number of lines increase the number of line shape parameters increases. Modelling of the complex refractive index by Equations (3.4) is therefore only useful in practice if the number of lines is small and if the individual lines can easily be differentiated. In Appendix A, generally valid relationships are derived between real and imaginary parts of a complex function. These Kramers-Kronig relations provide the tool for interconversions between real and imaginary parts of the complex refractive index independently of the number of lines.

Imaginary part. The shape of the line of the imaginary part of an individual line is a so-called *Lorentzian profile*. The amplitude is at a maximum at the resonance frequency ω_0 where it has the value A/Γ. At half height, the line width is equal to 2Γ; the parameter Γ is thus the half width at half height (HWHH). The physical meaning of the imaginary part of the refractive index is the close relationship to the absorption $a(\omega)$. This relation is known under the name "optical theorem":

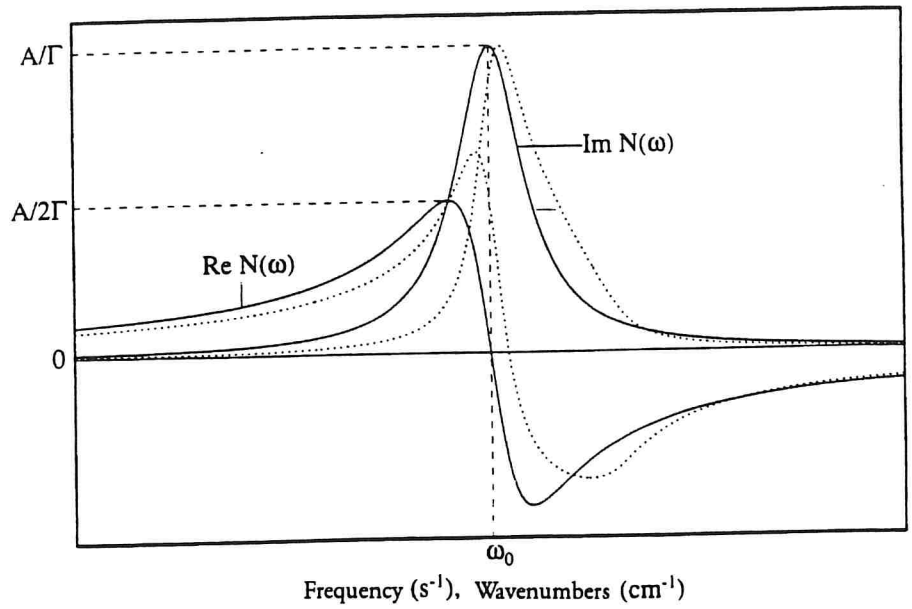

Figure 3.2: The complex refractive index for an individual absorption line. Dotted line: classical Equation (3.3), continuous line: quantum-mechanical Equation (3.4).

$$a(\omega) = \frac{2\omega}{c} n'(\omega) \qquad (3.5)$$

(Goldberger and Watson 1964, page 558). As is evident from Equation (3.5), in an individual line the absorption spectrum is the product of a Lorentz profile and the frequency, for several lines the amplitudes of the individual lines add.

For a molecule, the amplitudes, line widths and resonance frequencies of the individual absorption lines may be calculated in principle if the geometric structure of the molecule is known. This is because the spatial configuration of the individual atoms defines the potential in which the electrons move; if the Schrödinger equation is solved, the absorption spectrum can be calculated. However, an exact solution only exists for the hydrogen atom; for molecules one must be content with

approximations.*

In the present work, the absorption is a measured value. Modelling of the absorption spectrum is only necessary for the interpolation of data points or to extrapolate the spectrum beyond the range measured. For these purposes, a description of the absorption according to Equation (3.5) is sufficient.

Real part. The physical meaning of the real part is the refraction of the light: if light passes from one medium into another, the angles of entry and exit behave as in $\sin\alpha_1/\sin\alpha_2 = n_2/n_1$ (Snell's law). n is therefore called the *refractive index*, the wavelength dependency of n is termed *dispersion*. In the construction of lenses and prisms, materials are used which absorb only slightly in the spectral region of interest. As Figure 3.2 shows, $n(\omega)$ is there a monotonically increasing function, that is short-wave radiation is refracted more strongly than long-wave radiation. Because the function $n(\omega)$ has a negative gradient in the range ω_0-Γ to ω_0+Γ, the light refraction behaviour is reversed here; this interval is therefore termed the region of *anomalous dispersion*.

As can be seen from Figure 3.2, close to the resonance frequency, the real part is of the same order of magnitude as the imaginary part; they are identical at the frequencies ω_0-Γ and ω_0+Γ. If both the real part and imaginary part of the complex refractive index are known for a frequency range $\omega_{min}...\omega_{max}$, the optical properties of the material may be estimated from the course and range of values of the two curves. If the curves show a spectrum similar to that of Figure 3.2, the range measured includes a spectral region in which the absorption dominates the optical properties, otherwise

---

* Energy levels, oscillator strengths, binding forces and similar can be calculated for any desired molecules with the aid of the commercial programs PCMODEL and MMX (Serena Software).

the spectral regions of strong absorption lie outside the range measured and the optical properties in the range measured are dominated by light refraction which is closely connected to light scattering (compare Section 3.1.4). In this case it can be stated from the value of the real part whether an extension of the range measured towards the shortwave region or towards the longwave region leads more rapidly to a region of strong absorption. If a strong absorption band is situated in the longwave region ($\omega_0 < \omega$), then $n < 1$*, otherwise $n > 1$. Since all molecules absorb strongly in the UV, whereas they are generally transparent in the near infrared, n is generally greater than 1 in the visible.

The ratio n' to n - 1 is of interest in consideration of the optical properties of substances absorbing in the visible**. For a single line, the following equation applies:

$$\frac{n'(\omega)}{n(\omega)-1} = \frac{\Gamma}{\omega_0-\omega}.$$

The region of maximum absorption may be estimated with the aid of this equation. If $\omega_0 \gg \omega$, the ratio approximates the constant value Γ/ω_0.

As is shown by this brief discussion of the complex refractive index, the absorption of a substance in the IR and UV influences the optical properties in the visible. It is therefore often impossible in practice to correctly

---

* Since the refractive index n is equal to the ratio of the phase velocity of light in the material to that in vacuum, $n < 1$ means that the phase velocity of light is greater than that in vacuum. This does not contradict the theory of special relativity, according to which no signal can travel faster than light. This is because the phase velocity cannot be measured experimentally, so that it is not a physical process which could be used for information transfer. This problem is illustrated in the book by Born and Wolf (1989) in brief on page 18; the footnote there cites further literature.

** This ratio is of great importance in Mie theory, see Section 3.1.4, Equation (3.12).

describe absorption and scattering if a reliable measurement of the real and imaginary parts of the complex refractive index is not available.

3.1.4 Mie theory for spherical particles

The complex refractive index discussed in the last section completely characterizes the optical properties of a homogeneous isotropic substance whose physical size is very much greater or very much smaller than the wavelength of light*. However, to describe the optical properties of a water body in which the absorbing and scattering particles are not present in dissolved form but are suspended, knowledge of the complex refractive index is insufficient, just as it is for the suspended particles themselves. This is due to the fact that if the optical inhomogeneities are of the same order of magnitude as the wavelength, interference effects occur which influence the absorption and scattering behaviour.

Gustav Mie and Paul Debye independently of each other developed a method by which the optical properties of such substances may be calculated. Exact solutions of the equations of this "Mie theory" only exist for a few simple geometric shapes such as a sphere, cylinder, ellipsoid and enclosed sphere (sphere having refractive index m_1, enclosed by a spherical shell having refractive index m_2). Although these bodies generally do not even resemble the sometimes bizarre shapes of particles in water, Mie theory is useful for the discussion of radiation transfer in water as long as one is aware of its limits. If no reliable measured data exists, Mie theory is, furthermore, the only way of estimating scattering. Therefore, this section summarizes the most important Mie theory equations, in van de Hulst's

---

* The use of the term "optical" implies that the region of the electromagnetic spectrum under discussion lies in the visible or extends only slightly into the UV or IR. In this context, the terms "electromagnetic radiation" and "light" are used synonymously.

approximation (*anomalous diffraction approximation*), which are important for calculating scattering spectra. They may all be found in the standard book by van de Hulst (1957) which is abbreviated in the following citations by "vdH".

The most important measurable optical properties are absorption, scattering and attenuation (extinction). Their determination is described in Section 3.2. In the context of Mie theory they are described by the dimensionless numbers Q_a, Q_b and Q_c which each represent an efficiency factor: Q_a is the ratio of the absorbed energy to the energy impinging on the geometric cross-section, Q_b is the ratio of scattered to incident energy and Q_c is the ratio of absorbed *and* scattered energy to the incident energy (Bricaud et al. 1988). Therefore, independently of particle geometry, the following applies:

$$Q_c = Q_a + Q_b. \tag{3.6}$$

Q_a, Q_b and Q_c are also termed relative absorption, scattering and extinction cross-sections respectively. When the complex refractive index and the particle shape are known, Q_a can be determined taking into account Equation (3.5), Q_b may be calculated with the aid of the law of conservation of energy and Huygens' principle (vdH, Chapter 2): the energy of the scattered light is equal to the energy of the incident light and the spatial intensity distribution of the scattered light is calculated assuming that each point of the particle emits a spherical wave. Equations (3.9) and (3.11) given further below are the result of this statement for spherical particles. The discussion below relates first to the relative absorption cross-section Q_a and then to the relative extinction cross-section Q_c. The relative scattering cross-section Q_b is given by Equation (3.6) as the difference $Q_c - Q_a$.

Assuming the particle to be a sphere of diameter d and complex refractive index m = n - in' relative to the surrounding medium, and if λ is the wavelength of the electromagnetic radiation in the surrounding medium, the parameter

$$\alpha = \frac{\pi d}{\lambda}$$

is a measure of sphere size relative to λ. The absorption cross-section Q_a only depends on α and on the imaginary part n' of the complex refractive index. n' is linked to the absorption coefficient a_{cm} (unit m^{-1}) via the optical theorem (3.5). If ω is replaced in this by λ ($\omega = 2\pi c/\lambda$), this then gives:

$$a_{cm}(\lambda) = \frac{4\pi}{\lambda} n'(\lambda). \qquad (3.7)$$

The subscript *cm* stands for "cell matter" since it is the optical properties of the algal cells and not of the algal suspension which are of interest. The dimensionless parameter

$$\rho' = a_{cm} d = 4\alpha n' \qquad (3.8)$$

is now the parameter which determines the absorption behaviour. The following applies (vdH pages 175, 181):

$$Q_a = 1 + 2\frac{e^{-\rho'}}{\rho'} + 2\frac{e^{-\rho'}-1}{\rho'^2}. \qquad (3.9)$$

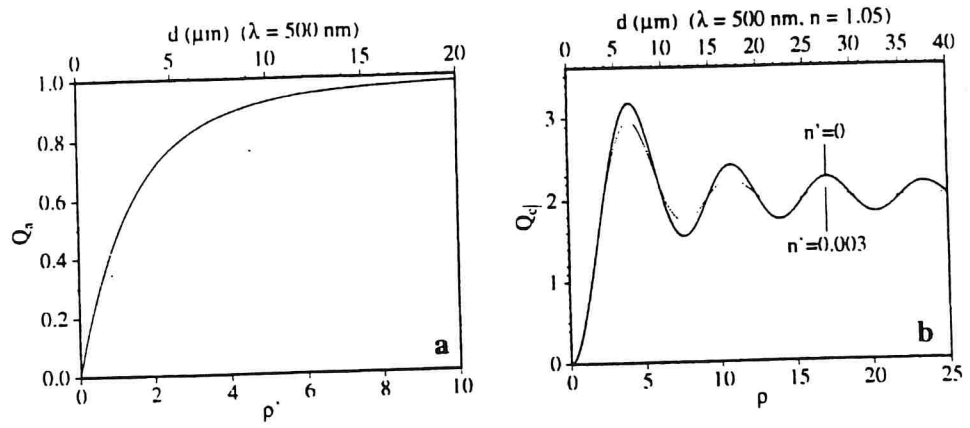

Figure 3.3: Efficiency factor for absorption (a) and attenuation (b) of a spherical particle. The dimensionless parameters ρ' and ρ are plotted on the bottom abscissa; see the text for definitions. The top abscissa gives the particle diameter d for a wavelength of 500 nm.

Figure 3.3a shows the function $Q_a(\rho')$. For $\rho' = 0$, $Q_a = 0$, when ρ' is small, Q_a is approximately proportional to ρ' and when ρ' is large, Q_a approaches the value 1 (*black body domain*, Morel and Bricaud 1981). For small values of ρ', the exponential function of ρ' may be developed ($e^{-\rho'} = 1 - \rho' + \frac{1}{2}\rho'^2 - \ldots$) and thus (3.9) may be represented as a power series. If the nonlinear elements are ignored, the following is obtained as an approximation of the linear region of Figure 3.3a:

$$Q_a \approx \frac{2}{3}\rho'. \qquad (3.9a)$$

For better representation of the particle size range, in addition to ρ', a further abscissa has been drawn in Figure 3.3a on which the particle diameter d for $\lambda = 500$ nm is plotted. The two x axes are interconverted by Equation (3.8).

Nonlinear light absorption effects may be explained by Equation (3.9) and Figure 3.3a; see the article by Morel and Bricaud (1981). The most important practical

consequence is that when ρ' is large, the Lambert-Beer law no longer applies, as this assumes proportionality between Q_a and ρ'. Because of the nonlinearity, when the pigment concentration in an algal cell increases (equivalent to a higher value of ρ') the absorption cross-section increases in a nonlinear fashion. This is evident in the fact that when the pigment concentration increases, the difference between absorption maximum and absorption minima becomes smaller. This flattening of the absorption spectrum when the packing density of the pigments increases (*package effect*, Kirk 1975a) was correctly explained for the first time by Duysens (1956). It complicates the comparison of absorption spectra. For this reason, Morel and Bricaud, in their work from 1981, extrapolate the absorption spectra of phytoplankton to the limit case d = 0, that is they extrapolate from the suspension to the solution. The extrapolation is possible if the particle size d is known. The method is described at the end of Section 3.2.1.

In scattering, in addition to the parameter α and the imaginary part n', the real part n of the complex refractive index is important. If the particle does not absorb (n' = 0) and the refractive index of the sphere is equal to the refractive index of the surroundings (n = 1), no scattering occurs. Therefore Q_c depends on m - 1 and the dimensionless scattering parameter

$$\rho^* = 2\alpha(m-1) = \frac{2\pi d}{\lambda}(m-1) \qquad (3.10)$$

is a useful parameter for the parameterization of Q_c. The following relationship applies (vdH page 176):

$$Q_c = 4\ Re\left\{\frac{1}{2} + \frac{e^{-i\rho^*}}{i\rho^*} - \frac{e^{-i\rho^*}-1}{\rho^{*2}}\right\}. \qquad (3.11)$$

In this form, the equation corresponds to Equation (3.9) for absorption but with the variable ρ' replaced by the

variable $i\rho^*$. The thick curve in Figure 3.3b shows Q_c for the case when absorption is negligible, that is for $n' = 0$. In this case, the complex scattering parameter ρ^* becomes real,

$$\rho = 2\alpha(n-1) = \frac{2\pi d}{\lambda}(n-1), \qquad (3.10a)$$

and (3.11) becomes (vdH page 176)

$$Q_c = 2 - \frac{4}{\rho}\sin\rho + \frac{4}{\rho^2}(1-\cos\rho). \qquad (3.11a)$$

The parameter ρ is the phase difference in steradians between the light passing through the particle and the light passing around the particle (Bryant et al. 1969). Since ρ contains the diameter d of the particle, its refractive index n and the light wavelength λ, for a given particle size distribution of non-absorbing spheres, the dependence of the attenuation cross-section on n and λ may be investigated. Bryant et al. (1969) confirmed the validity of Equation (3.11a) for scattering by latex spheres in water and in a mixture of water and glycerol and likewise for scattering by the bacterium *Escherichia coli*.

When ρ is large, Q_c tends towards 2, that is the attenuation cross-section is twice that of the geometric cross-section. The reason for this "extinction paradox" is constructive interference in the sphere shadow (Bryant et al. 1969).

For light-absorbing particles, the imaginary part n' of the refractive index is greater than zero. In this case, Equation (3.11) takes the form (vdH page 179)

$$Q_c = 2 - \frac{4}{\rho}e^{-\rho\tan\xi}\cos\xi\sin(\rho-\xi) - \frac{4}{\rho^2}e^{-\rho\tan\xi}\cos^2\xi\cos(\rho-2\xi) + \frac{4}{\rho^2}\cos^2\xi\cos2\xi. \qquad (3.11b)$$

The parameter ξ indicates how large n' is in relation to n - 1:

$$\tan \xi = \frac{n'}{n-1},$$

$\rho' = 2\rho \tan\xi$ and $\rho^* = \rho(1 - i \tan\xi)$. When $n' = 0$, $\xi = 0$ and the thick curve of Figure 3.3b is obtained. A value $n' > 0$ leads to the maxima of Figure 3.3b being smaller and the minima greater, that is with increasing absorption the amplitude of the periodic modulation decreases. The positions of the minima and maxima remain the same. This is illustrated by the thin curve: it represents Q_c for $n = 1.05$, $n' = 0.003$ ($\tan\xi = 0.05$). As in Figure 3.3a, a second x axis has also been drawn in Figure 3.3b in order to illustrate how Q_c behaves as a function of the observable variable d. The two axes are interconverted by Equation (3.10a).

3.1.5 Absorption of arbitrarily shaped particles

Shadowing and *package effect*. Absorption and scattering behaviour of spherical particles may be calculated with the equations introduced in the preceding section. However, water constituents are not spherical; the phytoplankton especially can adopt highly bizarre shapes. Kirk (1975a, 1975b, 1976) studied the effects on the absorption spectrum if the spherical shape is changed to more realistic shapes. One result of his calculations is shown in Figure 3.4.

It is most unfavourable for light absorption if all the pigments are located in a single large spherical algal cell or algal colony (lowest curve). If the sphere is deformed, the absorption cross-section increases as can be seen in the elliptical particle example (second curve from the bottom). The most efficient absorption of light is shown by many small spherical cells uniformly distributed in the water (top curve). Absorption which is almost as effective is shown by the long thin cylinders

(second curve from the top) which may be considered an approximation of thread-like cell colonies.

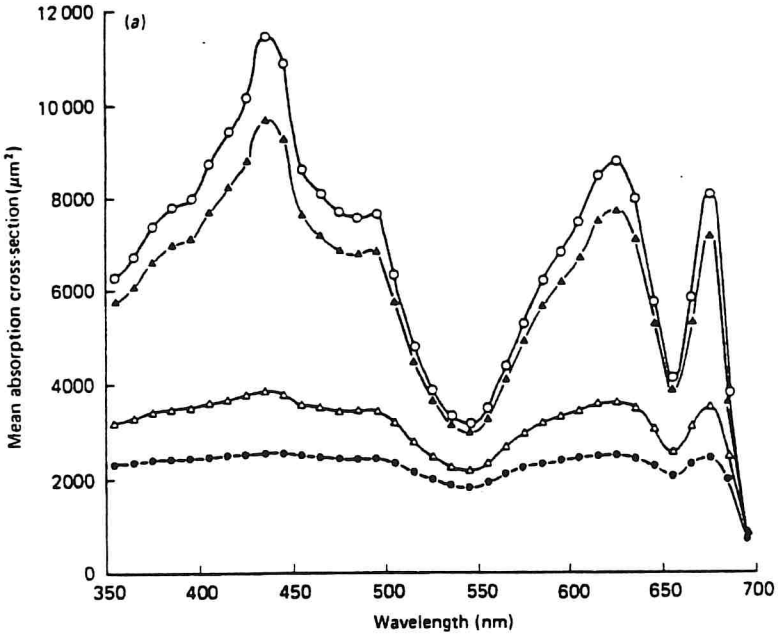

Figure 3.4: Dependence of the absorption cross-section on particle shape. From Kirk (1976). ●: Sphere with d = 57.6 μm, Δ: ellipsoid having axes of 230.4, 28.8, 28.8 μm, ▲ : cylinder of length 3537 μm and diameter 6 μm, o: 884 small spheres of diameter 6 μm. The volume is 10^5 μm^3 in each case, and the pigment concentration is identical.

This obvious dependence of the absorption cross-section on the distribution of pigments in the water is due to the mean free path length of the light: in the limit case when the pigment is dissolved in the water, the light impinges on the absorbing pigment everywhere in the water therefore it is maximally attenuated. In contrast, if the pigments are packed in individual cells, many photons pass by the cells so that some of the light stream does not interact with the pigments at all and because of the relatively high packing density within the cells, the shadowing is higher. The package effect is therefore governed by the mean projected surface area of the particles: the more this increases, the more light is

absorbed.

As has been explained with reference to Figure 3.3, the change of the absorption cross-section is determined by the absorption coefficient. Because of the nonlinear dependence, the absorption cross-section changes with packing density in the region of strong absorption more markedly than in the region of low absorption. For example, in Figure 3.4 the ratio of the absorption cross-sections of cylinder and large sphere is 3.82 at 435 nm, but only 1.16 at 695 nm.

The change in absorption amplitude and spectrum with spatial distribution of the pigments is therefore due to the projected area of the cells but not to their shape: identical projected areas give the same absorption spectrum. The results of Mie calculations for spherical particles are therefore applicable to particles of any shape as far as the absorption behaviour is concerned. Approximation of the spherical shape in scattering is more problematical.

Compensation for the shadowing effect in phytoplankton. The four curves of Figure 3.4 show how the absorption cross-section of a suspension changes with the projected area of the suspended particles. However, algae compensate for this shadowing effect by reducing the packing density of the pigments in large cells: according to Agustí (1991) the packing density of chlorophyll *a* is correlated with the cell volume by $c_i/V = 0.0065 \cdot V^{-0.16}$ (c_i = intracellular chlorophyll *a* concentration in pg/cell, V = cell volume in μm^3). A packing density of 0.001 pg/μm^3 results for the large sphere of Figure 3.4 (d = 57.6 μm) and 0.003 pg/μm_3 for the small spheres (d = 6 μm). In Figure 3.4, the same packing density was assumed for both cases. In order to return to identical pigment concentrations, instead of one large sphere, three must now be used, that is the amplitude of the lowest curve of Figure 3.4 must be multiplied by the

factor 3. The difference in absorption cross-section becomes markedly lower as a result of this. In contrast to the model particles of Figure 3.4, in the case of real algal cells, the absorption of a suspension is thus virtually independent of size and shape of the cells: the absorption, to a good approximation, is proportional to the chlorophyll concentration only, $a \sim c_i^{0.92}$ (Agustí 1991).

3.2 Determination of optical properties

The preceding sections explained how the complex refractive index is the decisive material property for interaction with electromagnetic radiation. Apart from this, the absorption and scattering behaviour only depend on the shape of the particle and its size relative to the wavelength. This is illustrated by the equations in the preceding section which apply to the simple case of spherically shaped particles. However, the efficiency factors employed in that section are not accessible directly by experiment; therefore the relationship with measured parameters will be derived in this section.

3.2.1 Inherent optical properties

The principle behind the measurement of optical parameters is illustrated in Figure 3.5. The medium whose optical properties are to be determined is illuminated by a light source*. Some of the incident radiation is absorbed, the remainder is scattered. These processes are indicated in the drawing: the symbol a represents the absorption processes, the symbol b the scattering processes. The light which, after passage through the medium, has a direction parallel to the incident direction, is termed transmitted light; it has apparently passed unimpeded through the medium. The remainder of the incident light interacts with the medium and is absent

* The light source is drawn as the sun so that the diagram can simultaneously illustrate reflection measurements at a water surface; a lamp serves as light source in laboratory measurements.

from the transmitted beam. This process occurring during passage of light through the medium is termed extinction or attenuation. The *attenuation coefficient* c has found acceptance as a measurement of this. It is the sum of the *absorption coefficient* a and the *volume scattering coefficient* b which describe the transmitted light losses:

$$c = a + b. \qquad (3.13)$$

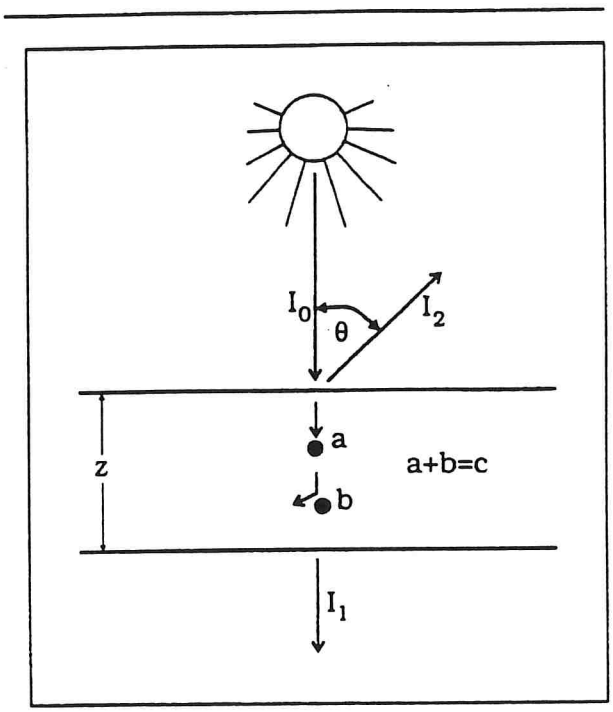

Figure 3.5: Definition of the inherent optical properties a, b, c and $\beta(\theta)$.

Since the losses depend on the path length through which the light passes in the medium, the unit of a, b and c is m^{-1}. It should be noted that in this treatment the transmitted light is not counted with the scattered proportion, that is scattering is taken to be zero for a scattering angle $\theta=\pi$. The values of a, b and c depend on the number N of particles in the sample volume V and, moreover, on their geometrical cross-section s. The following relationship with the efficiency factors applies (Morel and Bricaud 1981):

$$a = \frac{N}{V} s Q_a \,,\; b = \frac{N}{V} s Q_b \,,\; c = \frac{N}{V} s Q_c \,. \qquad (3.14)$$

The particles which absorb or scatter the light are not of identical size in practice but have a particle size distribution

$$F(d) = \frac{1}{V} \frac{dN}{dd} \,. \qquad (3.15)$$

$V \cdot F(d)\, dd$ is here the number of particles in the volume V which have a size $d \pm \frac{1}{2} dd$, d for spherical particles being related to s by $s = \pi d^2/4$. Obviously, $N = \int_0^\infty V\, F(d)\, dd$. The integral

$$f = \int_0^\infty F(d) \frac{\pi d^2}{4} \, dd \qquad (3.16)$$

is the projected area of the N particles in the sample volume. If all particles are the same size,

$$f = \frac{\pi d^2}{4} \frac{N}{V} = \frac{3N}{2d} \frac{V_0}{V} = f_0 \frac{3}{2d} \,. \qquad (3.16a)$$

$V_0 = \pi d^3/6$ is the particle volume,

$$f_0 = N \frac{V_0}{V} \qquad (3.17)$$

is the "dilution factor" (Sathyendranath et al. 1987) or *"biomass concentration"* (Morel and Bricaud 1981). f has the dimension m^{-1} and links the measured values a, b and c with the efficiency factors:

$$a = f \bar{Q}_a \,,\; b = f \bar{Q}_b \,,\; c = f \bar{Q}_c \,. \qquad (3.18)$$

The bar denotes that these are averaged values. If all the particles are the same size, $\bar{Q} = Q$. The consistent definitions $\bar{Q}_a$, $\bar{Q}_b$ and $\bar{Q}_c$, therefore result from

comparison of Equation (3.18) with (3.14). For example, the following is obtained for $\bar{Q}_a$ from

$$a = \frac{N}{V}\frac{\pi d^2}{4} Q_a = \int_0^\infty \frac{V\,F(d)\,dd}{V}\frac{\pi d^2}{4} Q_a(d) = \int_0^\infty Q_a(d)\frac{\pi d^2}{4} F(d)dd \equiv f\,\bar{Q}_a :$$

$$\bar{Q}_a = \frac{1}{f}\int_0^\infty Q_a(d)\,\frac{\pi d^2}{4}\,F(d)\,dd\,, \tag{3.19}$$

see Bricaud and Morel (1986). $\bar{Q}_b$ and $\bar{Q}_c$, are defined similarly. Since the chlorophyll concentration C is the most important parameter for most hydrographic questions, a, b and c are frequently normalized to a concentration of 1 mg of chlorophyll per m^3 of water*. The normalized values are given an asterisk:

$$a^* = \frac{a}{C}\,,\quad b^* = \frac{b}{C}\,,\quad c^* = \frac{c}{C}\,. \tag{3.20}$$

In order to calculate the absorption and scattering characteristics for an individual particle, the *intracellular* chlorophyll concentration c_i is the governing factor instead of C:

$$a^*_{cm} = \frac{a_{cm}}{c_i}\,,\quad b^*_{cm} = \frac{b_{cm}}{c_i}\,,\quad c^*_{cm} = \frac{c_{cm}}{c_i}\,. \tag{3.20a}$$

The subscript *cm* stands for "cell matter". For a single particle, $f_0 = 1$ and $\bar{Q} = Q$, and it thus follows from (3.18) that:

$$a^*_{cm} = \frac{3}{2}\frac{Q_a}{c_i\,d}\,,\quad b^*_{cm} = \frac{3}{2}\frac{Q_b}{c_i\,d}\,,\quad c^*_{cm} = \frac{3}{2}\frac{Q_c}{c_i\,d}\,. \tag{3.20b}$$

In general the spectra (3.20) differ from the spectra (3.20a) since the optical inhomogeneities in the suspension lead to a flattening of the spectrum, as was explained in Section 3.1.4. The spectra (3.20a), in

---

* In optical remote sensing, C is frequently the sum of the concentrations of chlorophyll a and pheophytin a.

contrast, apply to an individual particle, where it is assumed that the pigments are homogeneously distributed in the interior. Because of this homogeneous pigmentation, the transition from (3.20) to (3.20a) denotes the transition from suspension to solution. In other words, Equations (3.20a) and (3.20b) apply to the limit case that the diameter of the cell in which the pigments are enclosed is zero ($d \to 0$), see Morel and Bricaud (1981).

If the chlorophyll concentration C in the sample volume V, the particle number N and the particle size d are known, c_i may be calculated: the volume of all N particles is NV_0. The chlorophyll is concentrated in this volume; it has the mass $c_i \cdot NV_0 = C \cdot V$, therefore

$$c_i = C \frac{V}{NV_0} = \frac{C}{f_0} . \tag{3.21}$$

When light is measured, a radiant flux is detected, generally as a function of wavelength λ. It is termed *radiant intensity* I if it is given in the units W sr^{-1} nm^{-1}, that is when the flux relates to the solid angle covered by the instrument. I_0 is the intensity of the light beam impinging on the medium, I_1 is the intensity of the transmitted beam after passing through the path length z and $I_2(\theta)$ is the intensity of the light beam at an angle θ to the incident direction (see Figure 3.5). The defining equation for the attenuation coefficient below then follows from the Lambert-Beer law $I_1 = I_0 e^{-cz}$:

$$c = \frac{1}{z} \ln \frac{I_0}{I_1} . \tag{3.22}$$

In order to determine the attenuation coefficient, the radiant intensities I_0 and I_1 must be measured and inserted into the ratio. The logarithm to base ten of this ratio is generally termed *absorbance* or *optical density* (O.D.). In older literature especially, optical density is frequently given instead of attenuation. The

conversion formula is as follows:

$$c = \frac{\ln 10}{z} O.D., \quad O.D. = \log_{10} \frac{I_0}{I_1}.$$

Since no scattered light must be included in the measurement of I_1, the detector must detect the light beam I_1 free from divergence. In practice, this can only be realized as an approximation by mounting a baffle in front of the detector. Bricaud et al. (1983) estimate the unavoidable proportion of scattered light detected in their laboratory setup in the measurement of attenuation by algal cultures to be 5%, although the divergence is only 0.25°. The reason for this is the highly marked forward-scattering of the algae.

In an absorption measurement, all of the scattered light must be included in the detection. This is achieved by measuring the sample in an integrating sphere. Light reflected at the interior wall of the sphere also then arrives at the detector, that is the proportion b of Figure 3.5 is virtually zero. Because $c = a + b \approx a$, a measurement then gives the absorption coefficient a by Equation (3.22).

Quantitative description of the scattered light requires definition of a variable which indicates what fraction of the incident light is deflected in direction θ by scattering at a volume dV. This variable is termed *volume scattering function* $\beta(\theta)$, and its definition is

$$\beta(\theta) = \frac{dI_2(\theta)}{E_d \, dV}. \qquad (3.23)$$

In this definition, the incident light is described by the irradiance E_d (for definition see Equation 2.1) which has the units W m^{-2} nm^{-1}. $\beta(\theta)$ thus has the units m^{-1} sr^{-1}. The integral of $\beta(\theta)$ over all solid angles is obviously the fraction of the incident light which is not absorbed

in the sample, that is the volume scattering coefficient:

$$b = \int_{\phi=0}^{2\pi} \int_{\theta=0}^{\pi} \beta(\theta) \sin\theta \, d\theta \, d\phi = 2\pi \int_{0}^{\pi} \beta(\theta) \sin\theta \, d\theta. \qquad (3.24)$$

There are thus two methods of determining b: measurement of $\beta(\theta)$ for all scattering angles θ in order to calculate b therefrom by (3.24) (direct method), or measurement of a and c, since the difference c-a likewise gives b (indirect method). For remote sensing especially, the light scattered back into the upper hemisphere is of great importance. It is described by the *backscattering coefficient*

$$b_b = 2\pi \int_{0}^{\pi/2} \beta(\theta) \sin\theta \, d\theta \qquad (3.25)$$

The physical quantities a, b, b_b, c and $\beta(\theta)$ are termed, in accordance with Preisendorfer (1961, 1976) *inherent optical properties*, IOP. They are properties of the material and independent of the intensity and direction of the incident light, in contrast to the *apparent optical properties*, AOP.

A further important optical parameter is the refractive index n (real part). It is conventionally determined by the immersion method (Hodgson and Newkirk 1975), in which the substance to be examined is introduced into a surrounding medium of known refractive index. A mixture of two liquids having different refractive indexes is chosen as the surrounding medium so that the refractive index may easily be altered by changing the mixing ratio. If the refractive indexes of the surrounding medium and the substance to be examined are identical, the substance is transparent. However, for algal cells, reliable results are not obtained because the refractive index of the cell wall differs from that of the cell interior. The mean refractive index measured cannot be used for a correct calculation of the scattering behaviour (Bricaud and Morel 1986).

Determination of $n(\lambda)$ from $c_{cm}(\lambda)$. If the spectra $a_{cm}(\lambda)$ and $c_{cm}(\lambda)$ and the particle size d are known, the function $n(\lambda)$ may be calculated. With $c_{cm} = c_i \cdot c^*_{cm}$, from Equation (3.20b) the "experimental" function $Q_c^{exp}(\lambda) = 2dc_{cm}/3$ is calculated. By varying $n(\lambda)$, the "theoretical" function $Q_c^{th}(\lambda)$ is fitted to this "experimental" function; the calculation of the theoretical function from Equation (3.11b) includes the variables $\rho(\lambda)$ and $\xi(\lambda)$ which, apart from d only depend on the complex refractive index. The imaginary part $n'(\lambda)$ can be calculated via (3.7) from $a_{cm}(\lambda)$; the real part is the function which is wanted. In the program BRECH $n(\lambda)$ is determined by successive approximation: since n for algal cells is always in the range from 1 to 1.5, a test is made, for each λ, of at which of the values 1, $1+\Delta$, $1+2\Delta$,..., 1.5 of n (the increment Δ is, e.g. 0.05), the value $Q_c^{th}(\lambda)$ best agrees with $Q_c^{exp}(\lambda)$. The spectrum $n(\lambda)$ is obtained in this way with the accuracy Δ. If the interval $n(\lambda) - \Delta \ldots n(\lambda)+\Delta$ is examined in the subsequent step for each λ with an increment $\Delta' < \Delta$, this step gives $n(\lambda)$ at the higher accuracy Δ'. By successive diminution of the increment, $n(\lambda)$ may be obtained in this manner with any desired accuracy. This method was used to calculate the dashed line in Figure 3.8.

Calculation of $a_{cm}(\lambda)$. The absorption of an individual cell, $a_{cm}(\lambda)$, may be calculated from the absorption spectrum $a(\lambda)$ of the suspension if the particle diameter d and particle concentration N/V are known. d and N/V determine the dilution factor f (Equation 3.16a) which links the mean absorption cross-section $\bar{Q}_a(\lambda)$ to $a(\lambda)$. Mie theory describes the absorption cross-section by Equation (3.9). According to this, Q_a depends only on the dimensionless parameter $\rho' = a_{cm}d$. As is shown by Figure 3.3a, Q_a (ρ') is a monotonically increasing function. If

$\bar{Q}_a$ is identified with $Q_a(\rho')$, a unique value ρ' can therefore be given for each wavelength λ. The absorption spectrum of the individual cell is then $a_{cm}(\lambda) = \rho'(\lambda)/d$.

3.2.2 Modelling of scattering

The equations in the preceding section connect the parameters which can be measured directly with the optical properties of the water body and its constituents. They thus form the basis for analysis of optical measurements made on water. From the point of view of remote sensing, knowledge of the spectra $a(\lambda)$ and $b(\lambda)$ of the constituents is particularly necessary in order to determine their concentrations. As will be shown in the following sections, representative spectra may be found at most for absorption; virtually no measurements are available for the scattering behaviour of algae, and, moreover, it is much more sensitive than absorption to cell size. In practice, therefore, there is virtually always the problem when modelling the light backscattered from the water that although usable information is available to some extent on the absorption of the water constituents, there are no reliable scattering spectra. For this reason, a model was developed for estimating the scattering by the algae if the absorption spectrum is known. The additional information required is the mean particle size and the refractive index at a particular wavelength. In contrast to the model of Bricaud and Morel (1986), the particle size distribution does not need to be known, moreover, the time-consuming resolution of the absorption spectrum into individual absorption bands is dispensed with.

The model. The decisive reason why the scattering may be calculated if the absorption is known is that the same molecular parameters summarized by the complex refractive index are responsible for absorption and scattering. This has been explained in detail in Section 3.1. The real part of the complex refractive index determines the

scattering behaviour and the imaginary part determines the absorption behaviour. Appendix A gives a derivation of the Kramers-Kronig relations which permit the real part of a complex function to be calculated from the imaginary part and vice versa; these relations of highly general applicability also apply to the complex refractive index. Equation (A.4) is used to calculate the scattering. If the energy scale is converted to the length scale ($\omega = 2\pi c/\lambda$, $d\omega = -2\pi c\, d\lambda/\lambda^2$), the equation is as follows:

$$n(\lambda) = n(\lambda_0) + \frac{2}{\pi}(\lambda_0^2-\lambda^2)\, P \int_0^{\infty} \frac{\lambda'\, n'(\lambda')\, d\lambda'}{(\lambda^2-\lambda'^2)(\lambda_0^2-\lambda'^2)} . \qquad (3.26)$$

P is the principal value of the following integral, that is the contribution at the poles $\lambda'=\lambda$ and $\lambda'=\lambda_0$ is omitted. The spectrum $n(\lambda)$ can be calculated by (3.26) if, in addition to $n'(\lambda)$ the refractive index $n(\lambda_0)$ is known for a particular wavelength λ_0.

If $a_{cm}(\lambda)$ is known, $n'(\lambda)$ may be calculated immediately by Equation (3.7). It should be noted that a_{cm} is not a directly measured value, but one which can only be calculated from a measured spectrum $a(\lambda)$ on the basis of the dilution factor f_0.

When $n(\lambda)$ and $n'(\lambda)$ are known, the parameters ρ and ξ can be represented as a function of λ if the (mean) size d of the algal cells is known (Equations 3.10a, 3.12). Equation (3.11b) gives, from $\rho(\lambda)$ and $\xi(\lambda)$, the spectrum $Q_c(\lambda)$ and, from this by (3.18), $c(\lambda)$. $b(\lambda)$ is then the difference $c(\lambda) - a(\lambda)$.

If, instead of $n(\lambda_0)$ the value of b or c is known for a particular wavelength λ_0, the spectrum $b(\lambda)$ or $c(\lambda)$ may be calculated by first using an estimated value $n(\lambda_0)$ in

the calculation of $n(\lambda)$. The spectrum $b(\lambda)$ or $c(\lambda)$ is then computed and the value at λ_0 is compared with the known value. If they differ, $n(\lambda_0)$ is modified and the calculation performed again. This is repeated until satisfactory agreement is obtained.

Discussion of Equation (3.26). Equation (3.26) is a *subtracted* Kramers-Kronig relation (SKK), for which, in contrast to the "usual" KK relation (A.1), a value of $n(\lambda_0)$ must be known. If $n(\lambda)$ is computed by (A.1) for phytoplankton cells, $n(\lambda)\approx 1$ is obtained, more precisely in the blue $n<1$ and in the red $n>1$. If this function $n(\lambda)$ is used to calculate $b(\lambda)$, the results do not agree at all with the measurements, since the scattering is highly sensitive to errors in n. The reason the "usual" KK relations lead to unusable results is that the phytoplankton absorption in the IR and UV is not known. It is therefore ignored in the integration. This missing quantity in the integral is the difference from the correct value of n. Using the SKK relation, $n(\lambda)$ is calculated relative to the value $n(\lambda_0)$, as a result of which the result is more correct. As has been shown by Ahrenkiel (1971), the unavoidable error at the limits of the measurement range can be tolerated when the SKK relations are used (compare this with the discussion on Figure 3.12).

Apart from $n'(\lambda)$, Equation (3.26) depends on two parameters: λ_0 and $n(\lambda_0)$. $n(\lambda_0)$ is simply an additive constant to the function $n(\lambda)$; the effect of λ_0 on the function $n(\lambda)$ is not directly observable. It is only obvious that the function $n(\lambda)-n(\lambda_0)$ is zero at $\lambda=\lambda_0$. This is *de facto* the only influence of λ_0 as can be shown by testing: conversion from λ_0 to $c\cdot\lambda_0$ only shifts passage through zero of $n(\lambda)-n(\lambda_0)$; the spectrum is independent of λ_0. Since it is required that n is known

at the wavelength λ_0 or at $c \cdot \lambda_0$, this proves that the choice of λ_0 does not influence the result of $n(\lambda)$.

Illustration of the model. An illustration is given with the aid of Figures 3.6 to 3.11 of how the scattering spectrum is obtained from the absorption spectrum. To test the calculations, measurements published by Bricaud and Morel are used; I know of no other data set which would be as suitable for this purpose.

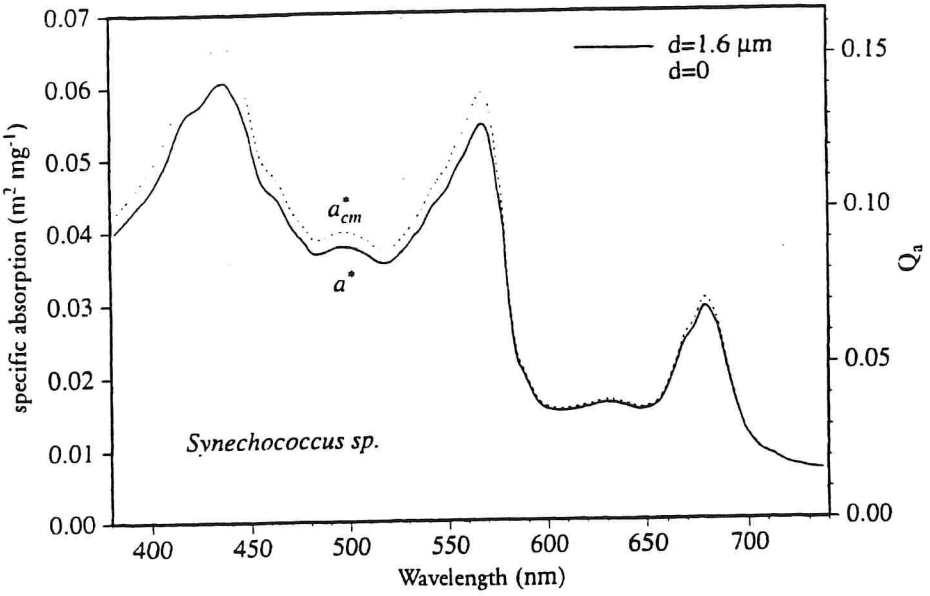

Figure 3.6: Specific absorption of a blue-green alga. Continuous line: measurement of Bricaud et al. (1988), dashed line: extrapolation to $d \to 0$.

Figure 3.6 shows the absorption spectrum for the blue-green alga *Synechococcus sp.*, type WH 8018. The spectrum is taken from the article by Bricaud et al. (1988). It was enlarged by a photocopier and then digitized with the aid of a digitizing tablet; these points were interpolated by a cubic spline and stored at intervals of 1 nm. Bricaud et al. report the following additional information on the algal culture: $d = 1.6\ \mu m$, $c_i = 2.20\ kg\ m^{-3}$, $C = 88.5\ mg\ m^{-3}$. The following may be calculated therefrom: $N/V = 1.88 \cdot 10^{13}\ m^{-3}$, $f_0 = 4.02 \cdot 10^{-5}$, $f = 37.7\ m^{-1}$; in addition, the spectrum $Q_a(\lambda)$ is obtained from Equation (3.20b) (right y-axis of Figure 3.6). The dashed curve

represents the extrapolation of the absorption spectrum for $d \to 0$ described at the end of Section 3.2.1, that is the spectrum $a^*_{cm}(\lambda)$.

The imaginary part $n'(\lambda)$ of the complex refractive index can be calculated by Equation (3.7) from the absorption spectrum $a_{cm}(\lambda) = c_i \cdot a^*_{cm}(\lambda)$. It is depicted in Figure 3.7.

In order to be able to calculate the refractive index $n(\lambda)$ from the function $n'(\lambda)$ of Figure 3.7, the value of n must be known for a particular wavelength λ_0. In the article by Bricaud and Morel where the optical measurements made on *Synechococcus sp.* are published, although an estimation of the refractive index can be found (n = 1.038), the associated wavelength is not reported. Moreover, the value was not determined by measurement, but n was optimized as a free parameter in a model for calculating $Q_c(\lambda)$, by adjusting the calculated function $Q_c(\lambda)$ to the measured function. For these reasons, the refractive index reported there is not usable as a reference value $n(\lambda_0)$.

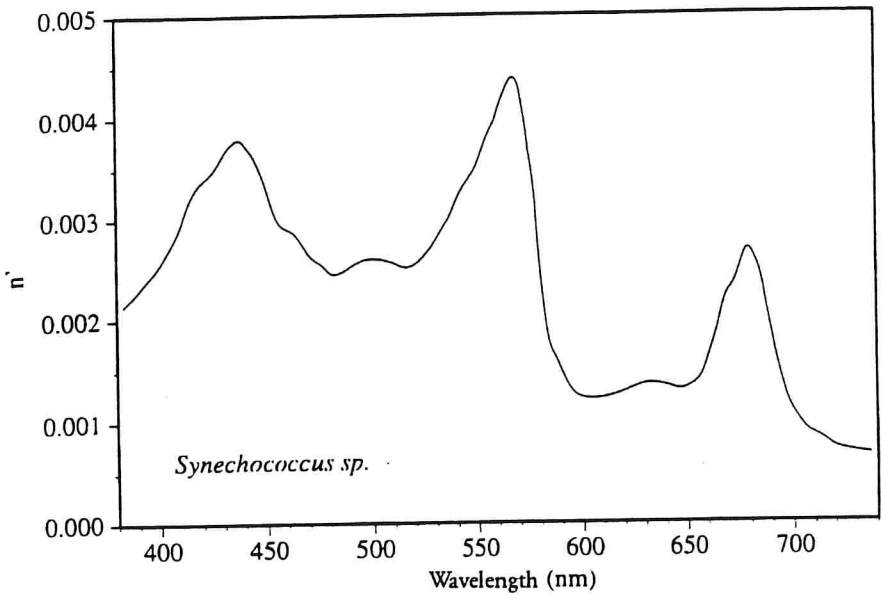

Figure 3.7: The imaginary part of the complex refractive index. Calculated from the data of Figure 3.6.

As was explained at the end of Section 3.2.1, $n(\lambda)$ may be calculated from the spectrum $c_{cm}(\lambda)$. Now, although the purpose of the model is to calculate this spectrum, so that if $c_{cm}(\lambda)$ is known, the model is not required at all, the use of $c_{cm}(\lambda)$ is justified here since the function is used to determine the value of n which could also be determined by a direct measurement. The dotted line in Figure 3.8 is the result of the calculation.

Obviously, the range of values of $n(\lambda)$ is close to the value 1.038 reported by Bricaud and Morel. A single value $n(\lambda_0)$ is used from the calculated spectrum $n(\lambda)$ as a reference value for Equation (3.26). λ_0 = 531 nm was chosen.

Using the value n(531) = 1.0344, the function $n(\lambda)$ was then calculated from the spectrum $n'(\lambda)$ of Figure 3.7 by Equation (3.26). This is the continuous line in Figure 3.8. The differences between the two lines of Figure 3.8 are discussed later. It should be noted that the values of n-1 are above the values of n'. In accordance with Figure 3.2, this means that the algal cells absorb more strongly in the UV than in the visible.

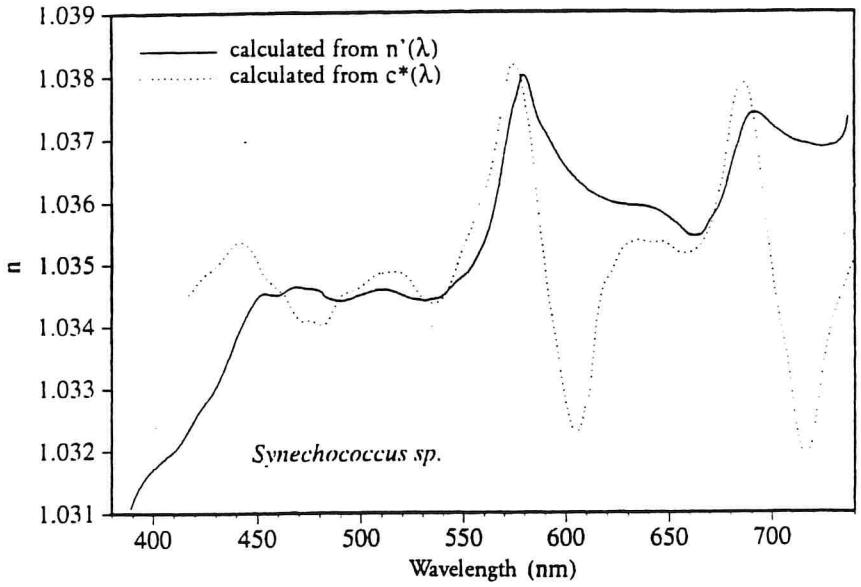

Figure 3.8: The refractive index n(λ). Continuous line: calculated from n'(λ) of Figure 3.7 with the aid of the Kramers-Kronig relation (3.26); dotted line: calculated from $c^*(\lambda)$ of Figure 3.11.

Unfortunately, it is not possible to compare n(λ) with measurements directly since I do not know of any spectrally resolved measurements of n. Virtually no measurements can be found in the literature on the refractive index of algal cells and the published values always relate to a single wavelength or have been averaged over a wide spectral range. In addition, Bricaud and Morel (1986) doubt that these measurements can be used to calculate scattering. I know of only one diagram showing the spectral course of n for algal cells, that is the curve shown as a dashed line in Figure 3.12. It is taken from the article by Bricaud and Morel (1986) and is the result of a model calculation.

Using Equation (3.10a), the function ρ(λ) results from the refractive index. It is shown in Figure 3.9. The values of ρ are between 0.6 and 1.1 and are thus in a range for which $Q_c(\lambda)$ is only slightly dependent on the refractive index and on the particle size distribution,

as comparison with Figure 3.3b shows. Moreover, for this range, $Q_c \sim \rho \sim \lambda^{-1}$. Therefore, on the basis of Figure 3.9, the statement that $Q_c(\lambda)$ has roughly the wavelength dependency λ^{-1} may be considered valid. The difference between n' and n-1 quantifies the function $\xi(\lambda)$ which is defined by Equation (3.12). A typical spectrum may be seen in Figure 3.10 as exemplified by *Synechococcus sp.*. Since n-1 varies about the mean by at most ± 10%, n' defines the spectrum of ξ; $\xi(\lambda)$ therefore resembles $n'(\lambda)$.

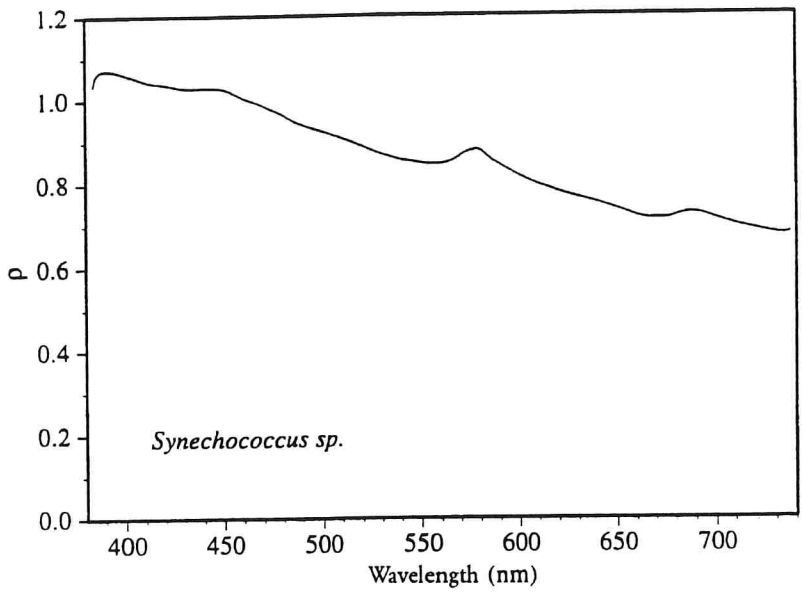

Figure 3.9: The function $\rho(\lambda)$.

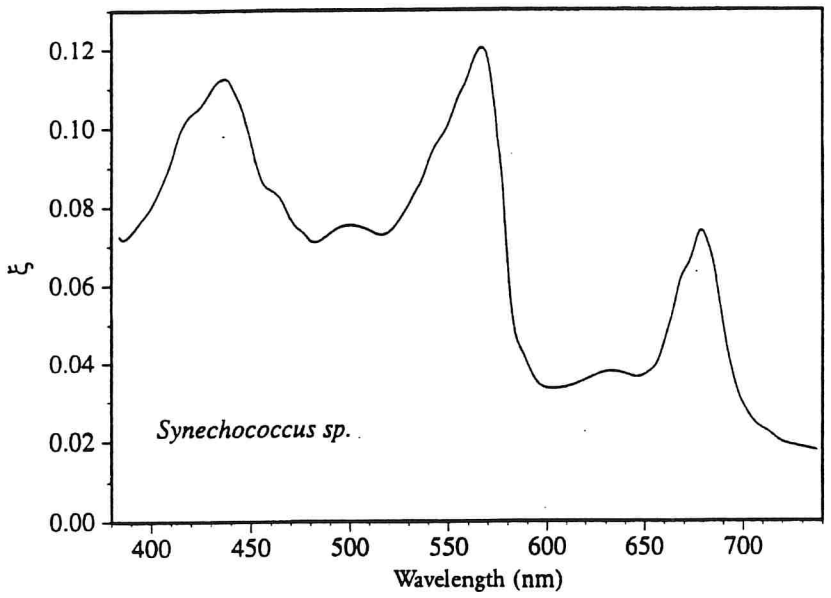

Figure 3.10: The function $\xi(\lambda)$.

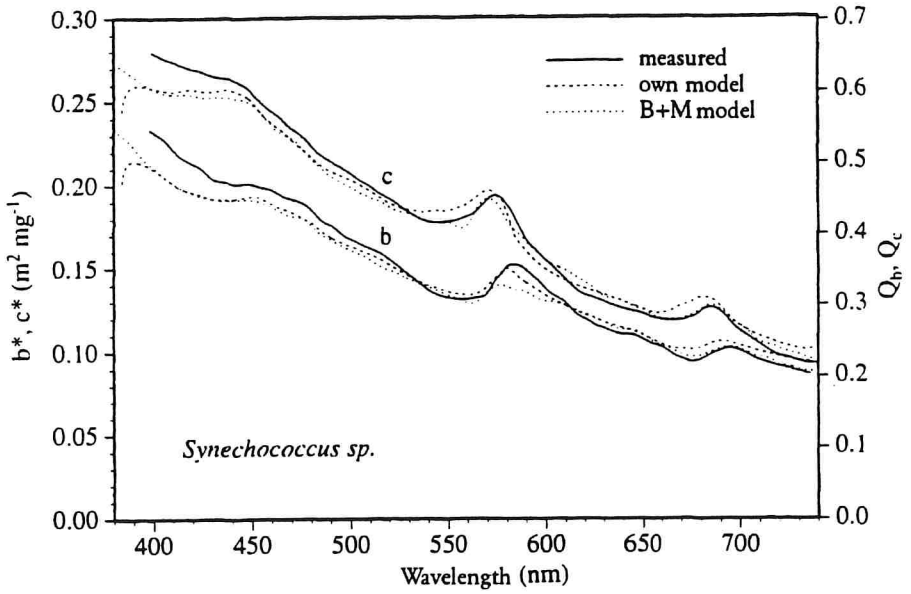

Figure 3.11: Attenuation c and scattering b.

Figure 3.11 shows the result of the modelling. The attenuation c was calculated from $\rho(\lambda)$ and $\xi(\lambda)$ by Equation (3.11b), and the scattering b is the difference between attenuation and absorption. As in Figure 3.6, the specific coefficients of attenuation or scattering are plotted on the left ordinate and the efficiency factors are plotted on the right ordinate. Conversion was carried out by Equation (3.20b).

Obviously, the measured spectrum was approximated very well by the model. The quality of the agreement is similar to that for the model of Bricaud and Morel.

Comparison with the Bricaud and Morel model. The model presented here is partially based on considerations published by Bricaud and Morel in various articles. In their article of 1986, they summarize their findings in a model with which the efficiency factors for attenuation, scattering and backscattering by homogeneous spherical particles in suspension may be calculated, if the particle size distribution, the absorption spectrum and the refractive index (real part) are known. The present model differs from this in several details. The two most important differences are as follows:

- the particle size distribution does not need to be known,
- calculation of the refractive index spectrum is significantly simplified.

Bricaud and Morel use the particle size distribution to extrapolate the absorption spectrum to the solution ($d \to 0$). This is important for establishing a database of absorption spectra (if the cell size of a species is variable, the absorption spectrum may be calculated for any d), but is not necessary for calculation of the scattering behaviour. In calculation of the scattering, they must return from the solution to the suspension, in which case they once more require the particle size distribution. In this step, they reverse the extrapolation $d \to 0$, so this can be avoided.

The reason why the extrapolation to $d = 0$ is necessary in the Bricaud and Morel model is the method by which $n(\lambda)$ is calculated from $n'(\lambda)$: the curve $n'(\lambda)$ is split into several individual lines using an equation similar to (3.4b). The result of this splitting is 3L line shape parameters (L = 9 = number of lines) which also determine

the spectrum of $n(\lambda)$. $n(\lambda)$ is calculated by an equation similar to (3.4a); it is the sum of L = 9 curves $n_i(\lambda)$ for the individual absorption bands. This method assumes that n and n' are additive values - this only applies if the absorption follows the Lambert-Beer law. As was discussed in Section 3.1.4, this precondition is not fulfilled with algal cells (keyword "package effect"), but is fulfilled at any rate in the limit case $d \to 0$ (compare this with Figure 3.3a).

For the conversion of $n'(\lambda)$ to $n(\lambda)$ with the aid of the Kramers-Kronig relations, the validity of the Lambert-Beer law is irrelevant, since the absorption is not subdivided into individual absorbers. The information which the absorption spectrum implicitly contains on the particle size distribution is also further contained in the spectrum $n(\lambda)$. The Kramers-Kronig relations thus have three great advantages:

- they make extrapolation of the absorption from the suspension to the solution superfluous,
- they do not require modelling of $n'(\lambda)$ which experience has shown to be time-consuming, since suitable initial values for the line-shape parameters must first be found,
- they utilize the information on the particle size distribution contained in the absorption spectrum (or in $n'(\lambda)$).

Figure 3.12 confirms that use of the Kramers-Kronig relations gives the same result as the modelling used by Bricaud and Morel. This figure shows the refractive index for the green alga *Platymonas suecica*. The two curves were calculated from the same spectrum $n'(\lambda)$ which is shown in the article by Bricaud and Morel (1986): the dashed line is Bricaud and Morel's result and the

continuous line was calculated from $n'(\lambda)$ by Equation (3.26); $n(500) = 1.079$ was used for both calculations. The same result is obviously obtained by using the Kramers-Kronig relations, and with significantly less effort. The slight difference is probably due to inaccuracy in digitizing the published spectra. The curves only differ markedly at the limits of the measurement range, since Bricaud and Morel extrapolate $n'(\lambda)$ beyond the measurement range, while the KK calculation was carried out outside the measurement range using $n'(\lambda) = 0$. If the KK calculation had been carried out with the same extrapolation, a very similar graph would have been achieved even at the limits. The difference at the limits of the measurement range thus illustrates the errors which are caused by the unknown IR and UV absorption. This error is obviously tolerable if the interval for $n(\lambda)$ is decreased at both ends by about 50 nm with respect to the interval of $n'(\lambda)$ for the evaluation.

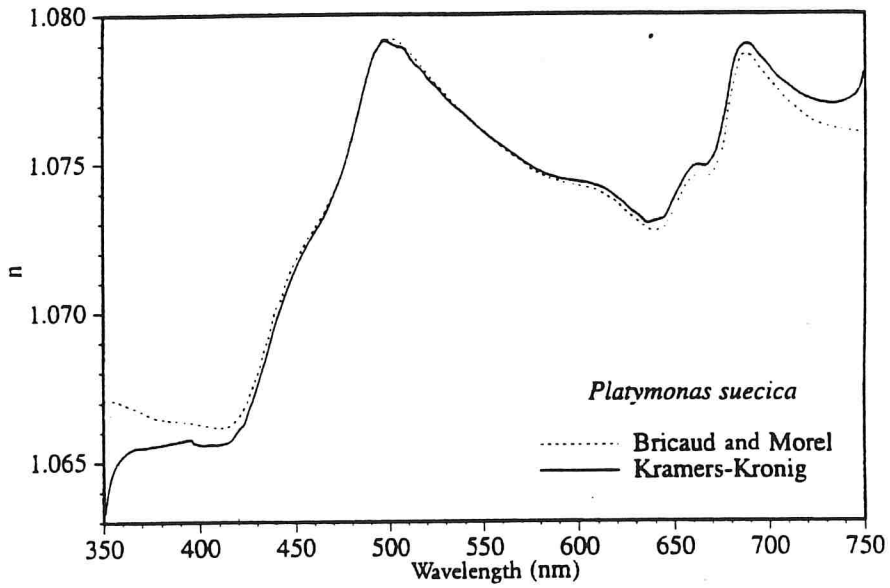

Figure 3.12: Comparison of two methods of calculating the refractive index $n(\lambda)$ from the function $n'(\lambda)$.

3.3 Pure water

The optical properties of pure water are not known

precisely in the visible and near UV. A model allowing correct calculation of absorption and scattering in this frequency region does not exist and experimental measurements are very difficult; see Morel (1974) for instance.

Absorption. Figure 3.13 illustrates the magnitude of the uncertainties regarding the absorption spectrum of pure water. The figure is taken from the review article by Smith and Baker (1981) and compares the most reliable measurements. For $\lambda > 600$ nm, the measurements agree well (the deviations are 10%), but for $\lambda < 600$ nm they differ considerably (by up to an order of magnitude!).

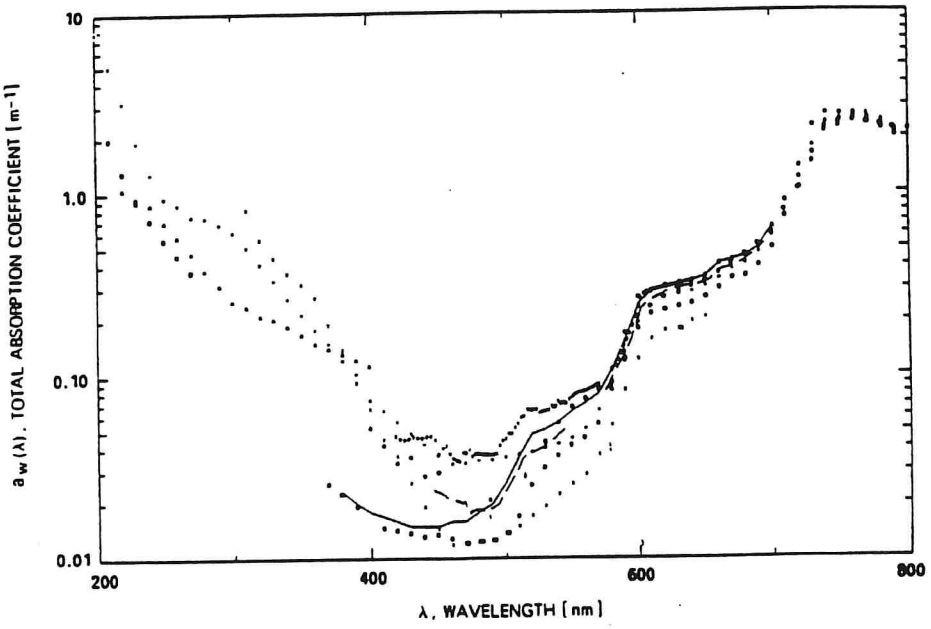

Figure 3.13: Absorption by pure water. Compilation of the most reliable measurements. From Smith and Baker (1981).

In addition to experimental error - water purity, suppression of scattered light - the temperature dependence of the absorption coefficient is responsible for these differences. Figure 3.14 underlines the importance of water temperature.

In their article, Smith and Baker (1981) derive a consistent absorption spectrum from a great number of laboratory measurements of absorption and *in situ*

measurements of attenuation. In slightly amended form, this is used in the present work, see Section 4.2.1. It essentially corresponds to the continuous line in Figure 3.13 which relates to the measurements by Morel and Prieur (1977). Smith and Baker estimate the accuracy to be +25% to -5% for $300 < \lambda < 480$ nm and +10% to -15% for $480 < \lambda < 800$ nm.

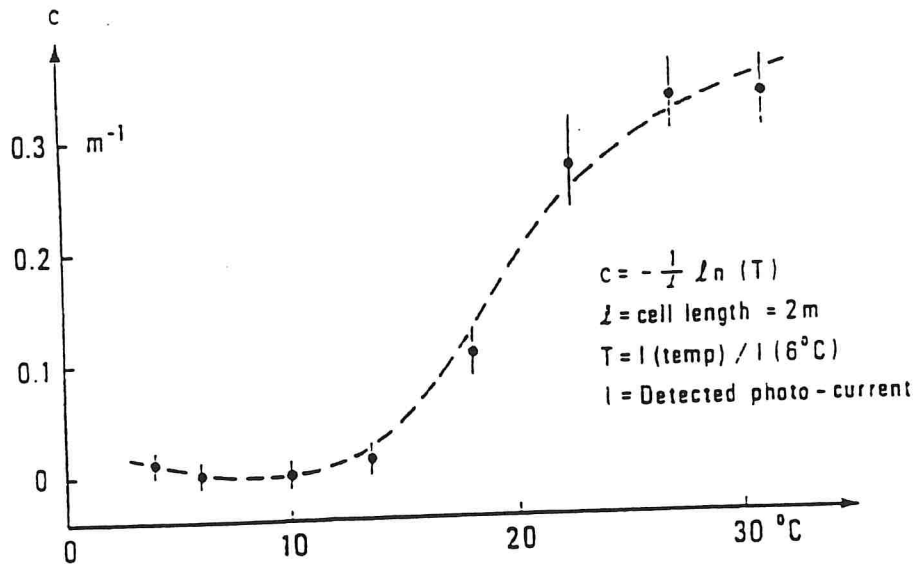

Figure 3.14: Temperature dependence of attenuation by water (400-600 nm). From Højerslev and Traberg (1990).

Water absorbs very strongly at $\lambda < 200$ nm and $\lambda > 700$ nm, therefore absorption measurements are simpler to carry out in these ranges and thus more precise, moreover useful models are available in this case: electronic transitions of the water molecule lead to absorption bands in the far UV; the vibration resonance frequencies (Raman levels) of isolated and coupled water molecules are the causes of the IR absorption. Figure 3.15 shows the absorption from 10^{-12} m to 10^{-4} m.

Scattering. In comparison with the absorption, scattering is negligible apart from in the region 400 to 500 nm (Morel 1974). However, since it is precisely this region which is of great importance for the detection of water constituents, a discussion of scattering by water is

necessary.

Whereas no model exists for absorption by water in the visible, there is a model for the scattering. It originates from Smoluchowski (1908) and Einstein (1910) and is known under the name *fluctuation theory*.

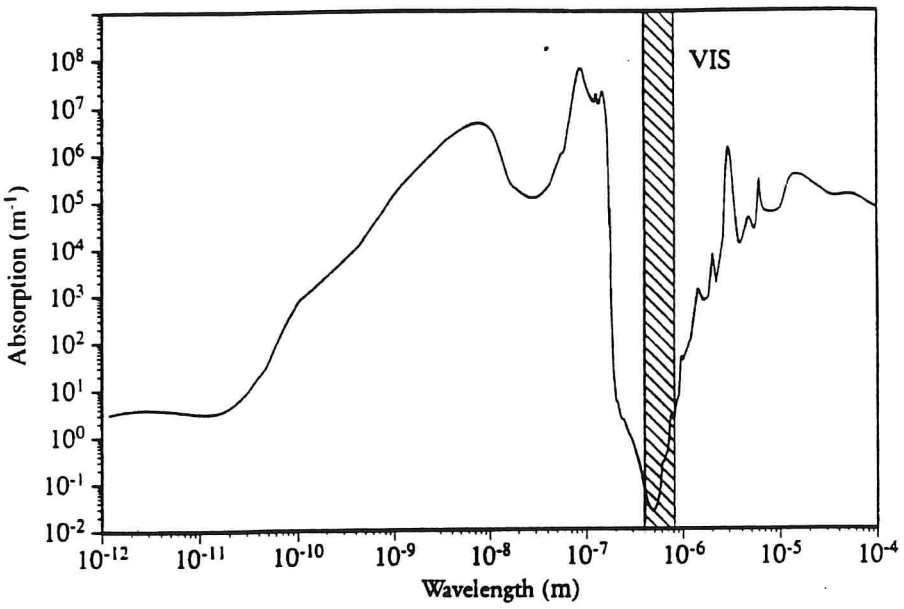

Figure 3.15: Absorption by pure water. From data by Hale and Querry (1973).

According to this model, density fluctuations cause light scattering in liquids. The following equation is obtained for the volume scattering function (Morel 1974):

$$\beta(\theta) = \frac{2\pi^2}{\lambda^4} kT\, n^2 \frac{1}{\eta} \left(\frac{\partial n}{\partial P}\right)_T^2 \frac{6+6\delta}{6-7\delta} \left(1 + \frac{1-\delta}{1+\delta} \cos^2\theta\right)$$

θ = scattering angle, k = Boltzmann constant, T = temperature in Kelvin, n = refractive index, η = isothermal compressibility, P = pressure. $\delta = I_{\parallel}(90)/I_{\perp}(90)$ is the proportion of unpolarized light for a scattering of 90°. The wavelength dependency of β does not exactly follow a λ^{-4} law, since n and δ are wavelength dependent.

Many liquids are correctly described by the model, but in the case of water, the experimental observations of the pressure and temperature dependency do not agree with the model predictions. Therefore, the analytical model is replaced by a semi-empirical one in which the experimental results are used instead of theoretical dependencies.

Morel has compiled all measurements of the volume scattering function $\beta(90)$ made after 1954, see Table 3.1.

λ(nm)	$\beta(90)$ for pure water in 10^{-4} m^{-1}									
366	6.80					4.53				5.63
405	4.05					2.90				3.63
436	2.89	2.95	2.86	2.45	2.32	2.12	2.54		2.82	2.64
546	1.05	1.13	1.07	1.08	0.86	0.83	1.08	1.10	1.16	1.00
578						0.66				0.78

Table 3.1: Experimental data of the pure water volumetric scattering function. From Morel (1974). The individual columns are measurements made by different experimenters, the last column contains values from Equation (3.27) for a proportionality constant of $6.68 \cdot 10^7$. The temperature range is from 18°C to 25°C.

As can be seen, the data set is not very extensive. It contains measurements made at only 5 wavelengths and they are markedly scattered. Morel fitted the data of Table 3.1 using a power law for the wavelength dependency. The result is as follows:

$$\beta(90) \sim \lambda^{-4.32}. \qquad (3.27)$$

Scattering by water in the visible is therefore approximately Rayleigh scattering. In practice, the volumetric scattering coefficient b is more important than $\beta(90)$. According to Morel (1974), for water, $b = 16.0 \cdot \beta(90)$. The scattering by water is thus described by the following equation:

$$b_w(\lambda) = b_w(\lambda_0)\,(\frac{\lambda}{\lambda_0})^{-4.32}. \qquad (3.28)$$

For pure water, Morel reports the value $b_w(500) = 0.00222\ m^{-1}$ at $\lambda_0 = 500$ nm; for sea water having a salinity of 3.5 - 3.8%, the scattering is higher by the factor 1.30, that is $b_w(500) = 0.00288\ m^{-1}$.

Equation (3.28) is generally used to describe the spectrum of the volume scattering function of water. It should be noted that according to the fluctuation theory, a wavelength dependency $\lambda^{-4} \cdot f(\lambda)$ is expected, $f(\lambda)$ not being a power of λ. Equation (3.28) therefore only represents an approximation obtained from a limited data set. One should be aware of this especially when extrapolating beyond the spectral range of Table 3.1.

3.4 Important pigments

The optical properties of a body of water are determined by the constituents which scatter or absorb light. The particles which only contribute to light scattering are inorganic substances. Sediments, in particular which are introduced into a body of water by rivers or which are swirled up by currents lead to a high proportion of scattered light in many waters.* Its spectrum can be calculated approximately if the particle size distribution is known. This has already been described in Section 3.1.4; no further discussion will be given here. In addition to the sediments, skeletons and wall deposits of calcium carbonate or silica present in many phytoplankton species (for example in diatoms) also scatter light. Increased light scattering is expressed as

* No information is available on the sediments suspended at the measuring point in Lake Constance. Their concentration is apparently low: the measuring point is situated far from currents which can transport sediments. If they were present at a detectable concentration they would be detected during filtration of the water samples routinely carried out for pigment determination.

a higher refractive index for these species.

All other substances which not only scatter but also absorb light are termed *pigments*. These may be divided into two groups: pigments which are dissolved or suspended in the water and pigments which are constituents of algal cells. The first group is chemically highly heterogeneous, but it shows a uniform absorption behaviour and is therefore not subdivided further for optical studies. These so-called *yellow substances* are discussed in Section 3.4.1. Table 3.2 gives a survey of the second group, the algal pigments. Although these molecules are chemically similar, their optical properties differ. They are discussed in Sections 3.4.2 to 3.4.6.

	Cyanophyceae	Rhodophyceae	Chrysophyceae	Xanthophyceae	Bacillariophyceae	Phaeophyceae	Chloromonadophyceae	Haptophceae	Eustigmatophyceae	Cryptophceae	Dinophyceae	Euglenophyceae	Chlorophyceae	Prasinophyceae	Charophyceae
Chlorophyll a	⊕	⊕	⊕	⊕	⊕	⊕	⊕	⊕	⊕	⊕	⊕	⊕	⊕	⊕	⊕
Chlorophyll b												⊕	⊕	⊕	⊕
Chlorophyll c			⊕	⊕	⊕	⊕	⊕	⊕	⊕	⊕	⊕				
Phycocyanin	⊕	⊕								⊕					
Phycoerythrin	⊕	⊕								⊕					
α-carotene		±			±					⊕			±	±	
β-carotene	⊕	⊕	⊕	⊕	⊕	⊕	⊕	⊕	⊕	±	⊕	⊕	⊕	⊕	⊕
Alloxanthin										⊕					
Antheraxanthin	+	+				+			±				+	+	
Crocoxanthin										+					
β-Cryptoxanthin	+	+		+					+			+	+		
Diadinoxanthin			+	⊕	⊕	±	⊕	+			+	⊕			
Diatoxanthin		+	⊕	⊕	±	+	+	+	+	+	+	+			
Dinoxanthin							±				+				
Echinenone	⊕		+									+	+		
Fucoxanthin			⊕		⊕	⊕		⊕			±				
Heteroxanthin				⊕					+						
Isozeaxanthin	+														
Loroxanthin													+		
Lutein		⊕											⊕	⊕	⊕
Micronone														+	
Monadoxanthin										+					
Myxoxanthophyll	⊕														
Neoxanthin		+		+	+				+			+	⊕	+	+
Peridinin											⊕				
Siphonaxanthin													+	+	
Siphonein													+	+	
Vaucheriaxanthin				⊕					+						
Violaxanthin						⊕			⊕				⊕	+	+
Zeaxanthin	⊕	⊕				+			±			+	⊕	+	+

Table 3.2: Algal pigments. From van den Hoek (1984). ⊕ = important, + = occurs, ± = rare or occurs in small quantities.

3.4.1 Yellow substance

The death of plants or animals results in the formation of numerous organic molecules and small particles by bacterial degradation processes. These substances occur in all water bodies. Since at high concentration they colour the water yellow to brown, Kalle (1937) coined the German name *Gelbstoff* for them, the term which is frequently also used in English in addition to the term *yellow substance* (which is a direct translation).

Because of the importance which yellow substance has for water colour, the ESA commissioned a study in 1984 with the title "The Influence of Yellow Substance on Remote Sensing of Sea" (GKSS 1986b). This study combines all the important findings on yellow substance. In the discussion below, most of the references are to this study; figures in square brackets indicate the particular chapter referred to.

Because "yellow substance" is a collective description for a large number of different molecules and particles few of which have been chemically characterized [1], this pigment cannot be unambiguously defined. A pragmatic definition is made use of: yellow substance is all those constituents of water passing through a filter of pore size 0.45 μm [8]. However, for practical reasons a different pore size is frequently used, for example Reuter [8] recommends 0.2 μm filters for absorption measurements of yellow substance in order to remove relatively large light-scattering particles.

Yellow substance concentration can be measured most accurately by fluorescence [3], but long-term measurements confirm that the fluorescing constituents are not identical with the absorbing constituents [6]. For interpretation of the radiance or reflection measured by passive sensors determination of concentration via the absorption of the filtrate is therefore more suitable.

According to Nyquist (1979) the yellow substance concentration in mg/l is given by the equation

$$C_Y = \frac{a_Y(\lambda_0)}{0.212}\,, \tag{3.29}$$

where $a_Y(\lambda_0)$ is the absorption of the filtrate in m^{-1} at λ_0 = 450 nm. For Lake Constance, use of this equation underestimates the concentration by about half, see Section 5.3.2.

By definition, all the yellow substance particles are smaller than the wavelength of light; most yellow substance constituents are even considerably smaller. Its scattering behaviour is therefore described by Rayleigh scattering ($b \sim \lambda^{-4}$). Since the scattering coefficient is very small in relation to the absorption coefficient, light scattering by yellow substance can be ignored when describing the optical properties of a water body.

The absorption spectrum of yellow substance has a very characteristic shape: it can be approximated well by an exponential function which increases towards the blue [2, 3] (see also Figure 3.16):

$$a_Y(\lambda) = a_Y(\lambda_0)\, e^{-S(\lambda-\lambda_0)}\,. \tag{3.30}$$

While the constant $a_Y(\lambda_0)$ is proportional to the concentration, the constant S depends on the composition of the yellow substance. This changes with time (for example because of photochemical reactions [6]), and in addition it changes from water body to water body. Nevertheless, many measurements of S agree surprisingly well. For example, the following is given from the extensive data set measured and analysed by Bricaud et al. (1981):

$$S = 0.0140 \pm 0.0032\ nm^{-1}.$$

For this result, 105 water samples from the Atlantic, the

Baltic and the Mediterranean were evaluated, samples from the coastal region also being used which are polluted by industrial effluents. Roesler and Perry (1989) carried out a literature search and compiled the values for S from 16 publications. The result is as follows:

$$S = 0.016 \pm 0.002\ nm^{-1}.$$

The decrease in absorption towards the red is therefore generally defined by a uniform decay constant. However, there are also notable exceptions to this rule. Thus, for instance, Doerffer and Amann (1984, 1986) found values for S up to 0.035 nm^{-1} in the "patch" of an algal bloom of the species *Gyrodinium aureoleum*; outside the patch, the values were 0.0115 to 0.0150 nm^{-1}. Because of the high correlation of S (and $a_Y(\lambda_0)$) with the cell concentration, these measurements verify directly the formation of yellow substance in the sea.

More exact measurements show that the exponential course of the absorption spectrum of yellow substance is only approximately correct. Figure 3.16 shows the spectrum of the attenuation measured by Diehl and Haardt (1980) in the Eckernförde Bay of the Baltic. From 400 to 600 nm, the measurements can be fitted well by two exponential functions (discontinuity at 460 nm), and above 600 nm, three weak absorption bands are found. Measurements by Reuter et al. [3] show that the absorption of yellow substance above about 600 nm differs significantly in differing water bodies. However, in this spectral region yellow substance absorbs only slightly in comparison to water, therefore Equation (3.30) is a sufficient approximation in practice for all types of waters.

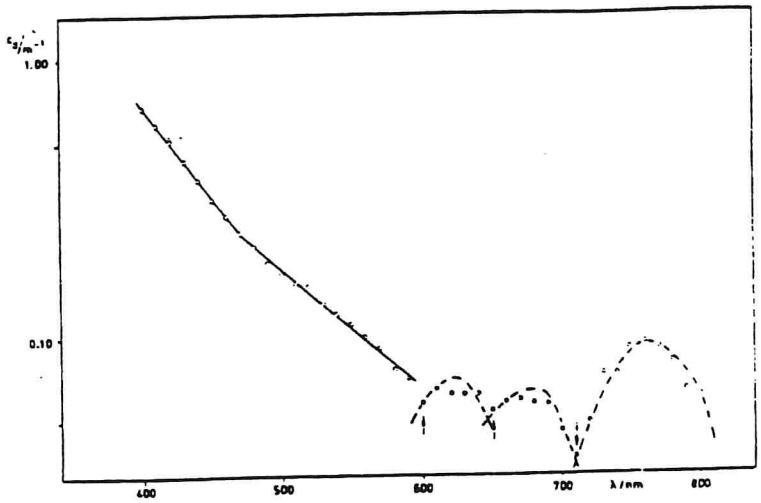

Figure 3.16: Attenuation of yellow substance. From Diehl and Haardt (1980). The ordinate has a logarithmic scale.

3.4.2 Chlorophylls

Chlorophyll a is the key molecule in photosynthesis, occurring in all photosynthetic organisms.* From Table 3.2, it can be seen that in addition to chlorophyll a, chlorophylls b and c also occur in phytoplankton, chlorophyll d has been found at high concentration hitherto in only one species (*Rhodocorton rothii*, class *Rhodophyceae)* (Strain 1958). Chlorophylls b, c and d can also absorb light and thus supply energy for photosynthesis, but only chlorophyll a participates in the so-called *primary processes* of photosynthesis which ultimately lead to the synthesis of high-energy molecules (NADPH).

Figure 3.17 shows the chemical structure of chlorophylls a and b. Chemically, chlorophylls are tetrapyrroles which can be derived from porphyrin. Chlorophyll a is a conjugated cyclic macromolecule having a planar "head" of four pyrrole rings. It is approximately 1.5·1.5 nm^2 in size. The head is esterified at ring IV via a vinyl group

*The only exception is photosynthetic bacteria in which bacteriochlorophyll forms the reaction centre. These primitive organisms are assumed to have arisen very early in evolution.

with phytol, a chain of about 2 nm in length which anchors the molecule in membranes. A magnesium atom which is bound in the centre of the molecule by two covalent and two complex bonds serves to coordinate the rings (Lawlor 1990).

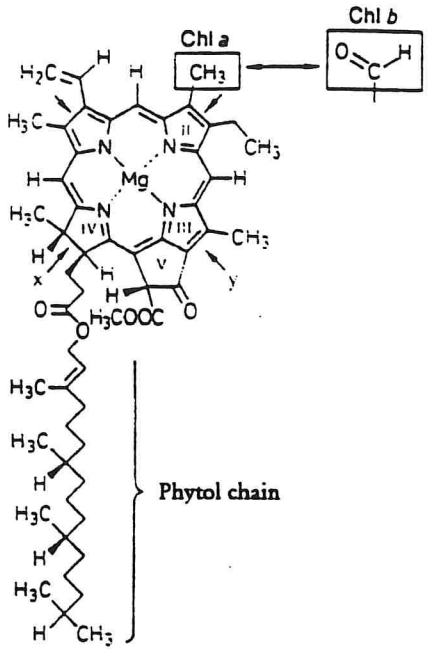

Figure 3.17: The chemical structure of chlorophylls. From Lawlor (1990).

Absorption. Light absorption takes place in the head of the chlorophyll molecule. As a result of the extended ring structure with ten double bonds, the electrons are delocalized over a large area so that the area for trapping a photon (absorption cross-section) is large. Since the resonance frequencies of the ring structure depend on the geometry, the dipole forces of the surroundings influence the wavelengths of the absorption maxima: if chlorophyll is in solution, the position and intensity of absorption depend on the polarity of the solvent (Lichtenthaler 1987); *in vivo*, the absorption properties are determined by a protein (Lawlor 1990).

Table 3.3 summarizes the absorption and fluorescence maxima of chlorophylls and phaeophytins in acetone and diethyl ether. The absorption spectra of the chlorophylls

are shown in Figure 3.18 for diethyl ether as solvent. Since chlorophylls c_1, c_2 and c_3 have similar absorption spectra they have not been further differentiated in the diagram. Chlorophylls absorb in the blue and in the red. Absorption in the red converts the molecule from the ground state to the first excited state (S_1), absorption in the blue converts it into the second excited state (*Soret band* S_2). Splitting states S_1 and S_2 into several vibrational states leads to the shoulders on the short-wave side of the absorption maxima.

The absorption spectra shown in Figure 3.18 are not *in vivo* spectra, since the absorption of individual pigments cannot be measured in an intact algal cell. However, for the interpretation of absorption spectra of intact algal cells it would be desirable to be able to define "representative" absorption spectra of the chlorophylls (and of the other pigments). This is not possible for two reasons:

1. In the algal cell, the chlorophylls have different functions. They therefore occur in differing protein surroundings so that the absorption properties of the individual molecules can differ.

	Acetone			Diethyl ether		
Chlorophyll a	430	660-663	*668*	428-430	660-662	*668*
Chlorophyll b	455	645-647	*652*	453-455	642-644	*648*
Chlorophyll c_1	442-444	630-631	*633*	438	625	*632*
Chlorophyll c_2	444-445	630-631	*635*	445-449	628-629	*632*
Phaeophytin a	410[1]	663[1]	*676*[1]	408-410	665-669	*673*
Phaeophytin b	433	657	*676*[1]	433-434	653-655	*661*

[1] 80%

Table 3.3: Absorption and fluorescence maxima of chlorophylls and phaeophytins in acetone and diethyl ether. Italics: fluorescence. From Rowan (1989).

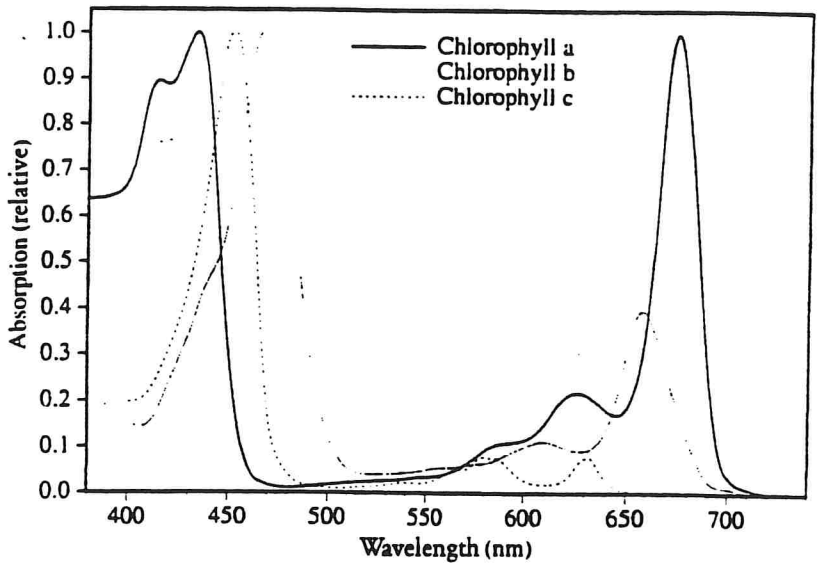

Figure 3.18: Absorption spectra of the chlorophylls. Solvent: diethyl ether. From Lichtenthaler (1987), Haxo and Fork (1959).

2. As the concentration of a pigment increases, the absorption spectrum becomes "flatter" (Duysens 1956), that is the differences between the absorption maxima and absorption minima become smaller.* The concentration of chlorophyll a, especially, is frequently high enough in an algal cell for this effect to occur. Table 3.4 makes clear how much the intracellular chlorophyll concentration depends on growth conditions and thus how the "effective" absorption spectrum also depends on growth conditions.

*This optical phenomenon results from the fact that from a certain concentration, light is virtually completely absorbed at the absorption maxima, whereas in other spectral regions the pigment is still transparent. If the pigment concentration increases further, the absorption changes only slightly at the absorption maxima while it increases significantly in the other spectral regions. Figure 3.3a illustrates this nonlinear relationship between absorption and concentration.

	60 µE m^{-2}	100 µE m^{-2}	180 µE m^{-2}	310 µE m^{-2}
10 °C	35.0	30.0	15.0	11.0
25 °C	12.0	7.0	5.4	4.3

Table 3.4: Dependence of the intracellular chlorophyll concentration on the growth conditions temperature and light intensity for the example of the blue-green alga *Synechococcus sp.* (Strain BO 8801). From Kenter (1991). Concentrations in fg/cell.

Fluorescence. Chlorophyll a fluorescence is also solvent-dependent, in the same way as absorption. *In vivo* chlorophyll a fluoresces at 685 nm and at 730 nm. The quantum yield is 0.35% (Günther 1986a), of which the peak at 685 nm accounts for about 75% (Günther 1986b, Haardt and Maske 1986). This proportion changes, inter alia, under nutrient stress and is thus of great interest in plant physiology.*

Reflectance spectra of water have a marked maximum at 685 nm whose amplitude is correlated with the chlorophyll a concentration. As the model calculations of chapter 6 show, this structure in the reflectance spectrum can be explained without fluorescence: between the absorption maximum of chlorophyll a at 670 nm and the steep rise in the absorption of water above 700 nm, there is a spectral region of low absorption having a minimum at about 685 nm (it is shifted to longer wavelengths with

*Stimulation of fluorescence by laser light makes the intensity sufficiently high to measure the intensity ratio or else the decay behaviour reliably even from the aircraft. An important future application is early recognition of damage to vegetation on land (initially forest); a sensor is currently being developed for this purpose (Günther et al. 1991, Dahn et al. 1992).

increasing amplitude of the absorption at 670 nm), which causes increased reflectance. Because of scattering at phytoplankton or at other suspended particles, the amplitude correlates with the concentration of these particles.

Although this explanation has been known at least since the work by Vasilkov and Kopelevich (1982), on the other hand, the opinion has been expressed in many publications that the peak at 685 nm is chiefly caused by chlorophyll a fluorescence, for instance in the article by Gordon (1979) in the ESA study with the title "The use of chlorophyll fluorescence measurements from space for separating constituents of sea water" (GKSS 1986a), but also in work by the present author (Gege and Hofmann 1990). As is shown by a simple energy estimation, the observed peak height is certainly not due to chlorophyll fluorescence and it is even questionable whether the fluorescence at 685 nm can be detected at all by passive measurements: assume that the incident solar energy is absorbed by chlorophyll a in a wavelength-dependent manner as shown in Figure 3.18. If the incident irradiance were constant over the spectral range, for example 1 W m^{-2} nm^{-1}, the proportion absorbed would be equal to the integral under the absorption curve times the constant; in the example chosen, this gives 96 W m^{-2}. (For a more exact calculation, the wavelength dependency of the incident radiation must be taken into account, but as is shown, for example, in Figure 2.2, this at most reduces the absorbed proportion.) Of this irradiance, about 0.3% passes into the fluorescence at 685 nm, that is 0.29 W m^{-2}. If the fluorescence peak is approximated by a Gaussian normal distribution with a width of 24 nm at half height, an emitted irradiance is obtained of 0.29 W $m^{-2}/[(2\pi)^{½} \cdot 24$ nm] = 0.0048 W m^{-2} nm^{-1} at the maximum, which is easily 200 times less than the chlorophyll a absorption at 440 nm and 670 nm.

3.4.3 Phaeophytins

The chemical structure of phaeophytins is almost identical to the structure of chlorophylls, with only the central magnesium atom missing. Artificial conversion of chlorophyll to phaeophytin is simply achieved by adding a weak acid, for example HCl. In algal cultures, the phaeophytins are generally degradation products of the chlorophylls of dead cells, but phaeophytin a, in particular, has a function in the living cell: it participates in charge separation and electron transfer.

In Table 3.3, in addition to the absorption and fluorescence maxima of the chlorophylls, those of phaeophytin a and phaeophytin b are reported. The absorption maximum of the phaeophytins in the blue, compared to chlorophylls, is shifted to shorter wavelengths and the specific absorption is somewhat higher; the maximum in the red is shifted to longer wavelengths and the specific absorption is markedly lower (Lichtenthaler 1987). Figure 3.19 shows the absorption spectra of phaeophytins a and b in diethyl ether.

As with the chlorophylls, the absorption spectrum of phaeophytins also depends on the electric fields which deform the molecule, that is the absorption of phaeophytins is solvent-dependent.

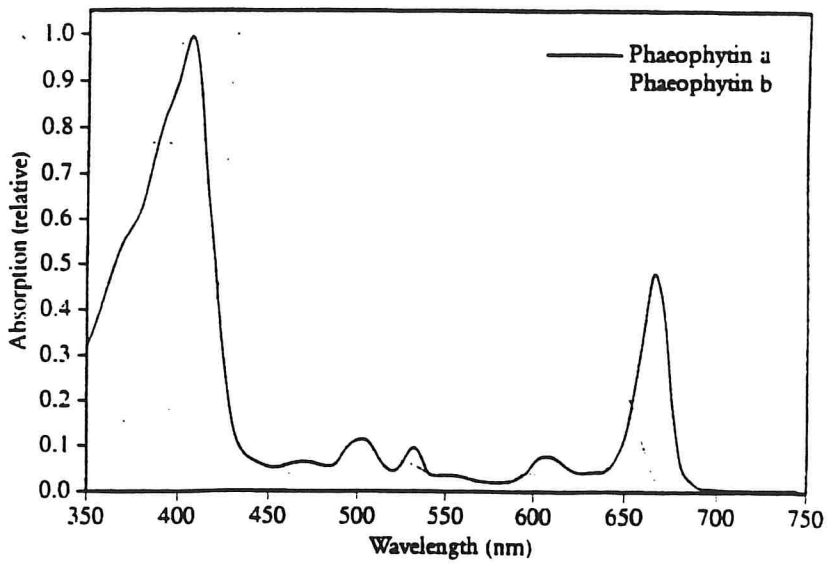

Figure 3.19: Absorption spectra of phaeophytin a and phaeophytin b in diethyl ether. From Lichtenthaler (1987).

3.4.4 Phycobiliproteins

In red algae, blue-green algae and Cryptophyceae, the phycobiliproteins* phycocyanin and phycoerythrin occur. Since these pigments absorb in the spectral region 540-650 nm which chlorophyll cannot utilize (the "green gap of chlorophyll"), these algal classes can survive in relatively deep water layers where the blue and red portion of the incident light has already been absorbed by the water or by algae living in the upper water layers. The phycobiliproteins transmit the absorbed energy to the reaction centres with an efficiency of almost 100%.

No fixed chemical formulae may be assigned to the molecules phycoerythrin and phycocyanin since they occur in various modifications. Their structural principle is shown in Figure 3.20: the phycobiliproteins are composed

*The correct terminology is "phycobiliproteids" since a protein is chemically bound to a nonprotein molecule (*prosthetic group*). However, the term "phycobiliproteins" or in brief "biliproteins" has found acceptance.

of a high molecular protein to which are bound several colour-imparting prosthetic groups, the so-called *chromophores*. These chromophores are tetrapyrroles as are the chlorophylls. The characteristic chromophore of phycocyanin is *phycocyanobilin*, that of phycoerythrin is *phycoerythrobilin*.

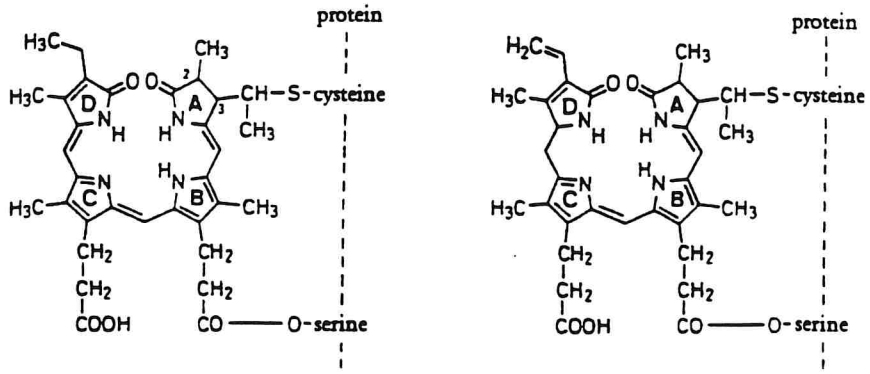

Figure 3.20: Chemical structure of phycoerythrin (left) and phycocyanin (right). From Richter (1988).

In addition to these, the phycobiliproteins can contain other chromophore types. The protein is composed of two subunits, a "light" (α) protein chain and a "heavy" (β) protein chain. Each subunit can bear 1 to 4 chromophores so that phycocycanins and phycoerythrins having 2, 3, 5 or 6 identical or different chromophores occur (Richter 1988). Differing spectral properties result therefrom.

The chromophores phycocyanobilin and phycoerythrobilin are isomers differing only in the position of one double bond. The cyclic form shown in Figure 3.20 is only one possible stage: the shape is subject to changes, for example stretching into the linear form because of different folding patterns of the bound protein. According to Scheer and Kufer (1977) the absorption in the visible increases relative to the absorption in the near UV, the more extended are the chromophores, and moreover the width of the absorption lines changes. The geometric configuration changes especially when the chromophores are separated from the protein (denaturation). As the examples in Table 3.5 show, the

quantum yield of the absorption in the visible markedly decreases in this case relative to that in the UV. Binding the chromophore to a protein therefore increases the efficiency factor for the algal cell, increases by a factor of 5 and above being achieved.

Table 3.6 gives a survey of the position of the absorption maxima of the phycobiliproteins from various algal species. The phycoerythrins may be classified into 3 groups thereby in accordance with the position of the absorption maximum in the visible (544 ± 1 nm, 554 ± 2 nm, 563-568 nm). A representative absorption spectrum is shown for each of these groups in Figure 3.21. The phycocyanins also have three characteristic absorption maxima in the visible (584 ± 1 nm, 615-625 nm, 643-645 nm); their absorption spectra frequently have a double peak structure. Figure 3.21 shows two typical spectra.

Phycobiliprotein extracted from	A_{VIS}/A_{NUV}		2Γ (cm^{-1})	
	with protein	denatured	with protein	denatured
Phycoerythrin *Rhodomonas lens*	3.6	1.3	2150	2590
Phycoerythrin *Phormidium persicinum*	2.4	1.4	1930	2460
Phycocyanin *Plectonema calothricoides*	2.2	0.4	2000	2330

Table 3.5: Examples of differences in the absorption spectrum of different phycobiliproteins. From MacColl et al. (1983). A_{VIS}/A_{NUV} = ratio of the amplitudes in the visible and near UV (see Equation 3.4b), 2Γ = line width at half height.

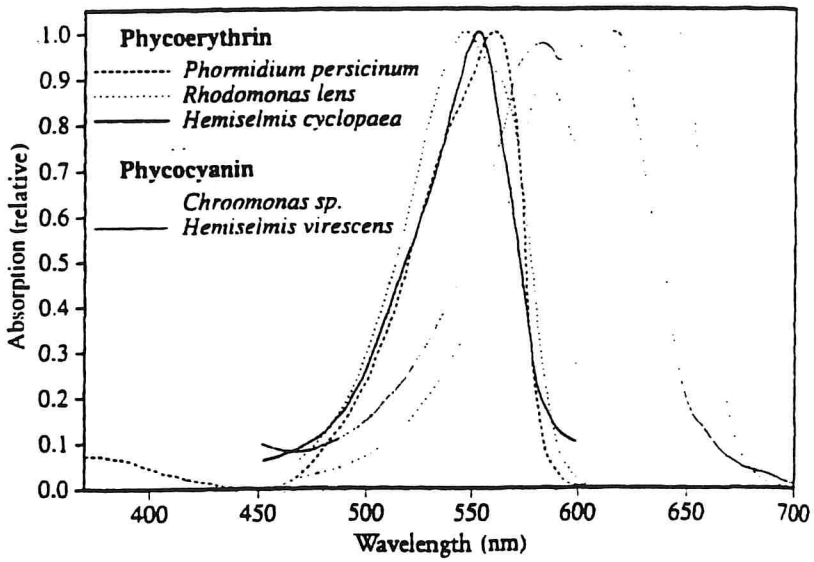

Figure 3.21: Typical examples of the absorption of phycobiliproteins. The legend indicates from which algal species the pigment was extracted.

Table 3.6 shows, furthermore, that the position of the absorption maxima can vary even within an algal species. In the case of such species, a differentiation into several forms is required which differ in the prevailing type of phycobiliprotein. One example of this is *Synechococcus*, for which two optically different forms are listed in Table 3.6. Furthermore, in the case of *Synechococcus* in addition to forms in which phycoerythrin dominates, forms also occur which principally contain phycocyanin (Kenter 1991).

Algal species	PHYCOERYTHRIN	Reference
Cryptomonas ovata var. *palustris*	565	Allen et al. (1959)
C. ovata var. *palustris*	285 568	Haxo and Fork (1959)
Phormidium persicinum	(542) 563	MacColl et al. (1983)
Cryptomonas atrorosea	542 — (560-570)	O'hEocha et al. (1964)
Plagioselmis prolonga	544 (560-570)	O'hEocha et al. (1964)
Rhodomonas lens	544 (560)	MacColl et al. (1983)
Rhodomonas lens	275 390 545	Haxo and Fork (1959)
Rhodomonas sp.	545	O'hEocha and Raftery (1959)
Cryptomonas sp.	545	O'hEocha and Raftery (1959)
Cryptomonas suberosa	543	O'hEocha et al. (1964)
Synechococcus sp. type DC-2, WH 7803	500 545	Alberte et al. (1984)
Synechococcus sp. type 1600, WH 8018	551	Alberte et al. (1984)
Hemiselmis rufescens	275 310 556	O'hEocha and Raftery (1959)
Cryptochrysis sp.	554	O'hEocha and Raftery (1959)
Hemiselmis cyclopaea	554	O'hEocha et al. (1964)
Chroomonas diplococcus	553	O'hEocha et al. (1964)
	PHYCOCYANIN	
Chroomonas sp.	585 (620) 650	O'hEocha et al. (1964)
Hemiselmis virescens	580 (620-625) 645	Allen et al. (1959)
Hemiselmis virescens	270 350 583 (620-625) 643	O'hEocha et al. (1964)
Hemiselmis virescens (?)	275 340 588 615	O'hEocha and Raftery (1959)
Hemiselmis virescens (?)	275 330 585 615	O'hEocha et al. (1964)
Cryptomonas cyanomagna	330 583 625-630	O'hEocha et al. (1964)
Cynanidium caldarium	615	Allen (1959)

Table 3.6: Absorption maxima of the phycobiliproteins extracted from different algal species. Wavelengths in nm. In brackets: shoulder in the spectrum.

Since the various types of phycobiliproteins differ in the absorption maxima positions, it has become the practice to classify them accordingly. For example, "phycoerythrin 566" denotes a phycobiliprotein whose absorption maximum in urea is at 566 nm. The chromophores of the α-subunit of this pigment are cryptobilin 596, and the β-subunit bears two different chromophore types, phycoerythrobilin and bilin 584 (MacColl et al. 1992). As is shown in this example, the chromophores are also

frequently characterized by their absorption maxima.

Fluorescence. The phycobiliproteins have characteristic fluorescence spectra, therefore their concentrations in water may be established highly precisely by active remote sensing methods (Exton et al. 1983, Hoge and Swift 1983). The quantum yield of the fluorescence stimulated by sunlight is presumably too low for passive methods. Table 3.7 shows the position of the emission maxima.

Phycoerythrin 545	580-586 nm	Phycocyanin 612	634-641 nm
Phycoerythrin 555	574-580 nm	Phycocyanin 630	648-657 nm
Phycoerythrin 566	617 nm	Phycocyanin 645	655-662 nm

Table 3.7: Fluorescence of phycobiliproteins. The emission maximum is given for the three types of phycoerythrin and the three types of phycocyanin established from Table 3.6. The references of Table 3.6 and the book by Rowan (1989) were used for the compilation.

3.4.5 Carotenes

β-Carotene occurs as an important pigment in all types of phytoplankton; in addition, in some algae α-, γ- or ε-carotene occurs in smaller amounts. The structural formulae of α- and β-carotene are shown in Figure 3.22.

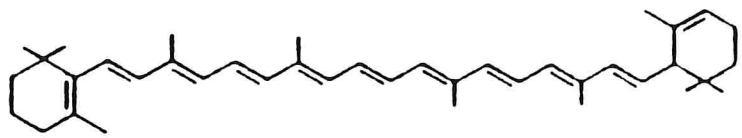

α-Carotene

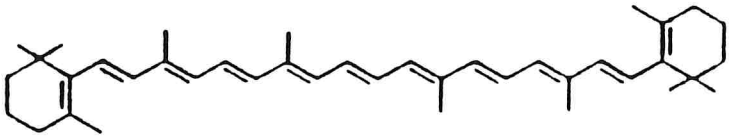

β-Carotene

Figure 3.22: Chemical structure of α-carotene and β-carotene. From Lichtenthaler (1987).

Carotenes are hydrocarbon chains made of isoprene units having nine or more conjugated double bonds in various positions. The 3 nm-long chain molecules are fat soluble. Carotenes principally serve in the cell as "solar protection": they remove an electron from the excited chlorophyll which would otherwise be oxidized by oxygen. Furthermore, the carotenes have a function as light-collecting pigments, but their efficiency in energy transfer is only 30 to 40% (Lawlor 1990).

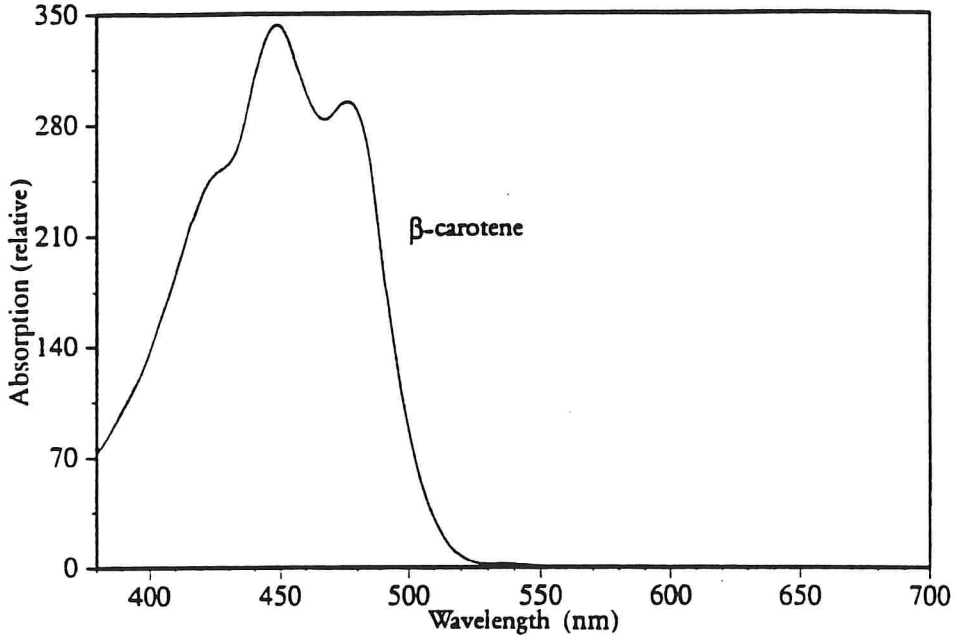

Figure 3.23: Absorption spectrum of β-carotene. Solvent: diethyl ether. From Lichtenthaler (1987).

Carotenes have three absorption maxima in the 400-500 nm region. The β-carotene absorption spectrum is shown in Figure 3.23 for diethyl ether solvent. The wavelength of the central maximum is given in Table 3.8 for 8 different solvents. If the carotenes are dissolved in acetone, diethyl ether, hexane or petroleum, the maxima for α-carotene are at 442-445 nm, and for β-carotene at 447-450 nm. However, if carbon disulphide is used as solvent, the maxima are shifted by about 40 nm to the

red. Carotene absorption is therefore highly solvent-dependent.

3.4.6 Xanthophylls

Xanthophylls are chemically related to carotenes; the two pigment classes are combined under the term *carotenoids*. Xanthophylls contain oxygen. They differ in the position of the oxygen in the ring structure. Figure 3.24 shows the chemical structure of some selected xanthophylls which occur in phytoplankton.

Xanthophylls have a similar function to carotenes, that is removing excited electrons and absorbing light for photosynthesis. Furthermore, some xanthophylls play an important role in chemical reactions in the chloroplasts, for example violaxanthin and zeaxanthin regulate the amount of NADPH and the redox state of the chloroplasts (violaxanthin cycle, Krinsky 1978). Figure 3.25 shows the absorption spectra of some xanthophylls. Table 3.8 summarizes the position of the absorption maxima of the most important xanthophylls, depending on the solvent used. The solvent dependency is very pronounced, it is therefore difficult to identify the xanthophylls present from the absorption spectra of living algal cultures.

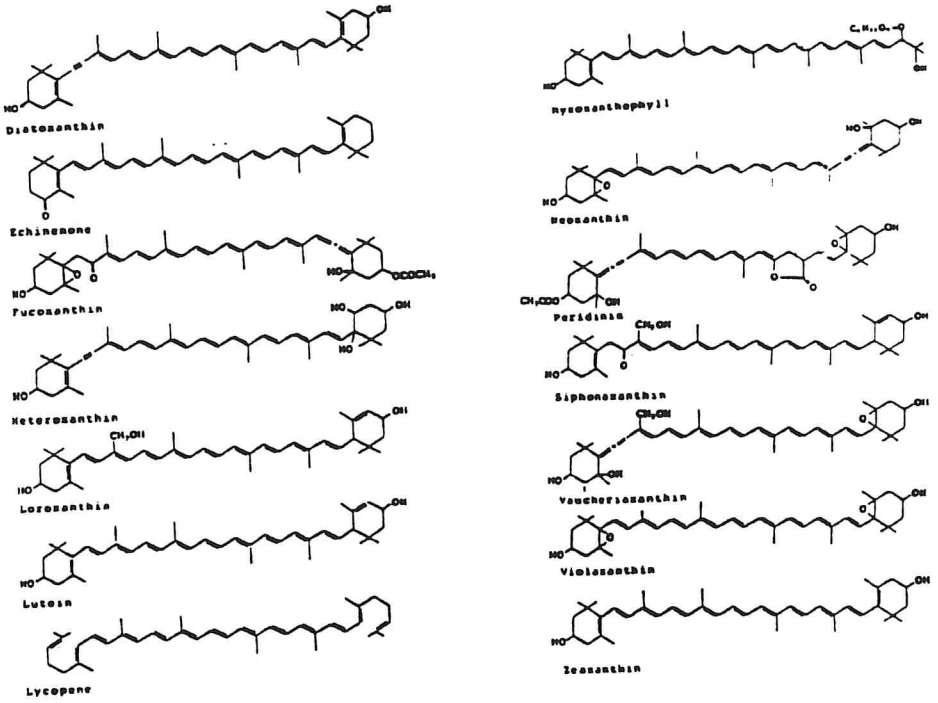

Figure 3.24: Chemical structure of 14 selected xanthophylls. From Rowan (1989).

	Acetone	Benzene	Carbon disulphide	Chloro-form	Diethyl ether	Ethanol	Hexane	Petro-leum
α-carotene	442-425	456	475-484	455-457	443-445	442-446	442-445	443-448
β-carotene	420-432	462-464	475-485	460-465	447-450	447-451	447-451	448-451
Alloxanthin	453	464		460-461	451	450-454	451	450
Antheraxanthin			476-478	456		444-447	443-445	443-445
Crocoxanthin		458		454	445	443-447	445	
β-Crypotaxan-thin	450-453	463	483	459-464	446-447	449-452	446-452	446-449
Diadinoxanthin	448-449		474	455	448	445-448	445-448	444-445
Diatoxanthin	448-454	463		458		449-453	447-450	448-451
Dinoxanthin	442		467			439-443	439-442	
Echinenone	459-460	470	488-494	471	455	453-461	459	455-458
Fucoxanthin	444-449	460-461	478	478	444-446	447-451	449-450	446-449
Heteroxanthin				448	442-445	442-448		
Isozeaxanthin			479				450-451	446-451
Loroxanthin	446			455	442	446		
Lutein	445	458	472-475	454-458	443-448	445-446	443-445	443-445
Monadoxanthin		456			446	447-448	445	
Myxoxantho-phyll	475-478	488		485-488		471-474		
Neoxanthin	436-445	445-453	463-466	445-449	437-444	436-438	435-439	435-442
Peridinin	465-471	465-467	480	470	453-454	472-475	454-457	
Siphonaxanthin				466	441	448-452		446-450
Siphonein				463-471	448	448-467		450-457
Vaucheriaxan thin	441			451		440-444		
Violaxanthin	440-442	451-454	468-470	449-452	441	439-441	439-443	438-443
Zeaxanthin	449-452	463	481-483	458-461	447-450	449-454	447-450	446-449

Table 3.8: Position of the absorption maxima of selected carotenes and xanthophylls in relation to the solvent used. The carotenoids have three absorption maxima in the blue, the central one is given in each case (it has the greatest amplitude). Wavelength in nm. From Rowan (1989).

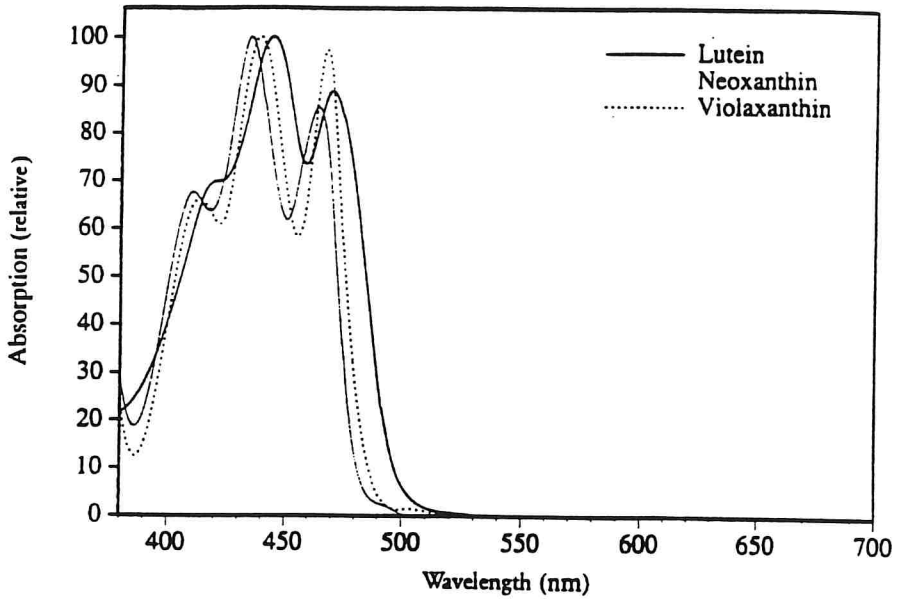

Figure 3.25: Absorption spectra of three selected xanthophylls. Solvent: diethyl ether. From Lichtenthaler (1987).

3.5 Phytoplankton

3.5.1 Absorption

The absorption spectra of phytoplankton are always characterized by the chlorophyll a absorption since chlorophyll a is essential for photosynthesis and is present in all species. The algae may be classified on the basis of the other pigments present, see Table 3.2. However, the concentration can be subject to great variations, even within one species, and, furthermore, the absorption spectra of many pigments are very similar. It is not possible, therefore, to differentiate the classes of Table 3.2 purely optically.

Identifying individual pigments on the basis of the

absorption spectrum of an algal culture is also made more difficult by the fact that the absorption depends on the chemical environment which can lead to a marked wavelength shift (up to 40 nm), particularly on extraction. *In vivo* as well, the position of the absorption maximum for the same pigment can differ (up to about 5 nm). The specific absorption coefficient also depends on the chemical environment (on extraction up to a factor of 5 or more cf. Table 3.5; *in vivo* the differences are difficult to quantify, but are estimated to be below 50%).

As an example of *in vivo* absorption spectra of phytoplankton, Figure 3.26 shows the spectra for 2 species which occur at high frequency in Lake Constance: *Stephanodiscus hantzschii* (class *Bacillariophyceae* = Diatoms) and *Cryptomonas ovata* (class *Cryptophyceae*). The algal cultures were grown at the Limnological Institute of the University of Konstanz and the absorption measurements were made with an integrating sphere (G. Hartmann, Institute of Physical Geography, Freiburg University); chlorophyll was determined photometrically by the method described in Section 5.1.3 (G. Hartmann).

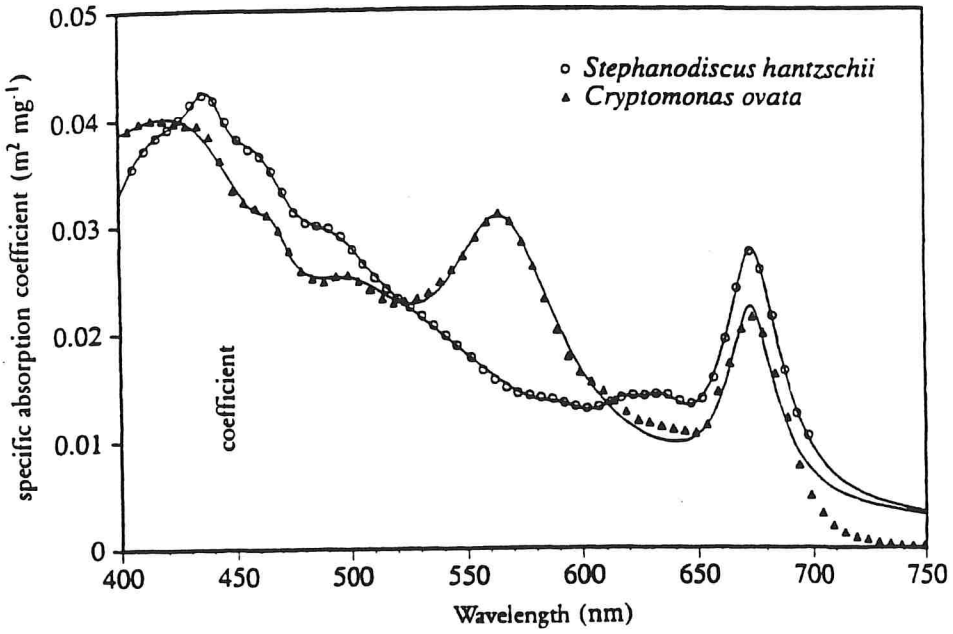

Figure 3.26: *In vivo* absorption spectra of two phytoplankton species which occur at high frequency in

Lake Constance.

According to theory (Equations 3.4b, 3.5; $\omega = 2\pi c\nu$), the absorption spectrum may be approximated by the following equation:

$$a(\nu) = \nu \sum_i \frac{A_i \Gamma_i}{(\nu_i - \nu)^2 + \Gamma_i^2}, \qquad (3.31)$$

wavenumbers being converted into wavelengths by $\lambda = 1/\nu$. The continuous lines in Figure 3.26 represent the fitted curves; the fitting is obviously highly successful. Table 3.9 lists the fitting parameters.

The maxima at 439 nm and 674 nm may be assigned to chlorophyll a and the minor maximum at 630 nm probably as well, compare Figure 3.18. *Cryptomonas ovata* contains phycoerythrin at high concentration.

Stephanodiscus hantzschii									
λ_i (nm)	416.7	438.4	460.9	494.3	536.6	591.5	617.2	634.6	674.2
Γ_i (cm^{-1})	2557	578	871	1099	2080	401	371	336	326
$2\Gamma_i$ (nm)	89.8	22.2	37.1	53.9	121	28.1	28.3	27.1	29.6
A_i (m^{-1})	0.0119	0.0007	0.0015	0.0017	0.0045	0.0001	0.0003	0.0003	0.0017

Cryptomonas ovata								
λ_i (nm)	370.0	418.5	439.9	466.4	503.6	566.5	629.4	673.5
Γ_i (cm^{-1})	3373	2381	1802	426	1208	968	897	278
$2\Gamma_i$ (nm)	93.8	84.2	70.2	18.5	61.5	62.3	71.3	25.3
A_i (m^{-1})	0.0849	0.0383	0.0265	0.0019	0.0155	0.0322	0.0011	0.0082

Table 3.9: Parameters of the fitted curves of Figure 3.26. λ_i = absorption maxima, $2\Gamma_i$ = line width at half height, A_i = amplitudes.

This pigment causes the marked maximum at 566.5 nm. The maximum of the two species at 418 nm may be assigned with

some certainty to phaeophytin a in accordance with Table 3.3. *Stephanodiscus hantzschii* according to Table 3.2 has the principal carotenoid contents β-carotene, diadinoxanthin and fucoxanthin; in contrast, *Cryptomonas ovata* principally contains α-carotene and alloxanthin. These probably form the peaks at 461 and 494 nm and at 466 and 504 nm respectively. Absorption spectra of phytoplankton always have at least one maximum in the range from 455 to 505 nm, the position depending on the species. Since individual species differ primarily in carotenoid composition, this pigment class is probably a substantial factor in determining the absorption in the 455 to 505 nm range. This is also confirmed by Figure 3.25 and Table 3.8.

Pigment concentrations can vary very greatly within one species. Absorption measurements for the same species therefore frequently differ markedly. For example, three optical density spectra have been found in the literature for *Cryptomonas ovata* (Allen et al. 1959, Haxo and Fork 1959, Farmer et al. 1983). Although the specific absorption coefficients cannot be derived therefrom since the chlorophyll concentration is not reported in the articles, the patterns of the three spectra and that of the measurement in Figure 3.26 can at least be compared qualitatively. Great differences are observed in the amplitudes of the individual maxima and also deviations in position.

Figure 3.27, in addition to the spectrum of *Cryptomonas ovata* already shown in Figure 3.26 (thick line) shows a further spectrum recorded from a culture which was grown under somewhat different conditions (dotted line). Clearly, the differences between the two spectra are just as great as the differences from other representatives of the class *Cryptophyceae* (the figure shows the spectra of *Cryptomonas rostratiformis*, *Cryptomonas marssonii* and *Rhodomonas minuta*). Individual species within this class, therefore, may not be differentiated on the basis of

spectral measurements. For modelling reflectance spectra, the absorption spectrum of the second culture of *Cryptomonas ovata* (thick line in Figure 3.27) was selected as a representative spectrum for all species of the class *Cryptophyceae*. The selection for other classes is discussed in Section 4.2.3.

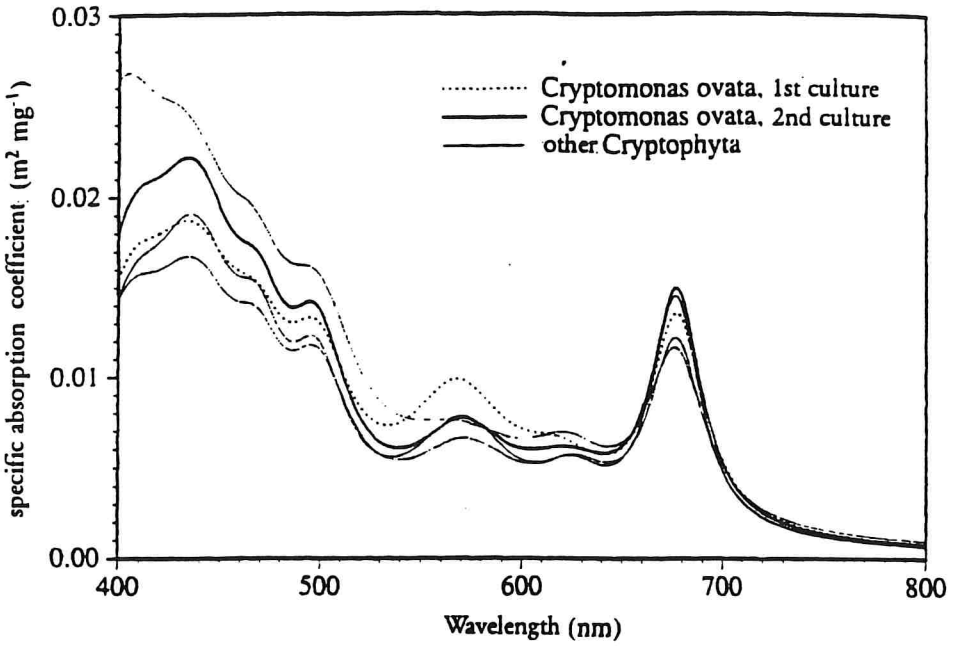

Figure 3.27: Absorption spectra of four Cryptophyta species which occur at high frequency in Lake Constance. Curves fitted to unpublished measurements made by G. Hartmann 1993 (with kind permission).

For the present work, many published absorption spectra were collected in order to build up a database. In the course of this it became apparent that during measurement little care is generally taken to avoid light losses by scattering. These errors in measurement have a greater effect in the case of small algal cells than with large ones since the wavelength dependency of the scattering is more marked in this case*. Attempts to use Equation (3.31) to fit absorption spectra which are obviously

*The setup used to take measurements is frequently described too imprecisely to estimate errors, particularly in older publications or in articles in biologically orientated journals. The examples in Farmer et al. (1983) demonstrate how markedly the measurement setup influences the spectra.

subject to error usually do not succeed. That is the quality of the fit gives an indication - at least a rough indication - of the reliability of a measured absorption spectrum.*

3.5.2 Scattering

Light scattering at phytoplankton has already been extensively discussed in Section 3.2.2. Essentially, size and refractive index govern the scattering amplitude and spectrum; the course of the curve is somewhat structured in the region of absorption maxima: on the longwave side of an absorption maximum the scattering coefficient has a minimum and a maximum on the shortwave side, compare Figure 3.11.

According to Figure 3.3, in small species $Q_c \sim \rho \sim \lambda^{-1}$, in the case of larger species Q_c approaches the value 2 with increasing absorption (increasing n'). Since the attenuation is principally caused by scattering, the following rule of thumb applies: scattering by small species (diameter less than 5 µm) is proportional to λ^{-1}, and scattering by large species is independent of wavelength. This rough approximation is helpful if no scattering measurements are available and it is not possible to model them because of a lack of data (specific absorption coefficient of the algal cells, refractive index).

---

*Care should generally be taken when using absorption spectra from the literature: the units are often reported erroneously ("absorption (%)"); it is sometimes unclear whether the ordinate has a linear or logarithmic scale. It is often not possible to derive specific absorption coefficients.

4. Reflectance model

4.1 Relationship of reflectance with absorption and scattering

The reflectance R was defined in Section 2.3.2 as the ratio of upwelling to downwelling irradiance beneath the water surface: $R = E_u/E_d$. The amount of light reflected in the water body depends on its absorption and scattering properties. The position of the sun and the angle of observation also influence the intensity of the detected radiation, since light scattering is highly dependent on the angle. In order to calculate the reflectance exactly, the *radiative transfer equation* must be solved. A complete solution is impossible since the boundary conditions - intensity distribution of the incident radiation for all zenith and azimuth angles, spatial distribution and optical characteristics of all scattering and absorbing particles in the water - are only known to an approximation.

Gordon et al. (1975) solved the radiative transfer equation by a statistical method, the Monte Carlo method. The result they obtained for the reflectance was a power series of the expression $b_b/(a+b_b)$. In practice this can be restricted to the linear term. The relationship between reflectance and absorption and scattering is then described as follows:

$$R(\lambda) = \gamma \frac{b_b(\lambda)}{a(\lambda)+b_b(\lambda)} . \qquad (4.1)$$

The proportionality factor γ depends on the spatial distribution of the incident radiation, that is on the position of the sun and on the cloud cover. If the sun is at the zenith in a clear sky, $\gamma=0.32$, and in the case of a uniformly overcast sky, $\gamma=0.37$. Prieur and Morel (1975) and Prieur (1976), by a different approximation method

(successively solving the radiative transfer equation for the succeeding orders of scattering) arrived at the equation $R = 0.33(1+\Delta)b_b/a$, the correction factor Δ depending on the radiance distribution and the volume scattering function. When Δ is small, Prieur's equation corresponds in practice to Equation (4.1) with $\gamma=0.33$, since, generally, $b_b \ll a$. In the original work it was stated that $\Delta < 5\%$ even in extreme cases; since then it has been shown that at least for hypothetical situations (sun against a black sky) the deviations can be considerably larger (between 25% and 55%: Kirk 1984, Gordon 1989), especially when single scattering dominates (Morel and Gentili 1991). The deviations are dependent on wavelength. Since it has not yet been possible to describe them quantitatively, in the present model Equation (4.1) is used with a constant $\gamma=0.33$.

The spectra $a(\lambda)$ and $b_b(\lambda)$ represent the spectra of the absorption and of the backscattering coefficient of the water body. They are defined in Section 3.2.1. a and b_b comprise the contributions of the water and its constituents:

$$a(\lambda) = a_w(\lambda) + \sum_i C_i\, a_i^*(\lambda) \qquad (4.2)$$

$$b_b(\lambda) = b_{b.w}(\lambda) + \sum_i C_i\, b_{b.i}^*(\lambda). \qquad (4.3)$$

a_w, $b_{b.w}$ denote the absorption and backscattering of the water (m^{-1}), C_i the concentration of constituent i (mg m^{-3}), a_i^* and $b_{b.i}^*$ denote the *specific* spectra of constituent i, that is based on a concentration of 1 mg per m^3 of water (units m^{-1} (mg m^{-3})$^{-1}$ = m^2 mg^{-1}).

If the spectra of the absorption and backscattering of the water and the constituents are known, the reflectance spectrum can be given in relation to the concentrations

C_i. The accuracy of this *reflectance model* is dependent on how well-known the spectra $a_w(\lambda)$, $a_i^*(\lambda)$, $b_{b.w}(\lambda)$, $b_{b.i}^*(\lambda)$ are. These optical properties of the water and the constituents were described in Chapter 3. To simplify, in summary, absorption measurements of some reliability exist, but there are virtually no measurements on scattering. However, the scattering spectrum can be estimated as was demonstrated in Section 3.2.2. The following section explains how the appropriate input spectra are selected or calculated for the model.

4.2 Model input spectra

4.2.1 Water

Absorption. As was explained in Section 3.3, the absorption spectrum of pure water can only be given imprecisely. The most reliable absorption spectrum is found in Smith and Baker (1981). By means of critical comparison of many published measurements made in the laboratory and very clear natural waters and from their own measurements, they derive a consistent absorption spectrum for the 400 to 800 nm region. This spectrum was initially used in modelling the reflectance spectra of Lake Constance. However, systematic deviations occured with this between measured and calculated reflectance spectra. Modifying the spectral regions 580 to 689 nm and 790 to 800 nm eliminated this systematic error. The continuous curve in Figure 4.1 shows this modified absorption spectrum and the unused data from Smith and Baker are shown in dotted lines.

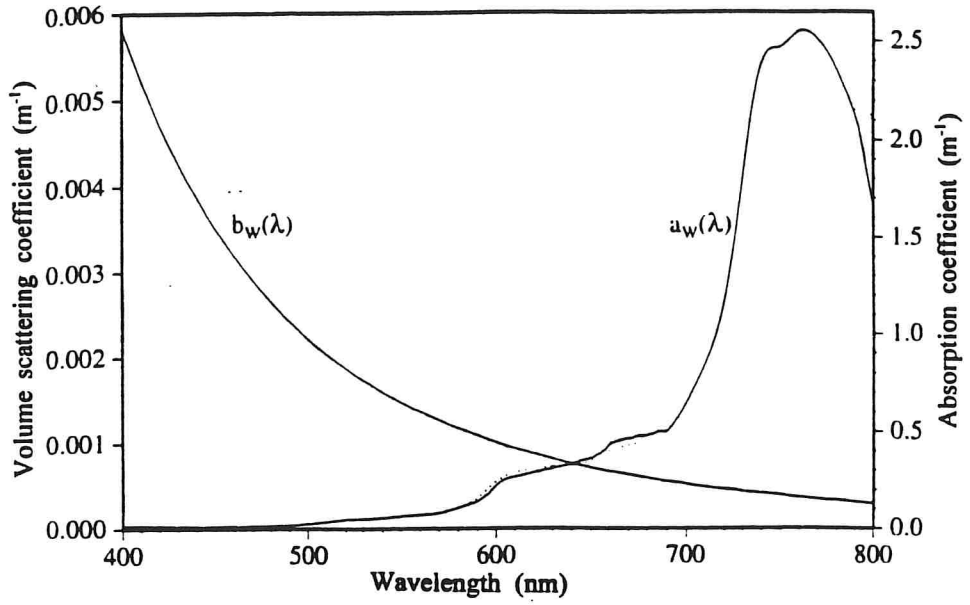

Figure 4.1: Spectra of the absorption and scattering of water used in the model. The dotted literature values were replaced by data from the present work, see text.

To modify the absorption spectrum of Smith and Baker, the absorption was derived from measured reflectance spectra. From Equation (4.1), the absorption can be calculated from the equation $a(\lambda) = \left(\frac{\gamma}{R(\lambda)} - 1\right) b_b(\lambda)$ if $b_b(\lambda)$ is known. It was assumed that $b_b(\lambda)$ is approximately constant for $\lambda > 700$ nm. The relative spectral course of $a(\lambda)$ is then obtained. $a(\lambda)$ was then scaled by fitting $a(\lambda)$ to the absorption spectrum $a_w(\lambda)$ of Smith and Baker, that is by minimizing the sum $\Sigma|a(\lambda_1)-a_w(\lambda_1)|^2$.* In the summation, only those channels λ_1 were used in which water absorption dominates ($\lambda > 700$ nm).

$a(\lambda)$ is calculated by the program BBA. Since the measured reflectance spectra can differ from the correct reflectance spectra by a scaling factor s and an offset

*Since this scaling factor equals b_b, the backscattering coefficient is obtained as by-product. This important value can generally be estimated only with difficulty since it is sensitive to the concentration and size distribution of the suspended particles and is only rarely determined in the laboratory.

o, a total of 3 free parameters (b_b, s, o) are fitted in the calculation. The scaling factor s scarcely affects the result so that s cannot be determined by the method. However, the offset o is determined reliably.

A relatively large number of absorption spectra were calculated in this way for a number of measurement days with markedly differing chlorophyll concentration. For $\lambda > 700$ nm, the agreement was good. To replace the literature values, the mean of 8 spectra $a(\lambda)$ from 28.5.91 was used, since the chlorophyll concentration was very low on this day (1.3 μg/l). Spectral regions where there was a significant difference were modified. As is shown in Figure 4.1, the modification is relatively slight, but it nevertheless has a marked effect in the modelling of reflectance.

Scattering. In the blue, Rayleigh scattering of the water constitutes a large part of the light reflected in a water body. It is approximated in the model by Morel's power law (3.28). For the constant $b_W(\lambda_0)$, the value for pure water is used: $b_W(500) = 0.00222\ m^{-1}$. Since the water molecule is very much smaller than the wavelengths of light, backscattering is just as great as forward scattering, that is $b_{b,W} = 0.5\ b_W$.

4.2.2 Yellow substance

Yellow substance absorption is approximated by the exponential function (3.30). The constant S describes the increase in absorption towards the blue. Yellow substance was determined on 25.6.91 at the measurement point in the Überlinger See, see Section 5.3.2. The value determined in this of $S = 0.022\ nm^{-1}$ is used for application of the reflectance model to the measurements made in Lake Constance. The concentration is not converted to mg/l, since the Nyquist equation (3.29) gives values which are too low for Lake Constance. Instead, the absorption of yellow substance at $\lambda_0 = 450$ nm is used as a measure of

concentration. Figure 4.2 shows the absorption of yellow substance, scattering is ignored.

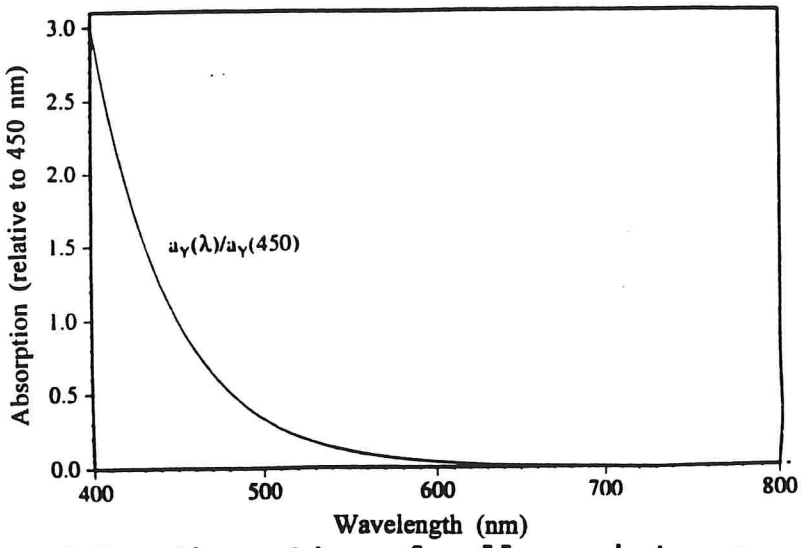

Figure 4.2: Absorption of yellow substance.

4.2.3 Phytoplankton

Determination of the phytoplankton concentration is the most importance purpose in the modelling of reflectance spectra. This proceeds with increasing accuracy the better the optical properties are known. As was explained in Section 3.5, neither the absorption spectrum nor the scattering spectrum is constant within a species, since the pigment concentration and size of algal cells depend on growth conditions.

In order to select absorption spectra suitable for modelling the phytoplankton in Lake Constance, a study was made of which species are typical of Lake Constance. The basis used was the cell count data which are presented in sections 5.2.4 and 5.5. These were used, as described in Section 5.2.5, to calculate the biovolumes of the individual species. Table 4.1 gives the frequency distribution in the columns "dominance" for the 34 days in 1990 and 1991 when reflectance spectra were also recorded. The first column shows the number of days on which the corresponding species dominated in terms of volume and columns 2 and 3 show how often it was observed to be the second and third most frequent species.

The phytoplankton species occurring with the highest frequency in Lake Constance is *Cryptomonas ovata*, but other Cryptophyceae species also have a very high frequency. As the table shows, absorption measurements could be made for all important representatives of this class or a spectrum could be taken from the literature. The measured spectra have already been depicted in Figure 3.27. As was explained in the associated text (Section 3.5.1), the changes in absorption within a species are just as great as the differences between the species. Therefore, in the modelling, the Cryptophyceae class was first characterized by a single spectrum, that of the species *Cryptomonas ovata*, since this occurred with the highest frequency. On days when *Cryptophyta* dominated however, the modelling of reflectance spectra was frequently unsatisfactory, especially in the spectral region around 550 nm. Therefore, the spectrum of *Rhodomonas lens* was additionally used, since it has a considerably pronounced maximum at 550 nm. In the article from which the spectrum is taken (Haxo and Fork 1959), the absorption spectrum is only given in relative units; to use it in the model, the spectrum illustrated in the original article was normalized to a specific absorption coefficient of $a^*(440) = 0.02\ m^2/mg$.

The algal class in Lake Constance with the second highest frequency is the diatoms (Bacillariophyceae).* Of the relevant species, only absorption measurements for *Stephanodiscus hantzschii* and *Fragillaria crotonensis* were available for the present work. The spectra have the same pattern but the specific absorption coefficient for *Stephanodiscus hantzschii* is twice that for *Fragillaria crotonensis*. Since the specific absorption coefficient of

*Averaged absorption spectra of diatoms are found in Farmer et al. (1983) and in von Smekot-Wensierski et al. (1992). Because of large spectral differences between individual species, the standard deviation is very high in both cases. Therefore, and because marine diatoms are used as the basis which are clearly separate from fresh water forms (Round 1975, page 260) they were not taken into consideration for Lake Constance.

Fragillaria crotonensis in the blue agrees better with the values derived from reflectance spectra on days when diatoms predominate, its absorption spectrum was taken to be characteristic for the diatoms of Lake Constance.

Class	Species	Dominance			Absorptionspektrum	
		1	2	3	Species	Class
Crypto-	Cryptomonas ovata	12	9	2	COVATA2.A [1]	COVATA2.A
phyceae	Rhodomonas lens	3	4	1	RHODOM.A [2]	RHODOM.A
	Crypt. rostratif.	2	3	1	CROST.A [1]	[1], [2]
	Rhodomonas minuta	2		3	RHMIN.A [1]	
	Crypt. marssonii		2	1	CMARS.A [1]	
Bacillario-	Steph. hantzschii	3	1	2	STEPH.A [1]	FRCROT.A
phyceae	Aster. formosa	2				[1]
	Fragil. croton.	1	2	1	FRCROT.A [1]	
diatoms	Diatoma elongatum			1		
	Melosira granvar.			1		
Dinophyceae	Ceratium hirund.	1	3			SMEK4.A
	Gymnodinium helv.	1	1	2	GYMSP.A [3]	[3]
dino-	Peridinium cinctum	1				
flagellates	Gymnod. lantzschii			1	GYMKOW.A [3]	
	Peridinium sp.			1		
Cyanophyceae	Microcystis 1-2 µm	2				
blue-green- algae	Microcystis 4 µm	1				
Chrysophyceae	Dinobryon diverg.	2		1		
	Mallomonas acar.		2			
Chlorophyceae	Chlamydomonas		1		CHLAMY.A [1]	MOUG.A
green algae	Chlorella sp.		1			[1]
Zygnemaph.	Mougeotia >80 µm		1		MOUG.A [1]	
green algae	Mougeotia <30 µm		1			

Source: [1] = Measurement by G. Hartmann (private communication 1993), [2] = Haxo and Fork (1959), [3] = von Smekot-Wensierski et al. (1992).

Table 4.1: Frequency of individual phytoplankton species in Lake Constance in 1990 and 1991. See sections 5.2.4, 5.2.5 and 5.5 for comments on the measurements. The

column "Dominance" lists the number of days for which the species was predominant or in the second or third position with respect to volume. The column "Absorption spectrum" gives the file names and the origin of the data.

No absorption spectra were available for the present work for the dinoflagellate species (Dinophyceae) which occur at high frequency in Lake Constance. Measurements were only found for two *Gymnodinium* species (tabulated in von Smekot-Wensierski et al. 1992), but in Lake Constance different subspecies are present. Because of this information deficit, for dinoflagellate absorption the spectrum used was that given by von Smekot-Wensierski et al. (1992, pages 27 ff). This apparently represents the Lake Constance dinoflagellates well, since in the modelling the relative proportion of dinoflagellates is determined accurately (see Section 6.3.5).

Of the blue-green algae (*Cyanophyceae*), according to the table, only *Microcystis* forms are important.* No absorption spectrum is available for this. It is uncertain how meaningful are the spectra found in the literature for other Cyanophyceae species (for instance the spectrum shown in Figure 3.6 of *Synechococcus* with a pronounced maximum at 560 nm originating from phycoerythrin): according to Section 3.4.4, precisely the absorption spectra of species containing phycobiliproteins are subject to great variations (*Synechococcus* was mentioned as a prominent example of this). For this reason, no absorption spectrum representing the blue-green algae was used for the reflectance model. On days when blue-green

*According to Kenter (1991), blue-green algae dominate the picoplankton (< 2 µm) in Lake Constance, particularly *Synechococcus* strains. The picoplankton is not taken into account in the cell count data available for the present work since it is too small for evaluation by light microscopy. It is therefore ignored in the present work. This is justified since its proportion is only about 10% of the total phytoplankton (chlorophyll a proportion; Kenter 1991, Table on page 47).

algae predominated, the modelling established green algae as the predominant class. Blue-green algae and green algae were therefore combined in the modelling into one "optical class".

No absorption spectra were available for the present work for the class Chrysophyceae. A representative spectrum of this class was therefore not used. On the two days when the species *Dinobyron divergens* predominated (17.7.90, 23.10.90) diatoms were established as the predominant class in the modelling of reflectance spectra. The Chrysophyceae are therefore integrated into the "optical class" of the diatoms in the modelling.

Absorption measurements made on green algae are frequently found in the literature, and are always highly similar. An absorption measurement is available for one species each of the two green algae classes Chlorophyceae and Zygnemaphyceae. Since the spectra are very similar, one joint absorption spectrum was selected for spectral characterization of the two classes, that is the spectrum of *Mougeotia* sp..

The five absorption spectra characterizing the phytoplankton in Lake Constance are shown in Figure 4.3. Since no measurements are available on light scattering, in modelling, it, together with the scattering by other suspended particles, is approximated by a function of type $B_0+B_1\lambda^n$, see Section 4.3.2.

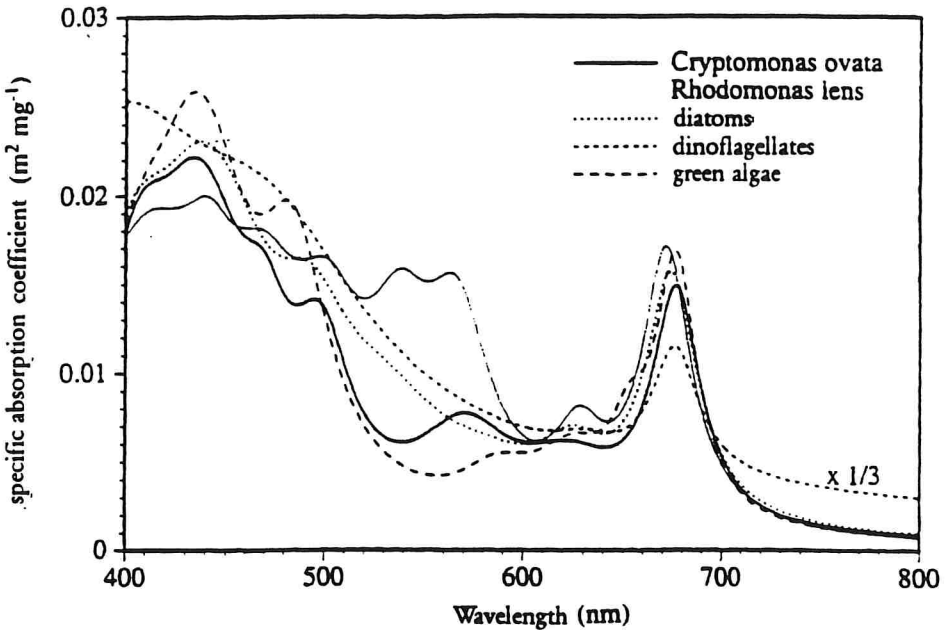

Figure 4.3: The absorption spectra of the phytoplankton classes relevant to Lake Constance.

4.3 Inversion of reflectance spectra

4.3.1 The problem of inversion

If the concentrations of the water constituents are known, the reflectance $R(\lambda)$ can be calculated from Equations (4.1), (4.2) and (4.3). In practice, the problem is the other way round: $R(\lambda)$ is measured and the concentrations of the constituents must be calculated from this. This is termed *inversion*. Since the constituents are determined via analysis of the absorption and scattering spectra, the problem of inversion is to derive the two spectral functions $a(\lambda)$ and $b_b(\lambda)$ from a single measurement $R(\lambda)$. Formally, this problem has no unequivocal solution. Inversion is only possible if prior knowledge of the permissible shapes of the curves of $a(\lambda)$ and $b_b(\lambda)$ is used. If these spectra differ significantly and $R(\lambda)$ is measured with sufficient resolution (spectral and radiometric), their separation is possible.

The variability of $a(\lambda)$ and $b_b(\lambda)$ is determined via the water constituents, by the phytoplankton especially, in the case of Lake Constance. Its concentration influences the absorption and the amplitude of the backscattering; the refractive index and size distribution principally effect the spectrum of the scattering. While phytoplankton absorption has a number of minima and maxima in the wavelength range from 400 to 800 nm, $b_b(\lambda)$ has virtually no structure. This difference allows separation of the two spectra.

Since the absorption of water in the red is considerably greater than the absorption of the phytoplankton, the scattering determines the reflectance in this case. Scattering can be approximated by the formula $B_0+B_1\lambda^{-1}$, (see Section 3.5.2). If for $\lambda > 700$ nm, $a(\lambda)$ is allowed to equal $a_w(\lambda)$ and $b_b(\lambda) = b_{b.w}(\lambda) + B_0$, equation (4.1) can be solved for B_0. The scattering can therefore be determined from the spectral region $\lambda > 700$ nm for the approximation $B_1 = 0$.

The value of B_0 determined is a good approximation for the scattering in the range 700 to 800 nm, since the wavelength dependency of scattering is negligible for this relatively small interval. How well this value represents the scattering in the overall measurement range 400 to 800 nm depends on two factors:

- on the value B_1,
- on the vertical layering.

The smaller B_1 is, the more $b_b(\lambda)$ approaches the constant B_0. The vertical layering relates to the signal depth: the coefficients B_0 and B_1 are proportional to the particle concentration determined over the signal depth. If the particle concentration is layered vertically, B_0 and B_1 are thus a function of the signal depth, which is a function of wavelength. To what extent the scattering

determined in the red - where the signal depth is very low - characterizes the scattering in the remaining measurement range therefore depends on the layering.

If the value determined for B_0 were to represent the scattering by the phytoplankton for the entire spectral range 400 to 800 nm, the spectrum $a(\lambda)$ could be calculated from Equation (4.1). It has been shown that phytoplankton absorption can be described by Equation (3.31) (see Section 3.5.1). Since the absorption by water and yellow substance are also known, this may be used as a check of whether the derived absorption spectrum can be correct: if fitting by Equation (3.31) is successful, the spectra $a(\lambda)$ and $b_b(\lambda)$ determined are consistent with $R(\lambda)$ and thus with the prior knowledge used. Inversion cannot achieve more. The circumstances under which the derived spectra are correct must be determined by comparison with *in situ* data.

4.3.2 General program structure

Two PC programs were written with different approaches for the absorption and scattering spectra: INVERS uses representative spectra for different algal classes and yields their concentrations as the result, WASSER models the phytoplankton spectra and yields curve parameters as the result, from which the pigment concentrations may be inferred and then, from these, the algal classes.

What the programs INVERS and WASSER have in common is that they separate the absorption and scattering contributions from a reflectance spectrum according to Equation (4.1) by varying parameters to minimize the difference between the measured spectrum and model curve (least square fit). The model curve is optimized by the Simplex algorithm which is explained in Appendix B.

The parameter measured was not reflectance $R(\lambda)$, but the

albedo $\rho(\lambda)$. They differ by an offset F_0 and a scaling factor F_1, see page 46, Equation (2.24a). The equation below is therefore used to fit measured spectra $\rho(\lambda)$:

$$\rho(\lambda) = F_0 + F_1 \gamma \frac{b_b(\lambda)}{a(\lambda) + b_b(\lambda)}.$$

If the light reflected at the water surface had the same spectrum as the incident light, the Fresnel reflection for a smooth water surface in the nadir direction would have the constant value $\sigma^+ = 0.02$. The offset would then be $F_0 = \sigma^+ = 0.02$ and the scaling factor $F_1 = (1-\sigma^+)(1-\sigma^-) = 0.45$ for $\sigma^- = 0.54$ (see page 40). In practice, these requirements are usually not met; in this case a spectrum proportional to the reflectance is generated from the measured albedo by varying the orientation of the white plate or by suitable manipulation of the measured spectra (cloud correction, see Section 2.3.5). It is known that the proportionality constants are only close to 0.02 or 0.45 under "ideal conditions", they frequently deviate markedly from these values. In the two programs, F_0 and F_1 are therefore fitting variables and can be varied during the fit.

In the calculation of a model reflectance spectrum, input spectra are required. The fitting programs either calculate these themselves or they read in the data from a file. The following spectra can be calculated by the fitting programs:

- yellow substance absorption according to Equation (3.30). Apart from $a_Y(\lambda_0)$, the exponent S is a fitting variable and is optimized as desired.

- scattering by water in accordance with Equation (3.28).

- particle scattering in accordance with the formula $B_0+B_1\lambda^n$. Apart from the amplitudes B_0 and B_1, the power

n may be optimized. According to Section 3.5.2, n = -1 is an acceptable approximation.

Parameters necessary for the calculation and the file names of the spectra are read from a parameter file (DEFAULT.INV, DEFAULT.WAS) at the start of the program. This ASCII file also contains all the important program parameters such as path names, the initial values of all curve-fitting parameters or control variables to establish which curve-fitting parameters are varied and which are kept constant. The file can be processed by any editor. Modifications to the program which effect the preset concentrations or number and type of input spectra can thus be made very easily without having to modify the source code (Turbo Pascal 7.0).

4.3.3 The INVERS program

The INVERS program uses the spectra for absorption and scattering of at most 6 phytoplankton classes or species to calculate the reflectance. These spectra are read in from files.

After a reflectance spectrum has been fitted, the curve-fitting parameters can be stored. This is performed in the form of a table which contains the names of the curve-fitting parameters, their values determined in the fit and, for those curve-fitting parameters which represent concentrations, the file names of the absorption and scattering spectra used. This table has the following appearance

File produced by INVERS (9.12.1993)
Reflectance spectrum: B45.REF

FITTING PARAMETERS		FILE NAMES	
Water =	1	Wasser.A	Wasser.B
Y =	0.00605	Y.A	0
CRYPT =	0.00637	COVATA2.A	0
DIAT =	0	FRCROT.A	0
DINO =	1.51	SMEK4.A	0
GREEN =	3.86	MOUG.A	0
RHOD =	0	RHODOM.A	0
AVERAGE =	0	BODENSEE.A	0
B0 =	0.0161		
B1 =	0		
F0 =	0.0244		
F1 =	1		
CHL =	5.37		

The files having the extension "A" are absorption spectra, and the files having the extension "B" are scattering spectra. In the case of yellow substance and the 6 phytoplankton absorption spectra, the scattering is ignored, which is designated by the inclusion of "0" in the file name. The scattering by phytoplankton is approximated, together with the scattering by all other suspended particles, by the equation $b_b(\lambda) = B_0 + B_1\lambda^{-1}$. The result of the fitting yielded by the program INVERS is:

- the absorption of yellow substance at 450 nm (m^{-1}),
- the concentrations of at most 6 phytoplankton classes (μg of chlorophyll a/l),
- the scattering parameters B_0 (m^{-1}), B_1 (dimensionless),
- offset F_0, scaling factor F_1 of the measured albedo spectrum (dimensionless),
- the total concentration of chlorophyll a ($\mu g/l$).

4.3.4 The WASSER program

Instead of using representative spectra of individual classes, the WASSER program models the phytoplankton absorption according to Equation (3.31) by a sum of Lorentzian functions and approximates the scattering by $B_0 + B_1\lambda^n$. The curve-fitting parameters are thus not directly the concentrations of the individual classes as in INVERS, but are amplitudes, line widths and wavelengths of the individual absorption peaks and amplitudes B_0 and B_1 and the power n of the scattering.

Before starting the program, the parameters must be provided. Typical values of the resonance frequencies and line widths of the phytoplankton in Lake Constance are given in Table 6.1. As is shown, the result of the fitting depends on the choice of initial parameters. If the same set of initial parameters were used for each reflectance spectrum, the result of the fitting would have a systematic error. In order to reduce this, it is advisable to vary the initial parameters. The reflectance spectra measured on the same day are frequently similar; differences in the resulting fitting parameters then reflect the accuracy in their determination.

5. Measurements

5.1 Instruments

5.1.1 Spectrometer

All measurements of radiance in the present work were made with the TN 1710 spectrometer (TRACOR Northern), owned by the DLR. Extensive spectrometer calibration measurements are documented as an internal DLR report (Gege 1992). Table 5.1 summarizes the instrument specifications, see the report for details.

General	
Data format	12 bit
Polarization sensitivity	< 5%
Clock accuracy	< 0.001 sec
Aperture angle of the entrance optics	1.8°
Detector temperature	about 0°C
Wavelength calibration	
Wavelength range	388-803 nm
Number of channels	512
Channel width	0.8 nm
Spectral resolution*	2.1-3.8 nm (λ < 670 nm) 5.7-11.6 nm (λ > 690 nm)
Absolute accuracy	±0.14 nm (λ < 715 nm) ±0.44 nm (λ > 715 nm)
Radiometric calibration	
Calibrated range of integration time	0.07 to 70 sec
Minimum radiance	0.4 mW m^{-2} nm^{-1} sr^{-1}
Absolute accuracy	± 5%
Relative accuracy	± 1.5% for SNR>600

Table 5.1: Spectrometer specifications

*For the first 12 days (18.4.-3.7.90) on which measurements were made, the spectral resolution was 29 nm, because the entrance slit was wrongly adjusted.

The spectrometer is composed of the entrance optics, image-forming grating, diode array and read-out electronics. In the entrance optics, the light is focused by a lens onto the entrance slit. The image-forming grating performs the spectral dispersion and focuses the spectrum onto the image plane in which the diode array is mounted. For a presettable time, the charges are integrated there, then digitized via an analog-digital converter and then read out into a memory. A computer may be connected via a serial interface; at the moment, an Atari 520 ST+ is used, in order to store the spectra on diskette. Further processing of the data, including subtracting the dark current, is performed with a PC.

In order to keep the dark current low, the diode array is cooled with a Peltier element. Water vapour would therefore condense or freeze out on the array, if the interior of the spectrometer were not free of water. This is prevented by using a nitrogen atmosphere: at the beginning of a series of measurements, gaseous nitrogen is vigorously passed into the instrument interior until nitrogen has displaced the air. The nitrogen flow is then throttled until the inflowing gas balances the losses. The slight over-pressure prevents air from penetrating into the instrument.

5.1.2 HPLC system

High pressure liquid chromatography (HPLC) utilizes differences in polarity to separate the individual pigments of a mixture.

An HPLC analysis begins with extraction of the pigments from the phytoplankton cells. This step is intended to dissolve the pigments out of the cell membrane as completely as possible and to transfer them into the liquid phase of the extraction medium. Acetone was used as solvent which covers all lipophilic pigments and their decomposition products, see Table 5.2.

The dissolved pigments are injected into a liquid mobile phase (acetone/water mixture) which is forced under high pressure (45-110 bar) through the separation column. In order to protect the separation column from impurities, the mobile phase stream first passes through a precolumn containing silica gel of 5 µm particle diameter. The separation column itself is packed with irregularly rounded silica gel particles of 5 µm diameter, the surfaces of which are derivatized with an octadecyl radical, a strongly lipophilic C^{18} unit. On passage through the column, unpolar pigments interact more strongly with the beads than the polar pigments, and therefore the lower the polarity of the pigment, the greater is the retardation of the passage through the column. The retention time is additionally dependent on the column length and the temperature. In the system used by the University of Konstanz, the separation column has a length of 25 cm and is operated at 40°C. In this case, the retention time for the slowest pigment, β-carotene, is 30 minutes.

After the separation column, the individual pigments are present in the mobile phase at different times. The mobile phase stream is therefore passed through various detectors which indicate the properties of the mobile phase as a function of time. Calibration measurements allow retention times to be established for individual pigments.

Chlorophyll a	++	Diatoxanthin	0
Chlorophyll b	+	Fucoxanthin	++
Chlorophyll c	-	Lutein	+
Chlorophyll a allomer	++	Neoxanthin	0
Chlorophyll a isomer	++	Phaeophorbide a (?)	-
Alloxanthin	++	Phaeophytin a_1	-
β-carotene	++	Phaeophytin a_2	-
Cryptoxanthin	++	Violaxanthin	0
Diadinoxanthin	+	Zeaxanthin	+

Table 5.2: Pigments covered by HPLC and their ease of determination. From Kenter (1991). Depending on the type of HPLC system, the concentrations of different pigments are determined with different accuracies. This is symbolized by the symbol used: "++" very good, "+" good, "0" fair, "-" poor.

In the system used, the detection equipment is two absorption detectors (Millipore-Waters 481, Spectra Physics 8450) and one fluorimeter (Perkin-Elmer M 3000), which are connected to two integrators (Shimadzu C-R3A, Spectra Physics C-R3A) and a two-channel recorder (Linseis). The absorption is measured at 430 nm and 460 nm, fluorescence at 670 nm (excitation at 407 nm). Because of frequently occurring faults with the Spectra-Physics detector, the 460 nm absorption could only be recorded for some of the samples, which chiefly impaired the accuracy of chlorophyll b measurement.

Since the specific absorption and fluorescence coefficients are known (or have been determined by calibration measurements), the concentrations of the individual pigments can be determined by integrating the recorded curves. The wavelengths selected on the detectors determine the accuracy of measurement. They were optimized for pigments indicated by the symbol "++" in Table 5.2.

Further details of the Konstanz HPLC system and the calibration measurements are described in Kenter (1991).

An extensive survey of separation columns, mobile phases and reference wavelengths suitable for analysis of algal pigments can be found in the book by Rowan (1989), Table 2-6.

5.1.3 Photometer

For many years, the Limnological Institute of Constance University has been determining the concentrations of the pigments chlorophyll a and phaeophytin a at the measurement point in the Überlinger See at depths of 0, 1, 2, 3, 4, 5, 6, 7, 8, 10, 12.5, 15, 17.5, 20, 22.5, 25, 27.5 and 30 metres photometrically at weekly intervals (in winter every 2 weeks). The water samples are filtered on board ship and analysed in the laboratory within a few hours, using Nusch's method (1980) to measure the extinction of the filtrate at 665 nm relative to the extinction at 750 nm and compare it with the extinction values after acidification with HCl.

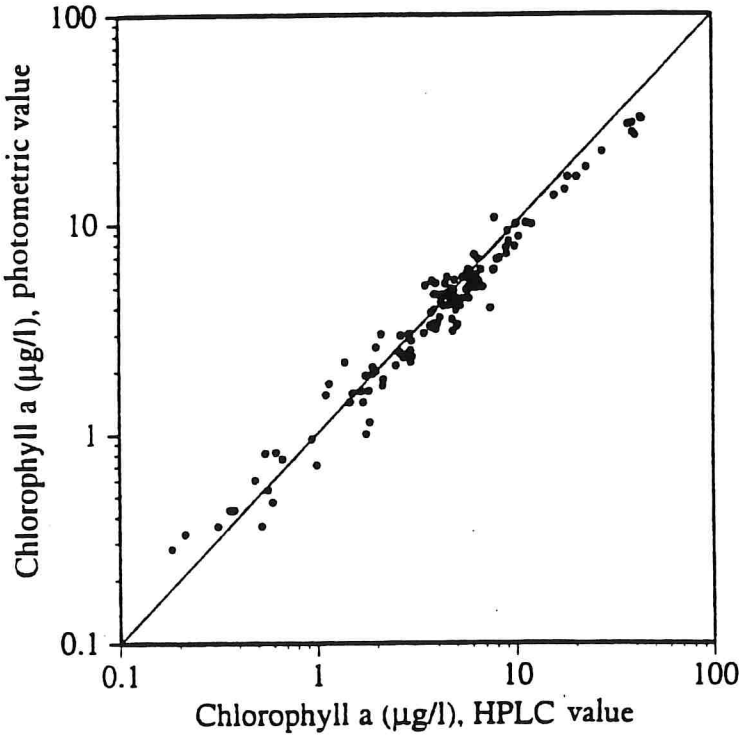

Figure 5.1: Comparison of the two methods for determining the concentration of chlorophyll a. The results of the HPLC analysis of 132 water samples taken on 22 days in

1990 at the depths of 0, 2, 5, 10, 15 and 20 m are plotted against the corresponding concentration values given by the photometric evaluation.

This photometric chlorophyll determination was performed independently of the HPLC analysis, permitting the accuracy of the determination of concentration to be estimated by comparing the results. In Figure 5.1, concentrations given by HPLC analysis for samples obtained on 22 days in 1990 are plotted against the values determined by photometry. The results correlate well ($r = 0.989$, $N = 132$), but at high concentrations the photometric value is always smaller than the HPLC value. As Figure 5.2 makes clear, this systematic error below 10 µg/l is 8.6%; above this it is 24%. Since the HPLC method is the more accurate, the photometric measurements were multiplied in the evaluation by the factor 1.086 ($C \leq 10$ µg/l) or 1.24 ($C > 10$ µg/l).

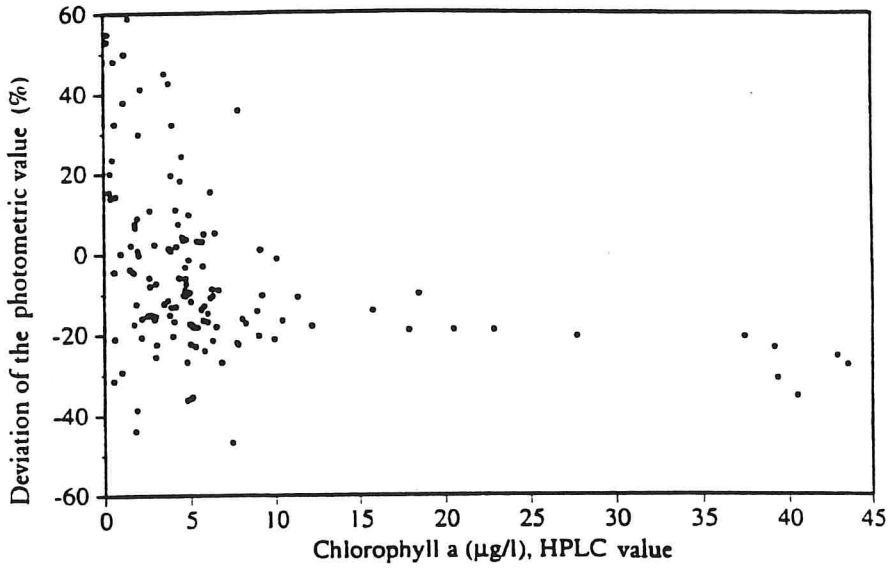

Figure 5.2: Accuracy of chlorophyll determination in dependence on concentration. Up to a concentration of 10 µg/l, the photometric values are on average 8.6% below the HPLC values for a standard deviation of 22%. Above 10 µg/l, the systematic deviation is 24%, the standard deviation is 8%.

Using this correction, for C > 10 µg/l, the agreement is very good, but at low concentrations the results of measurement are markedly scattered. If the standard deviation in the plot of Figure 5.2 is taken as a measure of the relative accuracy of the determination of concentration of chlorophyll a, it is 22% for C ≤ 10 µg/l and 8% for C > 10 µg/l. The absolute accuracy is ± 1.33 µg/l.

5.2 Correlation between chlorophyll a and other measurements

Chlorophyll a is the most important of the algal pigments since it is essential for photosynthesis and occurs in all species. It is therefore measured every time pigments are determined and the aim of every evaluation of optical spectral measurements is also at least determination of the chlorophyll a concentration.

In the *in situ* measurements on Lake Constance, in addition to chlorophyll a, the concentrations of phaeophytin a, carotenes, xanthophylls and of chlorophylls b and c were measured. As is explained below, these pigments correlate well with chlorophyll a. It is therefore unnecessary to develop an algorithm for derivation of their concentrations from spectral measurements independently of chlorophyll a. However, phaeophytin a is an exception. Such an algorithm would be very interesting for this pigment, since the phaeophytin concentration increases markedly when the water body contains dead algae.

Spectral measurements made on a water body permit the concentration of light-absorbing pigments or light-scattering particles to be derived, but not directly the abundance or biovolumes which the biologist uses to characterize a water body. Estimates are given in Sections 5.2.4 and 5.2.5 of how accurately abundance or biovolumes may be determined from spectral measurements.

Since the biovolume correlates better than the abundance with the chlorophyll a concentration (and therefore with the reflectance spectrum), figures given in this study on the relative proportions of individual species of the total population always refer to the biovolume.

5.2.1 Phaeophytin a

In Figure 5.3, the phaeophytin concentration P is plotted against the chlorophyll concentration C for 414 water samples taken in 1990 from depths of 0 to 30 metres. The majority of the measurements are close to the plotted straight line,

$$\ln P = -0.8565 + 0.7424 \cdot \ln C. \qquad (5.1)$$

The ratio of phaeophytin a concentration to chlorophyll a concentration is thus typically P/C = 0.23 to 0.42 (at C = 10 and 1 µg/l, respectively). However, there are also measurements where a considerably greater ratio was observed. These usually high phaeophytin concentrations occur in two cases:

1. at great depth (symbol: plus sign),
2. after a marked algal bloom (open symbols).

In both cases, the majority of the phytoplankton has died, and phaeophytin is known to be a decomposition product of chlorophyll (see Section 3.4.3). If in addition to chlorophyll a the concentration of phaeophytin a is also determined, an indication of the vitality of the algal population is obtained: the phaeophytin which is observed at a concentration above that calculated from Equation (5.1) originates from dead phytoplankton.

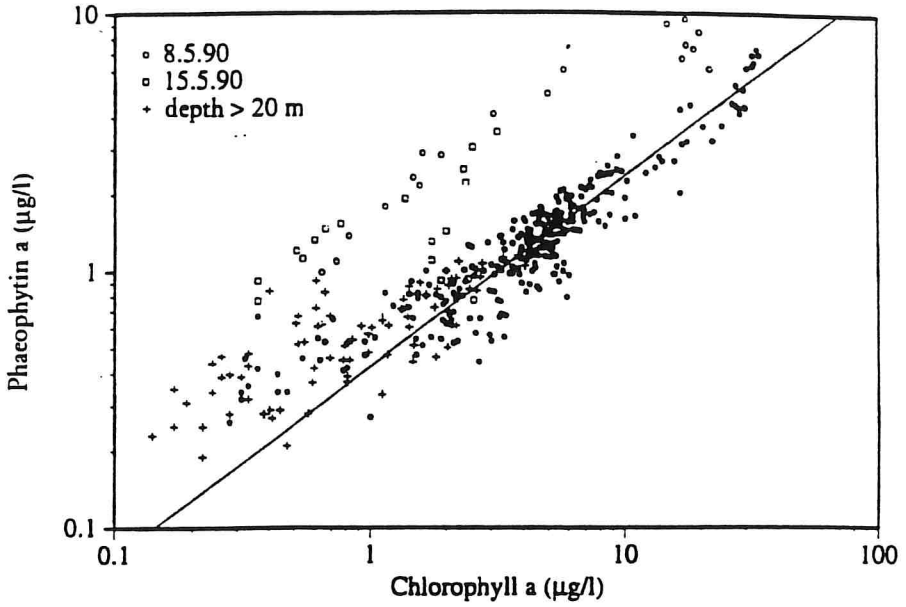

Figure 5.3: Relationship between phaeophytin and chlorophyll concentrations. 294 measurements taken from depths of from 0 to 20 m (filled circles) were used to calculate the regression line.

5.2.2 Carotenoids

In Figures 5.4 and 5.5, the concentration of carotenes (K) and xanthophylls (X) respectively is plotted against the chlorophyll concentration (C). The figures show the HPLC results of all 132 water samples from 1990 which were available for the present work. Both carotenes and xanthophylls correlate well with chlorophyll a, systematic deviations as occurred in the case of phaeophytin can not be observed. That is to say, in particular, that the relative proportion of the carotenoids is similar in different algal species. The equations of the regression lines for log log plots of Figures 5.4 and 5.5 are as follows:

$$\ln K = -3.316 + 1.201 \cdot \ln C, \qquad (5.2)$$

$$\ln X = -1.300 + 1.150 \cdot \ln C. \qquad (5.3)$$

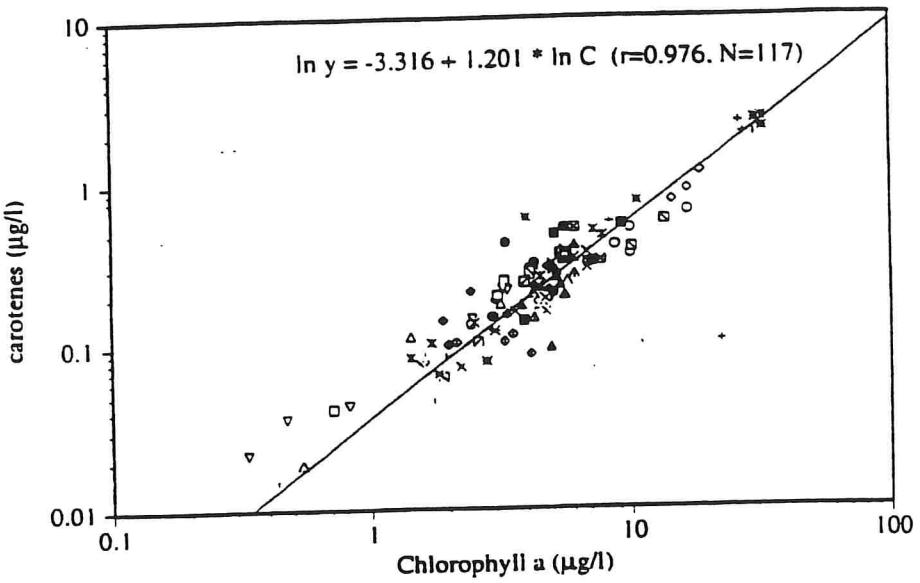

Figure 5.4: Correlation between carotene and chlorophyll concentrations. Each sampling day is indicated by a separate symbol.

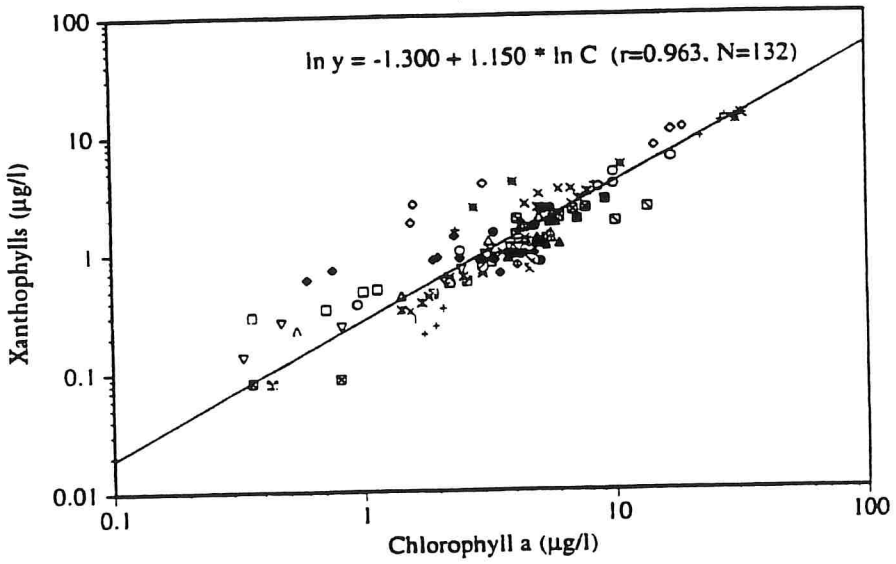

Figure 5.5: Correlation between xanthophyll and chlorophyll concentrations. Xanthophyll was not detected in 15 measurements; these measurements were discarded.

When the chlorophyll concentration is known, the carotene and xanthophyll concentrations can be estimated therefrom. The relative proportion of carotenes is typically K/C = 0.034 to 0.055, and the proportion of xanthophylls is X/C = 0.27 to 0.38 (for C = 1 to 10 µg/l). At a high

chlorophyll content, the relative proportion of carotenoids is higher than at low chlorophyll concentration. A clear explanation cannot be given for this: since carotenoids protect against sunlight, one would expect the opposite (von Smekot-Wensierski et al. 1992).

5.2.3 Chlorophylls b and c

As a further result of the HPLC analysis of the water samples taken in 1990, in Figures 5.6 and 5.7, the concentration of chlorophylls b and c is plotted against that of chlorophyll a. From Table 3.2, chlorophyll b or c is expected to be absent from some algal classes. Measurements made on days when such classes predominated are symbolized by open circles.

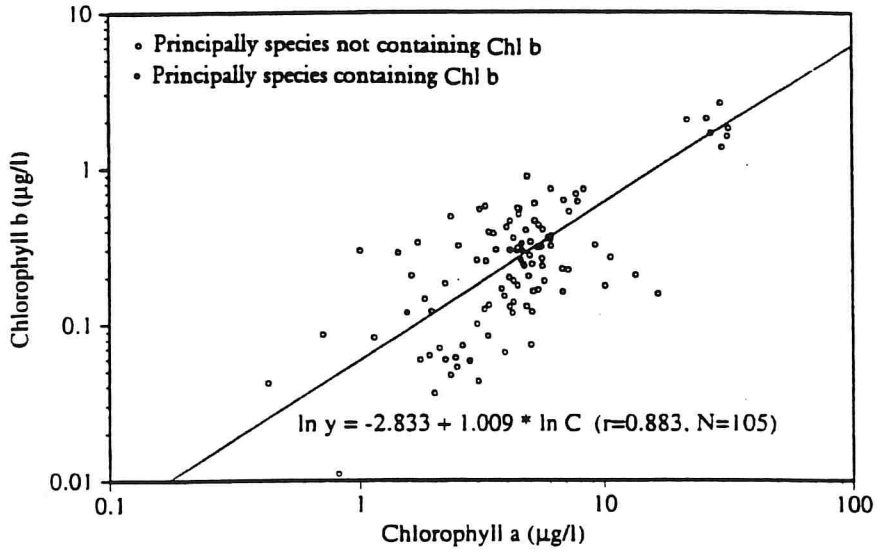

Figure 5.6: Correlation between the concentrations of chlorophyll a and chlorophyll b.

Chlorophyll b was generally absent from the predominant species; they contained chlorophyll c in its place. The few water samples where species containing chlorophyll b predominated do not show higher concentrations than the other samples; in water samples where species lacking chlorophyll c predominated, although the concentrations were beneath the expected value (beneath the regression line), they were still within the bandwidth of the samples containing chlorophyll c. Since the predominant

species usually constituted only 20-50% of the total volume of all species, the absence of a pigment in the predominant species can be compensated for by its occurring in several of the less frequent species and vice versa. The inaccuracy in the determination of the concentration and, above all, the variety of the phytoplankton lead to the high scattering of the measurements. Using the plotted regression lines

$$ln\ Chl\ b = -2.833 + 1.009 \cdot ln\ C, \qquad (5.4)$$

$$ln\ Chl\ c = -2.886 + 1.226 \cdot ln\ C. \qquad (5.5)$$

the concentrations of chlorophylls b and c may be estimated approximately if the chlorophyll a concentration is known - however, individual measurements are above or below the line by up to a factor of 5. Since the concentration of chlorophylls b and c is generally lower than chlorophyll a concentration by an order of magnitude and the specific absorption coefficients are comparable, the concentrations cannot be established more accurately from reflectance spectra than by using Equations (5.4) and (5.5).

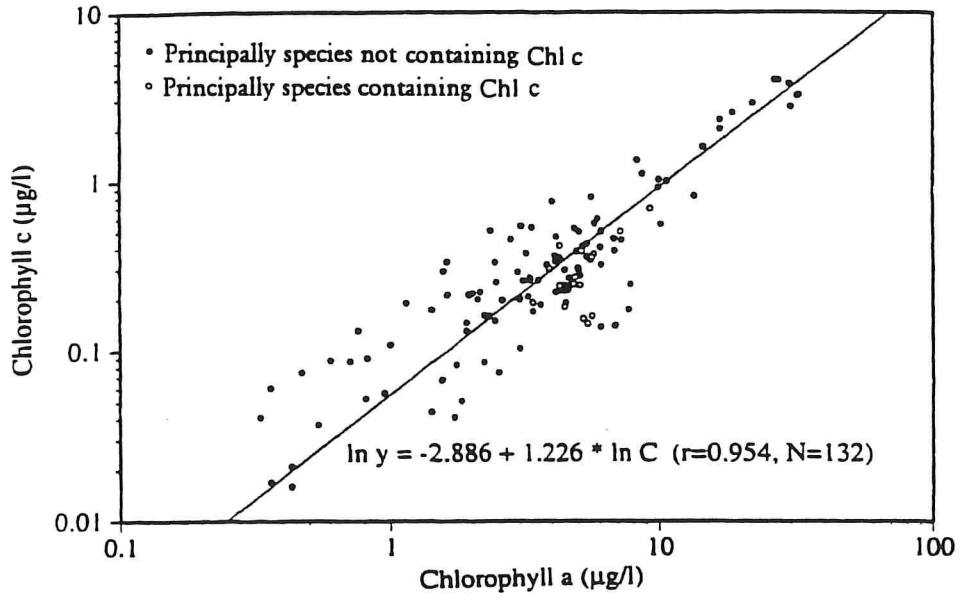

Figure 5.7: Correlation between the concentrations of chlorophyll a and chlorophyll c.

5.2.4 Abundance

In order to study the development of the phytoplankton in Lake Constance, mixed samples from the depth ranges 0 to 8 m and 8 to 20 m are routinely taken by the Limnological Institute of The University of Konstanz and the cells of all species of phytoplankton recognizable by light microscopy are counted from the mixed samples. These unpublished abundance data were kindly made available to me by Ursula Gaedke and Annette Schweitzer (Limnological Institute of the University of Konstanz.

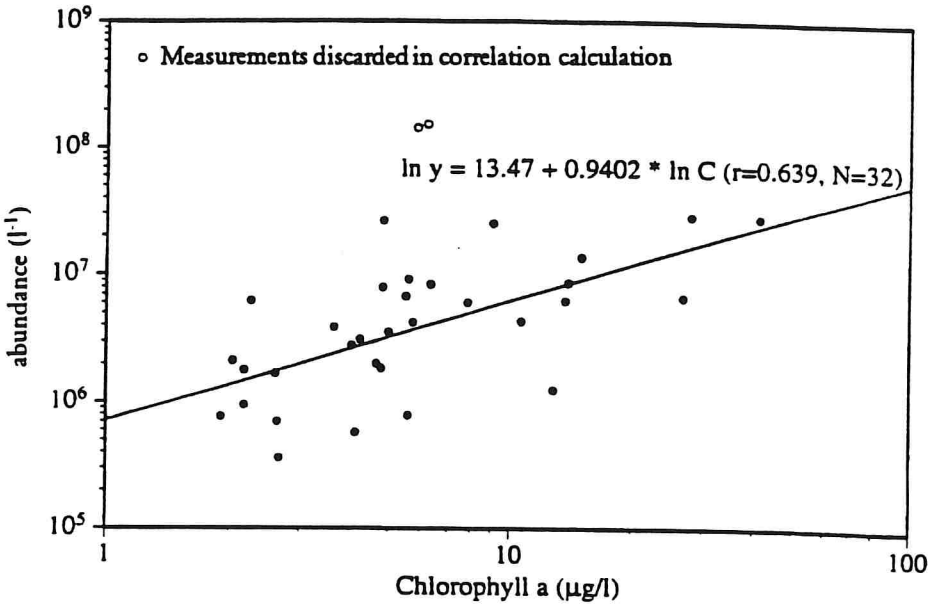

Figure 5.8: Correlation between the chlorophyll a concentration and the abundance (number of cells).

For 34 sampling days, in addition to the cell data, depth profiles of the chlorophyll a concentration (photometric measurements) were also available, which allowed calculation of the mean chlorophyll concentration for the depth range 0 to 8 m. This is plotted against the abundance (number of cells) in Figure 5.8. Although there is a correlation between the two parameters ($r = 0.64$), when the abundance Z is calculated from the chlorophyll a concentration using the Equation

$$\ln Z = 13.47 + 0.9402 \cdot \ln C, \qquad (5.6)$$

the mean error is 90% and the maximum deviation for this data set is as high as 736%. (The two measurements indicated of 24.7.90 and 7.8.90 were not included in the calculation.) The abundance, therefore, can only be estimated very inaccurately from spectral measurements using chlorophyll a absorption.

5.2.5 Biovolume

The mean cell volume is tabulated for each species occurring in Lake Constance; the tabulated values are the result of measurements made over several years. If the number of cells is multiplied by their average volume, the total volume is obtained for each species in the water sample. If this is summed for all species, the biovolume is obtained. In Figure 5.9, using the same dataset which forms the basis for Figure 5.8, the biovolume is plotted against the chlorophyll a concentration. The correlation is r=0.79, and the equation of the regression line is:

$$\ln B = 12.41 + 0.6488 \cdot \ln C. \qquad (5.7)$$

If the biovolume B is calculated from this equation, the mean error is 33%, and the maximum error is 146%. The biovolume is therefore more closely related to the chlorophyll concentration than the abundance and its order of magnitude may be reliably determined from spectral measurements.

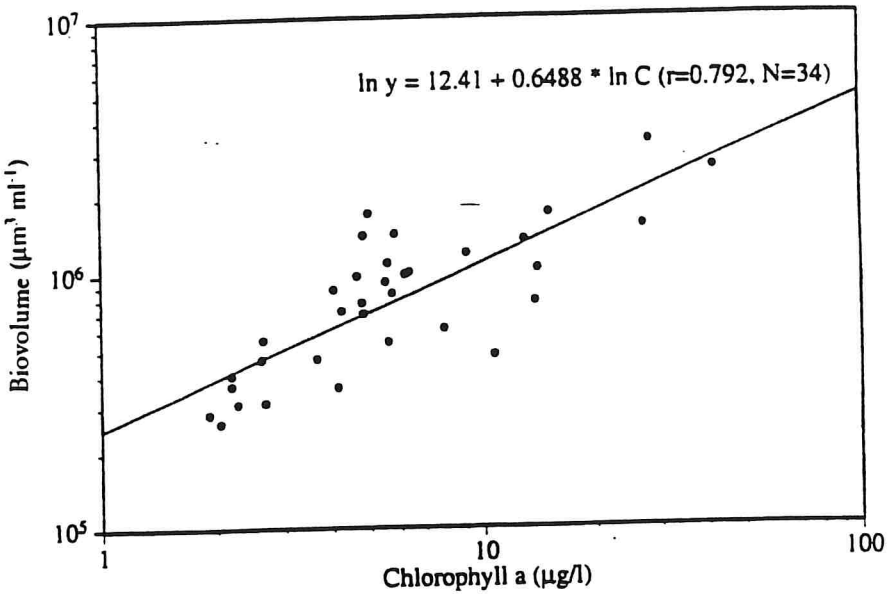

Figure 5.9: Correlation between the chlorophyll a concentration and the biovolume.

5.2.6 Secchi depth

If a white disc is lowered into the water, the depth from which it is no longer visible with the naked eye is termed *Secchi depth*. For the interpretation of remote sensing data, it is important to know which depth region the measurement signal originates from; here, the Secchi depth provides a reference point. As can be seen from Figure 5.10, Secchi depth is correlated with the chlorophyll concentration (cf. also Tilzer 1988) and may be estimated by the following equation:

$$Secchi\ depth\ (m) = 12.13 - 2.865 \cdot \ln C. \qquad (5.8)$$

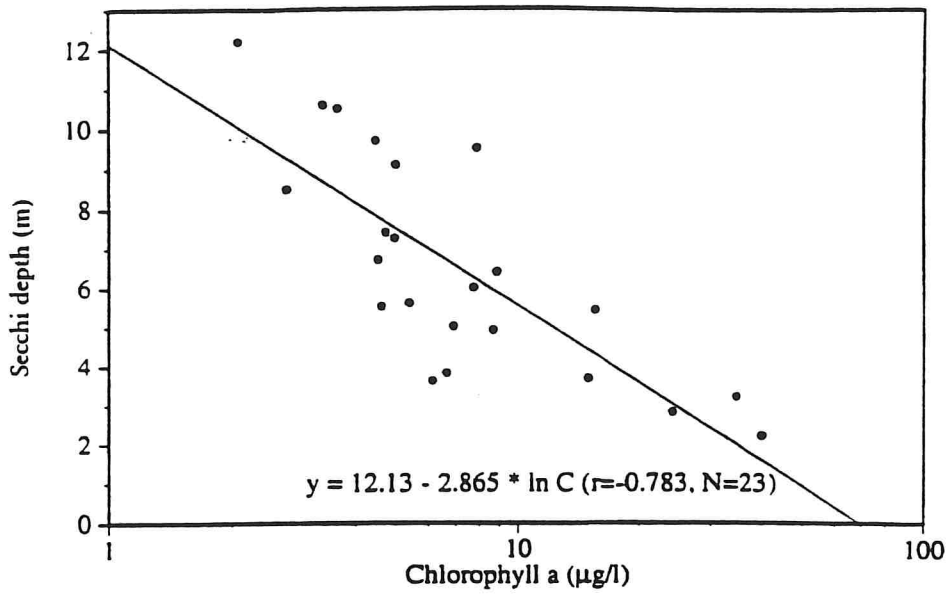

Figure 5.10: Correlation between Secchi depth and chlorophyll a concentration averaged from 0 to 2 m.

5.3 Yellow substance

5.3.1 Literature data on yellow substance in Lake Constance

Yellow substance has been little studied in Lake Constance. There are no publications from which a reliable estimate can be derived of the typical concentration or of the seasonal differences. The only studies known to the present author on yellow substance in Lake Constance are the three below.

Banoub (1973). The yellow substance concentration was determined for three transects through a reed area in the Gnadensee (between the island of Reichenau and the Bodanrücken), on the surface and at the bottom in each case. To relativize the results, the concentration was also determined 50 m and 500 m from the reed bed, so that in total 12 measurements were obtained in the open water. Concentration was determined optically by measuring the absorption of filtered water (Whatman GF/C glass fibre filter, no indication of pore size) in a quartz cuvette

with 10 cm path length at 260 nm. In parallel to this, the concentration was determined chemically (oxidation by acidic permanganate), and the correlation between the optical and chemical results was r = 0.74 (250 samples). The result for the measurement points outside the reed bed is summarized in Table 5.3; in the reed bed, the concentration is higher by up to three times.

	Surface	Bottom
50 m outside the reed bed	3.6 ± 0.4 mg/l	4.1 ± 0.2 mg/l
500 m outside the reed bed	3.3 ± 0.1 mg/l	3.2 ± 0.1 mg/l

Table 5.3: Yellow substance concentration in the Gnadensee 1970. From Banoub (1973). The Gnadensee is part of Lake Constance.

Maier and Geller (1973). This study introduced the possibility of rapidly obtaining a picture of concentration differences of dissolved organic substance and nitrate by using UV difference spectra: the difference in the UV absorption of two water samples is measured and information is thus obtained as to which sample contains more yellow substance or nitrate. The UV difference in this article is not calibrated to the absolute yellow substance concentration since, even without this calibration, it is possible to differentiate different bodies of water on the basis of yellow substance absorption. However, the absolute measurement of 13.7.77 can probably be considered as a typical concentration for the Überlinger See: the surface concentration was 1.5 mg/l, and 1.1 mg/l was observed at a depth of 60 m.

Stabel (unpublished). According to unpublished measurements made by Dr. Stabel (Lake Constance Water Supply Administration Union, Sipplingen), the yellow substance concentration in the Überlinger See varies from a minimum of 1.05 mg/l in winter to a maximum of 1.8 mg/l in summer (personal communication 23.5.91).

5.3.2 Measurement of yellow substance on 25.6.91

Because of the scarcity of information on yellow substance in Lake Constance, the *Joint Research Center* (Ispra, Italy) kindly offered to determine yellow substance. The results are listed in Table 5.4 and illustrated graphically in Figure 5.11.

The measurements summarized in Table 5.4 were carried out at the usual measurement point in the Überlinger See (see Section 5.4). 1 ml of NaN_3 solution was added to each of the water samples to avoid bacterial decomposition. The absorption $a_Y(\lambda)$ was measured with a single-beam photometer (Perkin Elmer LA 3840), the absorption of a cuvette filled with distilled water being deducted each time. In addition, to correct the scattering, the smallest value in the range 670-700 nm was subtracted. For absorption values below 0.5 m^{-1}, the error is at most 10%, for larger values it is smaller.

From Equation (3.30), the parameters a_Y (450) and S can be derived from the three measurements at 300, 375 and 400 nm, and they are listed in Table 5.4. The correlation is very high. The yellow substance concentration C_Y was calculated using Equation (3.29) from a_Y (450).

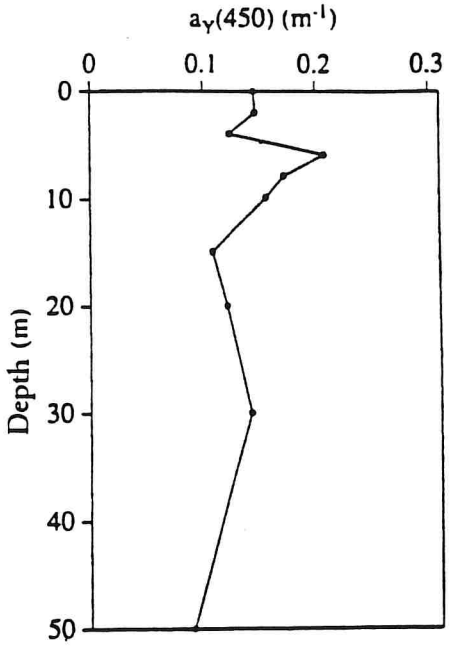

Figure 5.11: Yellow substance absorption in the Überlinger See on 25.6.91. Graphical display of the values given in Table 5.4.

The measurements yield a mean exponent $S = 0.0220 \pm 0.0012\ nm^{-1}$. S is thus greater than is the case for marine yellow substance (about $0.016\ nm^{-1}$), but the value of $0.035\ nm^{-1}$ observed by Doerffer and Amann (1984, 1986) in an algal bloom in the North Sea is still higher (compare Section 3.4.1).

The concentrations given in Table 5.4 are only half those which would be expected from Section 5.3.1. The reason for this is presumed to be the fact that equation (3.29), which was used to convert the absorption to concentration, does not apply in this case. It was derived by Nyquist for marine yellow substance which obviously has a different absorption behaviour. Apparently, when Equation (3.29) is used, the concentration of yellow

substance in Lake Constance is underestimated. However, absorption, not concentration is the critical parameter for description of the optical properties of the water. Therefore the results of measurements in Table 5.4 provide reliable information for modelling reflectance.

measured					calculated		
Depth	a_Y (m^{-1})				S	r^2	C_Y
(m)	300 nm	375 nm	400 nm	450 nm	(nm^{-1})		(mg/l)
0	3,789	0,690	0,460	0,146	0,0215	0,9964	0,688
2	3,634	0,700	0,440	0,147	0,0213	0,9990	0,695
4	3,900	0,670	0,396	0,124	0,0230	0,9995	0,583
6	4,450	0,897	0,592	0,208	0,0204	0,9979	0,981
8	4,070	0,820	0,506	0,172	0,0210	0,9996	0,812
10	3,660	0,820	0,430	0,156	0,0211	0,9969	0,738
15	3,940	0,670	0,360	0,108	0,0239	0,9999	0,510
20	3,547	0,720	0,350	0,121	0,0227	0,9956	0,569
30	3,280	0,620	0,420	0,142	0,0209	0,9960	0,668
50	3,470	0,540	0,320	0,091	0,0241	0,9990	0,430
100	3,540	0,680	0,400	0,137	0,0218	0,9999	0,645

Table 5.4: Measurement of yellow substance in the Überlinger See on 25.6.91. Measurements made by G.M. Ferrari. The concentration C_Y was calculated using Equation (3.29) which applies to marine yellow substance. Measured values from earlier years made by Maier and Geller (1979) and Stabel are about twice the calculated values.

5.4 Description of the measurement site

Figure 5.12 shows a map of Lake Constance. It extends from the south east to the north west over a length of

63 km and the mean water surface is at a height of 395 m above sea level. The large, deep main basin from the Bregenzer Bucht to the Constance Eichhorn is called the *Obersee*, the narrow north-west branch is the *Überlinger See* and the basin south of the Bodanrücken is divided into the *Gnadensee*, *Zeller See* and *Untersee*.

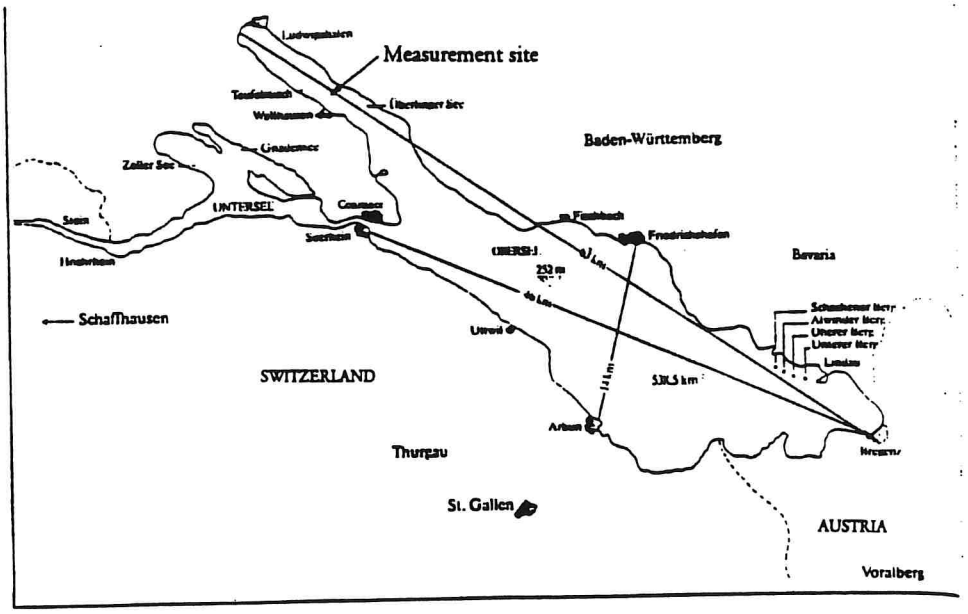

Figure 5.12: Lake Constance.

All the measurements in the present work were carried out in the vicinity of the deepest point of the Überlinger See (147 m) which is marked by a buoy. This is located roughly in the centre of the lake between Überlingen and Wallhausen and is indicated on the map. Whereas the Rhine introduces a high sediment load into the eastern part of the Obersee, the sediment content of the Überlinger See is low since the only significant inlet - the Stockacher Aache - delivers relatively little water. Its mouth is far from the measurement site at the north-western end of the lake. No information is available to the present author on exchange of water at the measurement site as a result of currents.

In this connection, an interesting phenomenon can be mentioned which has been documented for centuries on Lake

Constance and has only recently been able to be explained with certainty: "rise" and "flow". An oscillation of the water surface, stimulated by wind or atmospheric pressure differences, occurs in the longitudinal direction of the lake, resembling tides in the sea, but with a periodicity of 55 and 39 minutes; in the Überlinger See similar "seiches" of a few minutes duration also occur in the transverse direction. The associated currents can impede the mooring of ships. Usually, the water level changes by a few centimetres during this, but in rare cases such as the Constance water spectacle of 1549, the water level rose and sank by several metres. Internal waves between the epilimnium and hypolimnium can achieve amplitudes above 20 m (Geller and Güde 1989). This is due to self-oscillations of the lake, as has been shown by computer simulation (Wittum 1990).

5.5 Seasonal development of phytoplankton

Growth and decay of the phytoplankton are principally controlled by the incident light energy, available nutrients and the number of predators. None of these factors is constant: the light energy, apart from the seasonal cycle, is dependent on the cloud cover, the nutrients are introduced irregularly and are consumed by the algae themselves, and the number of predators (especially the zooplankton) is principally determined by the phytoplankton concentration. There are therefore several feedback loops in the population dynamics of a water body, for which reason the system is sensitive to changes in the boundary conditions.

For this reason the development of the phytoplankton concentration proceeds somewhat differently each year, and the change in species composition with time (*species succession*) cannot be predicted in detail. Only certain patterns are repeated seasonally: in winter insufficient light enters the water in order to maintain photo-synthesis, therefore the algal concentration is low in

winter and the nutrients introduced are not consumed. In spring the nutrients have accumulated and as soon as sufficient light is available, the algae begin to multiply rapidly (*algal bloom*). Species which are initially numerically predominant extend their dominance because of the exponential growth, but they can be overtaken by species having a shorter generation time. When the nutrients are consumed, growth stops and since the replenishment of nutrients is insufficient for many organisms, most of them quickly die. In addition, during the algal bloom the zooplankton finds a nutrient excess and likewise multiplies greatly. Therefore, at the end of the algal bloom, the phytoplankton concentration decreases rapidly as result of lack of nutrients and the large number of predators and a period of very low phytoplankton concentration follows. This period is called the *clear water stage*, since the Secchi depth is generally over 10 metres, compared with about 2 metres during the bloom.

The way in which the dynamics of the biocoenoses in Lake Constance lead to the clear water stage has been well studied and is an interesting example of the complexity of interactions in an ecosystem. According to measurements from 1976 (Lampert and Schober 1978), grazing of the phytoplankton by the zooplankton begins late, since the most efficient species, *Daphnia*, is consumed by another genus *Cyclops vicinus*. However, only the adult Cyclops are able to eat Daphnia and these die by the end of May. Following the disappearance of adult Cyclops, the Daphnia begin to multiply. Their concentration rises abruptly from the end of May and they substantially eliminate the phytoplankton because of their large number. This is the beginning of the clear water stage. There is now a lack of food for the zooplankton. The Daphnia develop resistant stages as they otherwise do in winter and can thus survive, but the majority of the Cyclops offspring starve. The Daphnia thus eliminate their predator by removing food from the predator's

offspring.

During the clear water stage, the nutrients reaccumulate. The zooplankton plays an important role in nutrient regeneration (Devol 1979). As the nutrient concentration increases, the phytoplankton concentration also increases and a second bloom occurs in the summer, but the concentration rarely achieves the high spring values. In the subsequent degradation phase, the concentration generally also does not fall to the low values of the spring clear water stage. Before the quiescent phase in winter, a further bloom frequently follows in autumn, especially when there is a long period of fine weather.

Phytoplankton development in Lake Constance is shown in Figure 5.13 for 1990 and 1991. The biovolume is the most meaningful parameter for comparison with spectral measurements (see Section 5.2.5), therefore the figure shows the biovolumes for the 5 most important algal classes of Lake Constance. Table 4.1 summarizes the predominant species.

The figure clearly illustrates the statement made initially, that phytoplankton development proceeds somewhat differently each year, but certain patterns recur. Until the beginning of March the phytoplankton concentration is low, but cell multiplication is then abruptly initiated. A decisive factor in this is, apart from the increased solar irradiance, the development of stable layering. This effects a considerable reduction of the mixing between the upper illuminated layer with the deep water so that the phytoplankton then remains long enough in a zone with favourable light conditions in order to make efficient photosynthesis possible.

In both years, the exponential increase in biovolume began in the second week in March and at first proceeded virtually identically. However, in 1991 this first bloom ended one week earlier than in the preceding year and

therefore did not achieve the high concentrations of 1990. The predominant species during this bloom was the Cryptophyceae *Rhodomonas lens* in 1990 and the diatom *Stephanodiscus hantzschii* in 1991.

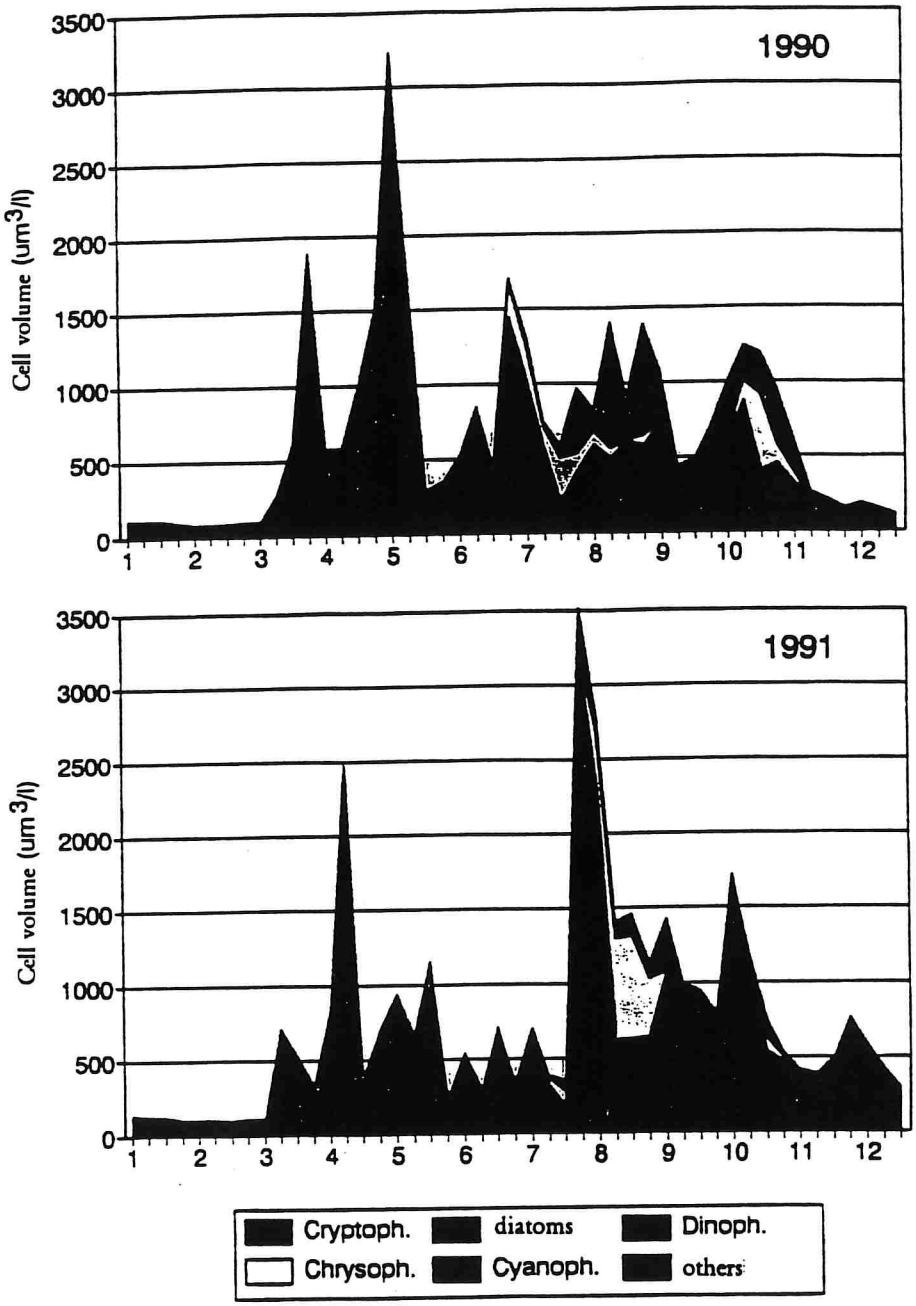

Figure 5.13: Phytoplankton development in Lake Constance. The diagram shows cumulative sums. From unpublished data by U. Gaedke and A. Schweitzer (with kind permission).

The second spring bloom was also more marked in 1990 than

in 1991. Although it began one week later, against this, it lasted 1 to 2 weeks longer and achieved extremely high concentrations which became noticeable as a red water coloration during the maximum on 2.5.90. The Cryptophyceae responsible for this, *Rhodomonas lens* and *Cryptomonas ovata* were still predominant until the beginning of June, then a greater species variety developed. This second spring bloom was also dominated by Cryptophyceae in 1991, but by a different species, *Rhodomonas minuta*. From the end of April until the end of May, in 1991 diatoms and dinoflagellates occurred in similar concentrations as the Cryptophyceae. They caused a third spring bloom which was absent in 1990. The *Chlorella* species which emerged on 22.5.91 at high concentration did not appear in the preceding year.

The clear water stage between the spring and summer blooms occurred in 1990 from 15.5. until 12.6. (with an elevated concentration on 6.6.) and occurred in 1991 from 28.5. until 16.7.. Cryptophyceae dominated in both years, principally *Cryptomonas* species (*C. ovata, C. rostratiformis, C. marssonii*). Their proportion of the overall volume of all species was generally above 80%.

A period of great species variety begins from the end of the clear water stage. A number of algal blooms follow until the end of October, the predominant species changing. The first bloom after the clear water stage was dominated in both years by diatoms, extreme concentrations occurring in 1991. (No spectral measurements were made on this bloom.) Then, for the first time in the year, Chrysophyceae and Cyanophyceae occurred at high concentrations. This development started 6 weeks later in 1991 than in 1990 and led to high cell concentrations until the December, whereas in 1990 the low winter values had already been measured at the beginning of November.

1990 was therefore characterized by a pronounced spring bloom and moderate concentrations in summer and autumn,

while in 1991, the spring bloom was overall rather weak, but the algal bloom in summer was vigorous and high concentrations were found until late in the year.

6. Determination of water constituents from reflectance spectra

Two PC programs were written to determine water constituents from reflectance spectra, WASSER and INVERS. They are described in Section 4.3. The programs differ in the treatment of the phytoplankton absorption: WASSER models this spectrum, INVERS uses 5 absorption spectra measured in the laboratory representing the predominant classes in Lake Constance. The program WASSER is suitable for the determination of concentrations of individual pigments, whereas phytoplankton may be classified by the INVERS program.

6.1 Spectral characterization of the phytoplankton in Lake Constance

When reflectance spectra are modelled by the WASSER program, inter alia, a set of parameters is obtained from which the phytoplankton absorption spectrum may be calculated to a good approximation as a sum of several peaks (Lorentzian functions), see Section 4.3.4 and Equation (3.31).

The position and width of these peaks depend on the algal class or species, and parameterization thus offers the possibility of identifying algal classes. The predominant pigments of the phytoplankton may be recognized on the basis of the position of the peaks in the absorption spectrum (characteristic frequencies). Figure 6.1 shows the histogram of these characteristic frequencies. It was calculated from the fits of 142 reflectance spectra measured on 22 days at Lake Constance.

An absorption peak was accepted in the histogram if its amplitude at the maximum (= $\nu A/\Gamma$, compare Equation 3.31) was at least 10% of the amplitude of the 430 nm peak. In the fit, the characteristic frequencies were calculated at a resolution of 0.1 nm, and the histogram was made in discrete steps of 1 nm.

The histogram allows the *in vivo* absorption maxima to be read off of those pigments occurring most frequently in the Lake Constance phytoplankton. These wavelengths are entered on the diagram. If they are compared with the absorption properties of extracted pigments which were described in Section 3.4, the assignment in Table 6.1 may be made. Table 6.1, in addition, gives the typical line widths of the absorption peaks. They were also calculated from the parameters from 142 fits of reflectance spectra.

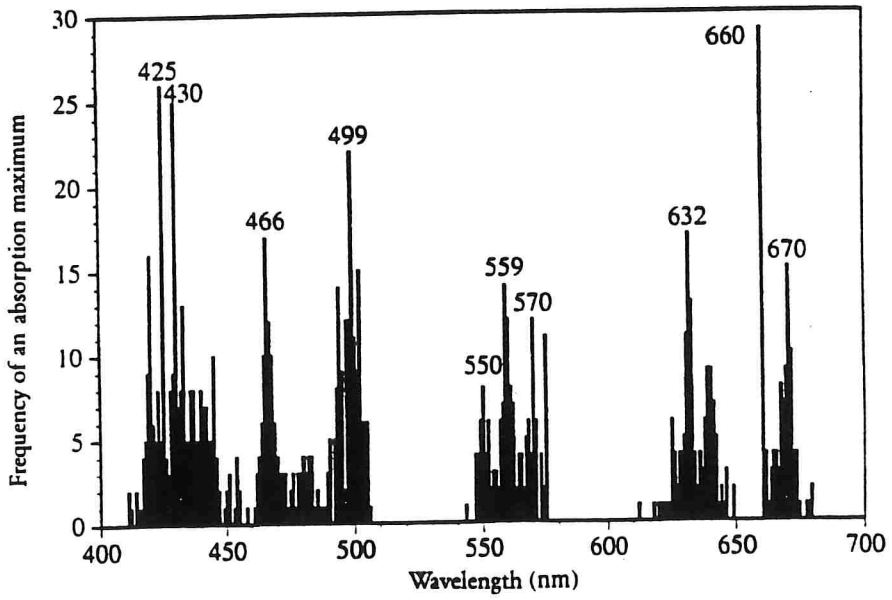

Figure 6.1: Histogram of the absorption maxima of the Lake Constance phytoplankton, determined by modelling 142 reflectance spectra measured over a period of 1½ years.

Characteristic frequency	Line width		Pigment
nm	nm	cm^{-1}	
425, 430	99±21	2619±533	chlorophyll a
466	88±32	1995±704	carotenoids
499	65±21	1309±425	carotenoids
550	70±35	1144±556	phycoerythrin
559	53±23	845±372	phycoerythrin
570	71±36	1085±543	phycoerythrin
632	53±17	663±216	chlorophyll a (?)
660, 670	42±22	474±244	chlorophyll a

Table 6.1: The most frequent *in vivo* absorption maxima of the Lake Constance phytoplankton.

Particularly at low concentrations, the position and width of the absorption peaks can only be determined imprecisely when reflectance spectra are modelled, as can be seen from the broad distributions in the histogram and from the high standard deviations of the line widths in Table 6.1. Which characteristic frequencies and line widths are given by the fit depends, as was explained in Section 4.3.4, on the preselection of the fitting variables. If the fitting parameters are given the values of Table 6.1, an acceptable fitting of reflectance spectra may be carried out even at low concentrations.

6.2 Pigment determination

The program WASSER is suitable for pigment determination, since it models the absorption of the phytoplankton as a sum of absorption peaks whose position, width and amplitude depend on the species and concentration of the individual pigments. On the following pages, a study is made of which wavelengths give the best correlation between the concentrations of individual pigments and the modelled absorption. It is shown that the optimal wavelength is not necessarily the absorption maximum. Table 6.2 summarizes the results.

Pigment	λ_p (nm)	α_p (µg/l)	β_p (mg m^{-2})	r	σ (µg/l)
Chlorophyll a	506	-2.40	65.1	3.71	3.71
Phaeophytin a	502	0.53	5.77	0.55	0.55
Carotenes	473	-0.20	3.01	0.17	0.17
Xanthophylls	477	-1.47	20.0	1.38	1.38

Table 6.2: Pigment determination by the program WASSER from the phytoplankton absorption using the algorithm $C_p = \alpha_p + \beta_p \cdot a(\lambda_p)$. C_p = pigment concentration (µg/l); $a(\lambda_p)$ = phytoplankton absorption (m^{-1}) at the wavelength λ_p; α_p, β_p = offset and gradient of the regression line; r = correlation coefficient; σ = mean error in pigment determination (standard deviation). By the program INVERS, the error in chlorophyll a determination is ±2.49 µg/l.

6.2.1 Chlorophyll a

A total of 225 reflectance spectra were modelled for 35 sampling days using the program WASSER. The result obtained, inter alia, is 225 phytoplankton absorption spectra. Figure 6.2 shows as an example a reflectance spectrum of 7.8.1990 and the phytoplankton absorption spectrum derived therefrom. All of the 225 derived absorption spectra greatly resemble absorption spectra of pure algal cultures. This verifies that the model is suitable for correctly calculating the phytoplankton absorption from the measured albedo spectra.

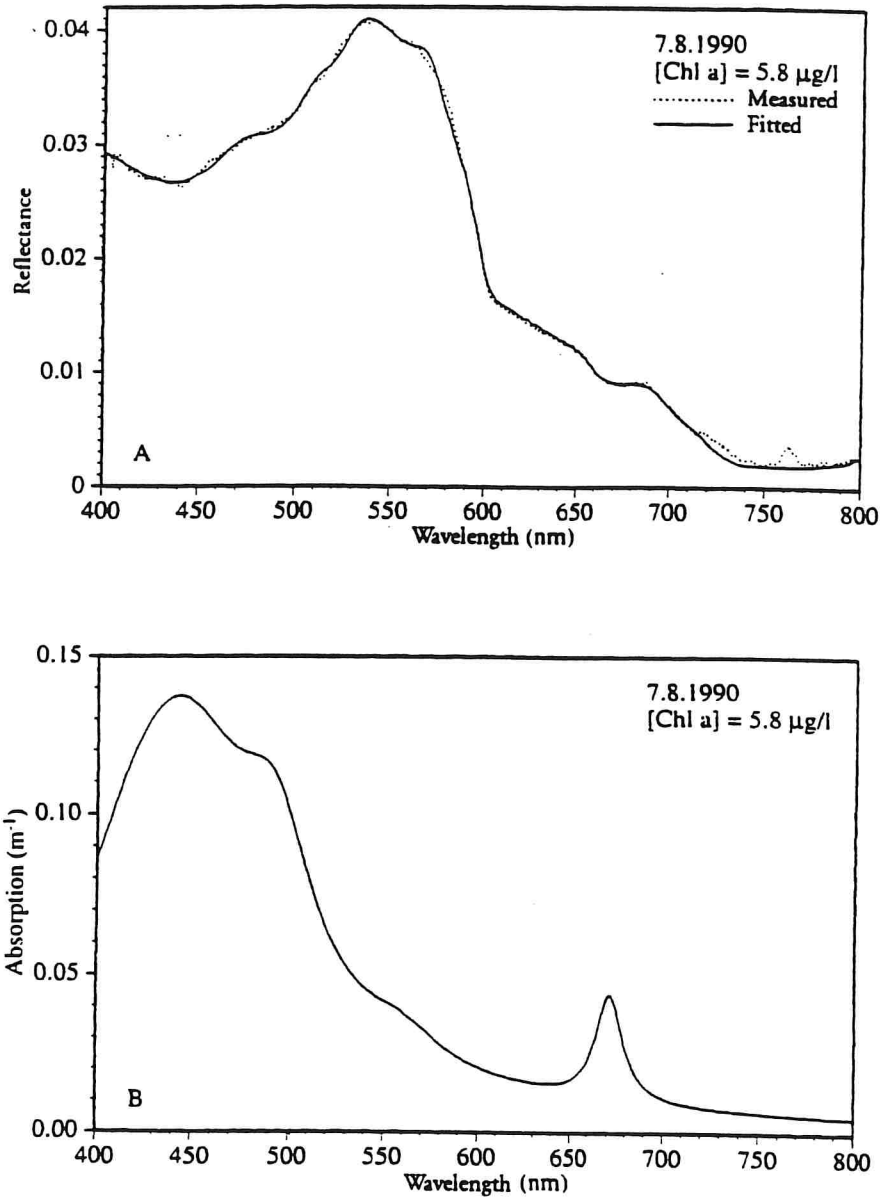

Figure 6.2: Example application of the program WASSER. A: Reflectance spectrum of 7.8.1990 and fitted curve; B: Phytoplankton absorption spectrum derived therefrom.

On the day when the reflectance spectrum shown in Figure 6.2a was measured, photometric evaluation of water samples from the depths 0 m, 1 m, 2 m gave chlorophyll a concentrations of 5.40, 5.02, 5.61 µg/l, that is a mean concentration of 5.34 µg/l. Multiplying by the correction factor 1.086 (see Section 5.1.3) gives a mean chlorophyll a concentration of 5.80 µg/l for a depth of 0-2 m. The concentration maximum was at a depth of 8 m on this

day (9.13 µg/l).

Since the *in vivo* absorption maximum of chlorophyll a is at 430 nm, according to Figure 6.1, a high correlation is expected between a(430) and the concentration. From the Figure 6.2B, an absorption of 0.131 m^{-1} can be read off for the wavelength 430 nm. In Figure 6.3, for all 35 sampling days, all the calculated values of absorption at 430 nm are plotted as a function of chlorophyll a concentration (mean for 0-2 m); the measurement for the example of Figure 6.2 is indicated by a rectangle. The regression line was calculated for the 154 pairs of values of Figure 6.3 measured at high spectral resolution (filled circles). The correlation at this wavelength is r = 0.929, the mean error in the determination of chlorophyll is 5.81 µg/l (standard deviation).

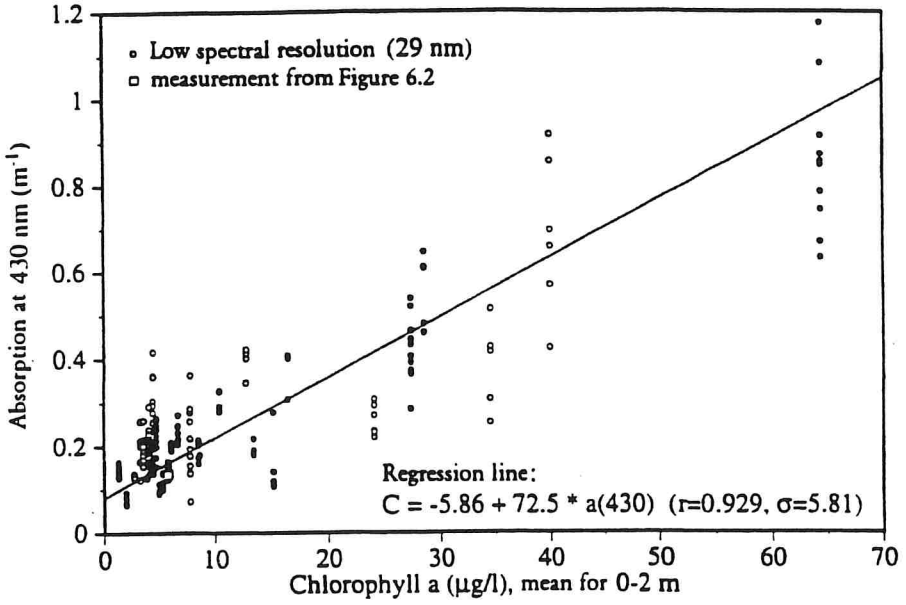

Figure 6.3: Phytoplankton absorption at 430 nm in dependence on the chlorophyll concentration. The measurements indicated "o" were not used to calculate the regression line.

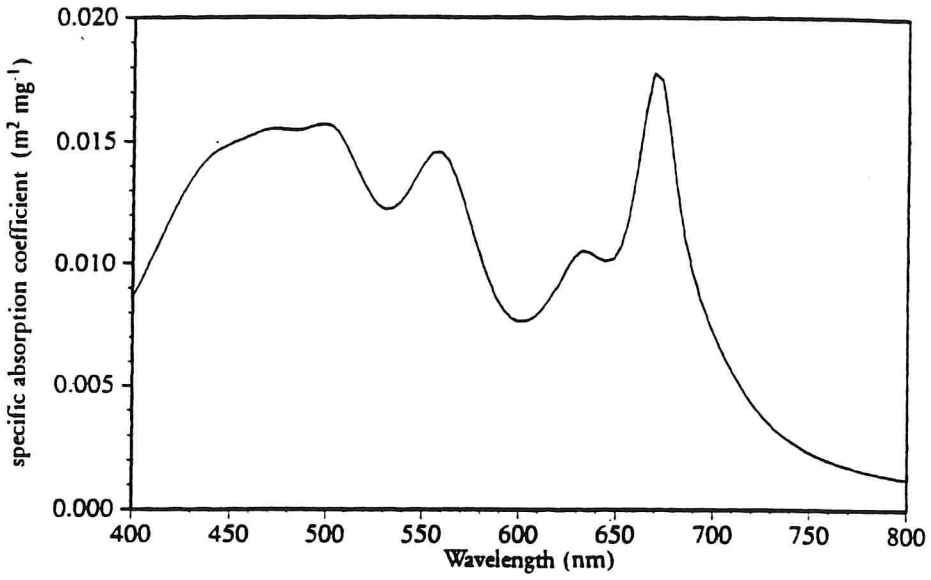

Figure 6.4: Mean specific absorption coefficient of the Lake Constance phytoplankton, derived by regression analysis.

The regression line, correlation coefficient and standard deviation were calculated in this manner in steps of 4 nm in order to discover the wavelength at which the error in chlorophyll determination is minimal. The reciprocal of the gradient of the regression line is shown in Figure 6.4 as a function of wavelength; Figure 6.5 shows the spectral dependence of the correlation coefficient and of the standard deviation.

The chlorophyll a concentration C is calculated from the phytoplankton absorption a using the equation $C = \alpha + \beta \cdot a$. A value close to zero is expected for the offset α (since absent phytoplankton does not absorb), therefore $1/\beta = a/C = a^*$ is the specific absorption coefficient of the phytoplankton. It is shown in Figure 6.4.

The spectrum of Figure 6.4 resembles in the shape of the curve and in amplitude the absorption spectra of Figure 4.3 measured on pure algal cultures. The greatest similarity is with the spectrum of *Rhodomonas lens*; only this

has a similarly marked absorption maximum at 550 nm. The reason for this is that the shape of the curve in Figure 6.4 is greatly influenced by the algal bloom on 16.4.91 in which *Rhodomonas lens* predominated: the absorption values, especially, for this day determine the gradient of the line in Figure 6.3 (these are the 10 values at 64 µg/l).

The correlation between the phytoplankton absorption and the chlorophyll a concentration is a maximum at 506 nm (r=0.949), and the standard deviation has a minimum here (4.96 µg/l). The chlorophyll a concentration can therefore be determined with the greatest accuracy at this wavelength. The equation for determination is as follows:

$$C = -2.40 + 65.1 \cdot a(506). \qquad (6.1)$$

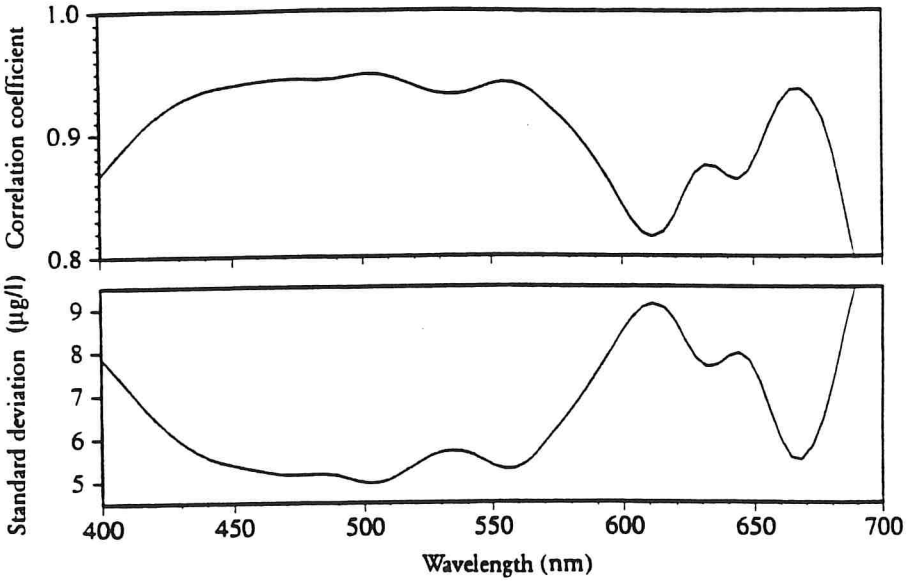

Figure 6.5: Correlation coefficient and standard deviation for the determination of chlorophyll a (mean for 0-2 m) with the program WASSER.

In Figure 6.6, the chlorophyll concentrations determined using Equation (6.1) are compared with the *in situ* data. Since several reflectance spectra are available for each sampling day but only a single *in situ* value, the

concentrations derived from reflectance spectra were averaged for one day.

The accuracy by which the chlorophyll a concentration can be determined from reflectance spectra is dependent to some extent on the spectral resolution; at a resolution of approximately 3 nm (cf. Table 5.1), the concentrations calculated using WASSER deviate on average by 3.71 µg/l from the *in situ* values (standard deviation), and at a resolution of 29 nm by ±4.04 µg/l*. As a comparison: the accuracy of the *in situ* measurement is ±1.33 µg/l (see Section 5.1.3). Determination of chlorophyll a concentration on the basis of phytoplankton absorption at 506 nm is therefore less accurate by a factor of 3 than analysis of water samples. The reasons for this are as follows:

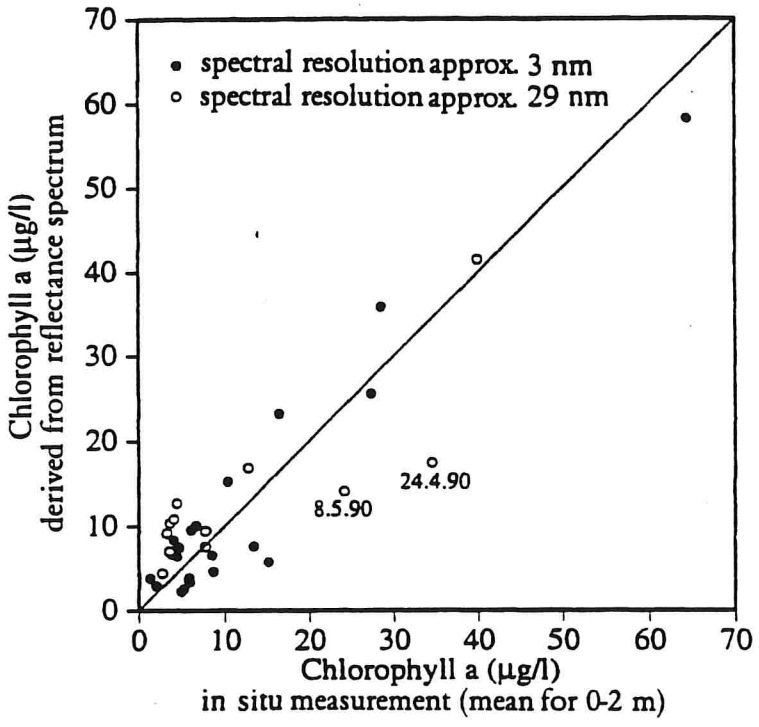

Figure 6.6: Comparison between measured chlorophyll a concentration and that determined by the program WASSER.

*The values of 24.4.90 and 8.5.90 are not taken into account in this as they are obviously outliers.

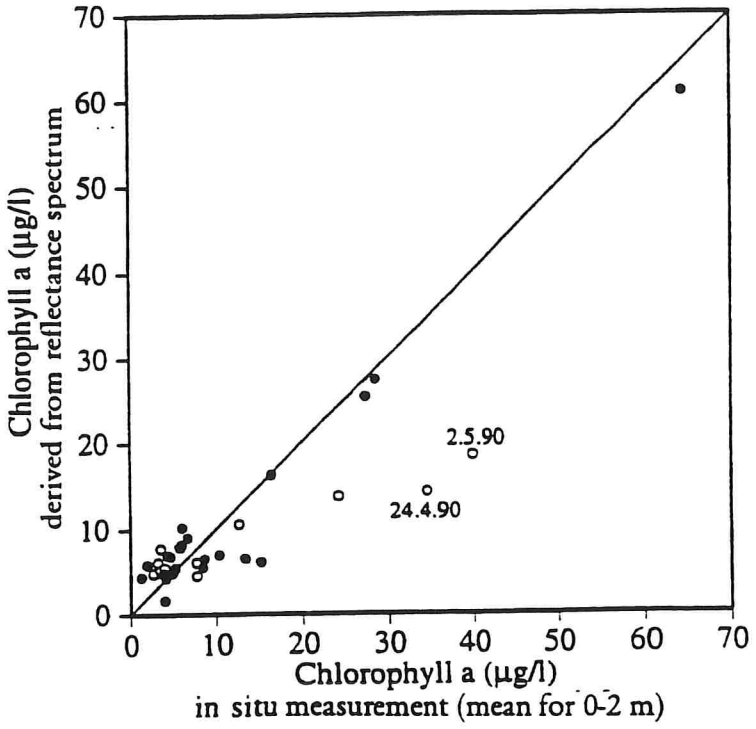

Figure 6.7: Comparison between measured chlorophyll a concentration and that determined by the program INVERS.

a) A slight current could generally always be observed at the measurement site. Since it always required a few hours after taking the water samples to begin the spectral measurements (because of lack of space on board ship), the two sets of measurements could not be carried out on the same body of water. If the chlorophyll distribution is inhomogenous in the vicinity of the measurement site, this can lead to a large error.*

b) The program WASSER assumes a specific absorption coefficient of the phytoplankton of $a^*(506) = 0.0153\ m^2/mg$. This is a mean; in fact, a^* depends on

*The chlorophyll concentrations derived, for example, from the algal bloom of 16.4.91 are between 43.7 and 74.1 µg/l. These large differences certainly represent the actual situations ("patches"), since at concentrations this high the phytoplankton absorption can be derived from the reflectance spectrum without any great error (these are the 10 values on the far right in Figure 6.3 at 64 µg/l).

the species, see Figure 4.3. The accuracy may be improved in this respect using a model which differentiates between the individual algal classes (such as the program INVERS).

c) The vertical profile of chlorophyll concentration is not taken into account. In the correlation calculations, one of which is depicted in Figure 6.5, a study was initially made of which depth gave the greatest correlation. However, weighted averaging which takes into account the visual range would be more realistic than inflexible averaging of the *in situ* data taken from a certain depth range. Only the initial stages of this approach were persued; an algorithm giving a higher correlation was not found.

d) Derivation of the phytoplankton absorption from the reflectance spectrum is not unequivocal. Errors in the calculation of the backscattering coefficient B_0 affect the resulting absorption as does an erroneous offset F_0 in the albedo.*

The chlorophyll a concentration is also a variable determined by the program INVERS, which was introduced in Section 4.3.3. It describes the phytoplankton absorption as a sum of the 5 absorption spectra from Figure 4.3. For the same reflectance spectra which were modelled by the program WASSER, a second fit was carried out by the program INVERS. Figure 6.7 shows the results of the chlorophyll a determination.

The mean deviation between the derived concentrations and the *in situ* values is ±2.49 µg/l (standard deviation) at a spectral resolution of 3 nm and ±3.22 µg/l at a

*If Equation (6.1) is replaced by an expression which additionally contains B_0 and F_0, an equation is actually found empirically which gives a somewhat higher correlation. However, no clear explanation can be given for the form of this equation, and so it was not used.

resolution of 29 nm, the two "outliers" of 24.4.90 and 2.5.90 being ignored. Determination of chlorophyll a concentration therefore proceeds more accurately with INVERS than with WASSER.

6.2.2 Phaeophytin a

A regression analysis for the phaeophytin a concentration was carried out following the same pattern described in the preceding section for chlorophyll a. Both the spectral course of correlation and standard deviation and that of the gradient β of the line resemble those of chlorophyll a, due to the high correlation between the chlorophyll a and phaeophytin a concentrations (compare Section 5.2.1). The smallest standard deviation is given by determining the phaeophytin a concentration P at the wavelength 502 nm (σ = 0.64 µg/l, r = 0.907). The algorithm is as follows:

$$P = 0.5325 + 5.765 \cdot a(502). \qquad (6.2)$$

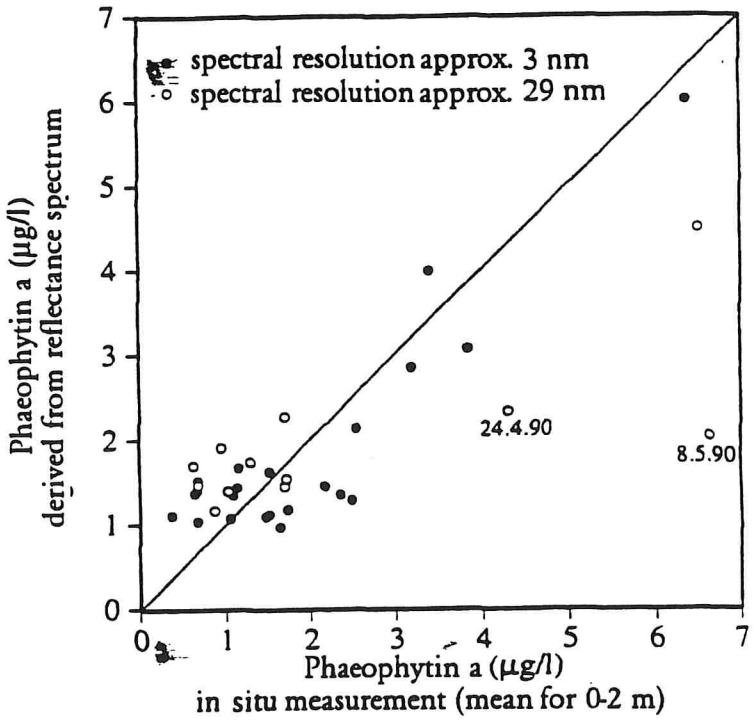

Figure 6.8: Comparison of results of phaeophytin a determination.

As is shown in Figure 6.8, the concentrations calculated from this equation correlate very well with the *in situ* measurements. The mean deviation of the data points "•", which were measured at high spectral resolution is ±0.55 µg/l. For the spectral measurements made at lower resolution (data points "o"), the standard deviation is ±0.69 µg/l if the two "outliers" of 24.4.90 and 8.5.90 are ignored, which were also outliers in the chlorophyll a (Figure 6.6) and carotenoid values (Figures 6.9 and 6.10).

The accuracy with which the sum and ratio of phaeophytin a and chlorophyll a may be derived from the phytoplankton absorption was also investigated. This showed that neither an algorithm for P+C nor for P/C increase the information content. Nevertheless, for the sake of completeness, the algorithms may be mentioned here:

$$P+C = -3.051 + 73.96 \cdot a(502), \quad r=0.940, \quad \sigma=6.37,$$

$$P/C = 0.2457 - 0.1516 \cdot a(461), \quad r=-0.571, \quad \sigma=0.0474.$$

6.2.3 Carotenoids

Regression analysis for the carotenoids was performed separately for the carotenes K and xanthophylls X. The following equations were found:

$$K = -0.1965 + 3.013 \cdot a(473) \qquad (6.3)$$

$$X = -1.47 + 19.96 \cdot a(477) \qquad (6.4)$$

The concentrations calculated from these equations are compared with the results of HPLC analysis in Figures 6.9 and 6.10. If the "outliers" of 24.4.90 and 8.5.90 are again omitted, the accuracy obtained is ±0.17 µg/l for

carotenes and ±1.38 µg/l for xanthophylls.*

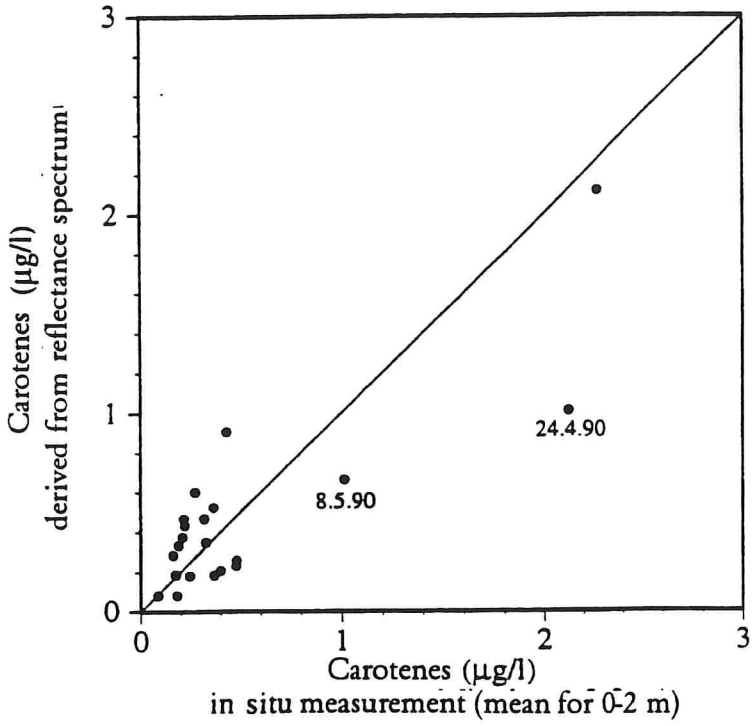

Figure 6.9: Comparison of results for carotene determination.

*High and low spectral resolution were not differentiated here since the range of values of the measurements at high spectral resolution is too low for a representative statement (*in situ* measurements are only available for 1990).

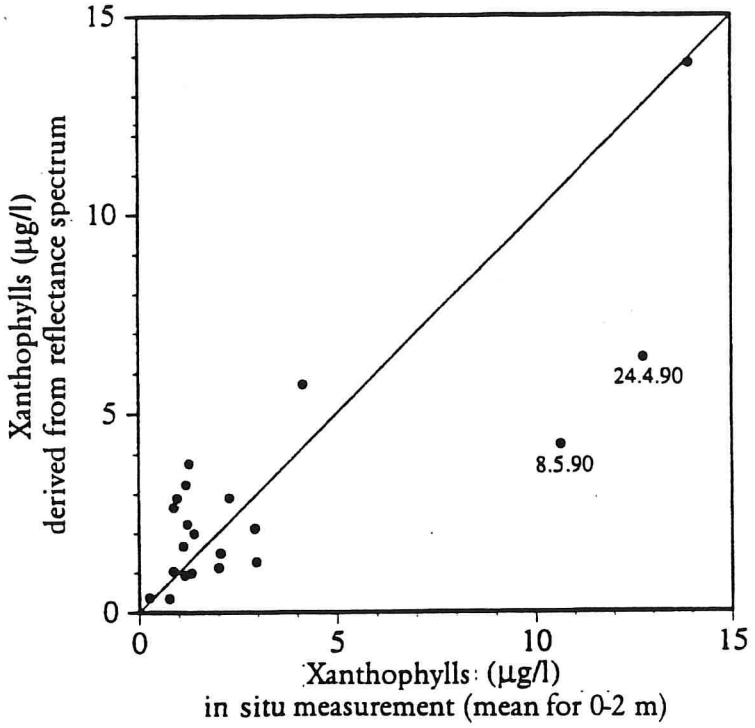

Figure 6.10: Comparison of results for xanthophyll determination.

6.3 Phytoplankton classification

The program INVERS was written for classification of phytoplankton. The absorption spectra of the 5 algal species introduced in Section 4.2.3 serve as characteristics for differentiation. As is shown below, the 4 "optical classes" of the Lake Constance phytoplankton given in Table 6.3 can be differentiated thereby. Classification on the basis of reflectance spectra proceeds with an accuracy of 12 to 25%, depending on the class.

Optical class	Biological classes	File name of the absorption spectrum	Mean error	Frequency of an error > 40%
Cryptophyceae	Cryptophyceae	COVATA2.A RHODOM.A	24.6%	18.8%
Diatoms	Bacillario-phyceae Chrysophyceae	FRCROT.A	14.2%	6.3%
Green algae	Chlorophyceae Zygnemaphyceae Cyanophyceae	MOUG.A	11.8%	0
Dinoflagellates	Dinophyceae	SMEK4.A	16.1%	3.0%

Table 6.3: Classification of the Lake Constance phytoplankton in the modelling of reflectance spectra by the program INVERS. The table gives the amount by which, on average for 33 sampling days, the derived concentrations differed from the *in situ* measurements.

6.3.1 Reflectance spectra fitting by the INVERS program and comparison with *in situ* data

The program INVERS is described in Section 4.3.3. Its critical degrees of freedom are the concentrations of the 5 phytoplankton species whose absorption spectra are shown in Figure 4.3. Weighted addition of the 5 spectra permits a large variety of absorption spectra to be produced which represent different species communities in Lake Constance. Figure 6.11 shows as an example the fitted curve and the derived phytoplankton absorption spectrum for the same reflectance spectrum which was

already used in Figure 6.2 to illustrate the program WASSER. The fitting was more successful in that case, since the shape of the curve of the phytoplankton absorption is variable to a greater extent in the program WASSER than in the program INVERS.

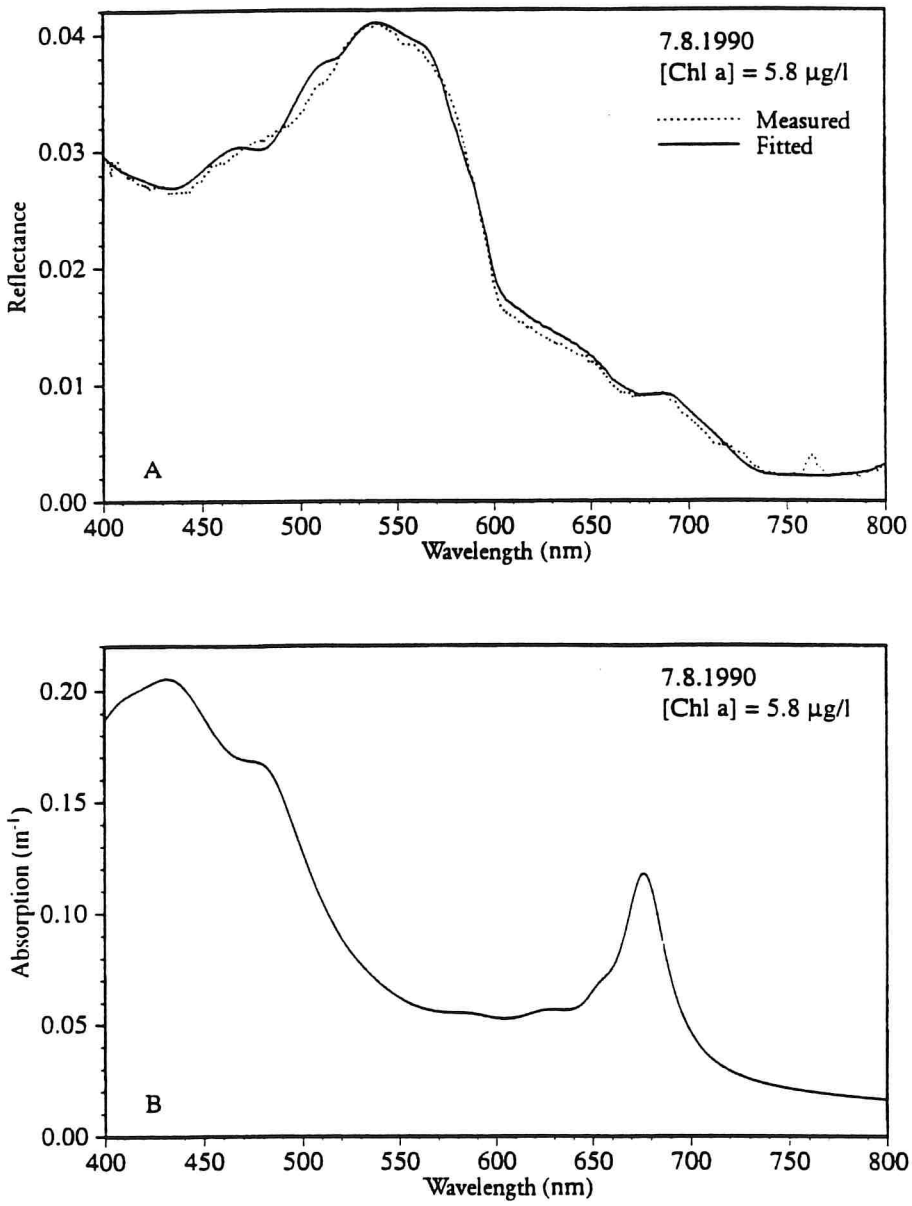

Figure 6.11: Example application of the program INVERS. A: reflectance spectrum of 7.8.1990 and fitted curve; B: phytoplankton absorption spectrum derived therefrom.

The example INVERS output file in Section 4.3.3 is a list of the fitting parameters for Figure 6.11. From this, the program determined a total chlorophyll concentration of

5.37 µg/l, 1.51 µg/l of which were apportioned to dinoflagellates and 3.86 µg/l to green algae. Negligibly small values were determined as proportions for the other 3 algal classes.

The example of Figure 6.11 shows one of 10 reflectance spectra made on this day (7.8.1990). Fitting by INVERS gives somewhat different values for each reflectance spectrum. If the results of the 10 fits are averaged, the concentrations given in Table 6.4 are obtained.

Absorption spectrum	Chlorophyll a		Biovolume	
	µg/l	relative	$\mu m^3/ml$	relative
COVATA2.A	0.09	1.4%	69812	4.9%
FRCROT.A	0.82	13.4%	349058	24.5%
SMEK4.A	1.14	18.7%	142473	10.0%
MOUG.A	4.08	66.6%	837740	58.8%
RHODOM.A	0	0	15672	1.1%
Total	6.12	100%	1424728	100%

Table 6.4: Comparison for 7.8.1990 between the chlorophyll a concentrations given from fitting by INVERS for 5 algal species and the biovolumes of the corresponding species given by *in situ* measurements. The *in situ* value for total concentration of chlorophyll a is 5.80 µg/l.

The 42 species found in the water sample on 7.8.1990 were assigned to the 5 absorption spectra as follows:

COVATA2.A: *Cryptomonas ovata, Cryptomonas rostratiformis.*

FRCROT.A: *Asterionella formosa, Fragillaria crotonensis, Synedra acus, Melosira granulata, Diatoma elongatum, Dinobyron divergens, Diatoma vulgare, Stephanodiscus sp., Nitzschia acicularis.*

SMEK4.A: *Ceratium hirundinella, Gymnodinium*

helveticum, Peridinium sp.

MOUG.A: *Pandorina morum, Staurastrum sp., Phacotus sp., Oocystis sp., Mougeotia sp., Aphanizomenon sp., Closterium aciculare, Microcystis sp., Pediastrum sp., Characium sp., Monoraphidium sp., Cosmarium sp., Elakatothrix sp., Planktosphaeria sp., Carteria sp., Sphaerocystis sp., Chlamydomonas sp., Tetraedron minimum, Scenedesmus bijugatus, Anabaena solitaria, Koliella sp., Coelastrum reticulatum, Lagerheimia ciliata, Anabaena circinalis.*

RHODOM.A: *Rhodomonas minuta, Rhodomonas lens.*

Unassigned: *Chrysochromulina parva, Erkenia sp.*

This assignment is given by the class membership of the species. In the class Cryptophyceae, a differentiation is made between *Cryptomonas* and *Rhodomonas* species, the other classes are combined to form "optical classes" in accordance with Table 6.3. The two unassigned species together make up a relative proportion of 0.71% of the biovolume.

The calculated chlorophyll a concentrations should actually be compared with measured concentrations. However, the chlorophyll a portion of the individual species cannot be separated out from the *in situ* measurements. As was shown in Section 5.2.5, the chlorophyll a concentration may be calculated from the biovolume with an accuracy of about 33%. This error of 33% relates to the conversion from any phytoplankton species chosen at random - within one class, the error is certainly smaller.

It follows from Table 6.4 that with the assignment described for 7.8.1990, there is good agreement between the results of fitting and the *in situ* data. Corresponding tables were compiled for all 33 sampling days for which, in addition to reflectance spectra, *in situ* data are also available. If for each "optical class" the relative proportions from the fitted curve are plotted

against the relative proportions from *in situ* data, it can be seen directly how good the general agreement is. These plots are shown in Figures 6.12 and 6.13 for the *Cryptomonas* and *Rhodomonas* species.

Each data point in the figures corresponds to one day: the *in situ* measurement is based on a mixed sample from the depth stage 0-8 m, the modelled value is the mean from the fitted curves of several reflectance spectra. Reflectance spectra at high spectral resolution (3 nm) are symbolized by filled circles, measurements made at low resolution (29 nm) by open circles (see Section 5.1.1 for spectral resolution). The thick diagonal line corresponds to agreement of modelled and measured proportions, the two thin diagonal lines correspond to a deviation of ±20%. The number of deviations can be read off from the histograms to the right of the plot; the bars have a spacing of 5%.

Example: The open circle in Figure 6.12 at (18%, 55%) denotes a deviation between the *in situ* value and fitted value of the relative proportion of *Cryptomonas* species by 18% - 55% = -37%. It is the only overestimation due to fitting by more than 20%. It is situated in the histogram as a bar of height 1 at -35%.

The histograms of Figure 6.12 and 6.13 are asymmetric. Two approximately symmetrical distributions may be differentiated ("bimodal histogram"): one having a centre of symmetry at 0%, the other approximately at +50% (Figure 6.12) or at -50% (Figure 6.13). The mode having a centre of symmetry at 0% has a width of about ±20%, therefore the corresponding data points in the plot are situated between the ±20% lines. The values of the second mode are the points which lie outside this 20% interval: in Figure 6.12, the "outliers" are at the bottom right in the plot, and in the top left in Figure 6.13. These are systematic errors in classification: if the *Cryptomonas* species are underestimated in the fit, the *Rhodomonas*

species are simultaneously overestimated. The two species cannot therefore be reliably kept apart in the fit, and are therefore combined in a joint optical class (Cryptophyceae). The plot and the histogram of this class are shown in the next section; the histogram is markedly more symmetrical than that of the individual species.

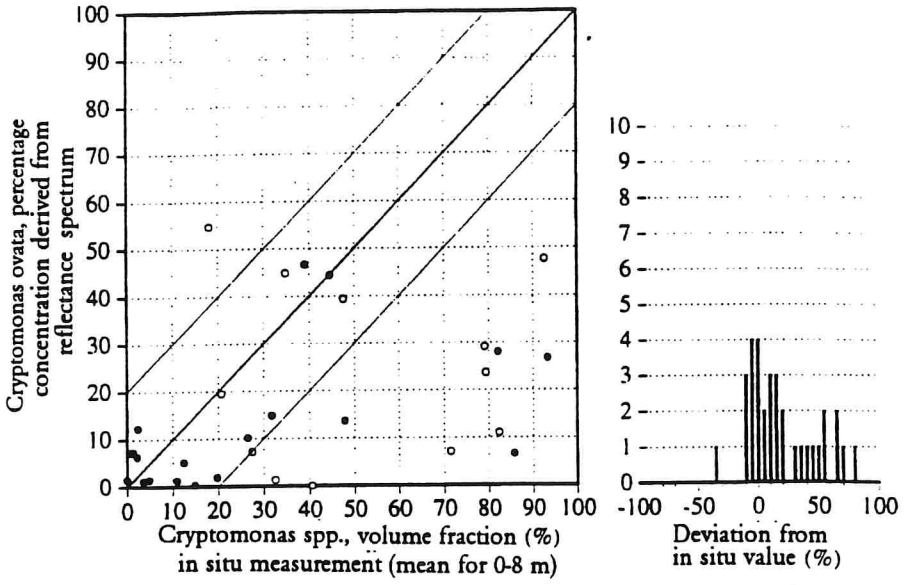

Figure 6.12: Comparison of the modelled and measured proportion of *Cryptomonas* classes of the total phytoplankton.

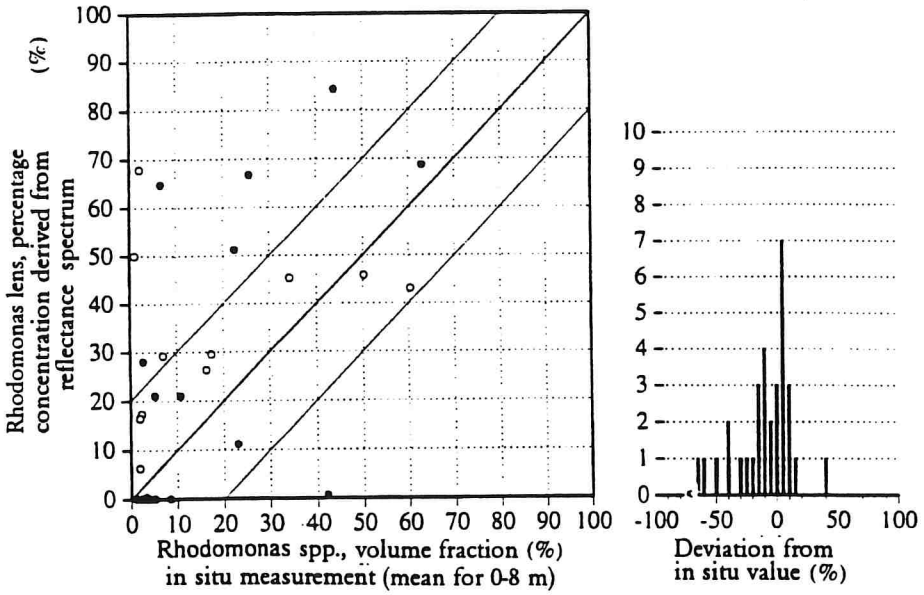

Figure 6.13: Comparison of the modelled and measured proportion of *Rhodomonas* species of the total

phytoplankton.

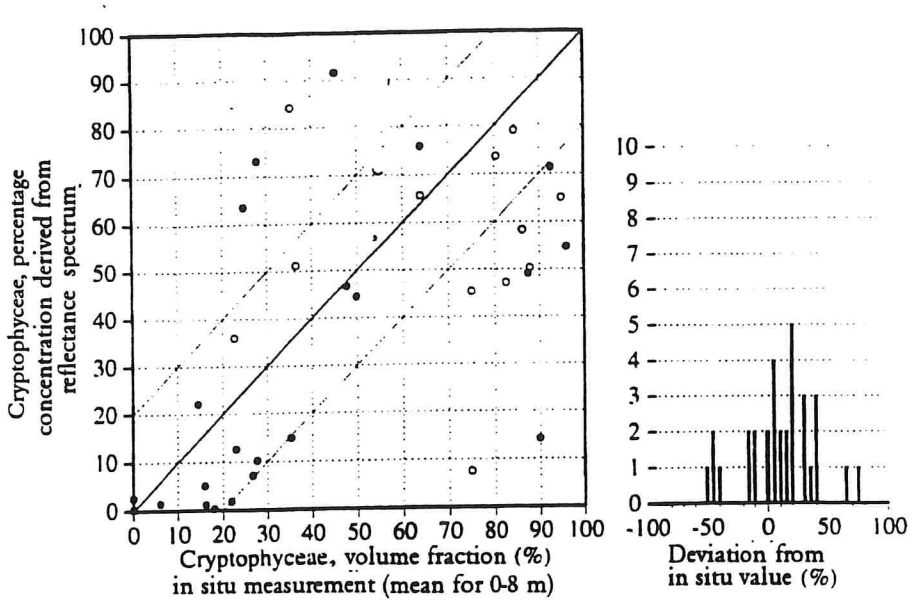

Figure 6.14: Comparison of the modelled and measured proportion of *Cryptophyceae* class of the total phytoplankton.

6.3.2 Optical class: Cryptophyceae

Of the more than 100 phytoplankton species occurring in Lake Constance, those with by far the highest frequency are species from the class Cryptophyceae, see Table 4.1. A characteristic of this class is the absorption maximum at 550 nm which is due to the pigment phycoerythrin. The concentration of this pigment greatly depends on the growth conditions and the amplitude of the 550 nm peak is therefore highly variable even within one species. This is the reason why, in modelling reflectance spectra, two different absorption spectra are necessary to characterize the optical class "Cryptophyceae": one having an indistinct 550 nm maximum represents a low phycoerythrin concentration and the other having marked absorption at 550 nm represents a high concentration. Although one absorption spectrum was measured using the species *Cryptomonas ovata* and the other using the species *Rhodomonas lens*, the two species are, as was shown in the preceding section, frequently confused during fitting.

Figure 6.14 shows that the sum of the *Cryptomonas* and *Rhodomonas* concentrations determined in the fitting correlates well with the bio-volume of the class Cryptophyceae. The error in the determination of the relative proportion is ±24.6%; on 6 of 32 days, the deviation was greater than 40%. The accuracy in this case is not significantly dependent on the spectral resolution: at high resolution (3 nm), the mean error is 23.5% and at low resolution (29 nm) it is 26.5%.

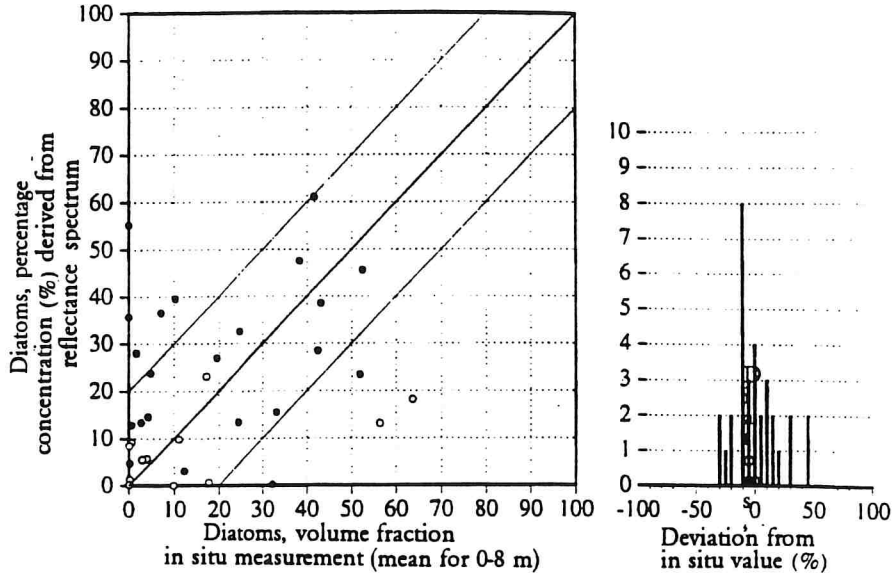

Figure 6.15: Comparison of the modelled and measured proportion of the optical class *diatoms* of the total phytoplankton.

6.3.3 Optical class: diatoms

For the diatoms, the program INVERS uses an absorption spectrum of the species *Fragillaria crotonensis*, file name FRCROT.A. This represents the classes *Bacillariophyceae* and *Chrysophyceae*. As Figure 6.15 shows, the relative proportion of diatoms is generally successfully determined with an error of less than 20%. On average the error is 14.2%. A deviation greater than 40% occurred on two sampling days. For the 12 sampling days on Lake Constance when the reflectance spectra were measured with low spectral resolution (29 nm), the mean error was

12.1%. On the other 20 sampling days with high spectral resolution (3 nm), the mean error is 15.5%.

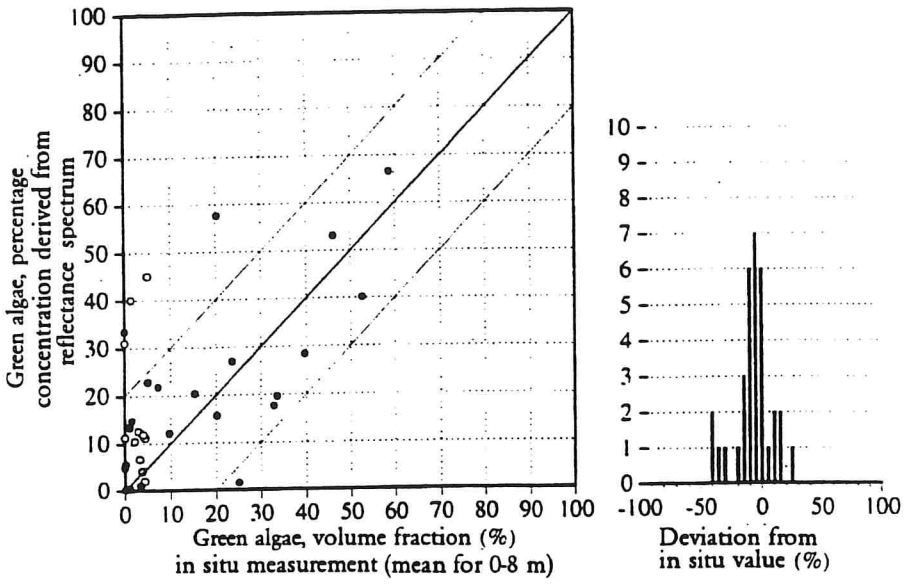

Figure 6.16: Comparison of the modelled and measured proportion of the optical class *green algae* of the total phytoplankton.

6.3.4 Optical class: green algae

The green algae are represented by one absorption spectrum of the species *Mougeotia*. As Figure 6.16 shows, the relative proportion of green algae is determined highly precisely in the modelling: the error is on average 11.8%, and an error above 40% was never observed. The reason why the proportion of green algae can be determined so precisely is possibly that its absorption properties scarcely change.

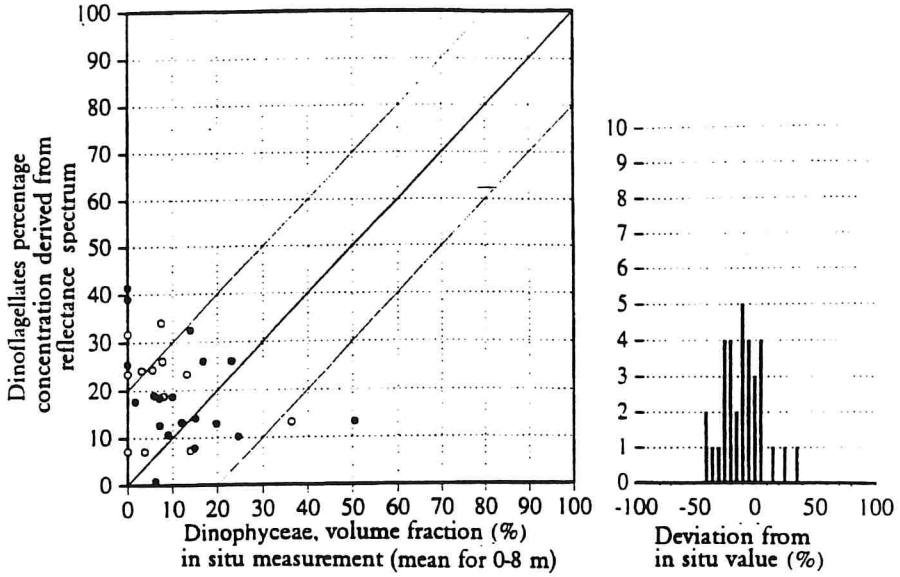

Figure 6.17: Comparison of the modelled and measured proportion of the optical class *dinoflagellates* of the total phytoplankton.

6.3.5 Optical class: dinoflagellates

For the dinoflagellates, the program INVERS uses an absorption spectrum, SMEK4.A, taken from the literature which was averaged from several individual spectra. The proportion of dinoflagellates in Lake Constance is always very low, generally below 30%. The modelling also always resulted in a low proportion of dinoflagellates and the proportions determined in this differ on average by 16.1% from the measured contents. Only once was the deviation above 40% when no dinoflagellates were found in the water sample: modelling yielded a percentage concentration of 42%.

6.4 The spectral region in the vicinity of 685 nm

In the region 600 to 800 nm, reflectance is marked by a minimum at 670 nm and a maximum at 685 nm. In modelling by the program INVERS which uses representative phytoplankton absorption spectra (see Section 4.3.3), it emerged that the shape of the curve can be described to an approximation with the absorption and scattering input spectra used: the minimum at 670 nm is due to the phytoplankton absorption at this wavelength (chlorophyll a), and the maximum at 685 m results from the minimum in the absorption between the chlorophyll a peak at 670 nm and the steep rise in the absorption of water above 700 nm, the amplitude depending on the intensity of particle scattering which can be derived from the reflectance at $\lambda > 700$ nm (see Section 4.3.1).

However, the agreement between measured and modelled reflectance was of variable quality. A possible reason is that the phytoplankton absorption spectra used do not represent the predominant species well on all sampling days. In order to by-pass this inflexibility in modelling by INVERS, fits were made with the program WASSER (see Section 4.3.4) which, in addition to the amplitudes, can also fit the absorption maxima and line widths within reasonable limits. In fact, all reflectance spectra which were not subject to obvious errors (compare Section 2.3.5) could be reproduced very well by this approach.

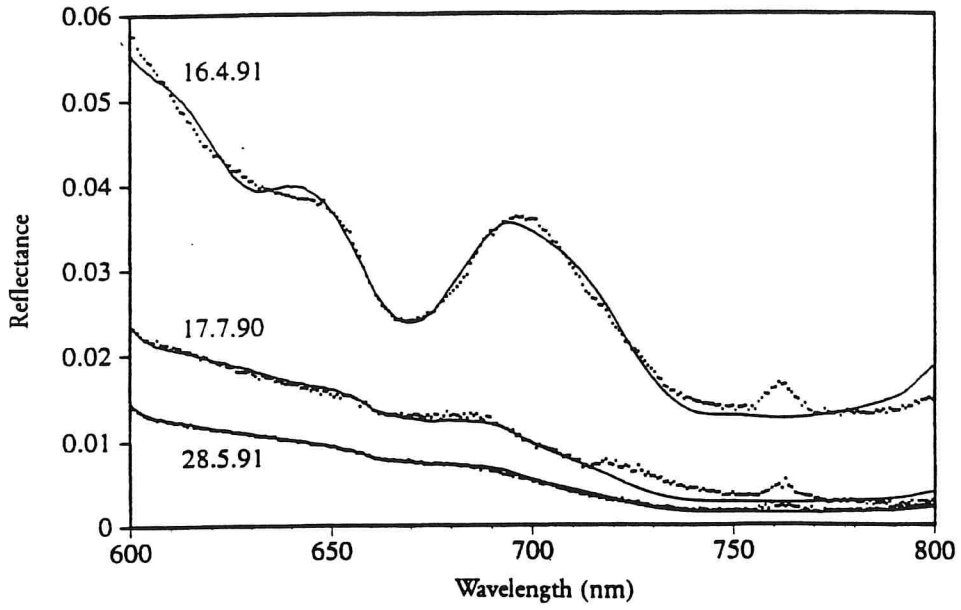

Figure 6.18: Examples of reflectance in the red spectral region. The points are measurements, the lines are the result of modelling. See also Table 6.5.

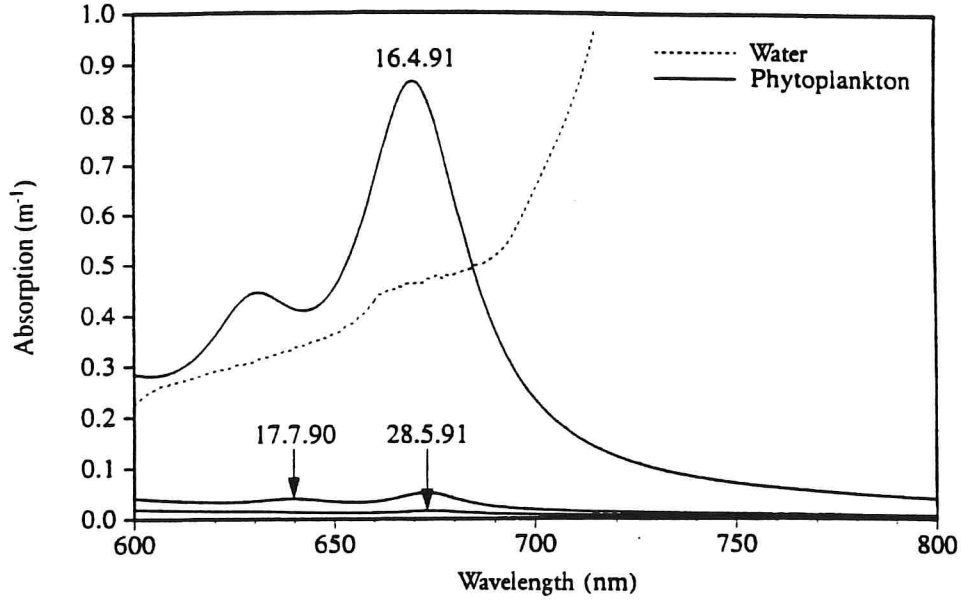

Figure 6.19: Absorption spectra calculated from the reflectance spectra of Figure 6.18. See Table 6.5 for the curve parameters.

Figure 6.18 shows as an example three reflectance spectra at different chlorophyll concentrations. Modelling by the program WASSER leads to the continuous lines. The associated absorption spectra are shown in Figure 6.19. Table

6.5 gives details of the reflectance spectra and the fitted parameters in the spectral region 600-800 nm.

As is shown in Figure 6.19, the absorption by the water constituents (phytoplankton) is only comparable with the absorption by water during the bloom on 16.4.91; in the other two examples, the constituents contribute less than 10% to the total absorption in the spectral region 600-800 nm. However, this is of the same order of magnitude as the inaccuracy in the value of the water absorption (compare Section 3.3) and the backscattering coefficient of the suspended particles can be significantly greater in this spectral region. Therefore, the absorption parameters (absorption maxima, line widths, amplitudes) can only be determined reliably at chlorophyll concentrations above about 5 to 10 µg/l. In contrast, the red spectral region is highly suitable for determining the backscattering coefficient (B_0).

Date		28.5.91	17.7.90	16.4.91
Chlorophyll a	µg/l	1.2	10.8	65
Algal Cells	ml^{-1}	1365	3639	16700
Reflectance spectrum	file name	B67.REF	B75.REF	B21.REF
Absorption maximum	λ (nm)	632.0	640.0	629.7
at 632 nm	Γ (cm^{-1})	325	300	361
	2Γ (nm)	26.0	24.6	28.6
	A (m^{-1})	$4.10 \cdot 10^{-5}$	$2.99 \cdot 10^{-4}$	0.00533
Absorption maximum	λ (nm)	674.4	673.5	670.1
at 670 nm	Γ (cm^{-1})	218	227	353
	2Γ (cm^{-1})	19.8	20.6	31.7
	A (m^{-1})	$1.06 \cdot 10^{-4}$	$5.31 \cdot 10^{-4}$	0.0183
Scattering	B_0 (m^{-1})	0.0107	0.0197	0.103
	B_1, n	0	0	0
Offset	F_0	0.00174	0.0255	0.00662
Scaling factor	F_1	1.11	1.18	0.698

Table 6.5: Data on the spectra of Figure 6.18. The values beneath the double line are results of modelling by the program WASSER.

7. Summary

The present study analysed what may be inferred about the constituents of a water body when solar radiation reflected in the water is measured by a sensor situated outside the water. The measurements were made in 1990/91 on Lake Constance, accompanying *in situ* data being made available by the Limnological Institute of Constance University. In order that the algorithms for determining concentration from reflectance are not restricted to Lake Constance, the relationships were not studied purely statistically but on the basis of a physical model. Therefore great attention was paid both to the systematic representation of the physics involved and also to description of the optical properties of the water constituents.

The results are summarized by the following points:

1. It was shown experimentally that the shape of the spectrum of the incident radiation can be represented as the sum of 4 base spectra (2.1).* Two base spectra may be determined theoretically (blue sky, aerosol scattering), and the other two were derived from measurements (direct solar radiation, clouds). All measurements of irradiance which were obtained over a period of 1½ years may be reproduced by these 4 spectra with a mean error of 0.11%, the largest error being 0.24% (2.1.6).

2. The ratio of upwelling irradiance to downwelling irradiance is termed *reflectance* if it is measured beneath the water surface and *albedo* if it is measured above. An equation linking these two spectra was derived (Equation 2.23).

---

*The first number denotes the chapter and the following numbers denote section and subsection.

3. A large part of the albedo of a body of water is light reflected at the surface. The spectrum of these specular surface reflections is different from that of the incident radiation (2.3.4) and consequently the reflectance spectrum is erroneous if it is derived from remote sensing measurements. A method was developed for correcting this error (2.3.5). Its use is known to be chiefly necessary in the case of a cloudy or overcast sky, and it is therefore termed *cloud correction*.

4. Measurements made when the sky is cloudy or overcast generally require cloud correction. A good indicator for such a requirement is the absorption band of water vapour at 722 nm (2.3.3).

5. In the case of uncorrected albedo spectra, the shape of the spectrum in the blue can be fundamentally distorted, likewise the amplitude of the maximum at 685 nm (2.3.3). The two errors are correlated.

6. Reflectance is exclusively determined by absorption and scattering of the water and its constituents (4.1). These optical properties may be summarized by a single parameter, the complex refractive index. In 3.1.1 to 3.1.3, the underlying physics is explained in detail, in 3.1.4 the relevant scattering equations are summarized (Mie theory), and in 3.1.5 the special characteristics of absorption by algal cells are discussed. The quantum-mechanical approach was applied here explicitly for the first time as far as the present author is aware to the optical behaviour of water bodies. It leads to two practical applications:

   a) With the aid of an elementary relation for complex numbers (Kramers-Kronig relations, Appendix A) the spectrum of the refractive index (real part) may be calculated from the absorption

spectrum (3.2.2). It was shown that the result agrees with a considerably more complex model by Bricaud and Morel (1986). It is thus possible to calculate the scattering spectrum if the absorption spectrum and the refractive index at a particular wavelength are known.

b) The absorption spectrum of algal pigments and also of living phytoplankton is, according to quantum mechanics, essentially the sum of Lorentz functions (Equations 3.4b, 3.5). Measured absorption spectra may accordingly be characterized by a few parameters (characteristic frequencies, line widths, amplitudes), and erroneous measurements as are frequently encountered in the literature may be recognized by the fact that the fit does not succeed in accordance with Equation (3.5).

7. The varied measurement parameters used in the relevant literature are systematically presented in Sections 3.1.4 and 3.2.1 and their relationship to the elementary parameters is emphasized. The systematization culminates in an iterative method for calculating the refractive index from absorption and attenuation and in a method for extrapolating the absorption spectrum of an algal cell to any cell size (to compare absorption spectra from different species, extrapolation to zero size is of particular interest).

8. The results of a literature search on the optical properties of water, the most important pigments and phytoplankton are summarized in sections 3.3, 3.4 and 3.5. Reliable characterization is only possible in the case of water; the optical properties of the constituents vary by nature considerably. Furthermore, there is a lack of useful measurements for them, principally on the scattering behaviour.

However, it is possible to give spectra for the phytoplankton absorption which characterize certain "optical classes".

9. The reflectance model is presented in Chapter 4. It is based on spectra of the absorption and scattering by water and optically differentiatable constituents and its purpose is determining the concentrations of these constituents on the basis of the reflectance spectrum. The concentrations cannot be derived explicitly from the spectra but only in an iterative process, so-called "inverse modelling". Two PC programs were written for this purpose which differ in their treatment of phytoplankton absorption: WASSER models this absorption spectrum, INVERS uses characteristic spectra for the individual "optical" classes.

10. The absorption of Lake Constance phytoplankton is typically characterized by 8 maxima in the spectral range 425 to 670 nm with line widths of 42 to 99 nm, which may be assigned to chlorophyll a, carotenoids and phycoerythrin (Table 6.1). These parameters, resulting from a statistical analysis, are optimal initial values in modelling reflectance spectra by the program WASSER (4.3.4).

11. When reflectance spectra are compared with cell count data, the critical factor is not the number of the phytoplankton cells but their volume (5.2.4, 5.2.5).

12. Well over 100 different phytoplankton species occur in Lake Constance. If they are grouped into 4 "optical classes", the relative proportions of the 4 classes may be determined from reflectance spectra with an accuracy of 12 to 25% (6.3). The program INVERS which carries out this separation employs two different absorption spectra for the optical class "Cryptophyceae" in this, in order to take into

account high natural variations in phycoerythrin concentration.

13. The accuracy of *in situ* determination of chlorophyll a concentration is ±1.3 µg/l (standard deviation; 5.1.3). The accuracy when it is derived from reflectance spectra is ±2.5 µg/l if the attributes in the absorption of the 4 optical classes are taken into account (6.2.1). The reason for the greater inaccuracy is principally the uncertain assignment of water sample and reflectance spectrum: the spectral measurements could only be performed several hours after the water sample was taken.

14. The ratio of concentration of phaeophytin a to chlorophyll a is a measure of the phytoplankton vitality, since when algal cells die off, chlorophyll a is converted to phaeophytin a (3.4.3). It is usually 23 to 42% (5.2.1), but at the end of algal blooms it can be higher by more than a factor of 3 (Figure 5.3). Although an algorithm was found by which the phaeophytin a concentration may be determined from reflectance spectra with a mean accuracy of ±0.6 µg/l (6.2.2), it does not reliably detect an increased phaeophytin concentration.

15. The phytoplankton classes principally differ in their carotenoid inventory (Table 3.2). The carotenoids cannot be reliably differentiated by spectral measurements, since they have similar absorption spectra (3.4.5, 3.4.6). At most, carotenoids not containing oxygen (carotenes) may be differentiated from those containing oxygen (xanthophylls). The accuracy with which the concentrations of these pigment classes can be derived from reflectance spectra was studied (6.2.3). The accuracy is no higher than when Equations 5.2 and 5.3 are used which describe the correlation with chlorophyll a concentration (5.2.2).

16. The shape of the reflectance spectrum around 685 nm, the subject of numerous publications, is correctly represented by the present model in terms of accuracy (6.4). The fluorescence of chlorophyll a which has a maximum at this wavelength is not contained in the model. It can certainly only be detected from passive measurements if both the absorption and the scattering by water and the water constituents are known in this spectral region with an accuracy which can be realized at best in the laboratory (3.4.2).

It is planned to use these results, which are obtained using a ship-board spectrometer, for the further development of algorithms for image processing of aircraft and satellite measurements. Image analysis has the fundamental problem of calculation time: powerful models which can in principle compute exactly the radiation transfer in water and in the atmosphere (Fischer and Graßl 1984), can for this reason only be used in practice for some few pixels and principally serve to check simpler models which are optimized for short computation times (Schiller and Doerffer 1993). Efforts are being made to implement this type of "simple" model in the image-processing system XDIBIAS of the DLR for the evaluation of data from specific remote sensors (e.g. ROSIS, MERIS, SeaWIFS). The results given above are to be used as a base.

8. References

S. Agustí: Allometric Scaling of Light Absorption and Scattering by Phytoplankton Cells. Can. J. Fish. Sci. 48, 763-767 (1991).

R.K. Ahrenkiel: Modified Kramers-Kronig Analysis of Optical Spectra. J. Opt. Soc. Am. 61, 1651-1655 (1971).

R.S. Alberte, A.M. Wood, T.A. Kursar, R.R.L. Guillard: Novel phycoerythrins in marine *Synechococcus spp.*: characterization, and evolutionary and ecological implications. Plant Physiol. 75, 732-739 (1984).

M.B. Allen: Studies with *Cyanidium caldarium*, an anomalously pigmented chlorophyte. Arch. Mikrobiol. 32, 270-277 (1959).

M.B. Allen, E.C. Dougherty, J.J.A. McLaughlin: Chromoprotein Pigments of Some Cryptomonad Flagellates. Nature 184, 1047-1049 (1959).

V. Amann, R. Doerffer: Aerial Survey of the Temporal and Spatial Distribution of Phytoplankton During FLEX'76. In: North Sea Dynamics, ed. Sündermann/Lenz. Springer 1983.

R.W. Austin: The remote sensing of spectral radiance from below the ocean surface. In: N.G. Jerlov, E. Steemann Nielsen (Eds.): Optical Aspects of Oceanography. Academic Press London, 317-344 (1974).

R.W. Austin: Coastal Zone Color Scanner radiometry. In: Ocean Optics 6, Proc. Soc. Photo-Opt. Instrum. Eng. 208, 170-177 (1979).

R.W. Austin: Gulf of Mexico, ocean-colour surface-truth measurements. Boundary-layer Meteorol. 18, 269-285 (1980).

M.W. Banoub: Ultra violet absorption as a measure of organic matter in natural waters in Bodensee. Arch. Hydrobiol. 71, 159-165 (1973).

V. Barale, P.M. Schlittenhardt (Eds.) Ocean Colour: Theory and Applications in a Decade of CZCS Experience. Kluwer Academic Publishers, Dordrecht (1993).

Bergmann, Schaefer: Lehrbuch der Experimentalphysik. Band III Optik [Textbook of experimental physics. Volume III Optics]. Walter de Gruyter, 8th edition (1987).

M. Born, E. Wolf: Principles of Optics. Pergamon Press, 6th edition (1989).

A. Bricaud, A. Morel, L. Prieur: Absorption by dissolved organic matter (yellow substance) in the UV and visible domains. Limnol. Oceanogr. 26, 43-53 (1981).

A. Bricaud, A. Morel, L. Prieur: Optical efficiency factors of some phytoplankters. Limnol. Oceanogr. 28, 816-832 (1983).

A. Bricaud, A. Morel: Light attenuation and scattering by phytoplanktonic cells: a theoretical modelling. Applied Optics 25, 571-580 (1986).

A. Bricaud, A.-L. Bédhomme, A. Morel: Optical properties of diverse phytoplanktonic species: experimental results and theoretic interpretation. J. Plankton Res. 10, 851-873 (1988).

F.D. Bryant, B.A. Seiber, P. Latimer: Absolute Optical Cross Sections of Cells and Chloroplasts. Arch. Biochem. Biophys. 135, 79-108 (1969).

R.P. Bukata, J.E. Bruton, J.H. Jerome: Conceptual approach to the simultaneous determination of the back-scatter and absorption coefficients of natural waters. Appl. Optics 19, 1550-1559 (1980).

M.S. Caceci, W.P. Cacheris: Fitting Curves to Data. Byte 340-362, May 1984.

D.K. Clark: Phytoplankton algorithms for the Nimbus-7 CZCS. In: J.F.R. Gower (Ed.): Oceanography from Space. Plenum Press, 227-238 (1981).

H.R.Condit, F. Grum: Spectral Energy Distribution of Daylight. J. Opt. Soc. Am. 54, 937-944 (1964).

C. Cox, W. Munk: Slopes of the sea surface deduced from photographs of sun glitter. Bull. Scripps Inst. Oceanogr. Univ. Calif. 6, 401-488 (1956).

H.G. Dahn, K.P. Günther, W. Lüdeker: Characterisation of Drought Stress of Maize and Wheat Canopies by Means of Spectral Resolved Laser Induced Fluorescence. EARSeL Adv. Remote Sensing Vol. 1, No. 2-II, 12-19 (1992).

A.M. Devol: Zooplankton respiration and its relation to plankton dynamics in two lakes of contrasting trophic stage. Limnol. Oceanogr. 24, 893-905 (1979).

P. Diehl, H. Haard: Measurement of the spectral attenuation to support biological research in a "plankton tube" experiment. Oceanologica Acta 3, 89-96 (1980).

R. Doerffer, V. Amann: The development of the horizontal distribution of a North Sea phytoplankton bloom. Special meeting on Causes, Dynamics and Effects of Exceptional Marine Blooms and Related Events, ICES, Copenhagen, 4-5 Oct. 1984.

R. Doerffer, V. Amann: The Influence of Exceptional Phytoplankton Blooms on Remote Sensing of Chlorophyll. In: GKSS 1986a, Appendix 8.

R. Doerffer, H. Graßl, B. Kunkel, H. van der Piepen: ROSIS - an advanced imaging spectrometer for the monitoring of water colour and chlorophyll fluorescence. SPIE Advanced optical instrumentation for remote sensing of the earth's surface from space, 1129, 117-121 (1989).

L.N.M. Duysens: The Flattening of the Absorption Spectrum of Suspensions, as compared to that of Solutions. Biochimica and Biophysica Acta, 19, 1-12 (1956).

A. Einstein: Theorie der Opaleszenz von homogenen Flüssigkeiten und Flüssigkeitsgemischen in der Nähe des kritischen Zustandes [Theory of the opalescence of homogeneous liquids and liquid mixtures close to the critical state]. Ann. Phys. 33, 1275 (1910).

R.J. Exton, W.M. Houghton, W. Esaias, L.W. Haas, D. Hayward: Spectral differences and temporal stability of phycoerythrin fluorescence in estuarine and coastal waters due to the domination of labile cryptophytes and stabile cyanobacteria. Limnol. Oceanogr. 28, 1225-1231 (1983).

F.H. Farmer, O. Jarrett, C.A. Brown: Visible Absorbance Spectra: A Basis for In Situ and Passive Remote Sensing of Phytoplankton Concentration and Community Composition. NASA Technical Paper 2094 (1983).

J. Fischer, H. Graßl: Radiative transfer in an atmosphere-ocean system: an azimuthally dependent matrix-operator approach. Appl. Optics 23, 1032-1039 (1984).

J. Fischer, U. Kronfeld: Chlorophyll Fluorescence within the Visible Spectrum: Measurements and Calculations. In: GKSS 1986a, Appendix 5.

G.G. Ganf, S.I. Heaney, J. Corry: Light absorption and pigment content in natural populations and cultures of a non-gas vacuolate cyanobacterium *Oscillatoria bourrellyi* (= *Tychomema bourrellyi*). J. Plankton Res. 13, 1101-1121 (1991).

P. Gege, H.P. Hofmann: Tank experiments for the natural fluorescence of phytoplankton at high concentrations. DLR Oberpfaffenhofen, Internal Report 552-1/90, 40 pages (1990).

P. Gege: TRACOR Northern TN 1710 - Kalibrationsmessungen [TRACOR Northern TN 1710 - Calibration measurements]. DLR Oberpfaffenhofen, Internal Report 552-5/92, 62 pages (1992).

W. Geller, H. Güde: Lake Constance - the largest German lake. In: W. Lampert, K.O. Rothaupt (Eds.): Limnology in the Federal Republic of Germany, SIL Munich (1989).

GKSS 1986a: The use of chlorophyll fluorescence measurements from space for separating constituents of sea water. ESA Contract No. RFQ 3-5059/84/NL/MD. GKSS Res. Centre Geesthacht.

GKSS 1986b: The Influence of Yellow Substances on Remote Sensing of Sea - Water Constituents from Space. ESA Contract No. RFQ 3-5060/84/NL/MD. GKSS Res. Centre Geesthacht.

M.L. Goldberger, K.M. Watson: Collision theory. Wiley (1964).

H.R. Gordon, O.B. Brown, M.M. Jacobs: Computed Relationships between the Inherent and Apparent Optical Properties of a Flat Homogeneous Ocean. Applied Optics 14, 417-427 (1975).

H.R. Gordon: Diffuse Reflectance of the ocean: the theory of its argumentation by chlorophyll a fluorescence at 685 nm. Applied Optics 18, 1161-1166 (1979).

H.R. Gordon: Dependence of the diffuse reflectance of natural waters on the sun angle. Limnol. Oceanogr. 34, 1484-1489 (1989).

H.R. Gordon: Radiative transfer in the atmosphere for correction of ocean color remote sensors. In: Barale and Schlittenhardt (1993), pages 33-77).

W. Greiner: Theoretische Physik. Band 3: Klassische Elektrodynamik [Theoretical Physics. Volume 3: Classical Electrodynamics]. Verlag Harri Deutsch, 3rd Edition (1982).

K.P. Günther: Biophysical processes of chlorophyll a fluorescence. In GKSS 1986a, Appendix 1 (1986a).

K.P. Günther: Analysis of the daily cycle of in vivo chlorophyll a stimulated by artificial light sources. In GKSS 1986a, Appendix 3 (1986b).

K.P. Günther, W. Lüdeker, H.-G. Dahn: Design and testing of a spectral-resolving fluorescence lidar system for remote sensing of vegetation. Proc 5th Int. Colloquium - Physical Measurements and Signatures in Remote Sensing, Courchevel, France, 14-18 January 1991, ESA SP-319, 723-726 (1991).

H. Haardt, H. Maske: Variability of excitation-, emission- and absorption-spectra normalized to the chlorophyll concentration. In GKSS 1986a, Appendix 16.

G.M. Hale, M.R. Querry: Optical Constants of Water in the 200-nm to 200 μm Wavelength Region. Appl. Optics 12, 555-563 (1973).

S. Hassing, O. Sonnich Mortensen: Kramers-Kronig relations and resonance Raman scattering. J. Chem. Phys. 73, 1078-1083 (1980).

F.T. Haxo, D.C. Fork: Photosynthetically Active Accessory Pigments of Cryptomonads. Nature 184, 1051-1052 (1959).

R.T. Hodgson, D.D. Newkirk: Pyridine immersion: a technique for measuring the refractive index of marine particles. Proc. Sot. Phot. Opt. Instr. Energ. 64, 62-64 (1975).

N.K. Højerslev, I. Traberg: A new perspective for remote measurements of plankton pigments and water quality. Københavns Universitet, Geofysisk Institut, Report No. 51 (1990).

N.G. Jerlov: Marine Optics. Elsevier Scientific Publ. Company (1976).

J.H. Jerome, R.P. Bukata, J.E. Bruton: Determination of available subsurface light for photochemical and photobiological activity. J. Great Lakes Res. 16(3), 436-443 (1990).

D.H. Jewson, J.F. Talling, M.J. Dring, M.M. Tilzer, S.I. Heaney, C. Cunningham: Measurement of photosynthetically available radiation in freshwater: comparative tests of some current instruments used in studies of primary production. J. Plankton Research 6, 259-274 (1983).

K. Kalle: Meereskundliche chemische Untersuchungen mit Hilfe des Zeissschen Pulfrich Photometers [Chemical oceanographic studies with the aid of the Zeiss Pulfrich photometer]. Ann. Hydrogr. Berlin 65, 276-282 (1937).

U. Kenter: Charakterisierung des autotrophen Picoplanktons des Bodensees nach Pigmentzusammensetzung und morphometrischen Merkmalen [Characterization of the autotrophic picoplankton of Lake Constance from pigment composition and morphometric characteristics]. Dissertation, Constance University (1991).

J.T.O. Kirk: A theoretical analysis of the contribution of algal cells to the attenuation of light within natural waters. I. General treatment of suspensions of pigmented cells. The New Phytologist 75, 11-20 (1975a).

J.T.O. Kirk: A theoretical analysis of the contribution of algal cells to the attenuation of light within natural waters. II. Spherical cells. The New Phytologist 75, 21-36 (1975b).

J.T.O. Kirk: A theoretical analysis of the contribution of algal cells to the attenuation of light within natural waters. III. Cylindrical and spheroidal cells. The New Phytologist 77, 341-358 (1976).

J.T.O. Kirk: Light and photosynthesis in aquatic ecosystems. Cambridge University Press (1983).

J.T.O. Kirk: Dependence of relationship between inherent and apparent optical properties of water on solar altitude. Limnol. Oceanogr. 29, 350-356 (1984).

C. Kittel: Einführung in die Festkörperphysik [Introduction to solid-state physics]. Oldenbourg Verlag, 6th Edition (1983).

F.X. Kneizys, E.P. Shettle, L.W. Abreu, J.H. Chetwynd, G.P. Anderson, W.O. Gallery, J.E.A. Selby, S.A. Clough: Users Guide to LOWTRAN 7. Air Force Geophysics Laboratory, AFGL-TR-88-0177 (1988).

N.I. Krinsky: Non-photosynthetic functions of carotenoids. Phil. Trans. R. Soc. London B284, 581-590 (1978).

U. Kronfeld: Die optischen Eigenschaften der ozeanischen Schwebstoffe und ihre Bedeutung für die Fernerkundung von Phytoplankton [The optical properties of oceanic suspended matter and its significance for the remote sensing of phytoplankton]. Dissertation, Hamburg University (1988).

W. Lampert, V. Schober: Das regelmäßige Auftreten von Algenmaximum und "Klarwasserstadium" im Bodensee als Folge von klimatischen Bedingungen und Wechselwirkungen zwischen Phyto- und Zooplankton [Regular occurrence of an algal maximum and "clear water stage" in Lake Constance caused by climatic conditions and interactions between phytoplankton and zooplankton]. Arch. Hydrobiol. 82, 364-386 (1978).

L.D. Landau, E.M. Lifschitz: Lehrbuch der theoretischen Physik. Band IV: Quantenelektrodynamik [Text book of theoretical physics. Volume IV: Quantum electrodynamics]. Akademie-Verlag Berlin, 5th Edition (1986).

D.W. Lawlor: Photosynthese [Photosynthesis]. Thieme (1990).

H.K. Lichtenthaler: Chlorophylls and Carotenoids: Pigments of Photosynthetic Biomembranes. Methods in Enzymology 148, 350-382 (1987).

R. MacColl, D.S. Berns, O. Gibbons: Characterization of Cryptomonad Phycoerythrin and Phycocyanin. Arch. Biochem. Biophys. 177, 265-275 (1976).

R. MacColl, D. Guard-Friar, K. Csatorday: Chromatographic and spectroscopic analysis of phycoerythrin 545 and its subunits. Arch. Microbiol. 135, 194-198 (1983).

R. MacColl, D. Guard-Friar, E. C. Williams: Spectroscopic studies on phycoerythrin 545, its bilins, and its isoproteins. J. Luminescence 51, 21-28 (1992).

D. Maier, W. Geller: Eine neue limnologische Methode zur Erkennung unterschiedlicher Wasserkörper in Seen [A novel limnological method for identifying different bodies of water in lakes]. Arch. Hydrobiol. 85, 229-243 (1979).

W.E.K. Middleton: The Color of the Overcast Sky. J. Opt. Soc. Am. 44, 793-789 (1954).

A. Morel: Optical Properties of Pure Water and Pure Sea Water: In: N.G. Jerlov, E. Steemann Nielsen (Eds.): Optical Aspects of Oceanography. Academic Press London, 1-24 (1974).

A. Morel, L. Prieur: Analysis of variations in ocean color. Limnol. Oceanogr. 22, 709-722 (1977).

A. Morel, A Bricaud: Theoretical results concerning light absorption in a discrete medium, and application to specific absorption of phytoplankton. Deep-Sea Research 28A, 1375-1393 (1981).

A. Morel, A.C. Smith: Terminology and Units in Optical Oceanography. Marine Geodesy 5, 335-349 (1982).

A. Morel, B. Gentili: Diffuse reflectance of oceanic waters: its dependence on Sun angle as influenced by the molecular scattering contribution. Appl. Optics 30, 4427-4438 (1991).

J.L. Mueller: The Influence of Phytoplankton on Ocean Color Spectra. PhD Thesis, Oregon State University (1974).

H. Neckel, D. Labs: Improved Data of Solar Spectral Irradiance from 0.33 to 1.25 μ. Sol. Phys. 74, 231-249 (1981).

J.A. Nelder, R. Mead: A simplex method for function minimization. Computer Journal 7, 308-313 (1965).

E.A. Nusch: Comparison of different methods for chlorophyll and phaeopigment determination. Arch. Hydrobiol. Beih. 14, 14-36 (1980).

G. Nyquist: Investigation of some optical properties of seawater with special reference to lignin sulfonates and humic substances. PhD Thesis Göteborgs Universitet, 200 pp. (1979).

C. O'hEocha, M. Raftery: Phycoerythrins and Phycocyanins of Cryptomonads. Nature 184, 1049-1051 (1959).

C. O'hEocha: Biliproteins of cryptomonad algae. Proc. Royal Irish Academy 63, 191-200 (1964).

T.R. Parsons, M. Takahashi, B. Hargrave: Biological oceanographic processes. Pergamon Press, Oxford (1977).

R.W. Preisendorfer: Application of Radiative Transfer Theory to Light Measurements in the Sea. Int. Geophys. Geod. Monogr. 10, 11-29 (1961).

R.W. Preisendorfer: Hydrologic optics, Vol. 1 (Introduction), NOAA, 218 pp. (1976).

L. Prieur, A. Morel: Relations théoriques entre le facteur de reflexion diffuse de l'eau de mer à diverses profondeurs et leur caractéristiques optiques [Theoretical relationships between the diffuse reflection factor of sea water at different depths and their optical characteristics]. (Abstract) Abstracts from the International Union of Geophysics and Geodesy, 16th General

Assembly held in Grenoble on 25 August - 6 September 1975 (Paris: International Union of Geophysics and Geodesy), pp. 250-251.

L. Prieur: Transferts radiatifs dans les eaux de mer [Radiative transfers in sea waters]. Thesis, Doctorat d'Etat, Univ. Pierre et Marie Curie, Paris, 243 pp. (1976).

G. Richter: Stoffwechselphysiologie der Pflanzen [Metabolic physiology of plants]. Thieme, 5th Edition (1988).

C.S. Roesler, M.J. Perry: Modeling in situ phytoplankton absorption from total absorption spectra in productive inland marine waters. Limnol. Oceanogr. 34, 1510-1523 (1989).

F.E. Round: Biologie der Algen [Biology of algae]. Thieme, 2nd Edition (1975).

K.S. Rowan: Photosynthetic pigments of algae. Cambridge University Press (1989).

S. Sathyendranath, L. Lazzara, L. Prieur: Variations in the spectral values of specific absorption of phytoplankton. Limnol. Oceanogr. 32, 403-415 (1987).

S. Sathyendranath, T. Platt: Angular distribution of the submarine light field: modification by multiple scattering. Proc. R. Soc. Lond. A 433, 287-297 (1991).

H. Scheer, W. Kufer: Studies on plant bile pigments. IV. Conformational studies on C-phycocyanin from *Spirulina platensis*. Z. Naturforschung Part C, 32, 513-519 (1977).

H.Schiller, R. Doerffer: Fast computational scheme for inverse modeling of multispectral radiances: application for remote sensing of the ocean. Applied Optics 32,

3280-3285 (1993).

H. Siegel: On the relationship between the spectral reflectance and inherent optical properties of oceanic waters. Beitr. Meereskd. Berlin 56, 73-80 (1987).

J.L. Simonds: Application of Characteristic Vector Analysis to Photographic and Optical Response Data. J. Opt. Soc. Am. 53, 968-974 (1963).

R.C. Smith: Structure of solar radiation in the upper layer of the sea. In: N.G. Jerlov, E. Steemann Nielsen (Eds.): Optical Aspects of Oceanography. Academic Press, 95-119 (1974).

R.C. Smith, K.S. Baker: Optical properties of the clearest natural waters (200-800 nm). Applied Optics 20, 177-184 (1981).

M. Smoluchowski: Molekular-kinetische Theorie der Opaleszenz von Gasen im kritischen Zustande, sowie einiger verwandter Erscheinungen [Molecular-kinetic theory of the opalescence of gases in the critical state, and some related phenomena]. Ann. Phys. 25, 205 (1908).

M.R. Spiegel: Komplexe Variablen [Complex variables]. McGraw-Hill (1982).

H.H. Strain: Chloroplast Pigments and Chromatographic Analysis. 32nd Annual Priestley Lecture. University Park, PA: Penn State University Press (1958).

I.J. Tehver: Raman profile with consideration for Condon and non-Condon terms. Optics communications 38, 279-283 (1981).

M.M. Tilzer: Secchi disk - chlorophyll relationships in a lake with highly variable phytoplankton biomass. Hydrobiologia 162, 163-171 (1988).

J.E. Tyler: Radiance distribution as a function of depth in an underwater environment. Bull. Scripps Inst. Oceanogr. 7, 363-412 (1960).

H.C. van de Hulst: Light scattering by small particles. Wiley, New York (1957).

C. van de Hoek: Algen [Algae]. Thieme, 2nd Edition (1984).

H. van der Piepen, R. Doerffer: Future Systems for Global Monitoring of Ocean Colour. In: Barale and Schlittenhardt (1993), pages 331-334.

A.P. Vasilkov, O.V. Kopelevich: Reasons for the Appearance of the Maximum near 700 nm in the Radiance Spectrum Emitted by the Ocean Layer. Oceanology 22, 697-701 (1982).

W. von Smekot-Wensierski, B. Wozniak, H. Graßl, R. Doerffer: Die Absorptionseigenschaften des marinen Phytoplanktons [Absorption characteristics of marine phytoplankton]. GKSS Research Centre Geesthacht, Report No. 92/E/105, 104 pages (1992).

G. Wittum: Mehrgitterverfahren [Multiple-grating methods]. Spektrum d. Wiss. 78-90, April 1990.

Acknowledgements

I thank Prof. H. Graßl, Director of the Max-Planck Institute for Meteorology in Hamburg, most sincerely for his supervision and expert opinion on the dissertation. I always left my discussions with him with renewed motivation and full of enthusiasm.

The present work was carried out at the Institute of Optoelectronics of the Deutsche Forschungsanstalt für Luft- und Raumfahrt (DLR) in Oberpfaffenhofen. The choice of topic and subject supervision were the responsibility of Dr. H. van der Piepen, and many thanks are due to him for this and for supplying contacts. I greatly appreciated the friendly collaboration in which I could work highly independently.

My thanks are due to Dr. M. Schroeder, Head of Department FO at the Institute for Optoelectronics, for my inclusion in the department for optical remote sensing, for his interest in my work and his involvement in procuring work contracts for me after my research studentship had expired.

I thank all colleagues in the Department for the excellent working atmosphere. I was able to profit from the experience and expertise of every single individual, since everyone readily provided advice. Mr. W. Mooshuber especially contributed to the success of my measurements, as he was helpful to me in the calibration and adjustment of the spectrometer and made his optics laboratory and calibration equipment available to me. I thank Dr. K. Günther and the visiting Chinese scientist Prof. S. Lin for much useful advice on the interpretation of my measurements. Mr. J. Schulz, who was always ready to have discussions with me, also helped me greatly.

The present work would have been impossible without the data from Lake Constance. For the possibility of

travelling on the research ship "Robert Lauterborn" and for supplying me with *in situ* measurements from the Limnological Institute of Constance University, I very sincerely thank its then director Prof. M.M. Tilzer, who has since become head of the Alfred Wegener Institute for Polar and Marine Research in Bremerhaven.

Unpublished cell count measurements were kindly provided to me by Dr. U. Gaedke and Dr. A. Schweitzer of the Limnological Institute of Constance University and I received measurements of pigment concentrations and visual ranges from Ms. B. Beese, Ms. Richter and Mr. U. Kenter. I thank all of them most sincerely for supplying the measurements and supplementary advice.

An important measurement of yellow substance concentration in Lake Constance was made by Mr. G.M. Ferrari. I thank him for travelling especially for this reason from Ispra, Italy, and I also thank Dr. P. Schlittenhardt, head of the Marine Application Department at the Institute for Remote Sensing Applications at the Joint Research Centre, Ispra, for organizing this measurement.

Very special thanks are due to the crew of the research ship, and especially the captain, Mr. Wiedemann. The crew frequently collected me especially from Überlingen, helped me to load and unload and set up the measuring equipment and complied with my wishes during measurement.

The absorption measurements on pure algal cultures which were made for me by Ms. G. Hartmann of the Institute for Physical Geography, Freiburg University, were very valuable to me and my special thanks are offered for these. I should also like to thank Ms. A. Pulvermüller of the Institute for Physical Geography for the copious discussions and correspondence. As a specialist in the remote sensing of Lake Constance, she was an indispensable source of information for me.

Any list of people who contribute to the success of a piece of work will never be complete. Every discussion about the work gives renewed impetus; here I may emphasize only the many discussions with Dr. R. Letterer. Relief from everyday tasks is also an important factor, and I give special thanks to my parents. My thanks are due to all those who helped me directly or indirectly.

Appendix A: Kramers-Kronig relations

Formulation

Complex numbers are frequently used in physics in order to give equations a more readable form. The complex notation is especially advantageous in the description of periodic processes, since, because of Euler's formula $e^{iz} = \cos z + i \sin z$, the cosine is converted into the exponential function which is more easy to handle.

A periodic process U is described by the equation

$$U(x) = U(0)\, e^{i(\omega x + \phi)}$$

the real part representing the amplitude and the imaginary part not being associated with any physical meaning. x represents a coordinate, for example position or time, ω is the length of the period and U(0) is the amplitude at x=0. The phase ϕ is a measure of the distance between the origin of the coordinates (x=0) and the point where the amplitude becomes maximum.

If two periodic processes are linked together by an equation

$$W(\omega) = \alpha(\omega)\, U(\omega),$$

then the complex function

$$\alpha(\omega) = \alpha'(\omega) + i\, \alpha''(\omega)$$

is termed a *response function*, since it describes a physical system which responds to a cause U with an action W.

Whereas in the case of U and W only the real part has a physical meaning, in the case of α, both the real part

α' and the imaginary part α'' have a physical meaning, since both are required to link together U and W. Because α' and α'' join together the same functions U and W, they are not independent of each other. If three conditions discussed further below are fulfilled, $\alpha''(\omega)$ can be calculated from $\alpha'(\omega)$ and vice versa. The interconversion formulae are called *Kramers-Kronig relations*. These are as follows:

$$\alpha'(\omega) = \frac{2}{\pi} P \int_0^\infty \frac{\omega' \cdot \alpha''(\omega')}{\omega'^2 - \omega^2} \, d\omega' \qquad \text{(A.1)}$$

$$\alpha''(\omega) = -\frac{2\omega}{\pi} P \int_0^\infty \frac{\alpha'(\omega')}{\omega'^2 - \omega^2} \, d\omega'. \qquad \text{(A.2)}$$

P designates the principal value of the following integral, that is the contribution at the pole $\omega=\omega'$ is omitted.

Proof

The derivation below follows the proof given in the book by Kittel (1983). The starting point is Cauchy's equation

$$\oint_C f(z) \, dz = 0.$$

This central equation of the theory of functions states that for an analytical (= continuously differentiable) function f(z), the integral over a single closed curve C is zero on the complex plane. The proof can be found, for example, in Spiegel (1982), page 103. We shall now consider the function $f(z) = \alpha(z)/(z \cdot \omega)$ and the following integration path:

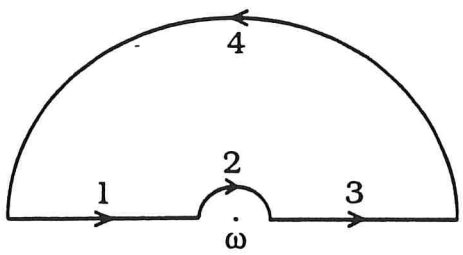

If f(z) is analytical in the upper half of the complex plane, according to Cauchy the integral is zero. We divide the integration path into the 4 parts shown:

$$\oint_C = \int_1 + \int_2 + \int_3 + \int_4.$$

If $\alpha(z)/z$ for $|z| \to \infty$ tends to zero, $\int_4 = 0$.

Let Section 2 be a semicircle of radius u and centre ω: $z = \omega + ue^{i\theta}$, $dz = iue^{i\theta}d\theta$. Since

$$\int_2 = \int_2 \frac{\alpha(z)}{z-\omega}\, dz = \int_{\pi}^{0} \frac{\alpha(\omega+ue^{i\theta})}{ue^{i\theta}} iue^{i\theta}d\theta = i\int_{\pi}^{0} \alpha(\omega+ue^{i\theta})d\theta$$

it follows for $u \to 0$: $\int_2 = -i\pi\,\alpha(\omega)$.

Sections 1 and 3 are by definition the principal values of the integral between $-\infty$ and ∞. It therefore follows that:

$$\bar{P}\int_{-\infty}^{\infty} \frac{\alpha(z)}{z-\omega}dz = i\pi\,\alpha(\omega).$$

This equation links together the real and imaginary parts. If α is divided into the real and imaginary parts, the equation then has the form:

$$P\int_{-\infty}^{\infty} \frac{\alpha'(z)}{z-\omega}dz + iP\int_{-\infty}^{\infty} \frac{\alpha''(z)}{z-\omega}dz = i\pi\,\alpha'(\omega) - \pi\,\alpha''(\omega). \qquad \text{(A.3)}$$

In order to obtain Equations (A.1) and (A.2), the integrals over negative frequencies must further be replaced by integrals over positive frequencies. For the imaginary part (A.3) the following is thus obtained:

$$\alpha'(\omega) = \frac{1}{\pi} P\left[\int_0^{\infty} \frac{\alpha''(z)}{z-\omega} dz + \int_{-\infty}^{0} \frac{\alpha''(p)}{p-\omega} dp\right].$$

If p=-z, dp=-dz, then for the last integral, it follows in the case $\alpha''(-z) = -\alpha''(z)$ that:

$$\int_{-\infty}^{0} \frac{\alpha''(p)}{p-\omega} dp = \int_{\infty}^{0} \frac{-\alpha''(z)}{-z-\omega}(-dz) = \int_{0}^{\infty} \frac{\alpha''(z)}{z+\omega} dz,$$

and where $\frac{1}{z-\omega} + \frac{1}{z+\omega} = \frac{2z}{z^2-\omega^2}$ (A.1) is obtained.

Similarly, by equating the real parts of (A.3), (A.2) is obtained, in which case $\alpha'(-z) = \alpha'(z)$ must be used.

Validity

The following three conditions on the function $\alpha(\omega)$ enter into the derivation of the Kramers-Kronig relations:

1. $\alpha(\omega)$ has no pole in the upper hemisphere.
2. $\alpha(\omega)/\omega$ disappears as $|\omega| \to \infty$.
3. $\alpha'(-\omega) = \alpha'(\omega)$ and $\alpha''(-\omega) = -\alpha''(\omega)$.

A discussion on their physical meaning follows.

Re 1. At a pole of α, the amplitude of W would be infinite. Because $\alpha = W/U$, this is only possible for U=0, but without cause there is no action. In physical systems, α has no pole.

Re 2. If the function $\alpha(\omega)/\omega$ does not disappear as $|\omega| \to \infty$, but tends towards a function $g(\omega)$, the subtracted

Kramers-Kronig relations are obtained, see Greiner (1982), p. 359. A practical application is discussed further below.

Re 3. The third condition represents the requirement for causality, if the coordinate x represents time t. In order to see this, consider

$$U(\omega) = e^{i(\omega t + \phi)}, \quad t < 0$$
$$W(\omega) = e^{i(\omega t + \phi')}, \quad t > 0.$$

Causality means that the cause occurs before the action: in the past $t<0$ only the function $U(\omega)$ existed, in the future $t>0$, only the function $W(\omega)$ exists. The formal conversion from $+\omega$ to $-\omega$ in condition 3 means that, in the exponent, $i\omega t$ becomes $-i\omega t$ and because only $\omega>0$ is physically meaningful, this means the transition from t to -t, that is the transposition of cause and action.

When U and W are transposed in the equation $W = \alpha U$, $U = \bar{\alpha}W = \bar{\alpha}\alpha U$ is obtained, that is $\alpha\bar{\alpha}=1$. In the response function $\bar{\alpha}$, the argument is $-\omega$: $\bar{\alpha}(-\omega)=\alpha'(-\omega) + i\,\alpha''(-\omega)$. Because $UU^*=1$ and $WW^*=1$, $\alpha = W/U = WU^*$ and $\bar{\alpha} = 1/\alpha = U/W = UW^* = (WU^*)^* = \alpha^*$, where * represents the complex conjugate parameter. Therefore, $\bar{\alpha}(-\omega) = \alpha'(\omega) - i\alpha''(\omega)$, which conforms exactly to requirement 3.

Subtracted Kramers-Kronig relations

In order to use a Kramers-Kronig relation, for instance (A.1), $\alpha''(\omega)$ must be known for $0<\omega<\infty$. However, in practice, α'' is only known in a finite interval, so that the integral (A.1) can only be solved approximately. The error cannot be estimated if there is no idea of the shape of the curve outside the interval; the error can be

particularly serious at the limits.

However, if the value of α' is known for a frequency ω_0, the unknown function $\alpha'(\omega)$ can be adjusted to this value $\alpha'(\omega_0)$. For if the difference

$$\alpha'(\omega) - \alpha'(\omega_0) = \frac{2}{\pi} P \int_0^\infty \omega' \cdot \alpha''(\omega') \left(\frac{1}{\omega'^2 - \omega^2} - \frac{1}{\omega'^2 - \omega_0^2} \right) d\omega',$$

is formed, the "subtracted Kramers-Kronig relation" (SKK)

$$\alpha'(\omega) = \alpha'(\omega_0) + \frac{2}{\pi} (\omega^2 - \omega_0^2) P \int_0^\infty \frac{\omega' \cdot \alpha''(\omega')}{(\omega'^2 - \omega^2)(\omega'^2 - \omega_0^2)} d\omega', \qquad (A.4)$$

is obtained which is much more accurate than (A.1) if α'' is only known in an interval, compare Ahrenkiel (1971). The SKK for the imaginary part is accordingly

$$\alpha''(\omega) = \alpha''(\omega_0) - \frac{2}{\pi} \omega(\omega_0^2 - \omega^2) P \int_0^\infty \frac{\alpha'(\omega')}{(\omega'^2 - \omega^2)(\omega'^2 - \omega_0^2)} d\omega'. \qquad (A.5)$$

Appendix B: Simplex algorithm

Many programs have been written for data evaluation which fit a model curve to measured data. In all of the programs, the optimization is carried out by the simplex algorithm. This algorithm was developed by Nelder and Mead (1965) and implementation as Pascal program followed the initial approach by Caceci and Cacheris (1984). In comparison with other conventional algorithms (stepwise descent, steepest descent, Newton-Ralphson, Marquardt) it has two great advantages: it always converges and no computing-time-intensive matrix operations need to be carried out, since it succeeds without differentiation. Moreover, its modular structure permits compact and clear programming, so that additional conditions may readily be inserted retrospectively, such as for example restricting the fitting variables to a defined interval.

If a data set consists of N measured values x_i, y_i, i=1...N and the model curve f(x) has M free parameters, the parameter

$$R = \frac{1}{N} \sum_{i=1}^{N} (f(x_i)-y_i)^2$$

is a measure of the deviation of the model curve from the data points. The aim of optimizing the model curve is to minimize the *residual* R. If a fictitious M+1-dimensional space is formed, whose coordinate axes form the M fitted parameters and the residual R, the objective may be formulated as searching for the minimum of the M+1-dimensional landscape.

In order to remain with the pictorial representation: the search for the minimum is performed by a structure - the simplex - which has M+1 so-called vertices ("limbs"). Each vertex is a point on the surface of the landscape and corresponds to a fit already carried out. One of these is the poorest (R is maximum). The simplex puts

this highest limb on a different point of the landscape. This process is repeated until the simplex is trapped in a minimum.

The decision which point of the landscape to calculate the function f(x) and the residual R for as the next one, follows a strategy which is described with reference to the adjoining figure.

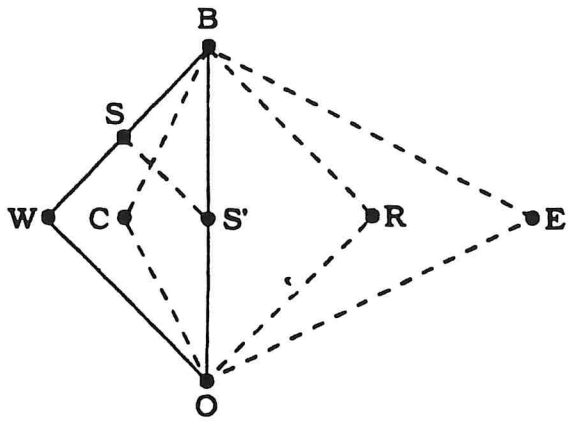

Possibilities for movement of the simplex. From Caceci and Cacheris (1984).

The simplex is the triangle WBO, where W represents the worst vertex (R is maximum), B the best (R minimum) and O all other. 4 positions are considered as the position of the simplex in the subsequent step: reflection of W on the line OB to the point R (the new simplex is the triangle RBO), contraction in the direction of this line to the point C (CBO), expansion beyond the line OB to the point E (EBO) and shrinking the simplex in parallel to the line WO (SBS'). Not all of the 4 possibilities are always computed, but they are tested in the sequence listed; if the new vertex is better than B, testing the remaining possibilities is dispensed with.

It can be shown (Caceci and Cacheris 1984) that the simplex is usually trapped in a minimum after $20 \cdot M^2$ iterations. If the landscape have several minima, the minimum found may, however, be a secondary minimum. Every

optimizing algorithm must deal with this problem. It is important therefore at the start, to assign suitable initial values to the fitting variables. In the fits which were carried out for the present work, it can be readily estimated how correct the resulting model curve is or how realistic the optimized values of the fitting variables are. Since all of the fits performed require a computing time less than one minute (80386 PC with a mathematics coprocessor), suitable initial values can be determined by testing if they cannot be estimated in other ways.

Appendix C: Software outline

A number of programs were written for the present work. The most important are described briefly in the following outline. The underlying algorithms can be found in the text; the numbers in italics indicate the number of the appropriate section. The programming language is Turbo Pascal 7.0.

Chapter 2

SKY Calculation of the transmission spectrum of the atmosphere by comparison of two measurements of irradiance. *2.1.3.*

CLOUD Calculation of the transmission spectrum of a cloud by comparison of two measurements of irradiance. *2.1.4.*

WEISS Resolution of a measured spectrum of irradiance into 4 base spectra. *2.1.6.*

REF Cloud correction for reflectance spectra. *2.3.3.*

Chapter 3

BRECH Determination of the shape of the spectrum of the refractive index from the attenuation spectrum. *3.2.1.*

ACM Extrapolation of an absorption spectrum from the suspension to the solution. Method of Bricaud and Morel (1981). *3.2.1.*

AB Calculation of attenuation and scattering from the absorption spectrum. The refractive index is calculated with the aid of the Kramers-Kronig relation (3.26); for attenuation, Mie theory is used in the approximation by van de Hulst (1957). *3.2.2.*

Chapter 4

INVERS Inversion of reflectance spectra according to Equation (4.1). Measured spectra are used for the absorption and scattering of the phytoplankton. *4.3.3.*

WASSER Inversion of reflectance spectra according to Equation (4.1). The absorption spectrum of the phytoplankton is approximated by Equation (3.31) and the scattering by all the water constituents is approximated by the formula $B_0+B_1\lambda^n$. *4.3.4.*